Evaluation of limestone and associated clays as industrial raw materials in NE Libya

A thesis submitted to the University of Manchester for the degree of Doctor of Philosophy in the Faculty of Science and Engineering

1999

Saad Kh. Abdalla

The Department of Earth Sciences

ProQuest Number: 10757060

ProQuest 10757060

Dedication

This thesis is dedicated to the memory of my late father "Mr. Khamis Abdalla" whom I lost during my sojourn in the city of Manchester, England. His understanding and compassion in times of crisis and difficulty, which gave me confidence that I would one day finish my project. His hope was that I will finish this study and I am very glad to fulfill his ambition.

LIST OF CONTENTS

CHAPTER 3 METHODOLOGY

CHAPTER 9 MINERALOGY AND MINERAL CHEMISTRY
OF CELESTITE-BEARING FORMATIONS

LIST OF FIGURES

LIST OF TABLES

LIST OF PLATES

LIST OF ABBREVIATIONS

API	American Petroleum Institute
AES	Atomic emission spectrometry
BSE	Backscattered electron images
CEC	Cation exchange capacity
C	Cement
CL	Cathodoluminescence
DSC	Differential scanning calorimetry
E	Echinoderm fragments
EDS	Energy dispersive spectrometer
EGME	Ethylene glycol monoethyl ether
EPMA	Electron probe microanalysis
FTIR	Fourier transform infrared
FGD	Flue gas desulphurisation
GCC	Ground calcium carbonate
HP	Hydrostatic pressure
HMC	High Mg-calcite
ICP	Inductively coupled plasma spectrometry
IOP	Iron ore pelletising
ISO	International Standards Organisation
JSM	Jeol scanning microscope
IR	Infrared
KBr	Potassium bromide
LOI	Loss on ignition
LSF	Lime saturation factor
Lst.	Limestone
LCM	Low Mg-calcite
M.	Member
Mx	Matrix
NMR	Nuclear magnetic resonance
OBMs	Oil based muds
OCMA	Oil Companies Materials Association
PCC	Precipitated calcium carbonate

LIST OF ABBREVIATIONS

ppm	parts per million
PRC	Petroleum Research Centre
ROP	Rate of penetration
R	Coralline algae
SBMs	Synthetic based muds
SE	Secondary electron images
SEM	Scanning electron microscopy
TGA	Thermogravimetric analysis
UV	Ultra violet
WBMs	Water based muds
WDS	Wavelength dispersive spectrometer
XRD	X-ray diffraction
XRF	X-ray fluorescence

ABSTRACT

The Al Jabal Al Akhdar in the eastern part of Libya comprises sedimentary carbonate rocks, represented by the Apollonia, Darnah, Al Bayda, Al Abraq, Al Faidiyah and Ar Rajmah Formations of Eocene to Quaternary age. The purity of limestone varies from impure (< 85.0 % $CaCO_3$) to very high purity (> 98.5 % $CaCO_3$). The highest limestone quality is exposed in the Al Faidiyah Formation at Al Fatayah Cement Quarry. For cement manufacture, limestone of the Benghazi Member at the Benghazi Cement Quarry, is used. The quality of this limestone is consistent but the clay content is more variable. From a commercial viewpoint, the main impurities such as dolomite, quartz and clay minerals (montmorillonite, kaolinite and glauconite) show some variation in certain Formations. Their distribution is a very important factor in grade control for the production of very high or low quality limestone. The limestones have a widespread and expanding range of end uses at relatively low cost. The primary use of carbonate rocks in the study area is in construction (aggregates), paints, oil well drilling mud, carpets and plastics. Future possible uses include animal feedstuffs, agriculture, glass, iron and steel, flue gas desulphurisation (FGD), soda ash and paper.
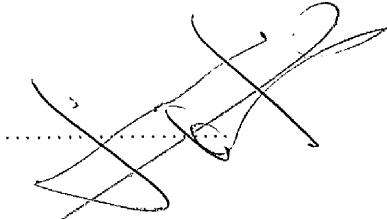
The Faidia Clay Member of the Al Faidiyah Formation consists of dark green clay; a very plastic sticky mass, with soap like textures. It is composed of montmorillonite, kaolinite and chlorite. Of these, montmorillonite constitutes by far the highest percentage. The Faidia Clay contains a variable proportion of non-clay minerals, such as fine quartz grains, calcite, ilmenite, dolomite, gypsum, K-feldspar, anatase and hematite. The Faidia Clay has been studied from the point of view of use as chemical additives for oil well drilling mud and specially for deep hole drilling, where high pressure and temperature occur. Standard bentonite tests show it is non-swelling, has a surface area 385 - 420 m^2/g (48 – 53 % smectite) and cation exchange capacity (C.E.C) 50 – 57 meqs/100 gms. With these characteristics, it is unsuitable for drilling fluid muds. Possible future uses include foundry moulding sands, decorative floor, bleaching and animal feed industries.

Celestite grade 88.3 % $SrSO_4$ occurs at the Benghazi Cement Quarry, as geodic nodules in the Middle Miocene rocks of the Ar Rajmah Formation. Detailed mineralogical and chemical data have been collected on the celestite and associated sediments. Sr contents vary from 161-8042 ppm and the average values (in Sr/Ca

x1000 atom ratio) for limestones in the Ar Rajmah Formation were 1.45 at Benghazi Cement Quarry, 0.44 at Ar Rajmah Quarry (mainly dolomite) and 0.77 at Wadi Al Faj Quarry.

Declaration

No portion of the work referred to in the thesis has been submitted in support of an application for another degree or qualification of this or any other university or other institute of learning.

Saad Kh. Abdalla

Author

The author obtained a B.Sc. degree from Garyounis University, Benghazi, Libya in Geology in 1985. From 1985 – 1986 he worked as Mud Engineer in Jowfe Oil Company, Benghazi, Libya, then as Geologist in the Water and Soil Department, Benghazi, Libya (1986 – 1990) and later as an expert in water well drilling, Benghazi Court. From 1990 – 1992 he worked in the Research Department in Jowfe Oil Company, and from 1992 – 1996 he worked in Wireline, DST and Production Test Department in Jowfe Oil Company, Benghazi, Libya. Since January 1997, he has engaged on the present research topic, in the Department of Earth Sciences, The University of Manchester.

Finally, I wish to express my particular heartiest thanks to my wife Dr. Faiza Al Shari and my children Naziha, Aya, Ahmed and M. Khamis for their patience, understanding, support and encouragement during the period of this study.

Chapter 1

INTRODUCTION

1.1 Introduction:

This thesis is a study of three different raw materials, limestone, clay and celestite in the Al Jabal Al Akhdar (in Arabic means the green mountain) area of the eastern part of Libya. Each raw material is discussed separately in three different chapters. Each chapter discusses the specific industrial requirements of the raw material and its industrial end-use. These raw materials occur in economic amounts, especially limestone and clay, and the aim of this thesis is to study these materials in the light of specific industrial applications. Although the amount of celestite in the area is small and of relatively poor quality, it was studied to gain an understanding of the chemistry and mineralogy of the mineral. It was also studied to gain an understanding of other much larger and purer deposits, which are of economic importance, fore example in the central part of Libya. The suitability of the three raw materials as components in oil drilling mud was also investigated. Evaluations of the Al Jabal Al Akhdar limestones, clays and celestite resources need to involve far more than a basic geological appraisal and should include laboratory determinations of mineralogical, chemical, physical and petrography of the rock types. The evaluation also should include a comparison with national and international specifications for each potential end-use.

1.1.1 Regional setting:

Libya is situated on the Mediterranean coast of north Africa. It covers an area of about 1.8 million square kilometres, extending about 1900 kilometres from east to west (coastline) and 1500 kilometres from north to south. Egypt and Sudan border it to the east and southeast, Tunisia and Algeria to the west and to the south lie Chad and Niger. Libya, situated on the Mediterranean foreland of the African shield, lies between Latitude 20° N and 33° N, and Longitudes 10° E and 25° E. Libya covers an area of about 1.6 million square kilometres along the northern coast of Africa. Libya includes a large part of the Sahara Desert, which extends across north Africa from the Atlantic Ocean to the Red Sea. Libya contains three climatogeographic zones: 1) the Mediterranean zone has an annual rainfall of as much as 600 mm and has a climate comparable to some parts of southern Europe, but southward this gradually gives way to intense desert conditions. The Mediterranean zone is the most heavily populated and most suitable for agriculture; 2) a semidesert area which is chiefly grazing land;

and 3) a desert zone containing several fertile oases. The Cyrenaica desert extends from the slopes of the Al Jabal Al Akhdar area at about 31°N to the southern border of Libya. The climate of Cyrenaica has average temperatures of about 20 to 25°C. Rainfall increases with increasing elevation from the coast to the upper Al Jabal Al Akhdar area, decreases towards the interior, and is rare in the desert. The rainy season is from October to March with January and December as the wettest months; drought is normal between June and September (Goudarzi, 1970).

1.1.2 Stratigraphy of the study area:

The sedimentary sequence exposed at the surface of the study area ranges in age from Eocene to Quaternary (Chapter 4) and is described in Table (1.1) as follows;

Table (1.1) Brief description of the Formations (Eocene to M. Miocene) in the study area

Group	Age	Formation	Member	Description
Al- Jabal Al- Akhdar	M. Miocene	Ar Rajmah	Wadi Al-Qattarah	Massive, white, fossiliferous limestone with dolomite to white, soft to medium hard, porous oolitic limestone with gypsum
			Benghazi	
	U. Oligocene to L. Miocene	Al Faidiyah	Faidia Limestone	Soft, greenish grey calcareous clay with glauconitic grains followed by the upper Member which is white, fossiliferous limestone
			Faidia Clay	
	M. to U. Oligocene	Al Abraq	-	Cream yellowish grey, medium grained, fossiliferous limestone
	L. Oligocene	Al Bayda	Algal Limestone	Grey to yellowish, soft, glauconitic, fossiliferous marl to white, fossiliferous, medium grained, thick bedded algal limestone
			Shahhat Marl	
	M. to U. Eocene	Darnah	-	Hard, massive, medium-to coarse-grained nummulitic limestone
	L. to M. Eocene	Apollonia	-	Light coloured, soft, fine- grained, chalky limestone with chert nodules, rhythmically alternating with hard limestone

1.1.3 Mineral resources:

The study area is poor in mineral resources. This is due chiefly to the absence of magmatic rocks. It contains mainly limestone, dolomite, marl and clay deposits. No ore mineralization was found during the study, except for the sedimentary celestite

occurring at the base of Benghazi Member of the Ar Rajmah Formation. Iron ore (hematite) is rare, occurring in the Faidia Clay Member of the Al Faidiyah Formation. Limestone is available for lime production as it contains deposits of sufficient quality, thickness and accessibility (road sections). In Cyrenaica (Al Jabal Al Akhdar area) within the Darnah (Plate 1.1), and Ar Rajmah Formations, the grain size distribution is critical in the use of a number of different industrial rocks. Aggregate in construction is used in specified size ranges, depending on the end use (Plates 1.2 and 1.3) and Al Faidiyah Formations are extensively used for various applications such as concrete aggregates, road, tiles, blocks, paints, carpets and plastics. Limestone also used as a bridging material reducing fluid loss and when used in combination with polymers forms a tough impermeable filtercake in oil drilling wells. Suitable limestone and clay deposits are available in sufficient quantities to support a cement industry in Al Jabal Al Akhdar area (e.g. Benghazi Cement Quarry of the Ar Rajmah Formation and Al Fatayah Cement Quarry of Al Faidiyah Formation). These areas are also close to good transportation and to the market.
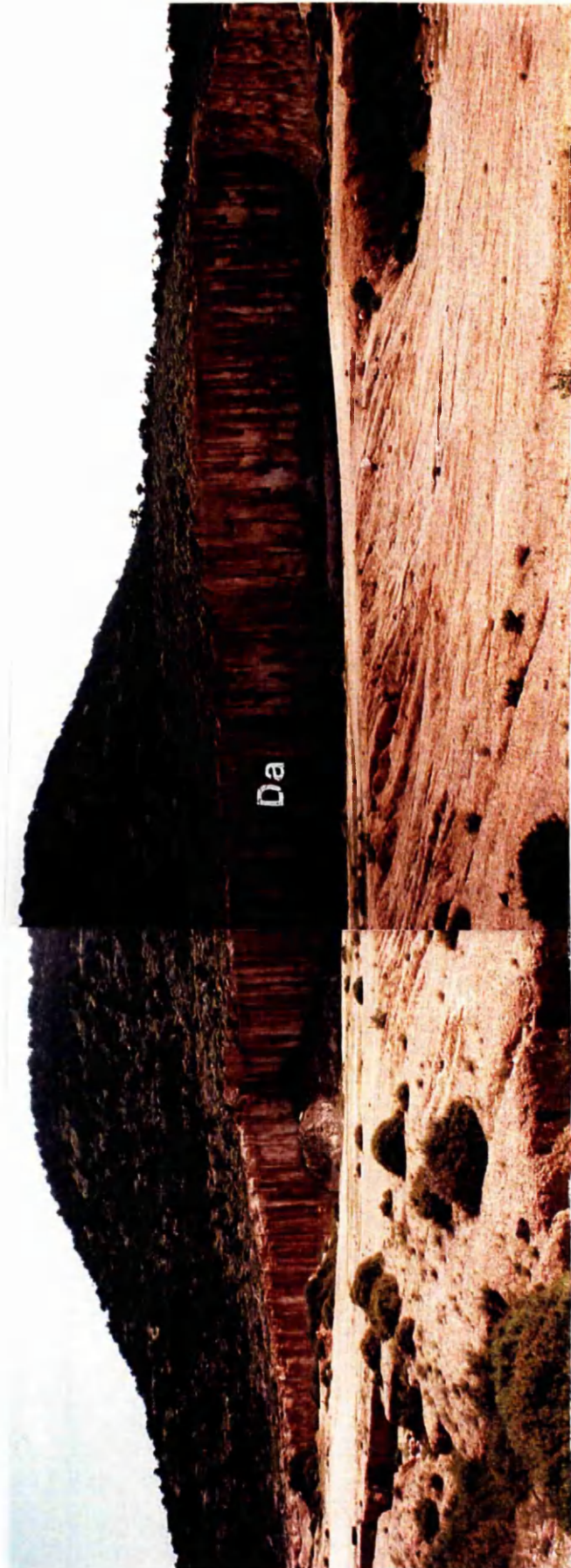
Plate (1.1) Showing Darnah Formation (Da) (Middle to Upper Eocene), in Qasar Libya Quarry, where it has been used for road aggregates.

Plate (1.2) Crushed limestone (see Plates 1.3) of Benghazi Member of the Ar Rajmah Formation (Middle Miocene). In Wadi Al Faj Quarry.
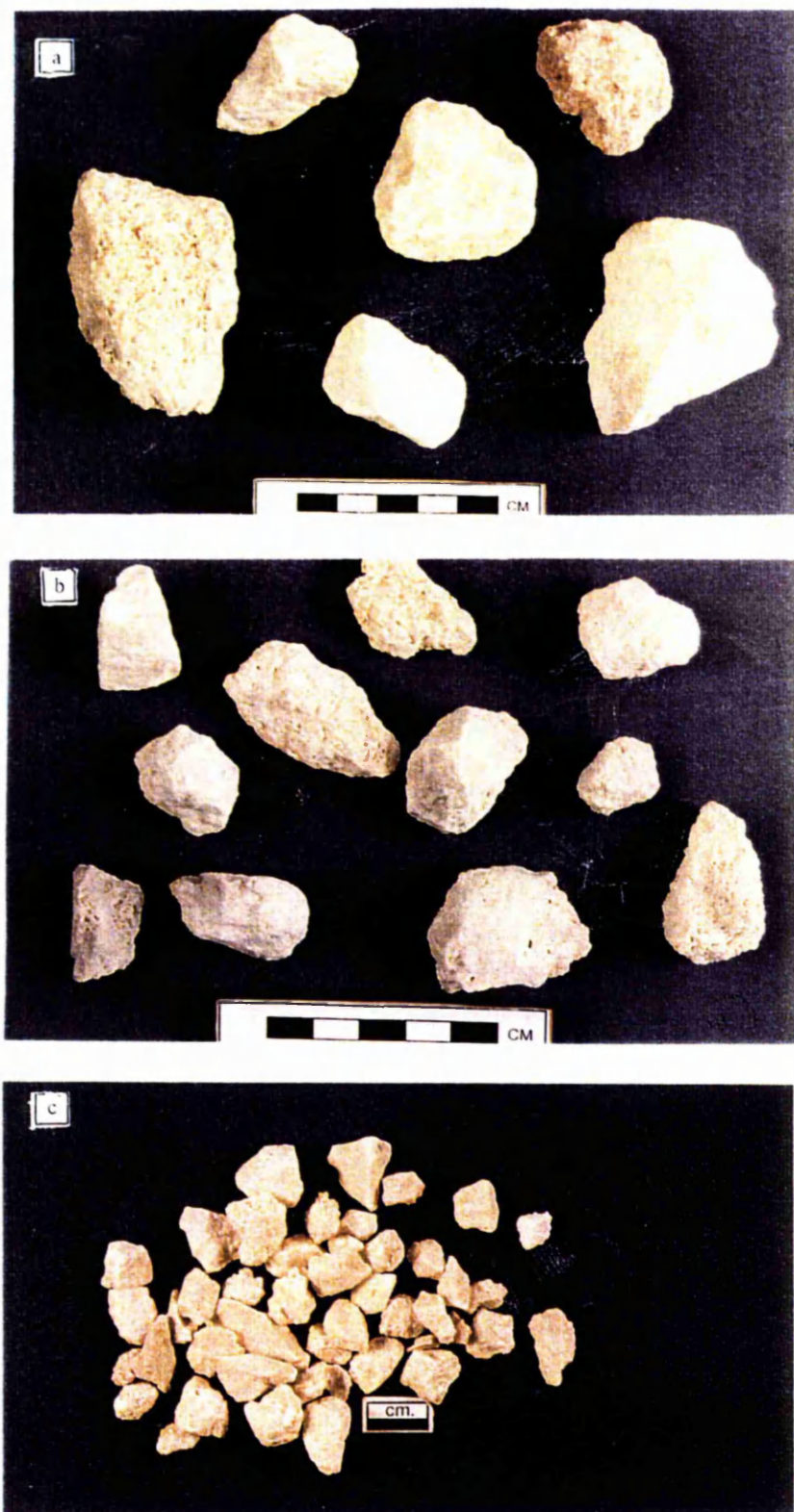
Plate (1.3) Crushed limestone of different grain sizes from Wadi Al Faj Quarry for building purposes; a) road aggregates; b) concrete aggregates; c) block and tile aggregates.

1.2 Limestones:

Limestones are extremely valuable raw materials and are widely used throughout industry, although the construction and cement manufacturing industries are generally the principal consumers. Limestones are amongst the most common rock types in the Al Jabal Al Akhdar area and are widely distributed in the study area (about 90% of the outcrop). There is a complete gradation from impure to very high purity limestone. The limestone is sometimes contaminated with other carbonate rocks such as dolomite $CaMg(CO_3)_2$, and other non-carbonates such as quartz, and clay minerals. Limestones in the study area are commonly compacted and well lithified, but softer porous varieties may also be found and used for certain applications. Chalk is a soft, white limestone and where found in Apollonia Formation, it is composed of planktonic foraminifera and it is characteristic of the Lower to Middle Eocene. It could be used as white filler. Principal mineral components were detected by X-ray diffraction (XRD), scanning electron microscopy (SEM) and $CaCO_3$ content (along with other carbonate components) accurately determined by thermogravimetry analysis (TGA). Thin-sections were also examined under a transmitted light petrographic microscope. A 35-mm camera was attached to the microscope. Each sample was described in terms of texture, fossil identification and type of porosity and in identifying accessory minerals, which were present at a level below the XRD detection limit. Chemical analyses of the major and trace elements present in the rocks of the Al Jabal Al Akhdar area was carried out by X-ray fluorescence spectrometry (XRF) and electron probe microanalysis (EPMA).

Lime is a manufactured chemical resulting from calcination of limestone or dolomite. The primary product is quicklime. When water is added, the resulting product is calcium hydroxide or slaked lime. Very high purity to high purity limestone is preferred because on calcination it loses 44 % of its weight and any impurities will be approximately doubled in amount in the lime. The production of good-quality lime depends largely on the type of kiln, conditions of calcination and the nature of the limestone raw material. The principal consumers of the lime are the steel industry where it is used as a flux, water treatment and flue gas desulphurisation (Harris, 1979; Evans, 1993; Harrison, 1993; Morgan, 1994).

1.3 Clay minerals:

Bentonite clay consists essentially of minerals of the smectite group. The structure, chemical composition, exchangeable ion type, swelling characteristics, and rheology are responsible for several unique properties and leading to very varied industrial applications (Highley, 1990; Inglethorpe *et al.*, 1993; Morgan, 1994; Manning, 1995; Reynolds and Moore, 1997). The terms non-swelling and swelling bentonites are synonymous with calcium and sodium bentonites. When mixed with water, swelling bentonite exhibits greater dispersion and better plastic, rheological properties than non-swelling bentonite. The grade is defined as the smectite content of the bentonite, whilst its quality is related to the inherent physico-chemical properties of the clay, either in its natural or modified form. Commercial bentonites usually contain more than 70 % smectite (Harben and Bates, 1990; Inglethorpe *et al.*, 1993). The major use of bentonites is in oil well drilling muds. Attapulgite and sepiolite, being the only clay mineral stable at high temperatures are favoured for muds used in drilling geothermal wells. These smectite clays have a phenomenal number of other uses, e.g. calcium bentonite is high value added chemical product used as bleaching, foundry moulding sands and as filler in animal feeding (Evans, 1993). Clay (bentonite) was found in the Lower part of the Al Faidiyah Formation (Faidia Clay Member). It consists of dark green clay, which is composed of montmorillonite, kaolinite and chlorite. It contains a variable proportion of other non-clay minerals such as quartz, calcite, ilmenite, dolomite, gypsum, K-feldspar, anatase and hematite. The clay of the Faidia Clay Member is used in producing building material. A major use of smectite (bentonite its commercial term) in Libya is in drilling muds for the petroleum industry, usually imported.

1.4 Celestite deposits:

Celestite ($SrSO_4$), is a member of the barite group of minerals and is the principal source of strontium. Celestite is similar to barite in many respects but it has a considerably lower density. Celestite occurs mainly in sedimentary rocks, particularly dolomite, dolomitic limestone and marls, either as a primary precipitate from aqueous solutions or more usually, by the interaction of gypsum or anhydrite with Sr-rich waters. (Harben and Bates, 1990; Ober, 1994; Chang *et al.*, 1996). Strontium compounds do not have any large-scale industrial uses like limestones and clay minerals. Useful compounds include; (Industrial Mineral, 1999)

- Strontium carbonate, $SrCO_3$. This carbonate is used in the manufacture of special glasses (colour television tubes) and for ferrites magnets.
- Strontium nitrate, $Sr(NO_3)_2$. This is responsible for red colours appearing in fireworks, signal flares and other pyrotechnic devices.
- Strontium chloride, $SrCl_2$. It is also used in fireworks to give a red flame.

Authigenic celestite is common as a minor accessory mineral in the Ar Rajmah Formation and is extremely coarsely crystalline and occurs both as a cement and as a replacement of other fracture-filling mineral such as anhydrite. Celestite in the study area is often associated with dolomite and gypsum in the Wadi Al Qattarah Member. Dolomites show very low strontium contents (Ar Rajmah Quarry). Strontium content within Ar Rajmah Formation is due to replacement of calcite by dolomite, inversion of aragonite to calcite and part of the strontium content of the originally aragonitic bioclasts could also have been mobilised during late diagenesis. All these factors should have provided considerable amounts of strontium.

1.5 Objectives of the study:

The study area has not yet been previously subjected to detailed geochemical and mineralogical investigations (especially for industrial minerals). Most previous studies have provided a general description of the lithofacies and some detailed work on the micropalaeontology (Gregory, 1911; Desio, 1935; Burollet, 1960; Pieteisz, 1968; Kleinsmiede and Van Den Berg, 1968; Goudarzi, 1970; Barr and Hammuda, 1971; Rohlich, 1974; Klen, 1974; El Hawat and Shelmani, 1993). For this reason the study was carried out and the main objective is to carry out a reconnaissance study to evaluate the limestone and associated rocks of the Al Jabal Al Akhdar area for industrial applications using different techniques. The main objectives were;

- Laboratory determination of chemical and mineralogical properties of the limestone using different techniques to evaluate its appropriateness for different industrial uses.
- Laboratory determination of mineralogical, chemical and physical properties of clay to assess its suitability in drilling muds for the petroleum industry.
- Geochemical study of the major and trace elements of Eocene, Oligocene and Miocene of Al Jabal Al Akhdar carbonate rocks, in order to differentiate rock types.

- Assistance in the evaluation of industrial mineral resources of the Eocene, Oligocene and Miocene rocks of the Al Jabal Al Akhdar area.
- The possibilities of using the limestones in other branches, especially in the chemical industries.
- Comparison of the results with national and international specifications for each potential end use.

The celestite in the study area has not yet been mentioned in the previous studies. The mineral has been studied to achieve the following objectives;

- To determine the source and the chemical and mineralogical properties of the celestite in the Al Jabal Al Akhdar area.
- To determine the strontium distributions in allochems, matrix and cement in the Al Jabal Al Akhdar Formations.
- To determine the possibility of using the celestite as a weighting agent in drilling muds for the petroleum industry.

Chapter 2

STRUCTURE AND STRATIGRAPHY

2.1 Introduction:

The geology of Libya is dominated by sedimentary rocks, occurring in distinct sedimentary basins. The basins of southern Libya are filled with Palaeozoic and continental Mesozoic strata. In northern Libya the Precambrian and the Palaeozoic strata are covered by marine Mesozoic and Tertiary sediments, which consist principally of carbonates and marl (Klitzsch, 1968). Many general investigations have been carried out on the geology of Libya including the geology of the Cyrenaica region. Most of these studies have concentrated on the surface outcrops of Al Jabal Al Akhdar, providing a general description of the lithofacies and some detailed work on the micropalaeontology. The sedimentary sequence exposed at the surface of Al Jabal Al Akhdar ranges in age from Cenomanian to Quaternary (Kleinsmiede and Van Den Berg, 1968; Klen, 1974; Zert, 1974; Rohlich, 1974; El Hawat and Shelmani, 1993).

2.2 Tectonic setting of Libya:

In Libya, the major diastrophic disturbances include the Caledonian and Hercynian orogenies during Palaeozoic times. These events caused uplifts, subsidence, tilting, faulting and intrusions, but compressional folds are very few. East – west and north – south trending faults are present, but two major fault systems trend parallel to the Red Sea and African rifts. Libya consists of five sedimentary basins, which have formed as a result of several tectonic cycles. These basins are the Sirte, Kufrah, Murzuk, Ghadamas and Marmarica basins (Figure 2.1), separated by intervening uplifts such as the Tripoli – Tibesti Uplift between the Ghadamis and Sirte Basin, the Gargaf Uplift between the Ghadamis and Murzuk Basins and the Tibesti – Sirte Uplift between the Sirte and Kufrah Basins (Figure 2.1). Many authors have discussed the tectonic setting of Libya in general, and the Sirte Basin and Al Jabal Al Akhdar in particular (Conant and Goudarzi, 1967; Klitzsch, 1968, 1971, 1981; Selley; 1968; Sanford, 1970; Klemme, 1971; Hea, 1971; Barr, 1972; Mikbel, 1977, 1979; Rohlich, 1980; Goudarzi, 1980; Kogbe, 1980; Mouzughi and Taleb, 1980; Gumati and Anketell, 1982; Harding, 1983; Van Houten, 1983; Brown *et al.*, 1985; El Arnauti and Shelmani, 1985; Gumati and Kanes, 1985; Almond, 1986; Reyment and Dingle, 1987; Sola and Ozcicek, 1990; El Hawat and Shelmani, 1993).

Klitzsch (1971) pointed out that NW – SE trending horsts and grabens have been formed as a result of the Caledonian orogeny in the Early Palaeozoic and that a major marine transgression in the Silurian and Devonian resulted in the deposition of

a thick sedimentary succession in troughs, and thinner sediments over the horsts (Figure 2.1). In the Late Palaeozoic and Mesozoic prior to the Late Cretaceous, and as a result of the Hercynian orogeny, another series of NE – SW horsts and grabens were developed approximately perpendicular to the Early Palaeozoic tectonic trends (Figure 2.1). The intersects of these fault systems (NW – SE and NE – SW) are near the central part of Libya and caused the largest outpourings of lava in Libya (Klitzsch, 1971; Goudarzi, 1980). Massa and Delort (1984) have pointed out that at the beginning of the Late Cretaceous a major tectonic event occurred which resulted in the collapse of the Sirte Uplift to form the Sirte Basin. Hea (1971) stated that the structure of the Sirte Basin is controlled by four major systems; Rift, Atlan (both with NW and NE alignments), the Merdian system (with N – S alignment) and the Mediterranean system (with E – W alignment). Barr (1972) noted that the Sirte Basin commenced in the Early Cretaceous when the Sirte Uplift was affected by extensive tensional stress, resulting in the development of NW – SE trending horsts and grabens. Selley (1968) has suggested that Sirte Basin was formed by large scale subsidence and block faulting commencing towards the end of the Early Cretaceous, which continued to develop into the Miocene. Van Houten (1983) pointed out that the Sirte Basin developed by fracturing and collapsing of NW – SE trending fault blocks during Late Jurassic – Early Cretaceous time. These movements formed large graben and horst blocks that trend NW – SE. Klemme (1971) pointed out that the fracturing of the Palaeo – Sirte Uplift may have begun in the Jurassic period. Gumati and Kanes (1985) have pointed out that the maximum subsidence of the Sirte Basin occurred during the Palaeocene and Eocene. Brown *et al.*, (1985) and Almond (1986) suggest that the collapse of the Sirte basin was due to the extensive fracturing of the African plate. Conant and Goudarzi (1967) indicated that the Sirte Basin is shallower in the south than in the north.

During Late Cretaceous and Early Tertiary times, there was a major marine transgression in the area, but influenced locally by opening of the Palaeo – Sirte Arch at the beginning of the Late Cretaceous. At the beginning of the Tertiary, extension of the sea continued until the Middle Miocene into the south of the eastern Murzuk Basin in the west and the Kufrah Basin to the east (Klitzsch, 1968; Conant and Goudarzi, 1967; Hancock and Kauffman, 1979). The Tertiary deposits in northeast Libya are generally dominated by deep and shallow marine carbonate sediments, shales and evaporites (Barr and Berggren, 1981).
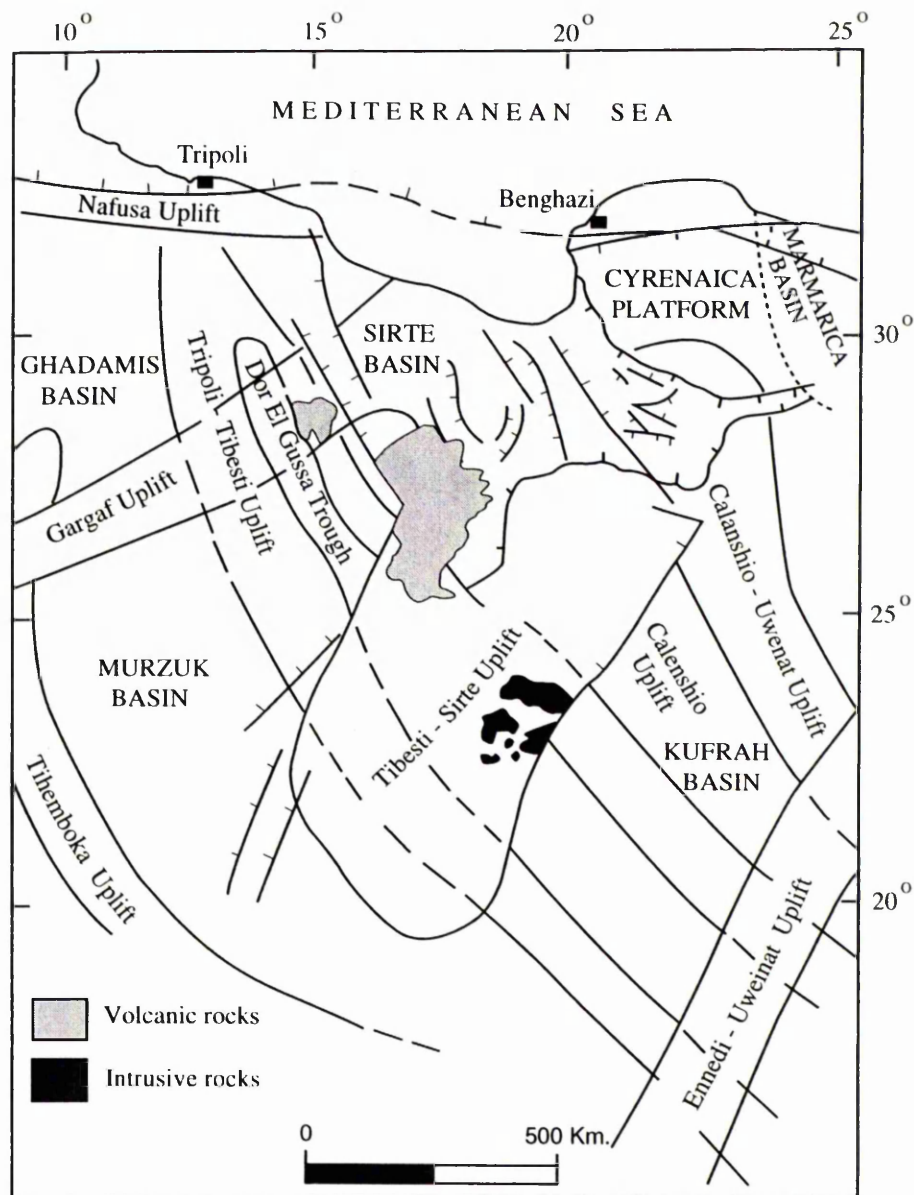
Figure (2.1) Schematic map of the major structural elements in Libya, showing the present day basins and uplifts of the central Sahara, resulting from a combination of the effects of two structural regimes, after Klitzsch (1971).

2.3 Cyrenaica region:

The north Cyrenaica region occupies the northeastern corner of Libya, where Al Jabal Al Akhdar is a part of this region. The region covers an area of around 200,000 square kilometres. It is bounded by the Longitudes 20°E and 25°E and the Latitudes from 29°N to 32°N. The region is surrounded by the Mediterranean Sea to the north, the Egyptian plains to the east, the Kufrah Basin to the south and Sirte Basin to the west and south west (Figure 2.2). The north Cyrenaica region is covered by Upper Cretaceous, Tertiary and Recent sedimentary formations. The Al Jabal Al Akhdar uplift is the major geologic feature of the region. The Upper Cretaceous rocks are exposed at the western margin of the uplift. The rest of the Cyrenaica region has Tertiary and Quaternary deposits at the surface. The tectonic activity in the north Cyrenaica region commenced from Caledonian times and continued to the Middle Tertiary (Rohlich, 1980). At this time the area was subjected to uplift, subsidence, tilting, faulting, folding and erosion. The general structure of the Cyrenaica platform includes the stable Cyrenaica platform in the centre and the relatively unstable Al Jabal Al Akhdar uplift in the north (Sola and Ozcicek, 1990).

2.3.1 Tectonic History of the Al Jabal Al Akhdar: (Rohlich, 1980)

Al Jabal Al Akhdar is described as a part of Cyrenaica. It is the highest geomorphologic feature in the Cyrenaica region, consisting of Upper Cretaceous and Tertiary marine deposits. The oldest cycle of sedimentation is built of Cenomanian – Coniacian deposits, represented by Qasr Al Ahrar and Al Baniyah Formations in the western part of the Jabal Al Akhdar area, which were deposited in a shallow neritic to a bathyal environment. The sedimentation was discontinued by the Santonian folding episode. This tectonic event is recorded in the folded and erosionally truncated beds of Al Bayniyah Formation. The first tectonic phase started in the Santonian time and produced along an ENE – WSW trending anticlinorium with high angle faults striking NE – SW, EW and NW – SE (Figure 2.3 and 2.4). The central part of Al Jabal Al Akhdar was subsequently deeply eroded to some hundreds of metres. In the north (coastal parts) marine sedimentation continued, where a succession of bathyal facies has been recorded (Barr and Hammuda, 1971). The next cycle of sedimentation in Al Jabal Al Akhdar commenced from Campanian to Landenian. The region was affected by transgression and deepening marine waters during the Palaeocene. This

Figure (2.2) Geographic location of Cyrenaica region, after Sola and Ozcicek, 1990.

Upper Escarpment

0   50   100 km
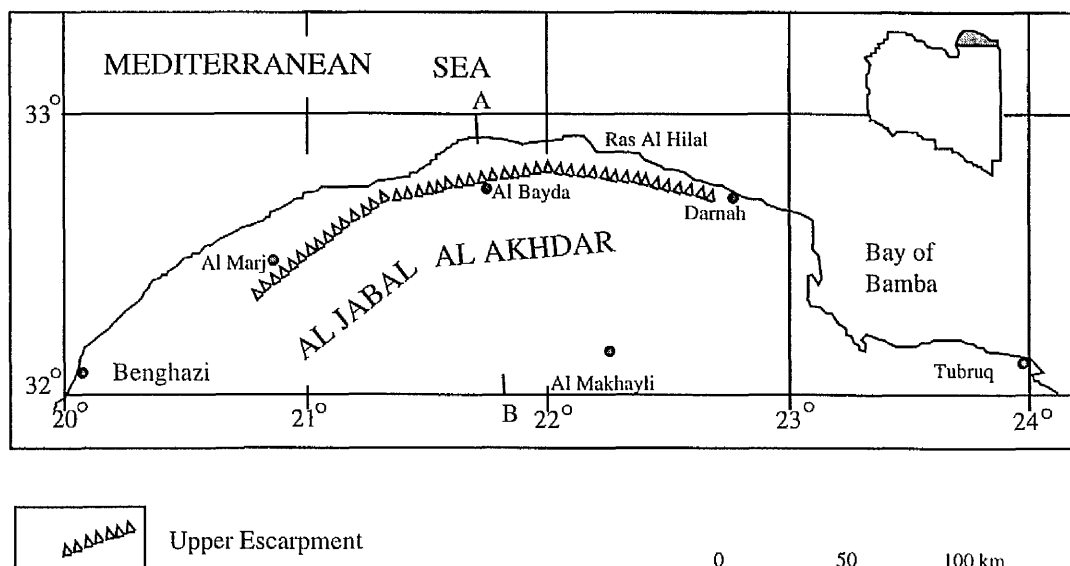
Figure (2.3) Sketch map of Al Jabal Al Akhdar and adjoining regions north of lat 32°. A - B line of the cross section in Figure (2.4), after Rohlich, 1980

N   S

Present Time

S.L

om   om

Early Oligocene

S.L

Landenian / Ypresian

Campanian

S.L

Santonian

S.L

0   10   20   30

om	Oligo - Miocene (Al Faidiyah Formation)
	Lower Oligocene
	Eocene
	Palaeocene

	Upper Senonian
	Cenomanian to Coniacian
	Lower Cretaceous
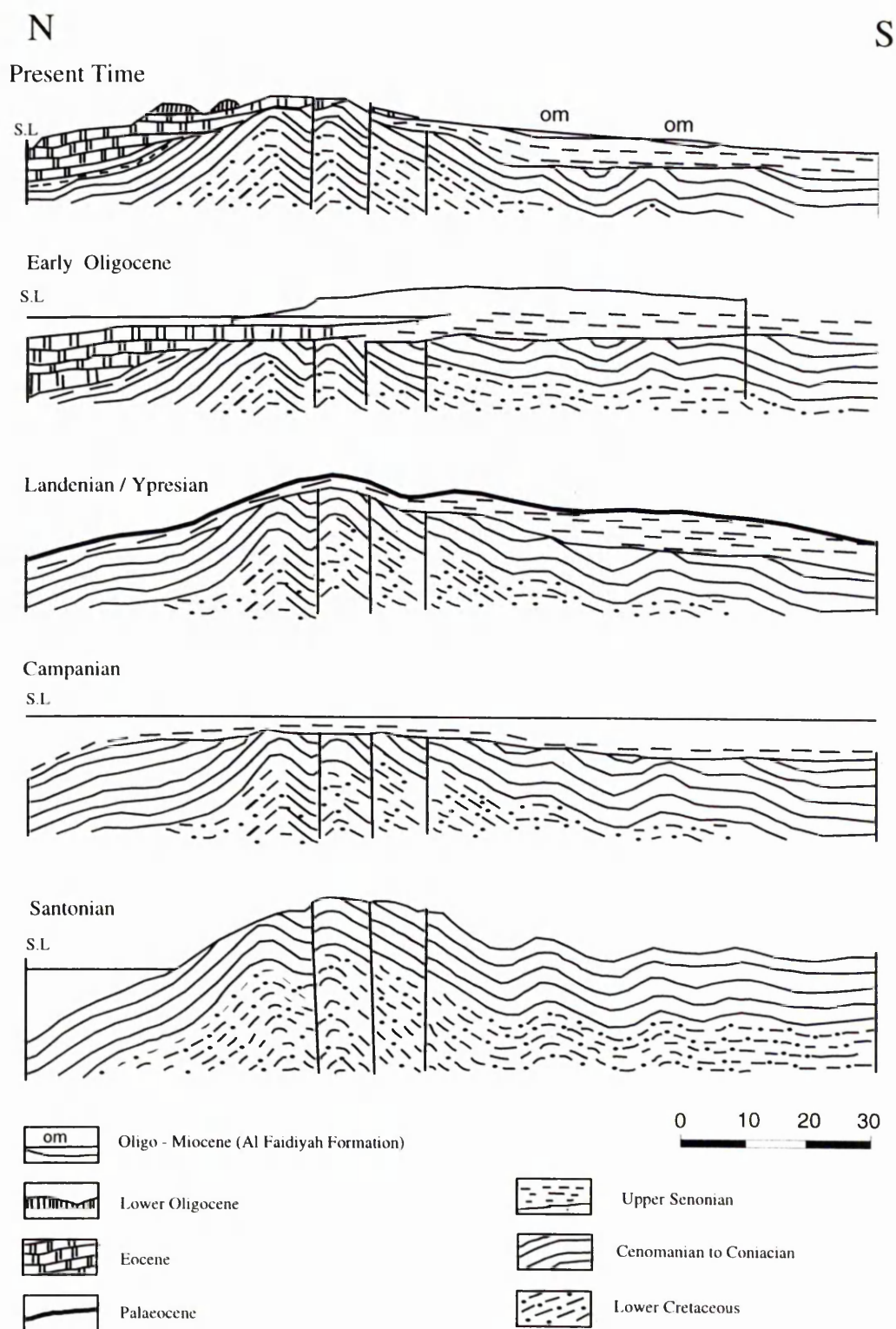
Figure (2.4) Scheme of the tectonic development of Al Jabal al Akhdar in cross sections, after, Rohlich, 1980.

interpretation is based on finely textured, chalky limestones containing planktonic foraminifera. There are two relics of Paleocene strata preserved; east of Al Uwayliah village, with a Landenian microfossil assemblage, and near Jardas Al Jarrari, with Danian assemblages described by Barr (1968b). This cycle of sedimentation ended with an Early Eocene. In the Early Eocene, folding was slight if compared with the Santonian episode, but affected a larger area. The folding and the subsequent erosion produced a regional unconformity separating Cretaceous from Tertiary rocks. The lack of the Paleocene strata is due to this erosion. The third cycle of sedimentation developed from Ypresian to Priabonian. During Late Ypresian and Lutetian times the sea covered the northern periphery of the Early Eocene uplift (nummulitic bank of Darnah and the deep neritic of the Apollonia Formations deposits). The southeast area of Al Jabal Al Akhdar remained dry land (Figure 2.5A). Further diastrophic movements took place at the end of Eocene, with the Early Oligocene marine transgression, which covered a small part of another different area to that of the preceding cycle (Figure 2.5B), allowing the deposition of Shahhat Marl and the overlying algal limestone Members. Further changes in the depositional area occurred after the Early Oligocene sedimentation, which was followed by regression that led to development of an unconformity surface. It was associated with a global-sea level fall at the end of Early Oligocene. The next cycle is represented by Al Abraq Formation (Middle to Upper Oligocene). Distribution of this unit reveals a new palaeotopographic feature, the ridge shown as 'A' in Figure 2.5C. In this ridge, the Al Abraq Formation is missing while both underlying and overlying Oligocene Formations are present, precisely dating the Oligocene diastrophic movement, which produced this ridge. At 'B' in the same Figure, no Oligocene sediments are found, whereas Middle Miocene sediments are preserved and lie between two fundamental faults. Withdrawal of the sea from the Al Jabal Al Akhdar area is dated as Late Oligocene, documented by the disconformable contact between the Al Abraq and Al Faidiyah Formations.
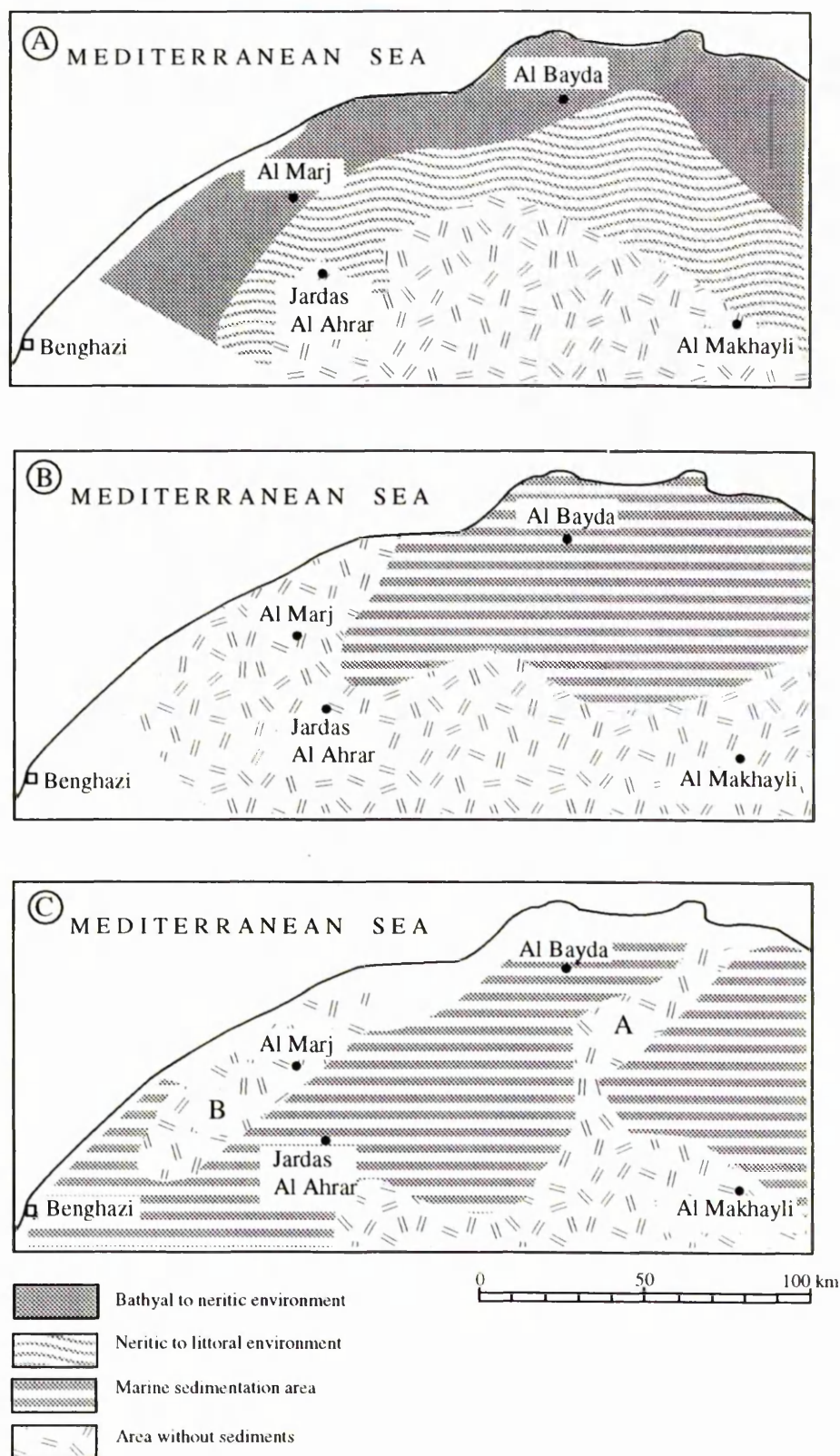
Figure (2.5) A- Eocene palaeogeography, B - Early Oligocene palaeogeography (extent of Al Bayda Formation), C - M. to Late Oligocene palaeogeography (extent of Al Abraq Formation), of Al Jabal Al Akhdar, after Klen (1974) and Rohlich (1974).

55

This contact represents the Oligocene Miocene boundary, and is found to be erosional everywhere in Libya (El Hawat and Shelmani, 1993). The inundation which produced the sediments of the Al Faidiyah Formation lasted from the latest Oligocene to the Early Miocene. The last Tertiary marine transgression in the Middle Miocene covered most of Cyrenaica and the Sirte Basin. It was followed by the deposition of the shallow marine facies of the Ar Rajmah Formation. The lack of Pliocene deposits is evidence that the Late Miocene had been a period of emergence throughout the Mediterranean region (separating the Tethys from the Paratethys). The principal fault directions in the Al Jabal Al Akdar area are NE – SW, E – W and SE – NW.

2.3.2 Stratigraphy of the surface geology of the Al Jabal Al Akhdar:

The sedimentary sequence exposed at the surface of the Al Jabal Al Akhdar ranges in age from Cenomanian to Quaternary (Figures 2.6 and 2.7). All Formations mentioned below are dated by faunal assemblages.

2.3.2.1 Qasr Al Ahrar Formation: (Cenomanian)

This consists of a sequence of green to yellow marl, thinly bedded, with intercalation of marly limestone, with glauconite and pyrite. It is overlain conformably by the Al Baniyah Formation.

2.3.2.2 Al Baniyah Formation: (Cenomanian – Coniacian)

Kleinsmeide and Van Den Berg (1968) described the Benia Limestone Member, introducing the name after the village Al Baniyah in northern Cyrenaica. Klen (1974) and Rohlich (1974) raised its rank to a Formation. It is consists of light coloured microcrystalline well-bedded limestone, marl, dolomitic limestones and grey dolomites. The lower contact with the Qasr Al Ahrar Formation and the upper boundary with Al Majahir Formation are unconformable.

2.3.2.3 Al Hilal Formation: (Albian – Coniacian)

Barr and Hammuda (1971) defined this Formation as the Al Hilal Shale. Marchetti (1934) was the first to assign these beds to the Upper Cretaceous. It is characterised by brownish and greenish thin-bedded shale, with glauconite and pyrite crystals. No lower contact is observed, but the upper part is gradational with the overlying Al Athrun Formation.

Era	Period	Epoch			South & Centre	Coastal & Off Shore
Cenozoic	Tertiary	Neogene	Miocene	Late		Ar Rajmah Fm.
				Middle		
				Early		Al Faidiyah Fm.
		Paleogene	Oligocene	Late		Al Abraq Fm.
				Middle		
				Early		Al Bayda Fm
			Eocene	Late		Darnah Fm. Darnah Fm.
				Middle		Apollonia Fm.
				Early		
			Pal.		Al Uwayliyah Formation	
Mesozoic	Creataceous	Late		Maastrichtian	Wadi Dukhan Fm.	Al Athrun Formation
				Campanian	Al Majahir Formation	
				Santonian-Coniacian		Al Hilal Formation
				Turonian	Al Baniyah Formation	
				Cenomanian	Qasr Al Ahrar Formation	

Figure (2.6) Surface and stratigraphic chart of Al Jabal Al Akhdar, N.E. Libya (Modified from El Hawat and Shelmani, 1993).
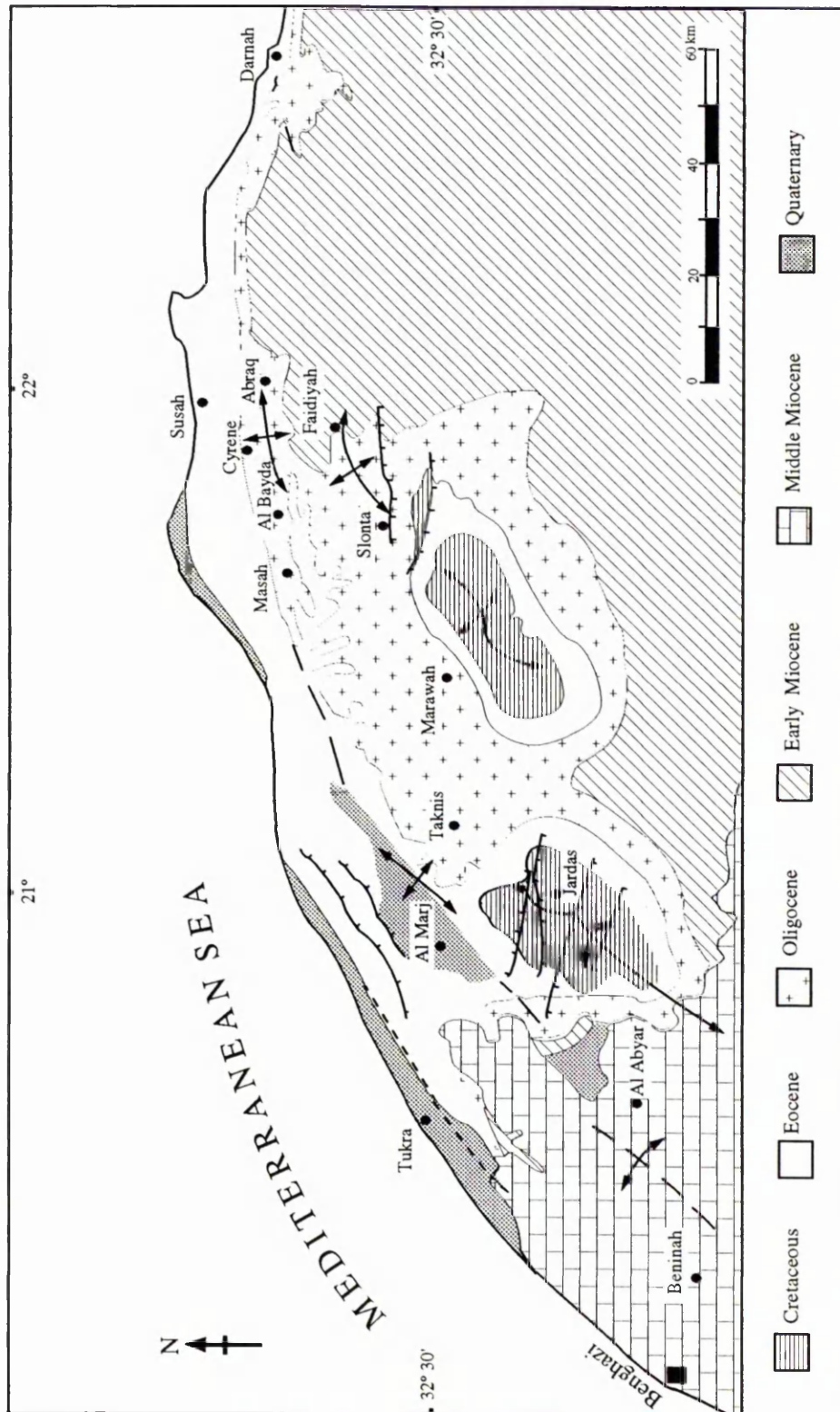
Figure (2.7) Geological map of Al Jabal Al Akhdar, after El Hawat and Shelmani,1993.

2.3.2.4 Al Majahir Formation: (Campanian)

Rohlich (1974) introduced the name after the former Majahir fortresses (Qasr Al Majahir). It is consists of cream coloured, medium bedded limestone, with dolomitic limestone and marl at the base. The upper part is conformable with the overlying Wadi Dukhan Formation.

2.3.2.5 Wadi Dukhan Formation: (Maastrichtian)

Kleinsmeide and Van Den Berg (1968) and Pietersz (1968) introduced the name Wadi Ducchan Formation. It consists of hard, grey to brown microcrystalline dolomites and dolomitic limestone. The upper part is conformable with the overlying Paleocene Al Uwayliyah Formation. The Al Majahir and Wadi Dukhan Formation are partly equivalent to the Al Athrun Formation of the coastal region.

2.3.2.6 Al Athrun Formation: (Coniacian – Maastrichtian)

This consists of white, microcrystalline to fine grained, thin-bedded limestone, with thin bands and lenses of greyish brown chert, and thin marly intercalations. The lower boundary is conformable with the Al Hilal Formation, whereas the upper boundary is unconformable with the overlying Eocene Apollonia Formation (Plate 2.1).

Paleocene:

Paleocene outcrops are relatively rare in Al Jabal Al Akhdar due to intensive tectonic activity and subsequent erosion (El Hawat and Shelmani, 1993).

2.3.2.7 Al Uwayliah Formation: (Paleocene)

Barr (1968b) introduced the name of the Al Uwayliah Formation after the village Al Uwayliah in northern Cyrenaica. It consists of white chalky limestone with green marl. The Al Uwayliah Formation has yielded Upper Paleocene foraminiferal assemblages of a deep marine environment. The lower boundary is conformable with the Upper Cretaceous dolomite of the Wadi Dukhan Formation and the Formation is unconformably overlain by Eocene rocks of the Apollonia and Darnah Formation.

Plate (2.1) The contact between the Al Athrun Formation (Ath.) (U. Cretaceous), and Apollonia Formation (Ap.) (Lower to Middle Eocene).

2.3.2.8 Apollonia Formation: (Lower to Middle Eocene)

Gregory (1911) first introduced the name Apollonia Limestone after the ancient Greek settlement Apollonia (now called Susah) located at the coastal region in the northern Cyrenaica. Pietersz (1968) introduced the name Apollonia Formation. It is represented by light coloured massive fine grained, siliceous limestone with chert nodules. In places the limestone is chalky and rarely marly. A characteristic feature of the limestone is the bituminous smell. The lower boundary is unconformable with the Upper Cretaceous Al Athrun Formation, whereas the upper boundary is gradational and shows an interfingering relation with the overlying Darnah Formation.

2.3.2.9 Darnah Formation: (Middle and Upper Eocene)

Gregory (1911) introduced the term Derna Limestone after the coastal town of Darnah in northern Cyrenaica. Burollet (1960) and Goudarzi (1970) named it as the Derna Formation, but Barr and Weegar (1972) retained the original term of Derna Limestone. It consists of hard, massive, medium to coarse grained nummulitic limestone, with intercalations of dolomitic limestone. The Formation is rich in fossils. The most abundant are large benthonic foraminifera, especially *Nummulites*, which sometimes form a dominant constituent of the rocks. The upper contact is unconformable with the Oligocene of the Al Bayda Formation.

2.3.2.10 Al Bayda Formation: (Lower Oligocene)

Rohlich (1974) introduced the name after the town of Al Bayda in northern Cyrenaica. It comprises two members; the lower, Shahhat Marl Member and an upper Algal Limestone Member. Kleinsmeide and Van Den Berg (1968) introduced the term lower Member, Shahhat, after the new name of the old city of Cyrene (Shahhat town). The Shahhat Marl Member consists of grey to yellowish, soft, glauconitic, fossiliferous marl and marly limestone. The Algal Limestone Member consists of thick bedded, white, fossiliferous, medium grained to microcrystalline algal calcarenite. In places slight dolomitization is observed. The upper boundary is unconformable with the overlying Al Abraq Formation.

2.3.2.11 Al Abraq Formation: (Middle to Upper Oligocene)

Rolich (1974) introduced the term after the village of Al Abraq (or Labrak) on the Al Bayda - Darnah highway in northern Cyrenaica. It consists of cream yellowish grey, medium grained fossiliferous limestones (partly calcarenite to calcilutite) with dolomitic limestone, dolomite and marl. The Formation is separated from the overlying Al Faidiyah Formation by a prominent clayey layer.

2.3.2.12 Al Faidiyah Formation: (Upper Oligocene – Lower Miocene)

Pietersz (1968) introduced the name Faidia Formation, derived from the village of Qaryat (in Arabic this means village) Al Faidiyah. It comprises two Members: the lower, Faidia Clay Member and an upper Faidia Limestone Member. The Faidia Clay Member consists of a soft, greenish grey calcareous clay with glauconite grains, followed by the upper Member of Faidia Limestone which is whitish, fossiliferous limestone.

2.3.2.13 Ar Rajmah Formation: (Middle Miocene)

Desio (1935) introduced the name Regima Limestone after the village of Rejma (present transcript Ar Rajmah). The Ar Rajmah Formation represents the last cycle of sedimentation during the Middle Miocene in the western part of Al Jabal Al Akhdar area. The Ar Rajmah Formation is divided into two Members; the lower, Benghazi Member and the upper Wadi Al Qattarah Member. The name of the Benghazi Member is taken from Gregory's (1911) Benghazi Limestone. It consists of massive, white sandy fossiliferous limestone, dolomitic in places, with occasional dark grey marl and calcareous clay. The upper part of the Ar Rajmah Formation is represented by the Wadi Al Qattarah Member, which is the end of Middle Miocene sedimentation in the western part of Al Jabal Al Akhdar. It is consists of white, soft to medium hard, porous, oolitic limestone with gypsum crystals.

Chapter 3

METHODOLOGY

3.1 Introduction:

Strategic evaluations of limestone and clay resources need to involve far more than a basic geological appraisal and should include laboratory determinations of chemical and mineralogical properties of these two raw materials. A variety of techniques were used in this study including X-ray fluorescence (XRF), scanning electron microscopy (SEM), electron probe microanalysis (EPMA; EDS and WDS), X-ray diffraction (XRD), cathodoluminescence (CL) and thin section description. Specific tests for industrial clays were also carried out (swelling test, cation exchange capacity (CEC), surface area test, and differential scanning calorimetry (DSC)) for the Faidia Clay Member of Al Faidiyah Formation (see chapter 7). All these were carried out at the University of Manchester laboratories.

3.2 Field procedures:

Seven quarries and three outcrops were selected from different localities in NE Libya of Al Jabal Al Akhdar area. These locations represent ages ranging from Eocene, Oligocene and Miocene time. The quarries are: Bachor, Qasar Libya (Eocene sediments) and Umm Ar Razam, Al Fatayah, Benghazi, Ar Rajmah and Wadi Al Faj (Oligocene and Miocene sediments). The three outcrops studied include: Bachor road-cut (Eocene sediments), Shahhat Susah road-cut (Eocene and Oligocene sediments) and Deryanah Al Abyar road-cut (Oligocene and Miocene sediments). In addition, samples and data have been collected which are related to this research from some national factories, where the limestone and clay materials are one of the main components. These industries are: glass (Al Aziziyah in Tripoli), PVC (in Benghazi), cement (in Benghazi and Al Fatayah), textiles (in Benghazi) animal food plant (in Benghazi) and bentonite and limestone for drilling fluid (in Jowfe Oil Co., Benghazi). Also two international cement industries have been seen in Derbyshire, UK. Samples were collected according to facies change, based on significant vertical and horizontal changes of colour, textures, and sedimentary and organic structures. The specific features of interest have been photographed. The samples collected from the study area have been described using a hand lens for identification of the rock components. Unweathered samples were chosen for both rock types (limestone and clay) wherever possible. Fieldwork was undertaken over 4 weeks in March to May, which is the most suitable time, because before there is heavy rain and after it is too hot (Mediterranean climate).

3.3 Petrographic techniques:

3.3.1 Hand specimen binocular microscope:

Hand specimens were examined optically and described using the binocular microscope. The features described include colour, grain-size, fossil identification and sedimentary and organic structures.

3.3.2 Polarising microscope:

Work involved examination of 93 polished thin sections in polarised light on the petrographic microscope. The examination of thin sections with a petrographical microscope (transmitted and reflected light) gives information on fabrics, textures and mineralogy. Petrographic observations useful in limestone and clay assessments include;

- General lithology

- Sedimentary and organic structures

- Palaeontology identification of grain types

- Colour variations

- Textures, size and shape sorting of the grains

- Carbonate and non-carbonate mineralogies

- Type of cements

The thin sections were impregnated with blue dye stained resin to colour and fill the pore space as an aid to calculation of porosity from the whole rock volume. Point counting techniques have been applied to all polished thin sections, in order to observe rock fabric, constituent grains, matrix, cement and porosity (amount and type), which were determined from a 300 grains count for each slide.

3.3.3 Cathodoluminescence (CL):

Cold CITL cathode luminescence 8200 *mk3*, Olympus BH2 microscope and Olympus camera PM20 were used. CL has been done for the Benghazi Member of the Ar Rajmah Formation (dolomite minerals), at Ar Rajmah Quarry and gives bright and stable luminescence (orange). Mn/Fe ratio is the main controlling factor influencing CL intensity in calcite and dolomite minerals (Reed, 1996).

3.4 Scanning electron microscopy:

The Scanning electron microscope SEM is primarily used to study the surface or near surface structure of bulk specimens. It is closely related to electron probe microanalysis (EPMA) but is designed primarily for imaging rather than analysis. The instrument used was a Jeol scanning microscope (JSM-6400). Images are produced by scanning the beam in a television-like raster and displaying the signal from an electron detector on the screen. The most commonly used types of image are secondary electron (SE) images, which show topographic features, and backscattered electron (BSE) images, which are used to reveal compositional variation (showing differences in mean atomic number). In BSE images, every mineral composition has its own intensity, e.g. calcite mostly appears as light grey if compared with dolomite (darker grey), in contrast with celestite, which displays a bright white as in the Benghazi Member of the Ar Rajmah Formation (i.e. generally different compositions usually have different brightness values). The brightness of each mineral depends on the mean atomic number of the mineral. The mean atomic number of calcite is higher than that of dolomite. Therefore it will reflect electrons more efficiently and give a paler image compared with dolomite. Celestite has a high mean atomic number and will reflect electrons very efficiently to produce an intense white image. The SEM is ideally suited to the study of fossil morphology and the morphology of individual sediment grains and intergrowths can be viewed in three dimensions (Heinrich, 1981; Grahame, 1987; Reed, 1996). The SEM is very effective for studying crystal morphology on a microscale and can also be extremely useful as an auxiliary tool for checking the size of objects such as the crystal size of clay separations intended for XRD work. In the study area the SEM was a useful additional tool and together with the other techniques provided excellent images of the carbonate rock limestone (e.g. celestite mineral and dolomitic limestone rock in the Benghazi Member) and the clay minerals in Faidia Clay Member of the Al Faidiyah Formation. Utilisation of the SEM for the study of the limestone has been done to trace the evolution of cements (it gives much more detail than thin sections), textures and pore geometry of dolomitised sediments in the Benghazi Member of the Ar Rajmah Formation.

3.4.1   Coating:

Most geological samples, being non-conductors of electricity, require a conductive coating. The preferred coating element for X-ray analysis is carbon,

because it has a minimal effect on the X-ray spectrum. It is also the best choice for CL studies. However, it is not ideal for SEM imaging, owing to its low secondary electron yield. For this purpose a metal with a higher SE yield is preferable, e.g. gold or gold palladium alloy. This type of coating is, however, less suitable for X-ray analysis or BSE imaging.

3.4.1.1 Rough samples:

Prior to mounting the sample the stubs to be used must be labelled and this is simply done by engraving a sample number on the underside of the stub. The specimen after that should be fixed onto the stub, which takes the form of a disc, usually made of aluminium and typically about 1 cm in diameter. The sample is glued to the stub. The glue used to stick the sample on the stub should be stable under high temperature and vacuum conditions (e.g. silicone rubber glue 'Loctite'). After the glue is fully dried the sample must be coated with gold using an International Scientific Instruments PS-2 Coating Unit, and becomes ready for SEM investigation. Careful consideration must be given to the thickness of the coating used, because it is useful for obtaining good resolution pictures. Thick coatings are more efficient conductors, but if the layer becomes too thick, it may obscure very fine surface detail and can interfere with microanalysis. Generally, it is better to apply a thin coating first and after that to examine the specimen in the SEM. Repeat the coating if necessary. Some of carbonate rocks in the study area required longer coating than other limestone rocks and clay samples, because specimens were porous. Rough samples were observed under the following operating conditions; working distance (WD) 39-25 mm, accelerating voltage 15 kV and probe current 1.50 nA.

3.4.1.2 Polished thin section carbon coating:

Thin sections were coated with a thin film of carbon using an Edwards 604 Carbon Evaporation Unit. The specimen was placed in a vacuum chamber with a carbon evaporation source consisting of pointed carbon rods (3 – 6 mm diameter) in contact under light pressure. A current of around 100 A is passed through the rods for a few seconds, causing carbon to be evaporated from the hottest region where the rods are in contact. The evaporated carbon atoms travel in straight lines. This coating method is suitable only for flat specimens and not irregularly shaped objects. Better coverage can be obtained by rotating the sample during coating. Thin sections coated

with carbon were used in BSE-SEM to examine the various cements and mineral compositions, which were impossible to identify using routine petrographic microscopy (Reed, 1996). In BSE-SEM, coated thin sections were used, with standard instrument parameters as follows: working distance 39-15 mm (where WD of 39 mm was used for quantitative analysis and WD of 15 mm was used for photography) accelerating voltage 15 kV, probe current 1.50 to 1.52 nA and a livetime of 45 seconds.

3.5 Electron probe microanalysis (EPMA):

When a finely focused beam of electrons hits the surface of a solid material it gives rise to a characteristics X-ray spectrum. From the wavelength (or energy) and intensity of the peaks in the spectrum the elements present may be identified and their concentrations measured by comparison with the intensity from materials of known concentration. The spatial resolution of the chemical analysis is of the order of a few cubic microns and elements from Beryllium to Uranium can be detected. Two methods of detecting the characteristic X-rays are commonly employed: the wavelength dispersive spectrometer (WDS) and the energy dispersive spectrometer (EDS) (Table 3.1).

Table (3.1) Summary of the differences between EDS and WDS X-ray detection systems;

EDS	WDS
Solid state device, no moving parts.	Mechanical device.
Acquires and displays entire X-ray spectrum simultaneously. Rapid assimilation of mineral type from the spectrum display.	Each spectrometer measures only one X-ray peak with up to five spectrometers working simultaneously.
Detects major and minor elements only.	Detects major, minor and trace elements.
Detection limit about 0.1 wt. %.	Detection limit about 0.01 wt. %.
Has poor peak to background ratio.	10 times better background ratio than EDS.
Poor peak resolving power, spectrum overlap problems e.g. Ba $L\alpha$ /Ti $K\alpha$ peaks overlap	Good peak resolving power, 10 times better than EDS. Good for trace element analysis and analysis of sulphide.

Areas for analysis are located under the electron beam by observing the specimen using a light-optical microscope. Specimens are usually in the form of polished thin sections. For this study, a Cameca Camebax microprobe (WDS and EDS) was used, where WDS was used to determined the chemical composition of celestite from the Benghazi Member of the Ar Rajmah Formation. EDS is used to analyse the chemical compositions of the clay of the Al Faidiyah Formation and the dolomitic limestone of the Benghazi Member. The thin sections used have a polished surface with carbon coating. Painting colloidal silver (silverdag) ensured a good electrical contact between surface and the stage (Long, 1977; Reed, 1996).

Electron probe micro-analyser (Cameca SX100):

Major EPMA features includes the following;

- Elements from Beryllium to Uranium, nearly the entire periodic table of elements, can be detected and quantified in a small sample volume.

- It is a non-destructive method. Generally there are no worries about the material analysed being eroded or changing during analysis

- Rapid survey techniques can provide information an bulk composition as well as micro-distribution of elemental concentrations.

- It is the most precise and accurate micro-analytical technique available.

- It has high sensitivity, stability and lack of peak overlaps compared to SEM/EDS and provides high quality SEM and BSE images. Detection limits for some elements under favourable operating conditions can be as low as 10 ppm.

These results are obtained by the detection and determination of secondary electron, backscattered electron, and X-ray emission excited by primary high energy electrons striking the specimen surface at the desired points. Major applications are found in geochemistry, mineralogy, physical metallurgy, nuclear metallurgy, material sciences including glasses, ceramics, cements, microelectronics, surface chemistry, and biochemistry of hard tissue. Anything hard which can be produced with a reasonably flat surface can be analysed in the electron probe micro-analyser. This powerful analytical tool was used to determine the Sr-content in fossils, cement, and matrix in the Apollonia, Darnah and Ar Rajmah Formations. X-ray element distribution mapping for Ca, Mg and Sr in coralline algae (Sample no. LB1) was performed using Cameca SX100 electron probe micro-analyser. Three wavelength dispersive spectrometers were used, each assigned to a single elemental peak position. A square

area of the specimen (500 microns by 500 microns) was scanned by stage motion under a static, focused beam. The fluctuation in X-ray intensity from each of the spectrometers was used to produce a two-dimensional map showing variation in elemental composition.

3.6 X-ray fluorescence (XRF):

A primary X-ray beam generated by an X-ray tube irradiates a sample of the material being analysed causing it to emit secondary (fluorescent) X-radiation. This contains wavelengths which are characteristic of each element in the sample. The procedures for sample preparation vary according to rock or sample type and the result being sought. The aim is to produce a homogeneous fine powder for analysis. All weathered material must be removed first using either a diamond saw or jaw splitter to produce a clean, fresh sample of rock. XRF analysis was used to determine the bulk chemical composition for the carbonate rocks and the clay materials of the study area. Sixty-nine samples were crushed and then powdered using a Tema grinding machine. Powdered samples must be finely ground (<50 μm) or 'flour-like'. The mass of powder was pressed and made into pellets with a boric acid back and edge designed to fit into Phillips sample holders. Care should be taken to avoid breathing the very fine dust and dust masks should be worn. The mass of powder used was about 2.0 g. There is no point in producing pellets containing much more than 2.0 g of sample since fluorescent radiation from the back of a very thick sample can not reach the primary collimator owing to mechanical apertures in the spectrograph. The amount of boric acid is not critical. The pressure required to form a coherent sample varies with the nature of the sample and corresponds to a required load of about 5 to 6 tonnes. A PW1450 (Phillips) wavelength dispersive spectrometer fitted with computer control and data processing was used for major and trace element analyses. The results are summarised in Appendix A5 (Tables 1 to 9) and described in Chapter 5.

3.7 X-ray diffraction (XRD):

X-ray diffraction is a basic tool in mineralogical analysis of sediments. It is widely used for mineral identification, particularly for minerals of very small size. XRD studies can provide information on the degree of order in dolomites as explained in Chapter 5. The carbonate sediments (limestone and dolomite) and clay samples of

the study area have been analysed using a Phillip X-ray diffractometer system, consisting of a PW 1730 X-ray generator and running PAXRD software (XRD). XRD patterns were recorded 65 to 5° 2θ (for carbonate sediments of the Ar Rajmah Formation) and 65 to 2° 2θ (for clay samples of the Faidia Clay Member). JCPDS powder diffraction cards were used to identify the minerals present in each samples and the using of the computer software was very helpful for XRD pattern interpretations.

3.7.1 Preparation of samples for XRD:

Carbonate rocks for powder diffraction studies were crushed homogenously and finely ground. Coarse particles in the sample will substantially reduce peak-to-background ratios and will produce diffraction patterns with abnormal peak intensity ratios. The fine powder of carbonate sediments was prepared for analysis using oriented mounts as a thin smear (by mixing the sample with a small volume of amyl acetate) on a glass slide. For clay mineral studies, the clays must be treated by different methods prior to X-ray examinations as described below.

3.7.1.1 Clay mineral separation:

About 250 grams of the clay were poured into plastic containers. Deionised water was added. An indelible marker was used to label the plastic containers, including your name, sample number and the size fraction. The mixtures were left in a mechanical agitator for about 12 hours (depending on the rock or sample type), running at very low speed to avoid any damage to the clay crystals and to suspend all size fractions. The large particles settled out, and the resulting suspension was decanted into clean tubes to a height of 30 cm. The tubes were supported in a water bath and all tubes labelled again. Half of the clay suspension of each sample was transferred to another settling tube, and both tubes made up to 30 cm with deionised water. They were left in the water bath for a specified time, for sedimentation from the top surface of the water column for a specified particle size. The tubes were covered in cling-film to avoid contamination. Less than 2 μm - > 0.5 μm and < 0.5 μm fractions were used, and Stoke's Law was applied for clay size separation. When size fractions have already been separated, the sample was transferred to the appropriate, clean centrifuge vessels. For the low speed centrifuge (should not be run

above 3000 rpm) plastic buckets were loaded and placed within the steel centrifuge buckets (each vessel holds about 200 to 250 ml.). For the high speed centrifuge (not above 10000 rpm) plastic test tubes were placed into the rotor (these vessels hold about 50 ml. each). Sample was added/removed by pipette until the vessels equalled each other in weight, to prevent the centrifuge from becoming imbalanced during operation. The timer was rotated to the desired time (about 10 to 15 minutes). The centrifuge was used to separate known size fraction particles from the remaining water. If the liquid did not clear after an hour of centrifuging time on the low speed centrifuge, the sample was transferred to the high speed centrifuge. When all samples had been centrifuged, the residue solid in the bottom of the vessel was removed using a rotamixer, adding small volumes of deionised water. Drying of the samples took place using the freeze dryer technique. The clay samples after that become ready for mounting on the glass slide for XRD.

3.7.1.2 Oriented mount slide preparation: (Untreated air dried)

A diffractometer pattern from a strongly oriented clay specimen may show only the 001 series of basal reflections with little or no evidence of *hkl* reflection (Brown and Brindley, 1980). About 0.1 g of each sample was mixed into a paste with amyl acetate and then spread out in a strip about 8 mm wide down the side of a 1 x 1.5 in. glass slide using the corner of a stainless steel spatula. The amyl acetate was left to dry at room temperature for several hours until completely dried (Lewis and McConchie, 1994).

3.7.1.3 Ethylene glycol solvation:

Most clay mineral samples should be analysed in an air – dried condition, an ethylene glycol-solvated condition and after enough heating to collapse any expandable layers. This treatment is used extensively to identify clay minerals. All samples were glycolated using ethylene glycol by exposing the air dried samples to the vapour of the reagent for at least 8 hours at 60 °C (Moore and Reynolds, 1997). The air dried samples were placed in a large desiccator dish with lid which contained 100 to 200 ml. of ethylene glycol. The samples were put on a platform with their faces up to avoid direct contact with the solvent. The dish was placed in an electrical oven at 60 °C. Samples were labelled with a diamond marker, because ethylene glycol may

remove identification marks that have been made with marker pens. The samples are left overnight. After that the samples were analysed directly by XRD.

3.7.1.4 Heating to 350 °C and 550 °C:

The samples were heated to identify some clay mineral types which respond to high temperature. After heating some clay mineral peaks collapse (e.g. kaolinite at 550 °C), whereas the others are unaffected. After heating at temperatures of 350 °C, kaolinite reflection as not very great and peaks remained in the same position. In the case of heating up to temperatures of 550 °C kaolinite reflections are completely destroyed or disappeared. The glycolated samples are placed in a high temperature electrical furnace and left for one hour. The samples were taken out and immediately analysed by XRD to avoid rehydration.

3.8 Nuclear magnetic resonance (NMR) spectroscopy:

NMR spectroscopy is based on the interaction between atomic nuclei and a magnetic field. All atomic nuclei have a positive charge due to the proton they contain. When the sample nuclei is placed between the poles of a strong magnet, the nuclei adopt specific orientations aligning either parallel to (with low-energy state) or against (antiparallel high-energy state) the magnetic field. The sample is held in a strong magnetic field and is irradiated with a pulse of radio-frequency (RF) radiation that contains the range (1-500 MH$_z$) needed for the width of the spectrum to be recorded. The energy needed to flip a given nucleus (^{1}H, ^{13}C) is influenced by its chemical environment (various forms of hydrogen present in the molecule). This effect is called the chemical shift. In addition, peaks from one nucleus are frequently split into characteristic patterns by intramolecular interaction with neighbouring magnetic nuclei. This effect is known as spin-spin coupling. The chemical shifts and the spin-spin couplings lead to the characteristic patterns of resonance, which make up an NMR spectrum. However, the important feature is that the intensity of a particular NMR signal is proportional only to the number of nuclei in that chemical environment, and this makes NMR an absolute quantitative technique (McMurry, 1998; Young and Lovell, 1991; Robinson, 1982). This technique is used to identify the brucite mineral in the coralline algae of the Ar Rajmah Formation. The experiment

has been done in the Chemistry Department, the University of Manchester by Dr. Frank Heatley.

3.9 Infrared (IR) spectroscopy:

The IR region of the electromagnetic spectrum contains radiation lying between the visible and microwave regions. The range of the absorption mostly occurs in the region 4000 – 650 cm^{-1}. The atoms in a molecule vibrate and so absorb energy. Because the vibrational energy is quantized, this means that a molecule will absorb only photons of certain specific energies, all other energies being transmitted with no charge in the molecule. This absorption of energy can be monitored to form a spectrum. The spectra obtained from IR spectroscopy occur in the form of bands rather than single transition, since a vibrational energy change in a molecule is accompanied by a number of rotational energy changes. Since atoms are linked to each other by chemical bonds, molecules consisting of three or more atoms have vibrational modes of two types: stretching and bending (McMurry, 1998). A TI Mattson Genesis series Fourier Transform Infrared (FTIR) spectrometer was used. The Genesis instrument is fully computer controlled with simple interactive software, and has a wavelength range of 7500 – 300 cm^{-1} and the highest resolution of 1 cm^{-1}. IR spectroscopy is used to identify the brucite mineral in the coralline algae of the limestone rocks of the Ar Rajmah Formation (Middle Miocene). The potassium bromide (KBr) technique was used, in which the KBr was ground as fine as flour before adding 1-2 mg (using a small spatula) of the sample and regrinding to mix thoroughly. The powder was transferred using a small piece of paper into the press stainless steel. The pressed pellet was placed in the sample holder, the IR beam passes through the disk and both the compound and KBr absorb some energy to give a spectrum. The experiment has been done with help and assistance from Sarah Blake, Chemistry Department, the University of Manchester.

3.10 Inductively coupled plasma-atomic emission spectrometry (ICP-AES):

ICP-AES is now established as one of the most widely used techniques of elemental analysis. All ICP-AES was conducted using V.G. Elemental (Model-Horizon). There are three essential components in an ICP-AES instrument: the source unit (the ICP torch); the spectrometer; and the computer. The source unit provides the

energy to generate the emission spectral lines. The spectrometer separates and resolves these lines and measures their signal strength. The computer enables the analyst to convert the signal into a numerical measurement of the concentration of the analyte elements. There is a wide diversity of instrument designs and configurations, but all use the same basic principles. It is easy to use and straightforward to install and set up routine elemental analysis (Walsh, 1997). ICP-AES has been used to analyse the range of elements in solution of celestite and gypsum minerals of the Ar Rajmah Formation.

3.11 Differential scanning calorimetry - thermogravimetric (DSC - TGA):

Differential scanning calorimetry (DSC) measures the temperature and the heat flow associated with phase transitions in materials as a function of time and temperature. Such measurements provide quantitative and qualitative information about physical or chemical changes that involve endothermic (heat absorption) or exothermic (heat evolution) process, or changes in heat capacity. DSC is used primarily to characterise polymers and other organic materials, but is applicable also to metals, ceramics and other inorganic materials (Lee, 1995). TGA is used to detect changes in weight with changes of temperature. Samples of the Faidia Clay Member and other clay standards as well as calcite, gypsum and celestite of the Ar Rajmah Formation, with some other standards such as strontianite and brucite minerals, were studied on a STA 1500 H machine and software version 5.40 for the DSC technique. The samples were heated continuously at a regular rate from 25 °C to 1200 °C at 10 °C/ min. (see chapter 7 and 9).

3.12 Spectrofluorimetry:

The term ''fluorimeter'' describes the instrument used to make sure if the celestite of the Ar Rajmah Formation has fluorescence spectra as well as the oil or not. The amounts of the celestite and the solvents used (HCl and water for celestite and chloroform for crude oil from Texas), have been described in chapter 10. A beam of light excites the specimen (celestite in suspension or crude oil in solution) in the cell and emission is observed and analysed at right angles to the incident beam. The output is the emission spectrum plotted by the recorder (Barltrop and Coyle, 1978). If emission of radiation appears to cease immediately after exciting radiation was shut

off, then the phenomenon is called fluorescence and if the emission of radiation continues after the exciting radiation was shut off, the emitting species then is called phosphorescent (Wayne, 1988). Fluorescence is emission of light with no change in the electronic spin state of the molecule. In phosphorescence, the electronic spin does change during emission, so molecules spend more time in an excited state prior to phosphorescence than fluorescence. Phosphorescence also occurs at lower energy (longer wavelength) than fluorescence. Phosphorescence is distinguished from fluorescence by the long-lived emission after extinction of the excitation source. Generally, fluorescence occurs within 10^{-9} to 10^{-7} seconds of excitation, while phosphorescence has a longer lifetime varying from 10^{-6} to 10^{-2} seconds depending upon the structure of the molecule (Harris, 1998). The type of light source required in luminescence primarily depends on whether excitation or emission spectra are being measured. The source of light used in this experiment was a xenon lamp (Lumb, 1978).

Immediately after the instrument is switched on, the monochromators will start to return to the approximate positions that they were in before the instrument was switched off. This resetting process may take up to one minute.

- Select the fluorescence mode, and if the fluorescence characteristic of the sample is known, select the appropriate excitation wavelength. For unknown samples use the pre-scan facility as follow;
- Select both monochromators by pressing the 'EX/EM' key.
- Press 'Low λ' and 'High λ' simultaneously to reset the limits to their default values, press 'Pre-Scan' key. The previously described separate sequence of excitation and emission Pre-Scan are combined without operator intervention with the emission monochromator driving to zero order in the first instance.

For scanning (single monochromator);

- Enter 'Low λ' and 'High λ' limit value for the scanning monochromator.
- Enter the appropriate fixed scale factor.
- Press 'Start/Stop' key to scan through the required spectral region.

This experiment has been done with great help from Dr. I. Watt and W. Richard, Chemistry Department, The University of Manchester.

Chapter 4

PETROGRAPHY

4.1 Introduction:

The Al Jabal Al Akhdar area contains Eocene (Darnah and Apollonia Formations), Oligocene (Al Bayda and Al Abraq Formations), and Miocene (Al Faidiyah and Ar Rajmah Formations) strata. These formations consist mainly of limestones, dolomites, marls, and marly limestones. Thin sections were examined petrographically using a microscope fitted with point counter (300 grains counted from each slide), in order to observe rock fabric, and determine the presence and abundance of constituent grains, matrix, and cement. The thin sections were impregnated with blue dye stained resin to distinguish and determine the porosity types from the whole rock volume. The localities of the samples are shown in Figure (4.1) and lithological symbols used in all columnar sections are shown in Figure (4.2). The description of these thin sections petrographically was based on Scholle (1978), Fuchtbauer *et al.* (1980), Flugel (1982), Adams *et al.* (1984), Moore (1989), Tucker *et al.* (1990), Tucker (1991), Carozzi (1993), Mackenzie and Adams (1994), and Purser *et al.* (1994). The textures of the studied samples were classified following the Dunham classification (Dunham, 1962, Figure 4.3), and the determination of porosity types used descriptive and identification schemes established by Choquette and Pray (1970, Figures (4.4), (4.5) and Table 4.1). The description of textures and fabrics of crystal mosaics based on Friedman (1965) (Table 4.2). A number of thin sections (93) were polished and studied using CL, SEM (BSE and SEI) to distinguish calcite from dolomite and especially to determine the presence of calcite cement within the dolomite crystals.

Table (4.1) Terms used to describe porosity (%)

0 -5	Poor
5 - 10	Fair
10 - 15	Good
15 – 20	V. Good
>20	Excellent

Table (4.2) Terms for describing textures and fabrics of crystal mosaics in sedimentary rocks (after Friedman, 1965).

For crystal shape	Anhedral - poor crystal shape	
	Subhedral - intermediate crystal shape	
	Euhedral - good crystal shape	
For equigranular mosaics	Xenotopic - majority of crystals anhedral	
	Hypidiotopic - majority of crystals subhedral	
	Idiotopic - majority of crystals euhedral	
For inequigranular mosaics	Porphyrotopic - where larger crystals (porphyrotopes) are enclosed in a finer grained matrix	
	Poikilotopic – where larger crystals (poikilotopes) enclose smaller crystals	
Size - scale	Micron – sized	0-10 μm
	Decimicron – sized	10-100 μm
	Centimicron – sized	100-1000 μm
	Millimetre – sized	1-10 mm
	Centimetre – sized	10-100 mm
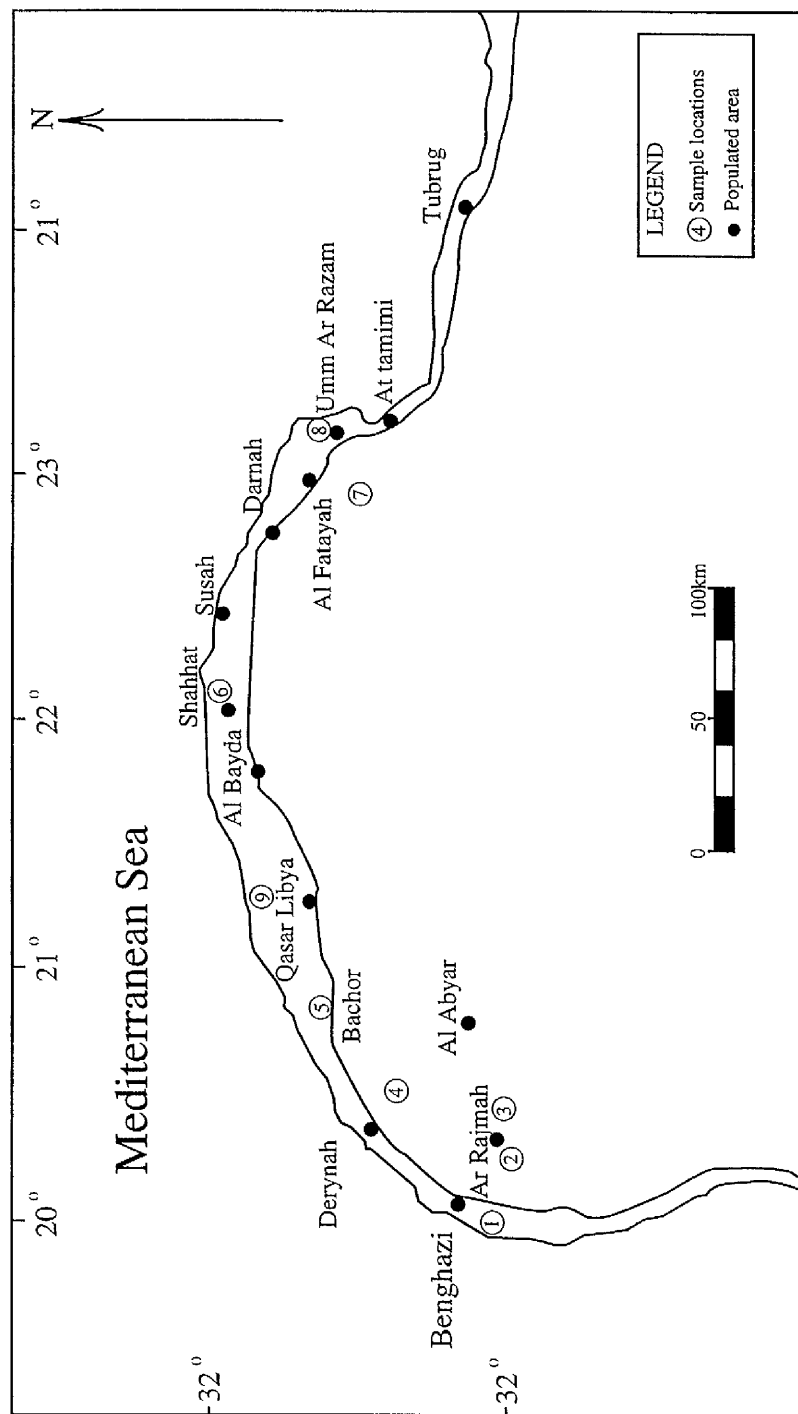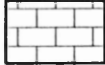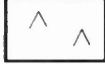
Figure (4.1) Location map of the studied area, north eastern part of Libya

LEGEND

Lithology

	Limestone
	Dolomite
	Dolomitic limestone
	Gypsum

	Marly Limestone
	Marl
	Oolitic Limestone

Fossils
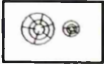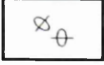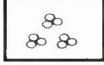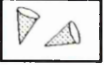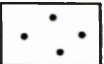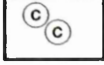
	Red algae
	Bioturbation
	Bivalves
	Gastropods
	Forams
	Shell fragments
	Celestite
	Bryozoan
	Chert nodules
	Snail tubes of gastropods

	Echinoids
	Brachiopods
	Ooids
	Nummulites
	Corals
	Glauconite
	Blocky

Figure (4.2) Lithological symbols used in all columnar sections (logs) in this study.

DEPOSITIONAL TEXTURES RECOGNIZED				
Original Components Not Bound Together During Deposion				Original components were bound together during deposition
Contains mud (particles of clay and fine silt size)			Lacks mud and is grain-supported	
Mud - supported		Grain - supported		
Less than 10 percent grains	More than 10 percent grains			
MUDSTONE	**WACKESTONE**	**PACKSTONE**	**GRAINSTONE**	**BOUNDSTONE**

(A)

Carbonate grain

Calcite mud

Secondary sparry calcite

Lime Mudstone

Lime Wackestone

Lime Packstone

Lime Grainstone
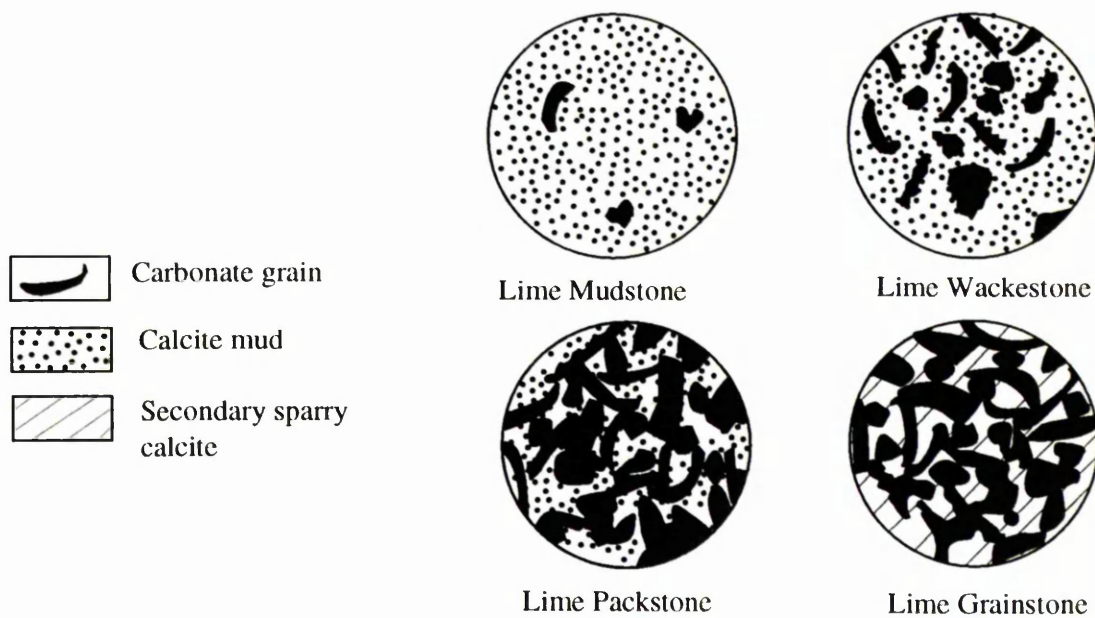
(B)

Figure (4.3) A.The textural classification of carbonates by Dunham (1962).
B. Diagrams illustrating terms proposed by Dunham (1962) for those carbonates in which components are not organically bound together.
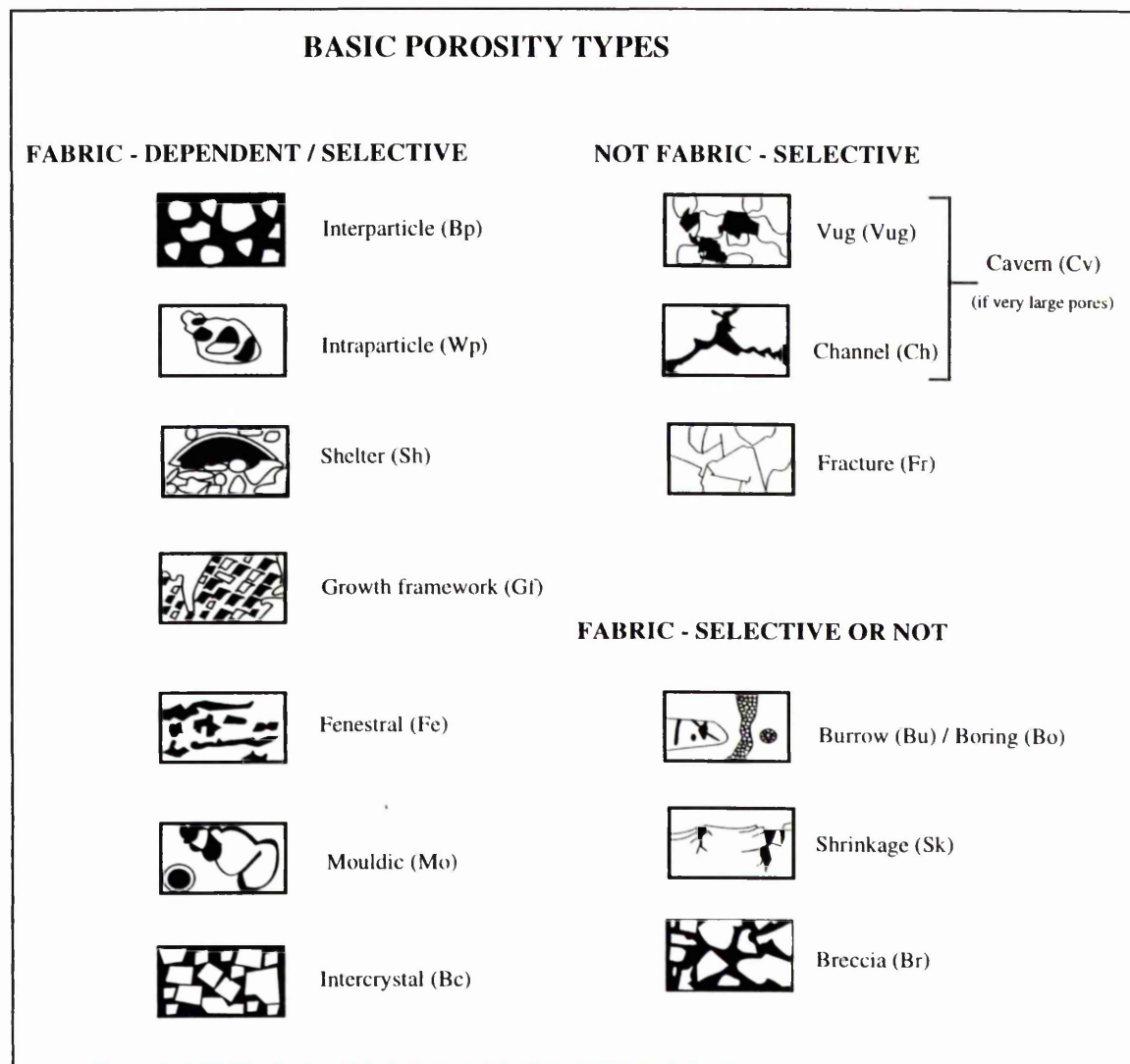
Figure (4.4) Classification of porosity in sedimentary carbonates after Choquette and Pray (1970)

PROGRESSIVE SOLUTION

| Initial state | Mould | Solution Enlarged | Vug |

PARTIAL ▼ INFILL

Matrix

Pore

Cement

| Reduced Mould | Reduced Solution Enlarged | Reduced Vug |

COMPLETE ▼ INFILL

| Filled Mould | Filled Solution Enlarged | Filled Vug |
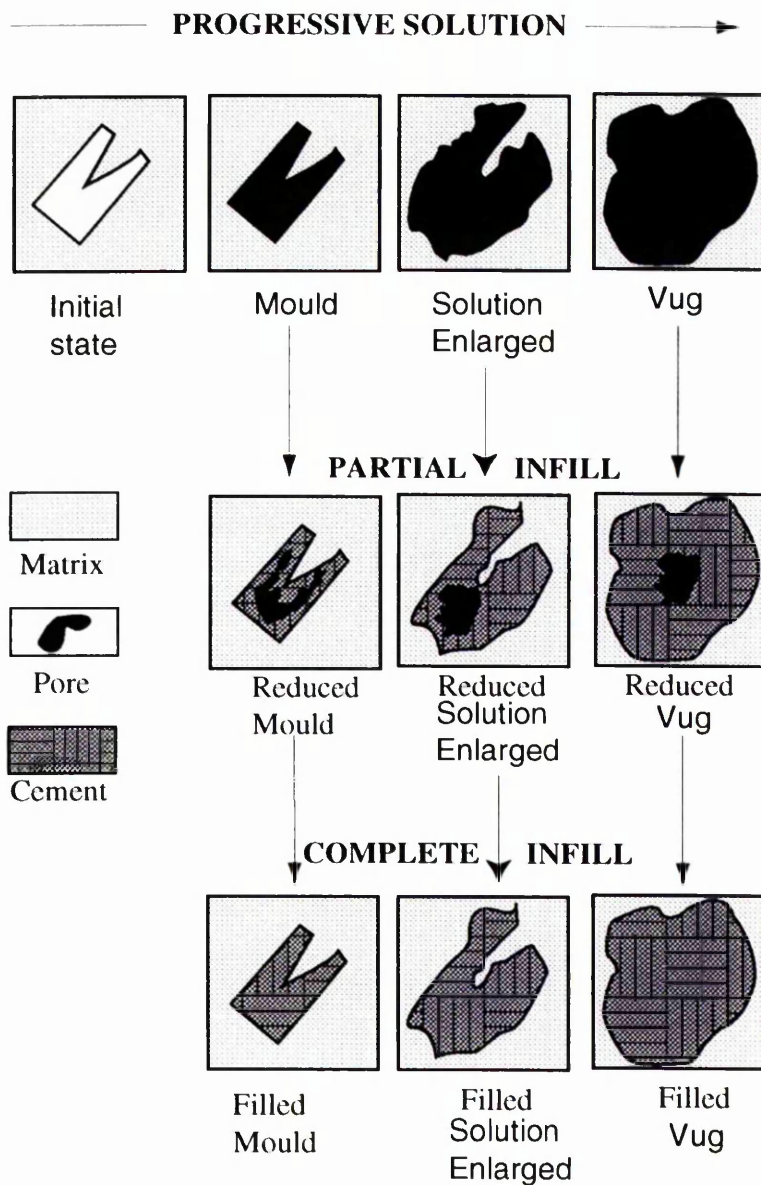
Figure (4.5) Common stages in evolution of one basic type of pore, a mould, showing application of genetic modifiers and classification code. From Choquette and Pray (1970).

4.2 Eocene

The oldest known Eocene deposit in Al Jabal Al Akhdar is the Apollonia Formation. The Apollonia Formation consists mostly of a thick sequence of well bedded light coloured, fine-grained limestone. The Apollonia Formation has two characteristic features; the presence of conspicuous brown cherty nodules, chert layers or lenses, and a bituminous smell (Goudarzi, 1970; Klen, 1974; Rohlich, 1974). The upper boundary is conformable with the Darnah Formation, which consists of fossiliferous limestone which is massive and well bedded, white to cream coloured. The most abundant fauna are large benthonic foraminifers especially *Nummulites*, which form a dominant constituent of the rock. Echinoids and bivalves are also common (Klen, 1974). On a regional scale, there is an interfingering between the Apollonia Formation and Darnah Formation (Rohlich, 1974). The higher percentage of planktonic foraminifers in the Apollonia Formation suggests a deeper environment of marine deposition, or deep neritic environment, and shallow neritic and littoral environment for the Darnah Formation (Klen, 1974).

4.2.1 Apollonia Formation (Lower to Middle Eocene) :

The section at Bachor (Figure 4.6) of the Apollonia Formation exhibits predominantly light coloured (white), soft, chalky limestone with chert nodules, rhythmically alternating with hard tan limestones. According to Barr and Berggren, (1980) this Formation results from a transgression, which commenced in the Early Eocene and lasted until the end of the Lutetian. The samples of the Apollonia Formation (Fig. 4.1, location no.5) are taken from Bachor Quarry (Plates 4.1 and 4.2). The Apollonia Formation consists of wackestone to mudstone, with echinoderm fragments, planktonic foraminifers (Plate 4.3), and contains up to 2 % dolomite crystals, micron sized, mostly in the matrix. The matrix (in sample no. AH) has been replaced by microspar (neomorphic spar).

Location	Age	Formation	Member	Meters	Lithology	Sedimentary structure Texture					Location of samples	Description
						Mudst	Wkcst	Pkst	Grnst	Bndst		
Bachor quarry	Lower to Middle Eocene	Apollonia		25 24 23 22 21 20 19 18 17 16 15 14 13 12 11 10 9 8 7 6 5 4 3 2 1 0							AS AH	Wackestone to Mudstone, white to creamy in colour, soft, with chalky limestone beds (10 - 20 cm thick) rhythmically alternating with hard tan limestones (about 50 cm thick), with chert nodules. Characterized by bituminous smell

Figure (4.6) Log of the Apollonia Formation, Bachor Quarry

Plate (4.1) The Apollonia Formation in the Tukra Bachor road-cut

Plate (4.2) White, soft, chalky limestone rhythmically alternating with hard limestone
(in Bachor Quarry)
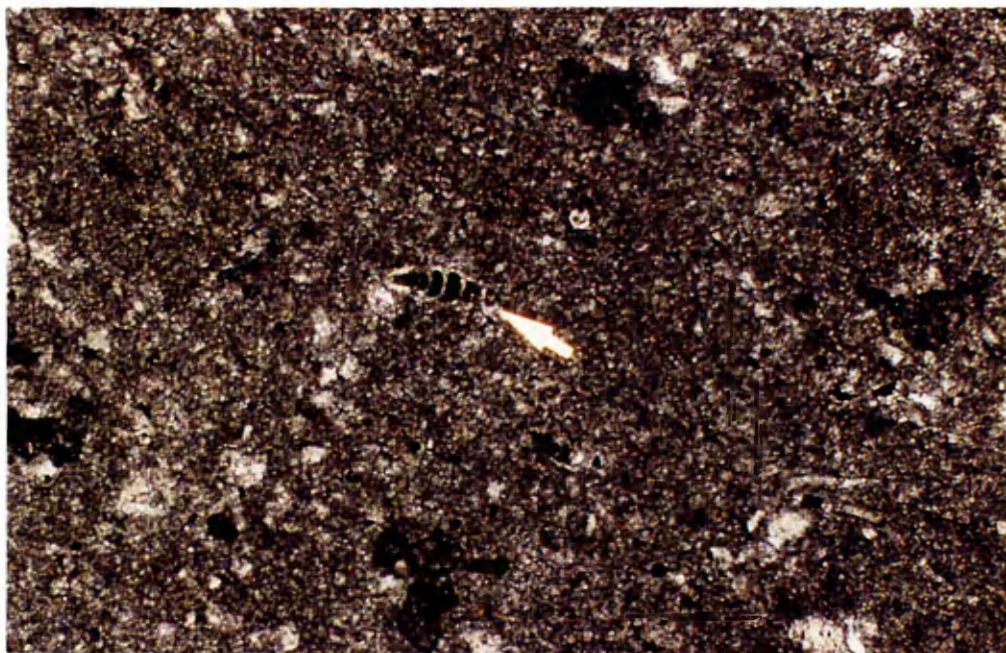
Plate (4.3) Planktonic Foraminifers, sample no. AS. Field view = 1.3 mm, (PPL).

4.2.2 Darnah Formation (Middle and Upper Eocene) :

The Darnah Formation has been studied at two localities: the new road-cut along Shahhat (Cyrene) - Susah (Apollonia), where the Darnah Formation represents the base of the section, and Qasar Libya Quarry (Fig. 4.1, locations no. 6 & 9). For this study the Darnah Formation is classified into two facies, according to the differences in nummulite grain size (Figure 4.7A). Facies (I) is composed of white to grey limestones, chalky in part, medium hard, with *Nummulites* of about 5 mm diameter. 22 % of the rock volume consists of *Nummulites* with other foraminifers (11 %), echinoderm fragments (7 %), matrix (51 %), and dolomite crystals (up to 1 % of the rock volume). Facies (II) consists of hard, white to cream limestones, containing *Nummulites* with variable size (up to 5 cm), and which comprise 48 % of the rock volume, with other foraminifers (1.3 %), echinoderm fragments (3 %), matrix (27 %), and dolomite crystals (0.5 %). Generally, the Darnah Formation is composed of massive limestone, whitish to cream, fine to medium grained, hard to medium hard in some places, chalky in part, containing mainly *Nummulites* (Plates 4.4, 4.5, and 4.6). Near the contact with overlying Al Bayda Formation echinoids were found in large numbers lying parallel to the contact (Plate 4.7). A packstone texture contains

Location	Age	Formation	Member	Meters	Lithology	Sedimentary structure					Location of samples	Description
						Texture						
						Mudst	Wkcst	Pkst	Grnst	Bndst		
Shahhat - Susah road cut	L. Oligocene	Al Bayda		46								
	Middle and Upper Eocene	Darnah		44 42							DE6	Nummulitic limestone (Facies I), chalky in part, white, m.hard, with *Nummulites* about, 5 mm in size, with molluscan shell fragments, echinoderm fragments, slightly dolomitized. The echinoids found in large numbers lying parallel to the contact with overlying Al - Bayda Formation
				40 38 36 34								
				32 30							DE5	Nummulitic limestone (Facies II), white to cream, hard, with *Nummulites* (ranging from 5 mm - 6 cm), echinoderm fragments, and Brachiopods
				28							DE4	Limestone (Facies I), white to cream, hard, with *Nummulites*, (ranging from 1 - 5 mm), echinoderm fragments, slightly dolomitized
				26 24 22								
				20 18							DE3	Nummulitic limestone (Facies II), white to cream, hard, with, *Nummulites* (*gizhensis*), (ranging from 3mm - 5 cm), echinoderm fragments
				16							DE2	Packstone(Facies I), white, chalky by part, medium hard, with *Nummulites* (<2mm), gastropods, and bivalves, oyster shell fragments
				14 12 10 8 6 4								
				2 0							DE1	Packstone (Facies I), whitish grey, m. hard, with small *Nummulites* (ranging from 2 - 4 mm), echinoderm fragments, slightly dolomitized

Figure (4.7A) Log of the Darnah Formation, Shahhat Susah road- cut

Nummulites (Plates 4.8, 4.9,and 4.10), echinoderm fragments with syntaxial overgrowths, shell fragments, clear dolomite crystals (0.4-1.6 % of the rock volume), some of which replace cement, which occurs mainly in echinoid spines and echinoderm fragments. The matrix is micrite with many fragmented bioclasts. Excellent primary porosity (intraparticle; Plate 4.11), and vuggy types.

Plate (4.4) Nummulitic bank, Darnah Formation (DE5), in Shahhat Susah road-cut

Plate (4.5) Large *Nummulites* (*gizhensis*), from Darnah Formation (DE3), Shahhat Susah road-cut
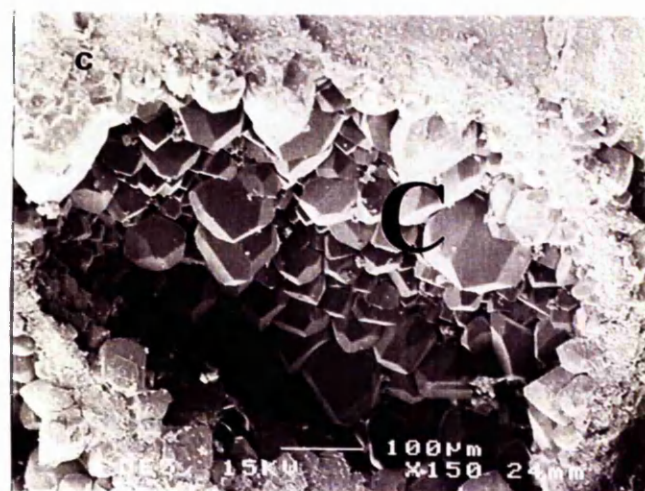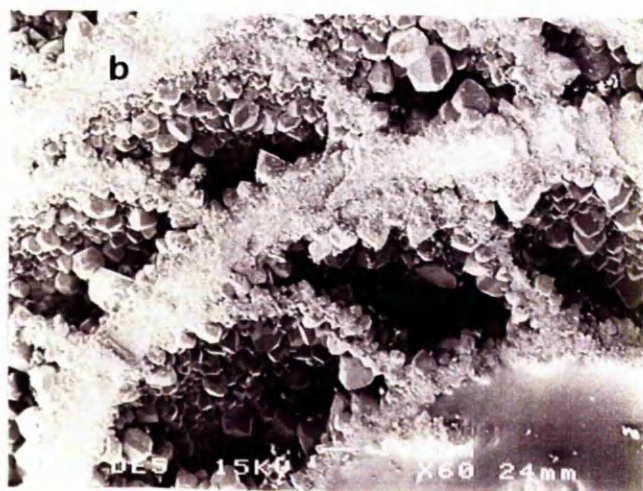
Plate (4.6) SEM-View of *Nummulite* grain (A) of Darnah Formation (DE5), (b) and (c) are close view of (A), showing the calcite cement (c), in the chambers of the grain.

Plate (4.7) Echinoid from the top of the Darnah Formation, Shahhat Susah road-cut.
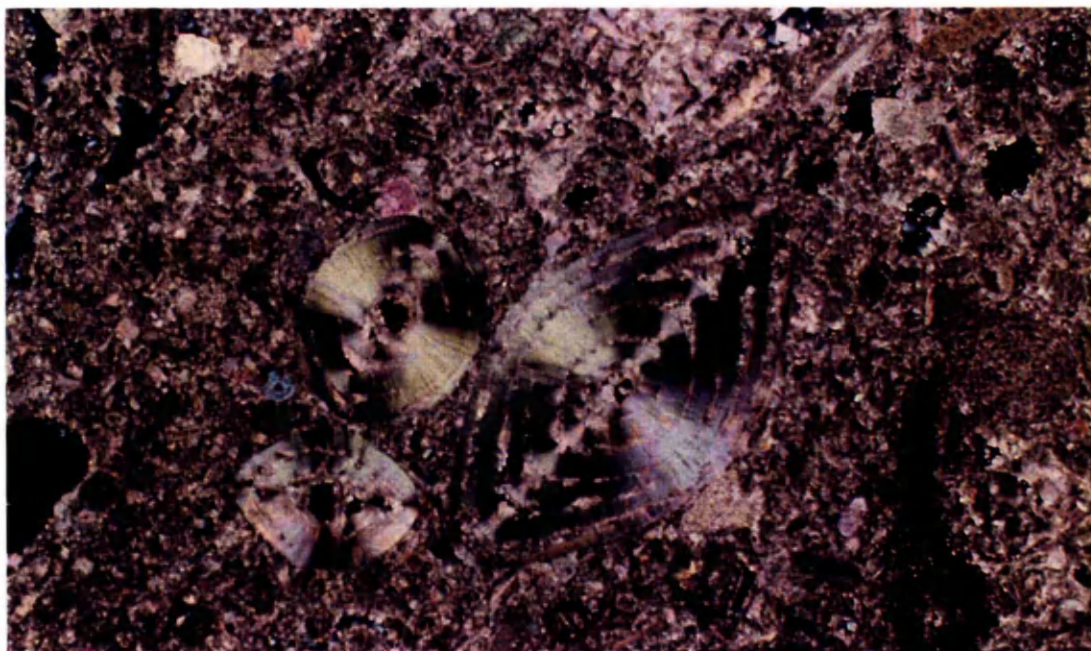
Plate (4.8) Nummulitic Packstone with echinoderm fragments, Facies (I) of Darnah Formation (DE1), Shahhat Susah road-cut. Field of view = 6mm, (XPL).

Plate (4.9) *Nummulites*, Facies (1) of Darnah Formation (DE2), Shahhat Susah road-
cut. Field view = 6mm, (XPL).
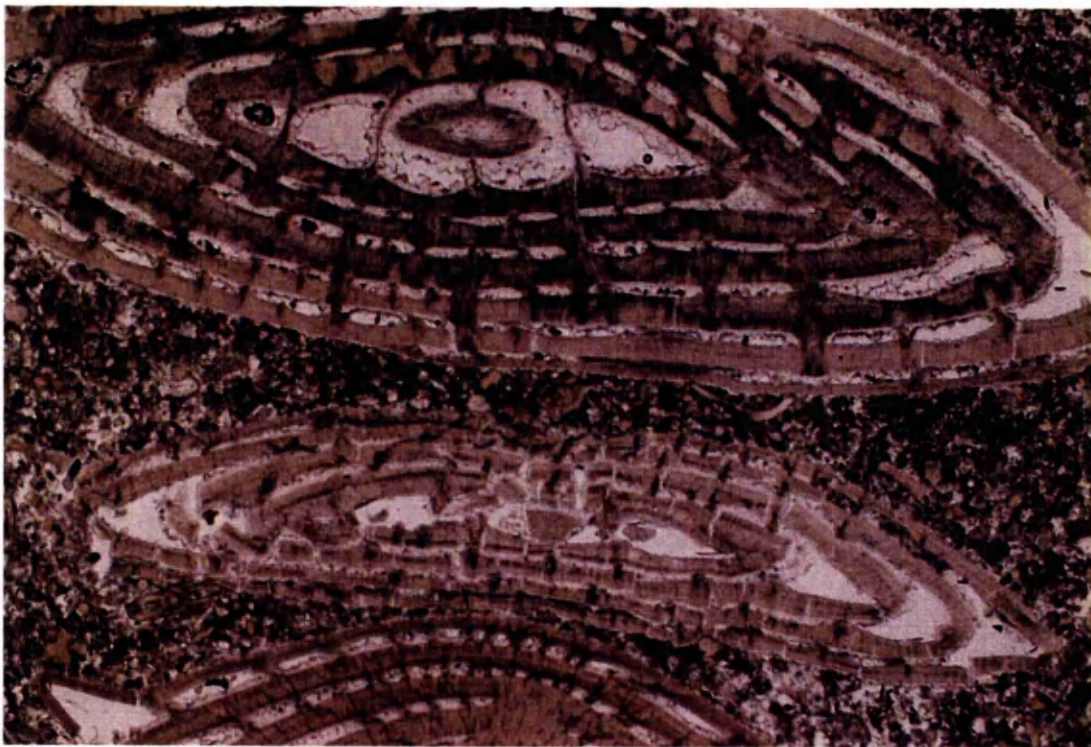
Plate (4.10) Packstone, showing slightly deformed *Nummulites*, an example of compaction, facies (I) of Darnah Formation (DE6). Field of view = 6 mm, (PPL).
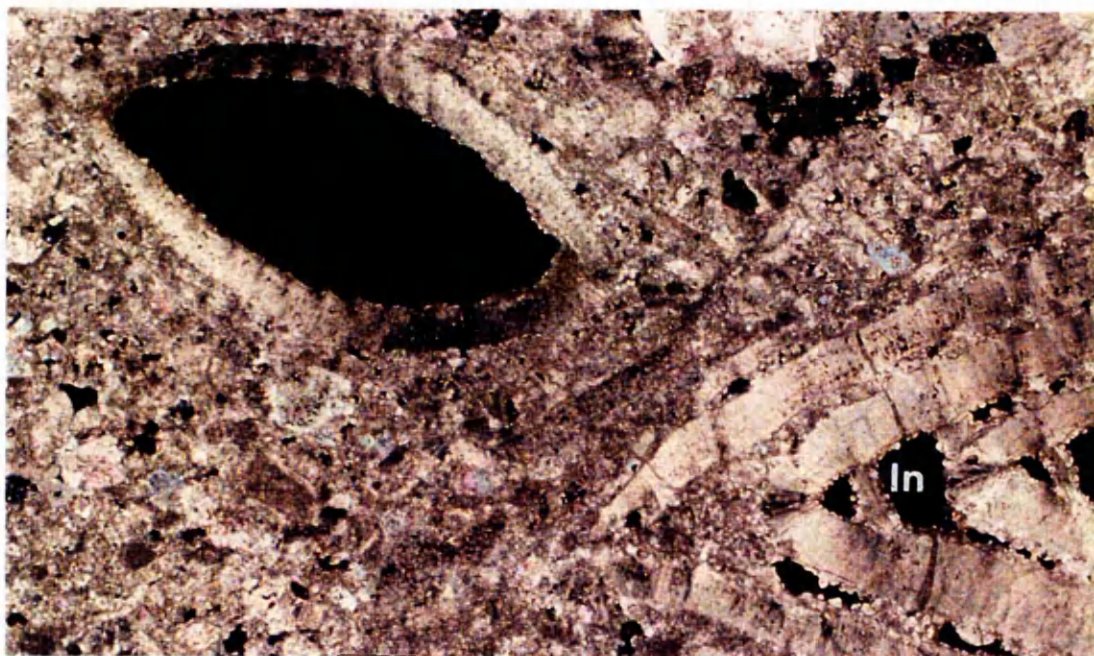
Plate (4.11) Packstone showing intraparticle (In) porosity, in *Nummulite* grains. Darnah Formation (Q.Libya U), in Qasar Libya quarry. Field of view = 3 mm, (XPL).

4.3 Oligocene

Oligocene rocks partly cover the Eocene rocks of the Al Jabal Al Akhdar area. With the Early Oligocene marine transgression a small part of Al Jabal Al Akhdar was covered by sea water allowing for the deposition of the Shahhat Marl Member and the overlying Algal Limestone Member. The submerged area was centred in Cyrene (Shahhat) where the maximum thickness of the Shahhat Marl is found. With increased transgression and / or subsidence an increasingly large area was covered by marine water as the Algal Limestone Member is found underlain by older formations in the structurally high areas (El Hawat and Shelmani, 1993). Oligocene units include the Shahhat Marl Member, which represents the basal Oligocene beds, the Algal Limestone Member of the Al Bayda Formation, and the Al Abraq Formation. The Al Bayda Formation suggests a neritic, largely shallow marine environment, and the marly facies indicates a relatively deep environment (Rohlich, 1974). The Al Abraq Formation is separated from the overlying Al Faidiyah Formation by a prominent clayey layer. The sedimentation of the Al Abraq Formation took place in a very shallow water environment (Goudarzi, 1970).

4.3.1 Al Bayda Formation (Lower Oligocene):

The Al Bayda Formation is composed of two members (Rohlich, 1974): the Shahhat Marl Member, and the Algal Limestone Member. Samples of this Formation have been taken from two different localities: Deryanah Al Abyar road-cut (Fig. 4.1, location no.4), and Shahhat Susah road-cut (Fig. 4.1, location no.6).

4.3.1.1 Shahhat Marl Member (Shahhat Susah road-cut):

The Al Bayda Formation in this section (Fig. 4.1, location no.6), consists of two members (Figure 4.7B). The lower boundary of Shahhat Marl Member is disconformable with the underlying Darnah Formation (sharp contact). The member consists of grey to greenish, highly fossiliferous, soft marl and marly limestone. The Shahhat Marl Member contains *Nummulites*, moulds of active bivalves (Plate 4.12), and burrows of *Thalassinoides* (Plate 4.13) and bivalves.

Location	Age	Formation	Member	Meters	Lithology	Sedimentary structure					Location of samples	Description
						Texture						
						Mudst	Wkest	Pkst	Grnst	Bndst		

Algal limestone, whitish, hard, with coralline algae, bivalves and *Nummulites*, and other foraminifera echinoderm fragments, bryozoans molluscan shell fragments, and quartz grains

Algal limestone, whitish, hard, with large coralline algae, echinoids, gastropods (*Vermetidae* family), *Nummulites*, bryozoans, gypsum crystals, and partly dolomitized

Marly limestone, greenish to yellow, soft, with bivalves, echinoderm fragments, quartz grains, and dolomite crystals

Marl, greenish to yellowish, soft, with bivalves, and dolomite crystals

Marly limestone, yellowish, soft, with bivalves (*Cardita* type), *Nummulites*, and echinoids (about 4 cm in diameter), burrows of *Thalassinoides*

Marly limestone, grayish, soft, with moulds of active bivalves, and burrows of *Thalassinoides*

Limestone, yellowish, thin bedded, medium hard, occurrence of bivalves, quartz grains and dolomite crystals

Figure (4.7B) Log of the Al Bayda Formation, Shahhat Susah road- cut

Plate (4.12) Moulds of active bivalves (sample no. SMP), in Shahhat Marl Member.

Plate (4.13) Burrows of *Thalassinoides* (sample no. SMP) of Shahhat Marl Member

A typical sample is a packstone with foraminifers *Nummulites* and discocyclinid species (Plate 4.14), echinoderm fragments, molluscan shell fragments, bryozoans, and quartz grains (1.5 % from the whole rock volume). The matrix is mainly micritic with common fragments of bioclasts and dolomite crystals (up to 0.9 % of the whole rock volume). Visible porosity is poor.

Plate (4.14) Longitudinal section of discocyclinid (arrowed) and *Nummulites*. The matrix is mainly micritic with many fragmented bioclasts (sample no. SUP). Field of view = 6mm, (PPL).

4.3.1.2 Algal Limestone Member (Shahhat Susah Road-cut):

The Algal Limestone Member of this section is made up of whitish, medium grained, hard, thick bedded algal limestone (Plate 4.15), with abundant echinoids (Plate 4.16) and gastropods (Plate 4.17).

It consists of packstone with coralline algae showing fine cellular structure (Plate 4.18), echinoderm fragments with syntaxial overgrowths, bryozoans, foraminifers, molluscan shell fragments, and quartz grains (2.5 % of the whole rock volume). It is partially dolomitized (up to 4 % of the whole rock volume). It shows very good vuggy solution porosity.

Plate (4.15) White coralline algae of the Algal Limestone Member of the Al Bayda Formation (Algal Lst. L), Shahhat Susah road-cut.

Plate (4.16) Echinoids in Algal Limestone Member of the Al Bayda Formation, in Shahhat Susah road-cut.

Plate (4.17) Vermetid gastropods in Algal Limestone Member of the Al Bayda Formation, Shahhat Susah road-cut.
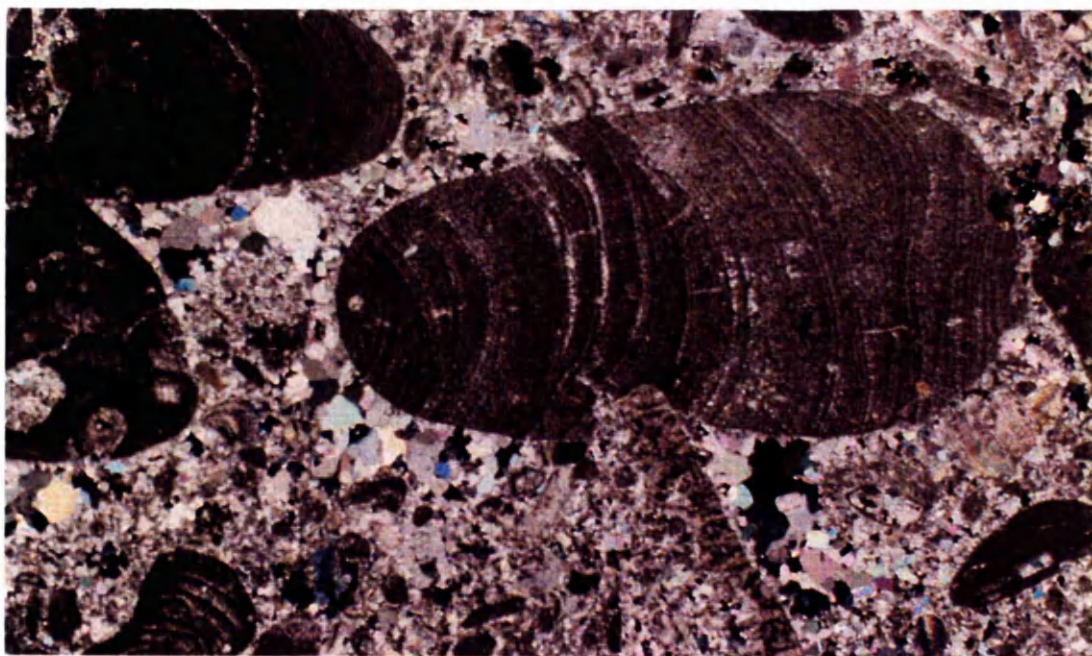
Plate (4.18) Coralline algae (well preserved) and equant spar drusy mosaics, filling pore spaces between the grains of the Al Bayda Formation (Algal Limestone Member), Shahhat Susah road-cut. Field of view = 6 mm, (XPL).

4.3.1.3 Algal Limestone Member (Deryanah Al Abyar Road-cut):

In this road cut only the Algal Limestone Member of the Al Bayda Formation is found (Figure 4.8). The overlying unit is the Al Abraq Formation. The Algal Limestone Member in this section is made up of whitish, medium grained, hard, fossiliferous limestone. It contains coralline algae, showing typical laminated (Plate 4.19) cellular structure (some in fragmented form), with *Nummulites* characterized by thick wall and radial fibrous structure (Plate 4.20), echinoderm fragments and bryozoans embedded in carbonate mud with micron sized clear dolomite crystals (up to 3.5 % of the whole rock volume). Multiple borings of the matrix have been infilled with bioclasts and the same micritic sediments. It contains good to excellent vuggy solutional porosity.

Plate (4.19) Coralline algae, with very typical lamination and regular cellular structure of the Al Bayda Formation (Algal Limestone Member). Field view = 6 mm, (PPL).

Location	Age	Formation	Member	Meters	Lithology	Sedimentary structure Texture					Location of samples	Description
						MUDST	WKEST	PKST	GRNST	BNDST		
Deryanah - Al Abyar road-cut	Middle Miocene	Ar Rajmah	Wadi Al Qattarah								QM.2	Gypsum, with scattered dolomite crystals filling fractures, and quartz grains
											QM.1	Oolitic limestone, white, hard, Ooids are regular concentric laminae, and often not well developed
	U. Oligo. - Mid. Mio.	Al Faidiyah	Faidia Limestone								1 TO 10	Glauconitic marly limestone, yellow to greenish, soft to medium hard, with interealation of green clays, echinoderm fragments, quartz grains, bryozoan, benthonic foraminifera, oyster fragments, the upper part is slightly dolomitized
	Middle to upper Oligocene	Al Abraq									A7	Packstone, marly limestone, yellowish, soft to medium hard, with *Nummulites*, echinoderm fragments, bryozoans, quartz grains, glauconite grains, coralline algae, corals, and slightly dolomitized
											A6	Packstone, marl, yellowish, soft to medium hard, with *nummulites*, echinoderm fragments, bryzoan, quartz grains, glauconite grains, large Oyster fragments, red-algae, and slightly dolomitized
											A5	Nummulitic limestone, yellowish, medium hard, with benthonic foraminifera, echinoderm fragments, bryozoans, and slightly dolomitized
											A4	Limestone, yellowish, hard, with abundant *Nummulites*, echinoderm fragments, bryozoans, and slightly dolomitized
											A3	Packstone, yellowish, hard, with abundant echinoderm fragments, benthonic foraminifera, bryozoans, and slightly dolomitized
											A2	Packstone, marly limestone, white to yellowish, soft, with molluscan shell fragments, large oyster fragments, coralline algae, and slightly dolomitized
											A1	Packstone, yellowish, hard, with benthonic foraminifera, coralline algae, echinoderm fragments, bryozoans, and slightly dolomitized
	Lower Oligocene	Al Bayda	Algal Limestone								Bayda	Algal limestone, whitish, medium grained, hard, with large coralline algae, fossiliferous; echinoderm fragments, molluscan shell fragments, bryozoans, slightly dolomitized

Figure (4.8) Log of the Al Bayda, Al Abraq, Al Faidiyah, and Ar Rajmah formations, Deryanah Al Abyar road-cut

Plate (4.20) *Nummulites sp.*, with thick wall and radial fibrous structure of the Al
    Bayda Formation (Algal Limestone Member). Field of view = 6 mm,
    (XPL).

4.3.2   Al Abraq Formation (Middle to Upper Oligocene):

The section studied was located in Deryanah Al Abyar road-cut (Fig. 4.1,
location no. 4). It consists of limestone (< 10 % of dolomite), nummulitic limestone,
and marl (Figure 4.8), containing abundant echinoids. The underlying unit is the Algal
Limestone Member of the Al Bayda Formation, and overlying it is the Al Faidiyah
Formation (Plate 4.21). The Al Abraq Formation consists of *Nummulites* (Plate 4.22),
echinoderm fragments with syntaxial overgrowths (Plate 4.23), miliolids, red algae,
bryozoan fragments, molluscan shell fragments (Plate 4.24), quartz grains (1.5 % of
the rock volume), and glauconite grains (especially in Samples A6 and A7, near the
contact with Al Faidiyah Formation). The unit is partially dolomitized (up to 3.8 % of
the rock volume), usually with micron sized clear dolomite crystals in the matrix.
Good to excellent porosity is present (including biomouldic, microvugs, and enhanced
interparticle types).

Plate (4.21) The contact (disconformity) between the Al Abraq Formation (Ab) and the Al Faidiyah Formation (ALF), Deryanah Al Abyar road-cut.
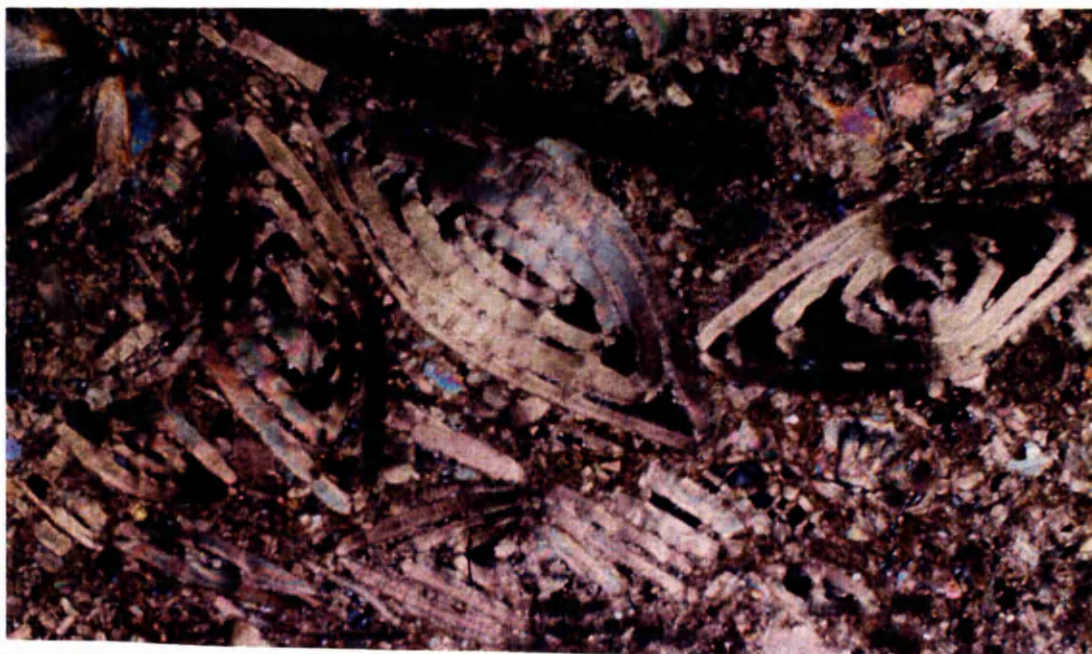
Plate (4.22) Packstone, with *Nummulites* (also in fragmental form), and intraparticle porosity, Al Abraq Formation (A4), Deryanah Al Abyar road-cut. Field of view = 6 mm, (XPL).
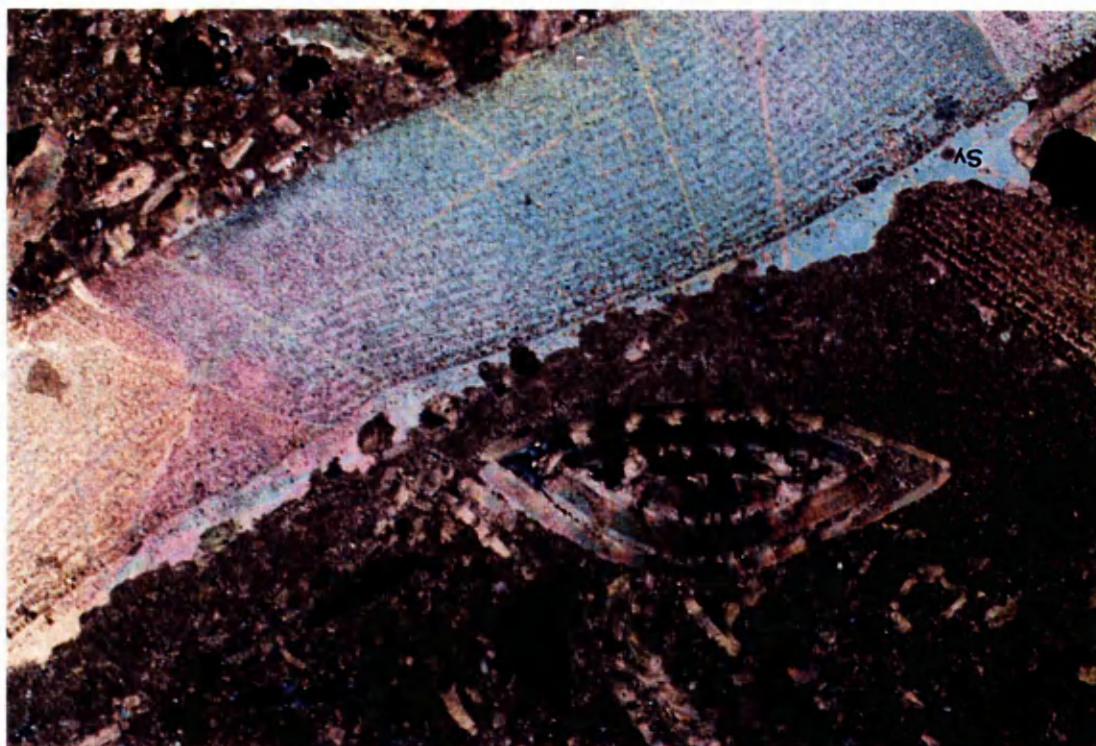
Plate (4.23) Large echinoid fragment with syntaxial overgrowth (Sy), Al Abraq Formation (A7), in Deryanah Al Abyar road-cut. Field of view = 6 mm, (XPL).

Plate (4.24) Large oyster fragments with foliated structure, and echinoderm fragments, Al Abraq Formation (A2), Deryanah Al Abyar road-cut. Field of view = 6 mm, (PPL).

4.4 Miocene

During the Late Oligocene-Early Miocene, tectonic activity took place, and the Oligocene-Miocene boundary is found to be erosional everywhere in Libya. The Al Faidiyah Formation, in Al Jabal Al Akhdar, has been dated as Late Oligocene (Rohlich, 1974; Klen, 1974; Zert, 1974)) based on the occurrence of *Nummulites fichteli*. Other geologists argue that the succession is Aquitanian in age (Pietersz, 1968; El Hawat and Shelmani, 1993). They attribute the occurrence of *Nummulites* to reworking of the underlying Oligocene formations which had been eroded from the adjacent structural highs. The Middle Miocene marine transgression covered most of Cyrenaica and the Sirte Basin. It was followed by the deposition of the shallow marine facies of the Benghazi Member of the Ar Rajmah Formation. Later a major regression took place throughout northern Libya, leading to the development of a regional disconformity surface extending from western Libya, Sirte basin, Al Jabal Al Akhdar, the Western Desert, the Nile delta and Sinai (El Hawat *et al.*, 1987; 1985; El Hawat *et al.*, 1993; El Hawat, in press) This is timed with the separation of Tethys from Paratethys, and the closure of the Mediterranean. This was the main event that eventually led to the Messinian salinity crisis. In Al Jabal Al Akhdar the Late Miocene sequence consists of Tortonian oolitic shoals followed by Messinian carbonates and evaporites (El Hawat *et al.*, 1993).

4.4.1   Al Faidiyah Formation:

The Al Faidyah Formation stratigraphically ranges from the Upper Oligocene to Lower Miocene. The Formation consists chiefly of limestone, whitish to yellowish, thick bedded to massive. It contains fossiliferous layers with dominant coralline algae. The basal part of the Formation referred to by Pietersz, (1968) as the Faidia Clay Member is mostly typified by a layer of green clay (Rohlich, 1974). The Al Faidiyah Formation has been studied at three localities;

4.4.1.1 Al Faidiyah Formation (Deryanah Al Abyar road-cut):

The Al Faidiyah Formation in this location is yellowish to greenish, soft to medium hard with rhythmical alternations of glauconitic marly limestone and green clay. (Plates 4.25 and 4.26) (Figure 4.8). It contains large, rounded to subrounded

glauconite grains (Plate 4.27), green to brownish in colour, echinoderm fragments with syntaxial overgrowths, benthonic foraminifers, molluscan shell fragments (Plate 4.28), bryozoans, and quartz grains (up to 12.6 % from the whole rock volume). The upper part commonly contains Nummulitid forams (also in fragmental form, Plate 4.29). The matrix is micrite with many fragmented bioclasts. It is slightly dolomitized (up to 2 % of the rock volume).

Plate (4.25) Rhythmical alternations of glauconitic marly limestone, and varying grain size, Al Faidiyah Formation. In Deryanah Al Abyar road-cut.

Plate (4.26) Palaeosol at the top of the section of the Al Faidiyah Formation in Deryanah Al Abyar road-cut.
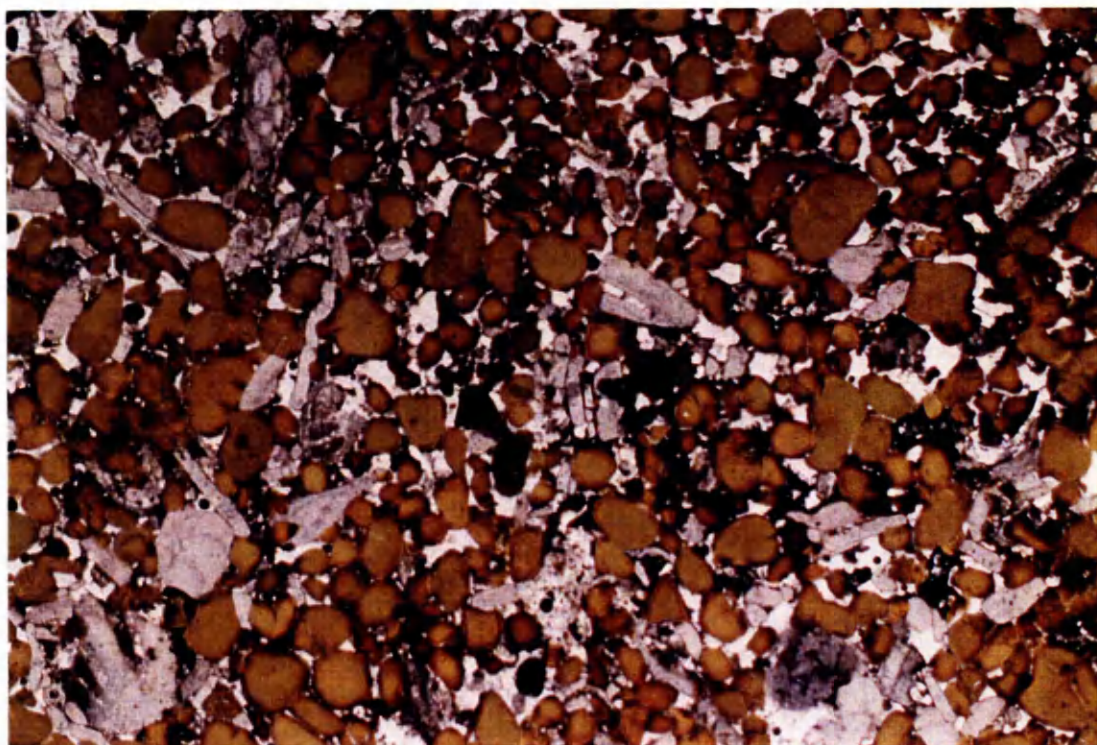
Plate (4.27) Abundant glauconite grains, Al Faidiyah Formation (1), Deryanah Al Abyar road cut. Field view = 6 mm, (PPL).
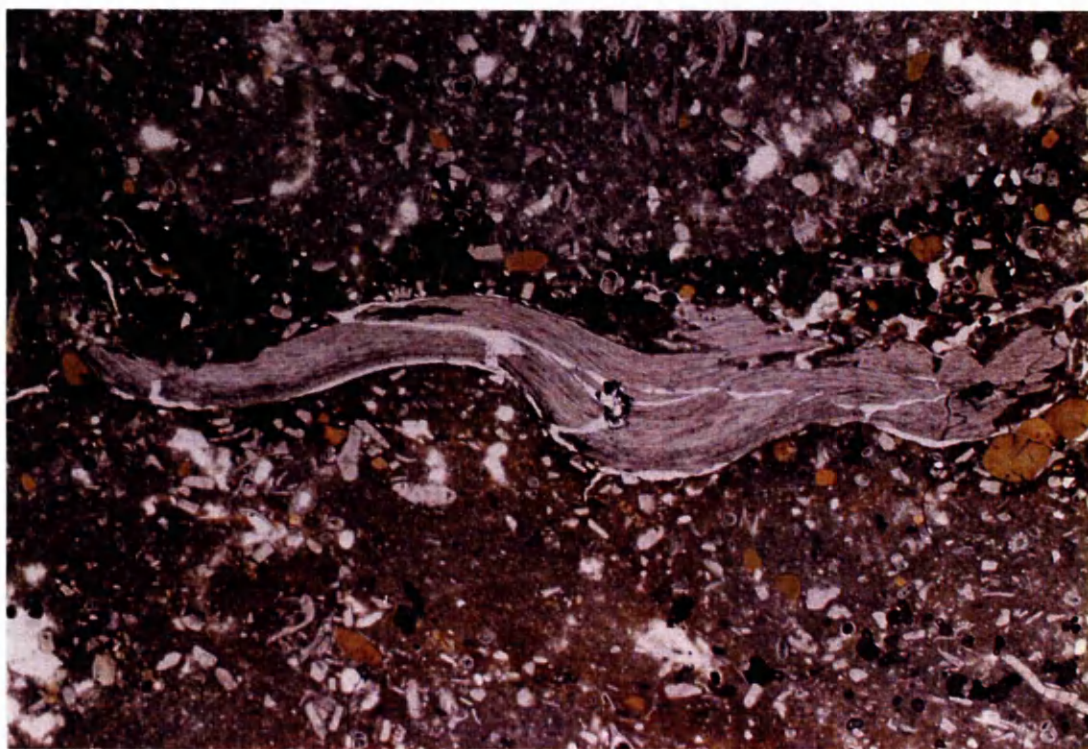
Plate (4.28) Large molluscan shell fragments and glauconite grains, Al Faidiyah Formation (3). Field view = 6 mm, (PPL).

Plate (4.29) Nummulitid forams (also in fragmental form), Al Faidiyah Formation (9).

Field of view = 6 mm, (PPL).

4.4.1.2 Al Faidiyah Formation (Al Fatayah Cement Quarry):

The Al Faidiyah Formation in this location (Fig. 4.1, location no.7) consists mainly of limestone (Faidia Limestone Member), with green clay in the lower part of the Formation (Figure 4.9). In addition to clay minerals the Faidia Clay Member contains gypsum crystals, microcrystalline dolomite, quartz grains, ilmenite, and muscovite flakes (see Chapter 7). The limestone of the Faidia Limestone Member is mostly white, medium to fine grained, medium hard, and contains coral reefs associated with the Aquitanian transgression (Figure 4.10). The reef framework is constructed of two genera of corals *Cyphastrea* (Plate 4.30) and *Aleveopora* (Plate 4.31), with abundant burrowing bivalves. It also contains encrusting red algae, echinoderm fragments with syntaxial overgrowths, molluscan shell fragments, large benthonic foraminifers (*Nummulites sp.* and Discocyclinids), bryozoans, gypsum crystals, glauconite grains, and equant spar drusy mosaic filled pores. It is dolomitized (1.7 %) especially in the lower part, with micron sized, euhedral dolomite, replacing matrix. There is excellent mouldic and vuggy solutional porosity.
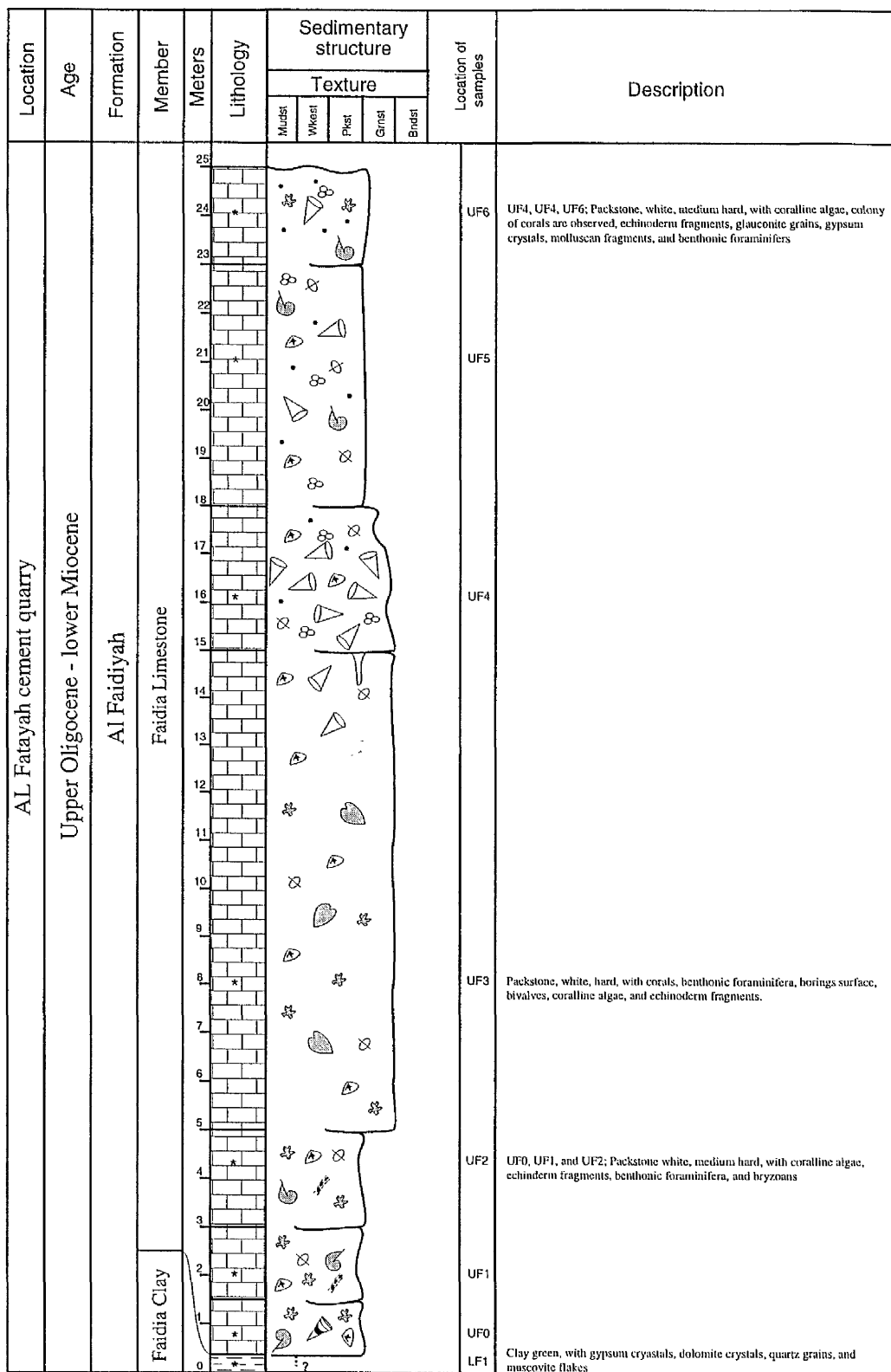
Figure (4.9) Log of the Al Faidiyah Formation, Al Fatayah cement Quarry
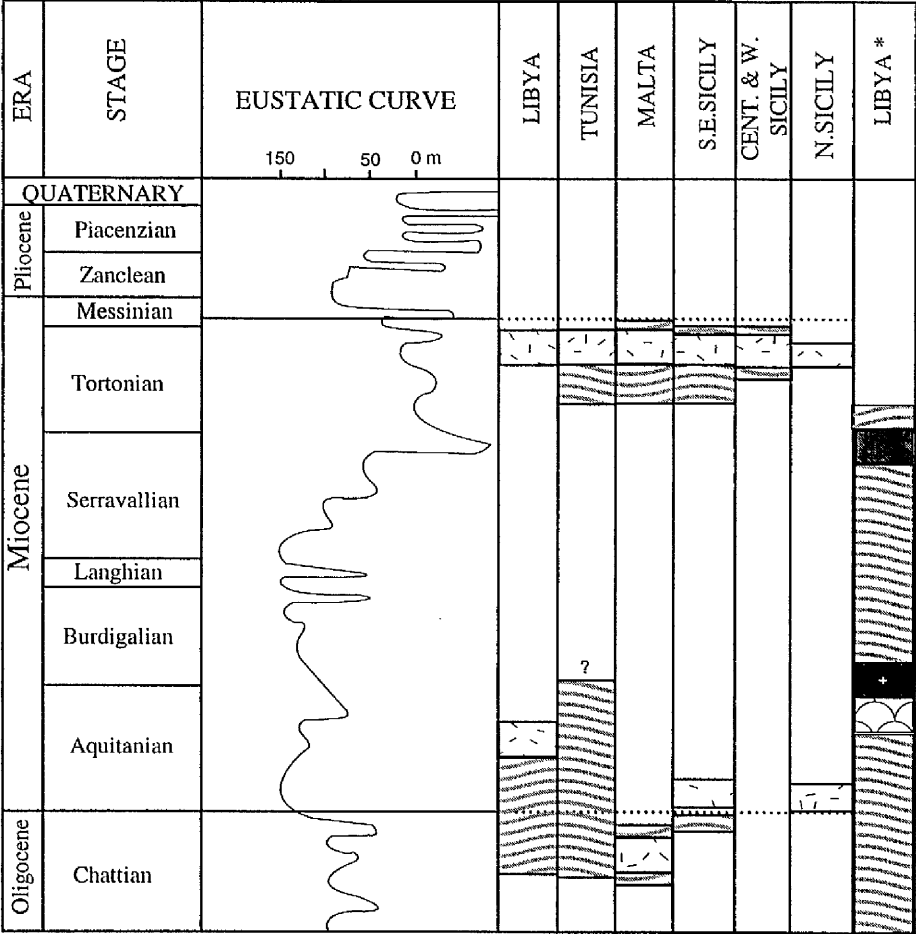
Figure (4.10) Stratigraphic distributions of the Miocene reefs of the central Mediterranean region (modified from Martyn, 1996).

Tarbellastraea

Porties

Aleveopora

Cyphastrea

Rhodalgal biostromes
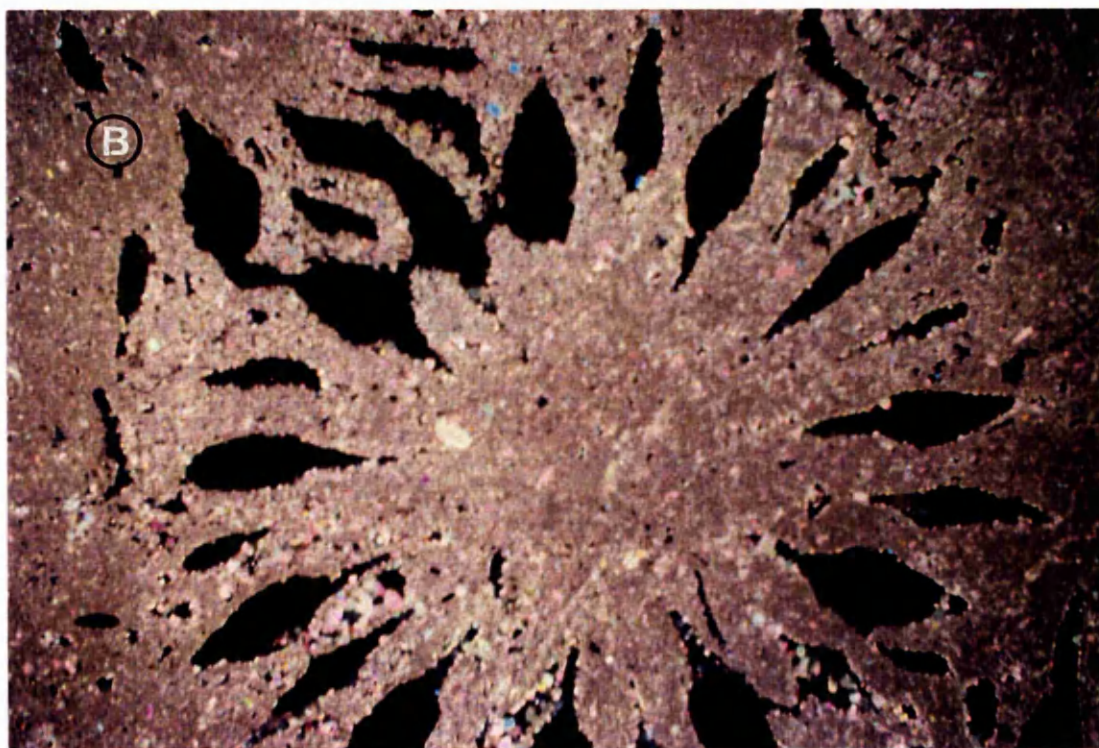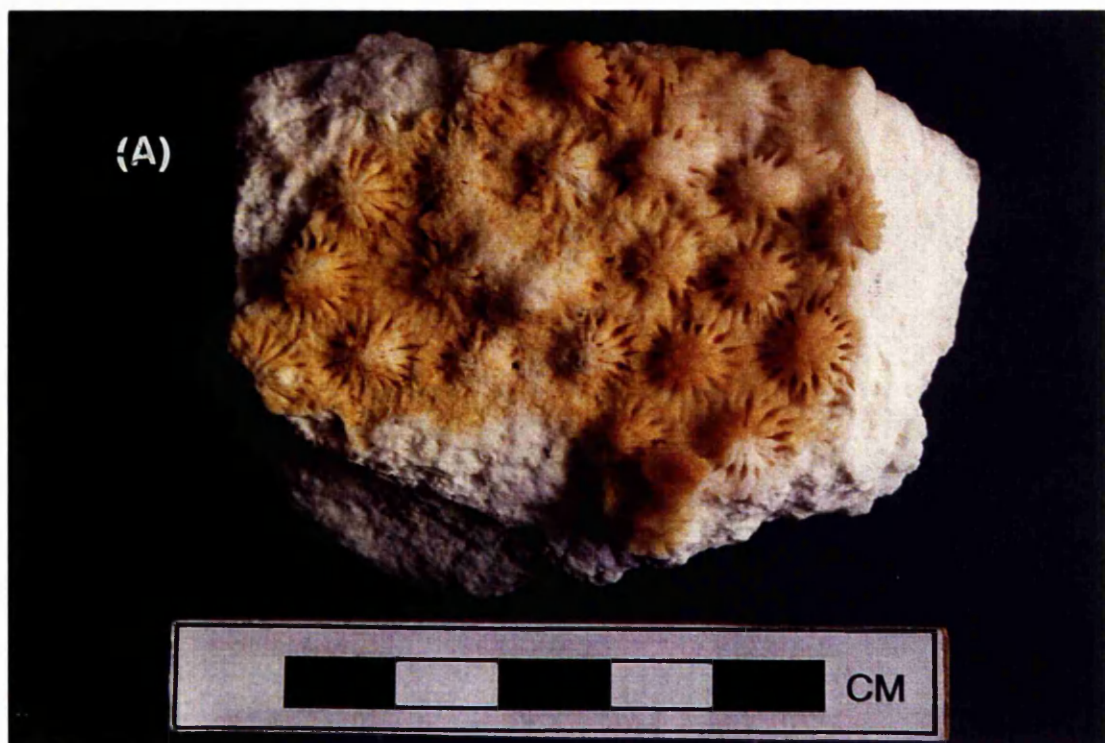
Plate (4.30) A). Typical coral reefs of *Cyphastrea sp.* (UF3), in Al Fatayah Quarry. B). Section of the same colony (A) under microscope showing mouldic porosity. Field of view = 6 mm, (XPL).
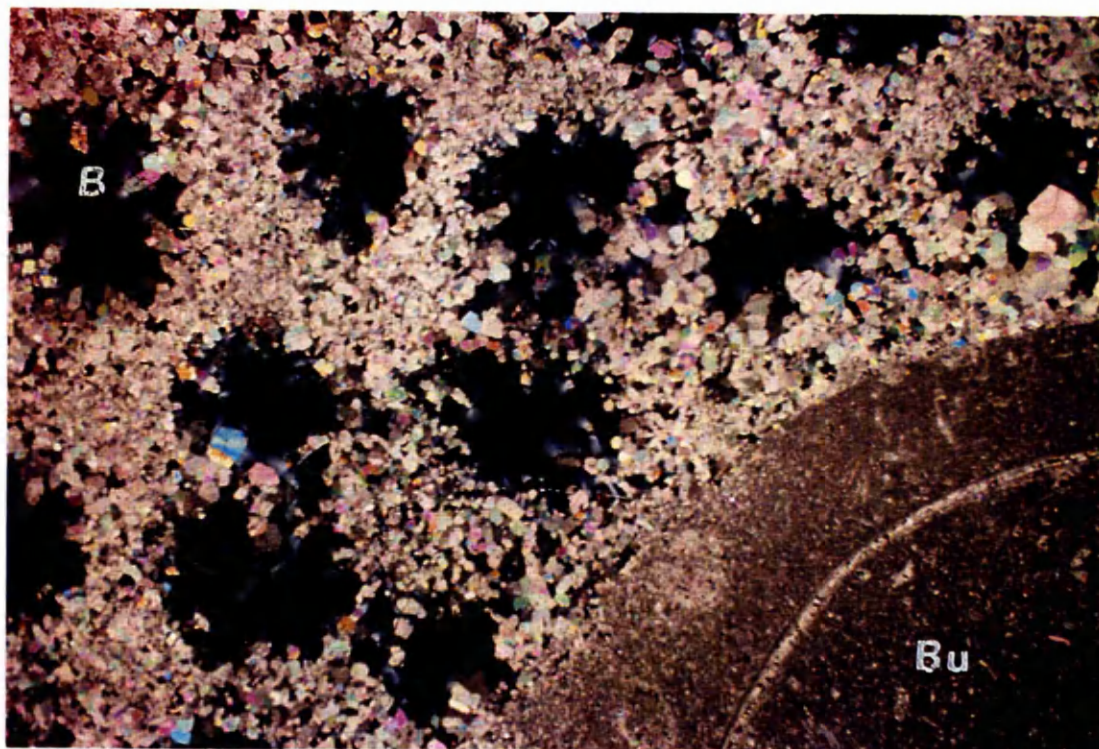
Plate (4.31) A). *Aleveopora sp.*(UF5), in Al Fatayah Quarry. B). with abundant boring of bivalves (Bu). The wall has been replaced by calcite, Al Faidiyah Formation. Field of view = 6 mm, (XPL).

4.4.1.3 Al Faidiyah Formation (Umm Ar Razam quarry):

This section of the Al Faidiyah Formation is located in Umm Ar Razam village (Fig. 4.1, location no. 8). The lower boundary of the Faidia Clay Member is disconformable with the Al Abraq Formation. The Lower Member of the Formation consists of green clay (Plate 4.32, and Figure 4.11) with gypsum crystals, micron sized dolomite, quartz grains, ilmenite (Plate 4.33) and muscovite flakes. The Faidia Limestone Member is composed of yellowish, medium hard limestone (Figure 4.11) with a packstone texture, and common bryozoans (Plate 4.34), echinoderm fragments with syntaxial overgrowths, benthonic foraminifers (Discocyclinids), glauconite grains (up to 1.5 % of the rock volume) and gypsum crystals. It is slightly dolomitized (up to 2 % of the rock volume), some of the echinoid spines are replaced totally by micron sized clear dolomite crystals. Good solutional porosity (vuggy type) is present.

Plate (4.32) The sharp contact between the Faidia Clay, and Faidia Limestone Members of Al Faidiyah Fm., in Umm Ar Razam Quarry.

Location	Age	Formation	Member	Meters	Lithology	Sedimentary structure					Location of samples	Description
						Texture						
						Mudst	Wkest	Pkst	Grnst	Bndst		
Umm AL Razam quarry	Upper Oligocene - lower Miocene	Al Faidiyah	Faidia Limestone	7 6 5							Ulst.2 Ulst.1 Uu	The upper part is limestone, yellowish, medium hard, medium grained, with gypsum crystals, quartz grains, and bryozoans, glauconite grains, and slightly dolomitized The lower part is glauconitic limestone, yellowish to greenish, medium hard, and medium grained, with common, bryozoans, showing well orientation, echinoderm fragments, and slightly dolomitized.
			Faidia Clay	4 3 2 1 0							Um Ul Us	Us, Ul, Um, and Uu;Clay dark green, blocky, with fine quartz grains, gypsum, dolomite crystals, and muscovite flakes

Figure (4.11) Log of the Al Faidiyah Formation, Umm Ar Razam Quarry
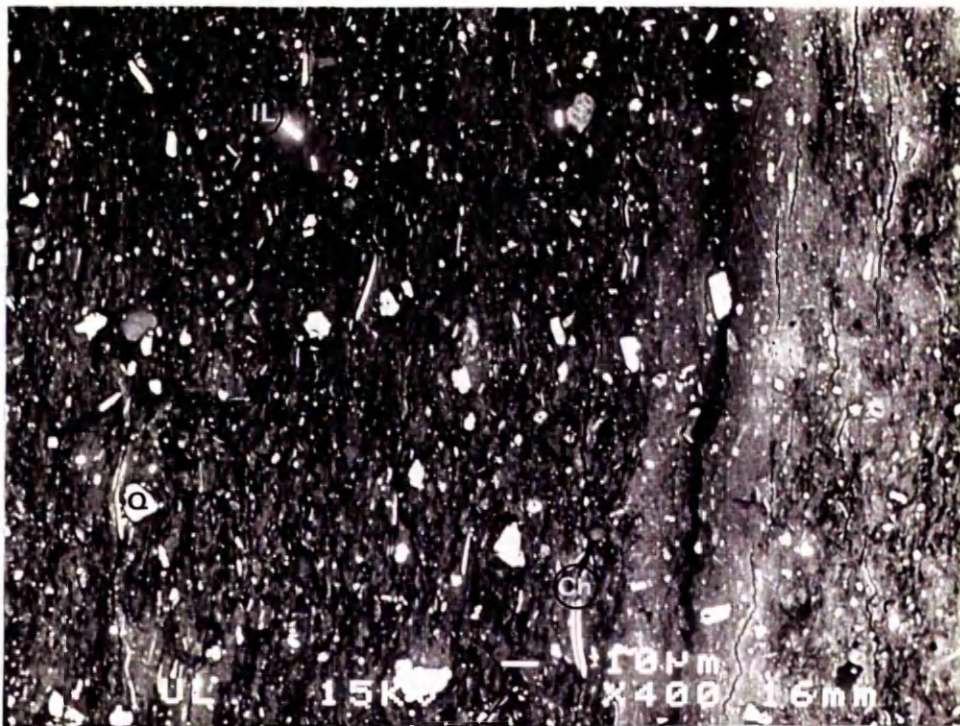
Plate (4.33) Scanning electron micrograph (BSE) of polished thin section of the Faidia Clay Member (UL), Al Faidiyah Formation. Showing quartz grains (Q), chlorite (Ch) and ilmenite (IL), all set in a matrix of clay.

Plate (4.34) Transverse cross section of bryozoan with regular hexagonal shaped chambers or cellular structure, Al Faidiyah Formation (ULst.1). Field of view = 6 mm, (PPL).

4.4.2 Ar Rajmah Formation (Middle Miocene):

The Ar Rajmah Formation is divided into two members: the Benghazi and Wadi Al Qattarah Members. This divison is based on the differences in lithology and faunal content (Klen, 1974; Rohlich, 1974).

4.4.2.1 Benghazi Member:

The Benghazi Member comprises mainly fossiliferous, dolomitic limestone to calcitic dolomite which is white to yellowish, hard to medium hard (Figures 4.12, 4.13, and 4.14) and with an abundance of fossils including large echinoids (Plates 4.35 and 4.36), sometimes bored (Plate 4.37), bivalves e.g. Pectinids (Plate 4.38) and gastropods. There is an abundance of coralline algae and one species of coral (*Tarbellastraea sp.*), in the lower part of the member in Benghazi Cement Quarry (Plate 4.39). It also contains brachiopods and echinoid spines, bryozoans and foraminifers. The upper part of the member (Wadi Al Faj Quarry) is frequently oolitic. Celestite is also observed (see Chapter 9).

Dolomite:

Dolomite is common in the Benghazi Member, in varying amounts. The lower and upper parts of the member contain about 2-8 % dolomite whereas in the middle part (Ar Rajmah Quarry), there is 10 – 80 % dolomite. Generally dolomite crystals were present as limpid euhedral crystals with a planar (idiotopic), inequicrystalline (micron to decimicron in size) fabric (Plate 4.40). It occurs both as fabric selective replacement of the carbonate mud matrix and as a cement. Grains of primary high-Mg calcite (HMC), such as red algae (Plates 4.41 and 4.42), foraminifers, and echinoderm fragments are often more susceptible to dolomitization than low-Mg calcite (LMC); (Buchbinder, 1979; Armstrong *et al.*, 1980; Sibley, 1980; Tucker, 1991). Mimetically replaced allochems were found, which show good preservation of the depositional fabric of the original limestone. Some dolomite crystals have a hollow centre (Plate 4.43). This may be the result of complete removal of metastable dolomite and/or more soluble calcite zones (Sibley, 1982; Ward *et al.*, 1985; Theriault *et al.*, 1987).

Calcite Cements:

There are four types of cement observed in the Ar Rajmah Formation;

- Equant spar drusy mosaic (Plate 4.44).

- Syntaxial calcite overgrowths.

- Poikilotopic calcite spar (Plate 4.45).

- Isopachous cement (Plate 4.48).

Porosity:

Overall, the Benghazi Member is quite porous and point count estimates of porosity range from 4 to 38 %. Pore types observed include primary interparticle and intraparticle porosity as well as vuggy and mouldic (Plate 4.46). Vugs are the most commonly encountered pore type. Some solution porosity and mouldic types are filled partially by calcite crystals (reduced porosity) (Plate 4.47).

4.4.2.2 Wadi Al Qattarah Member:

This member occurs close to the main road to Dreyanah Al Abyar (Fig 4.1, location no.4). It is composed of hard, white, porous, oolitic limestone, with gypsum in the upper part of the member (Figure 4.8). Thin sections show grainstone texture with ooids, and superficial ooids. Isopachous cement is observed allowing some compaction, but preserving most of the primary depositional intergranular porosity (Plate 4.48). This circumgranular calcite crust cement is characteristic of phreatic precipitation (Moore, 1989). Gypsum occurs in the upper part of the member together with quartz grains, and very minor amounts of scattered micron sized dolomite crystals, filling fractures.

Location	Age	Formation	Member	Meters	Lithology	Sedimentary structure — Texture					Location of samples	Description
						MUDST	WKEST	PKST	GRNST	BNDST		
Benghazi cement Quarry	Quaternary			26.8 26 25 24 23 22							LB8 LB7 LB6	Weathering Clay (terra rosa soil)
	Middle Miocene	Ar Rajmah	Benghazi (Lower part)	21 20 19 18 17 16 15 14 13 12 11 10 9 8 7 6 5 4 3 2 1 0							LB5	Packstone, whitish to grey, medium grained, hard and partially dolomitized
											LB4	Packstone, white to yellowish, medium hard, with coralline algae and corals
											LB3	Packstone, whitish to yellowish, coarse grained, medium hard, moulds of bivalves, gastropods, bryozoans
											LB2	Packstone, white to yellowish, with corals, mouldic organisms, gastropods, celestite and Strontianite
											LB1	Packstone, yellowish to gray, medium hard, with large echinoids, coralline algae, oyster fragments and *Nummulites*.

Figure (4.12) Log of the Benghazi Member (Lower part) of Ar Rajmah Formation, Benghazi cement Quarry.

Location	Age	Formation	Member	Meters	Lithology	Sedimentary structure / Texture					Location of samples	Description
						Mudst	Wkest	Pkst	Grnst	Bndst		
Ar Rajmah Quarry	Middle Miocene	Ar Rajmah	Benghazi (Upper part)								UBB2MUP	Calcitic dolomite, white to grayish in colour, hard, fine to medium grained
											UBB2U	Calcitic dolomite, grayish, hard, with shell fragments of bivalves (3 mm in size)
											UBB2L	Calcitic dolomite, white to grayish, m. hard, with moulds of bivalves
											UBB1	Dolomitic limestone, white to grayish, hard, with coralline algae and bivalves
											UBA3U	Dolomitic limestone, white to grayish, hard, with moulds of bivalves
											UBA3L	Calcitic dolomite, grayish, hard, fine to medium grained
											UBA2	Calcitic dolomite, white to grayish, hard, medium grained, with bivalves (4 mm in diameter max.)
											UBA1	Dolomitic limestone, fossiliferous, white, hard, with moulds of bivalves, gastropods and quartz grain

Figure (4.13) Log of the Benghazi Member (middle part) of Ar Rajmah Formation, Ar Rajmah Quarry

121

Location	Age	Formation	Member	Meters	Lithology	Sedimentary structure / Texture (Mudst, Wkest, Pkst, Grnst, Bndst)	Location of samples	Description
Wadi Al Faj Quarry	Middle Miocene	Ar Rajmah	Benghazi	5–4			RQ3	Highly fossiliferous -limestone, yellowish, coarse grained, hard, with ooids, moulds of bivalves and gastropods
				3			RQ2	Sandy limestone, highly fossiliferous, white to yellowish, hard
				2			RQ1U	Highly fossiliferous Oolitic limestone, white, hard, coarse grained, with moulds of bivalves and gastropods
				1–0			RQ1L	Dolomitic limestone, white, hard, fine grained, with moulds of bivalves (7 cm in diameter) and quartz grain

Figure (4.14) Log of the Benghazi Member (upper part) of Ar Rajmah Formation, Wadi Al - Faj Quarry

4.5 Weathering Clay (Quaternary):

Quaternary deposits rest on the Middle Miocene sediments at the Benghazi Cement Quarry, and mainly consist of terra rosa soil (weathering clay), reddish to brown in colour (Plates 4.49 and 4.50). It consists of three layers, the middle layer mostly contains coarse to fine grained alluvial sediments. This weathering clay is very important for cement making, and it is one of the essential major raw materials when mixed with limestone rocks in the Benghazi Cement Quarry.

Plate (4.35) A massive limestone bed of the Benghazi Member (lower part), Benghazi Cement Quarry. Displays a; LB1, b; LB2, c; LB3, d; LB4, e; LB5.
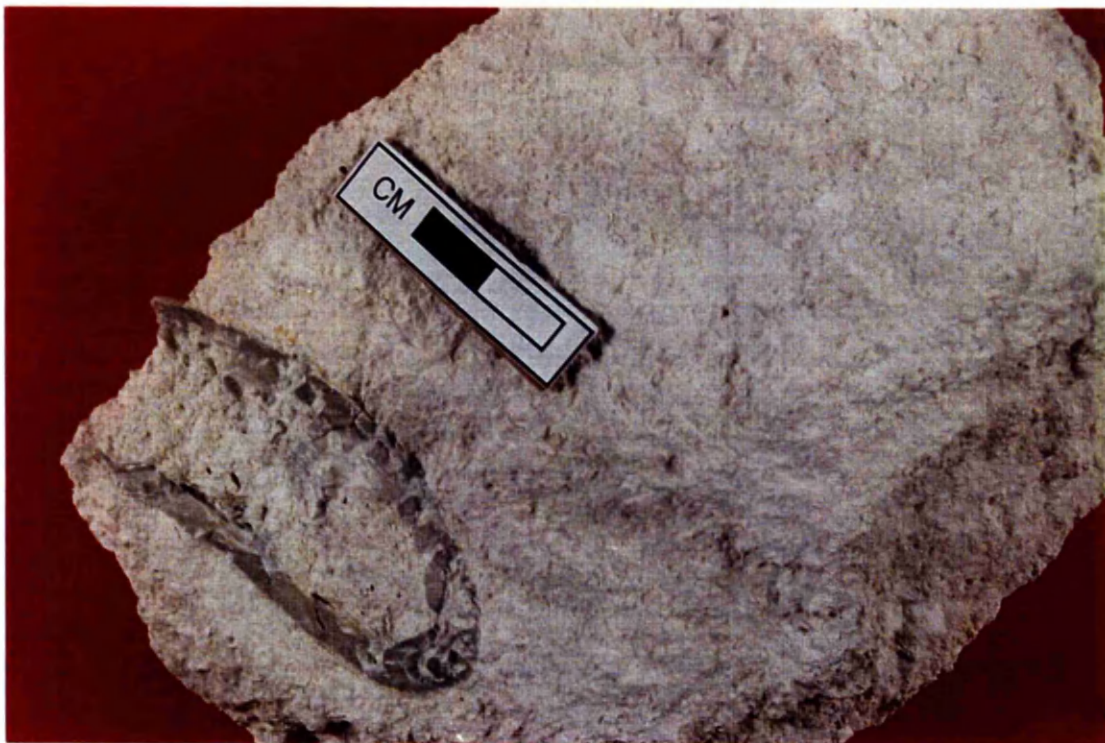
Plate (4.36) Echinoids, Benghazi Member (lower part) of the Ar Rajmah Formation, Benghazi cement Quarry.
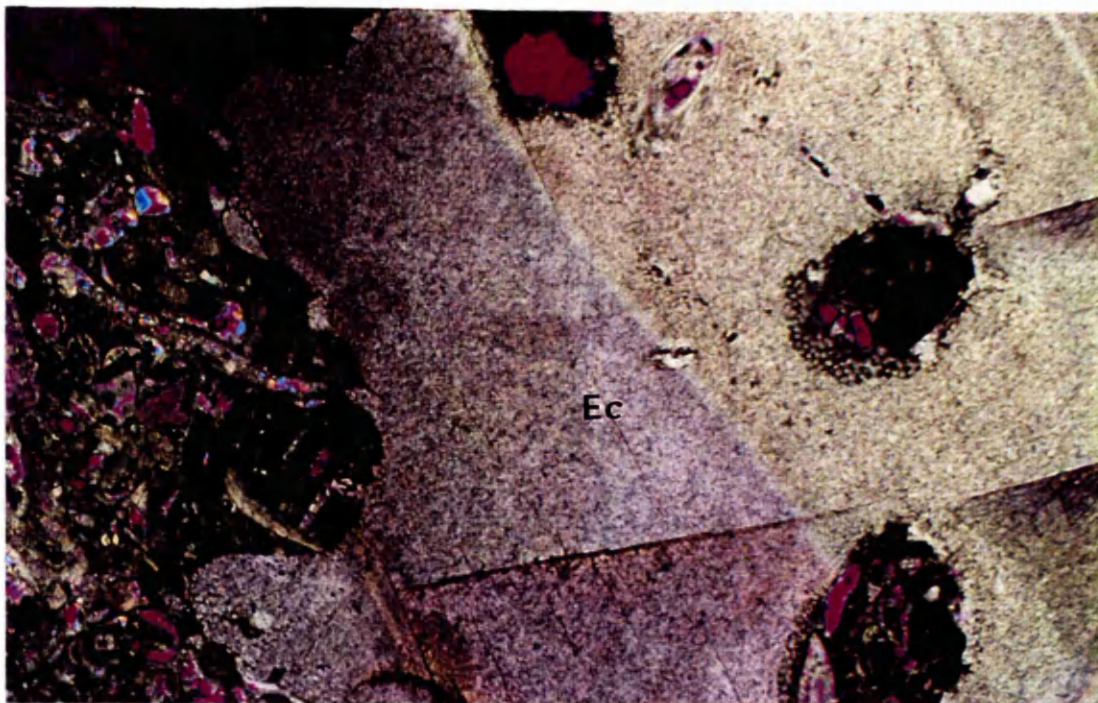
Plate (4.37) Large echinoderm fragment (Ec), with borings, filled with carbonate matrix and bioclasts, Benghazi Cement Quarry. Field of view = 6 mm, (XPL, with gypsum accessory plate).

Plate (4.38) Pectinid, Benghazi Member (UBA1) of the Ar Rajmah Formation, Ar Rajmah Quarry.
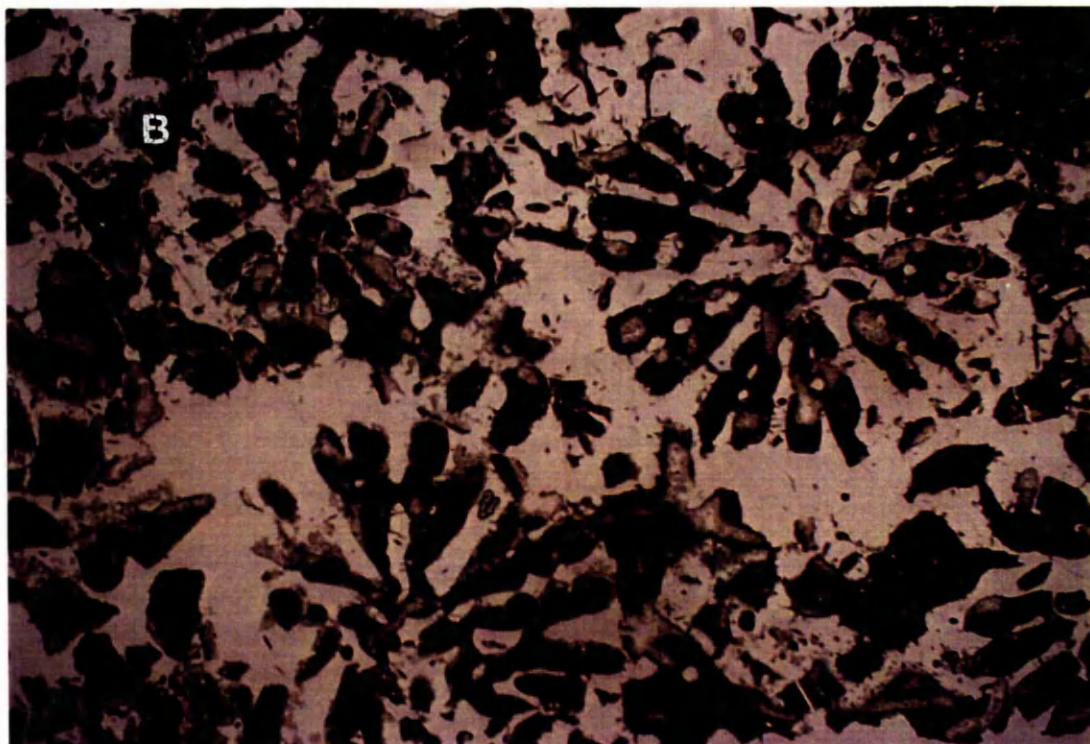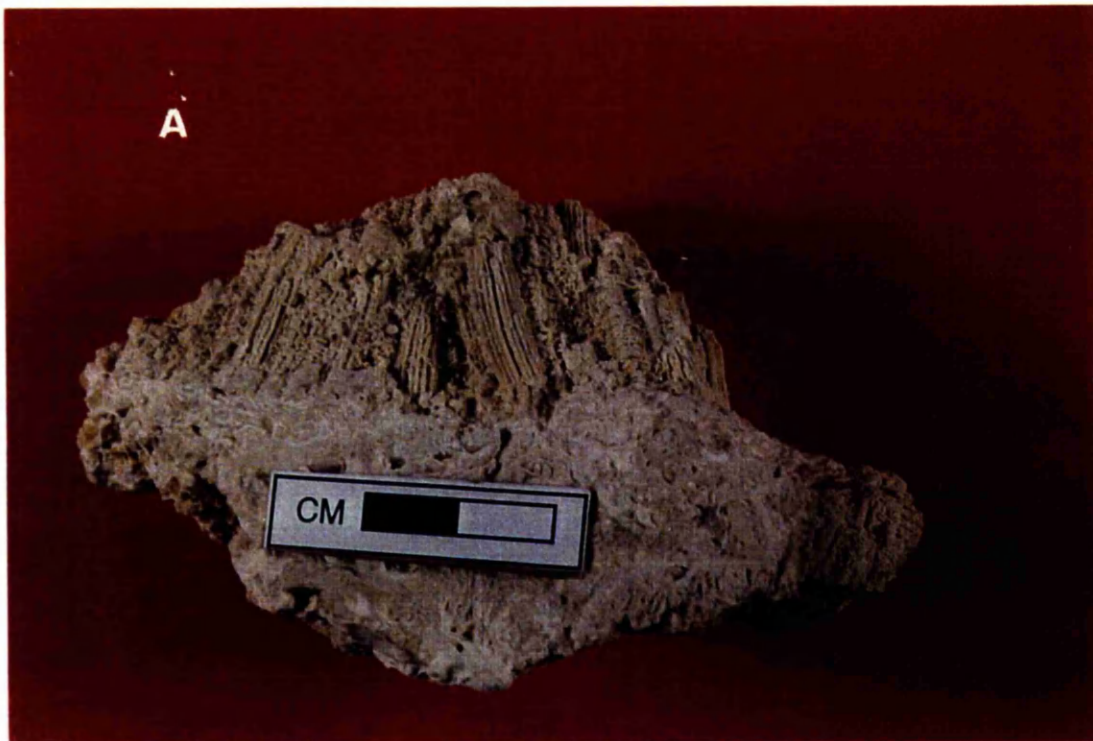
Plate (4.39) A). Side view of coral *Tarbellastraea*, also illustrating the coralline algae.

   B). Section of the same coral (A) under the microscope. Field of view = 6
   mm, (PPL)
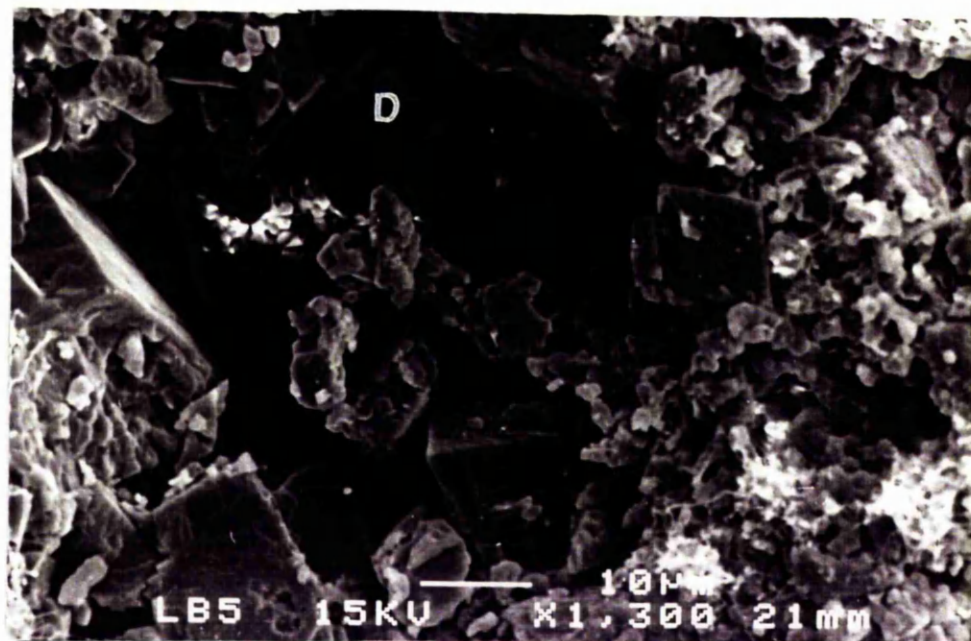
Plate (4.40) Scanning electron micrograph of the void-filling dolomite, Ar Rajmah Formation (LB5), Benghazi Cement Quarry.
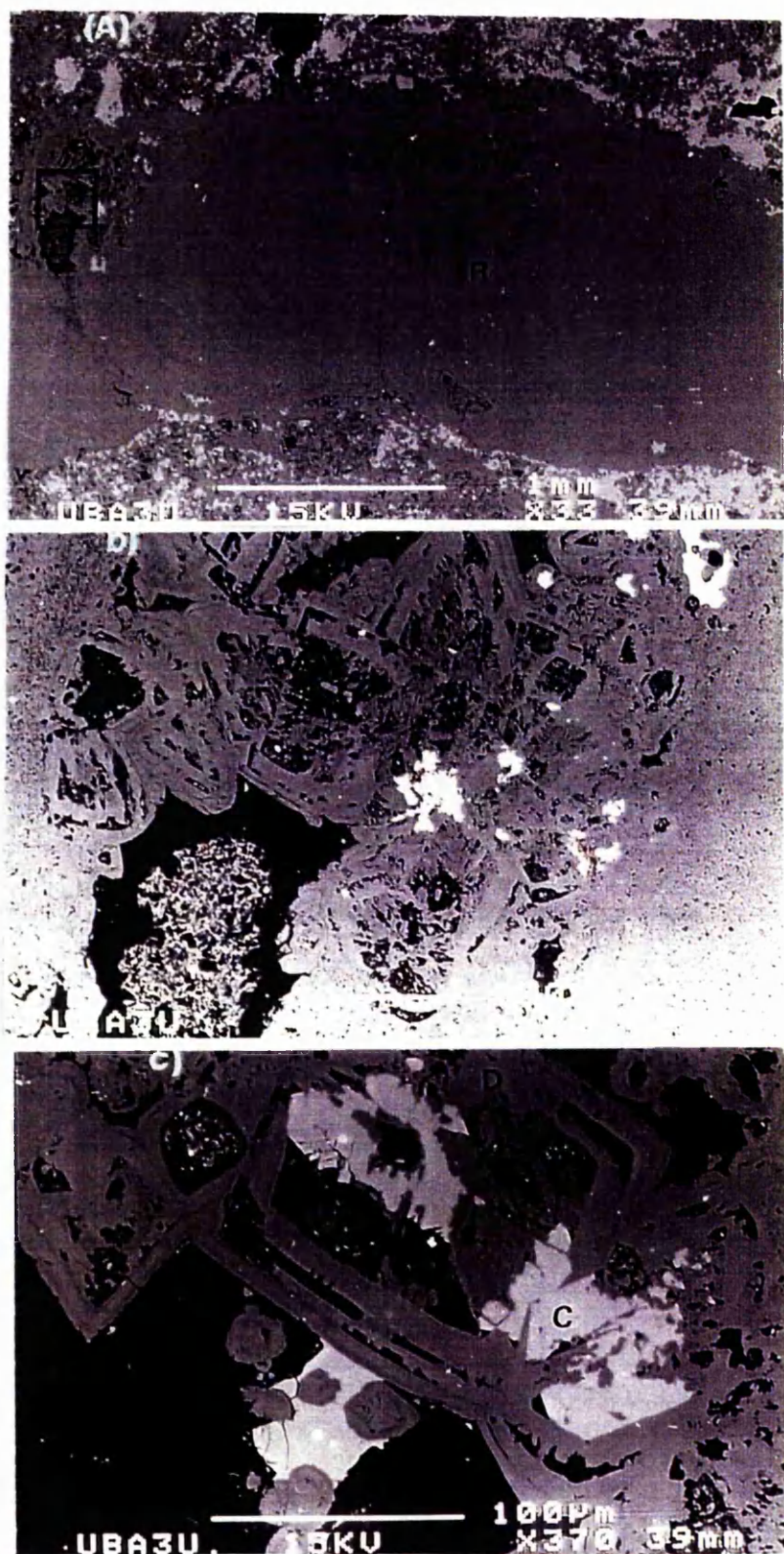
Plate (4.41) Scanning electron micrograph. a). Red algae (R), b and c close up view showing some euhedral dolomite (D) crystal cores filled with calcite (C). Ar Rajmah Quarry.
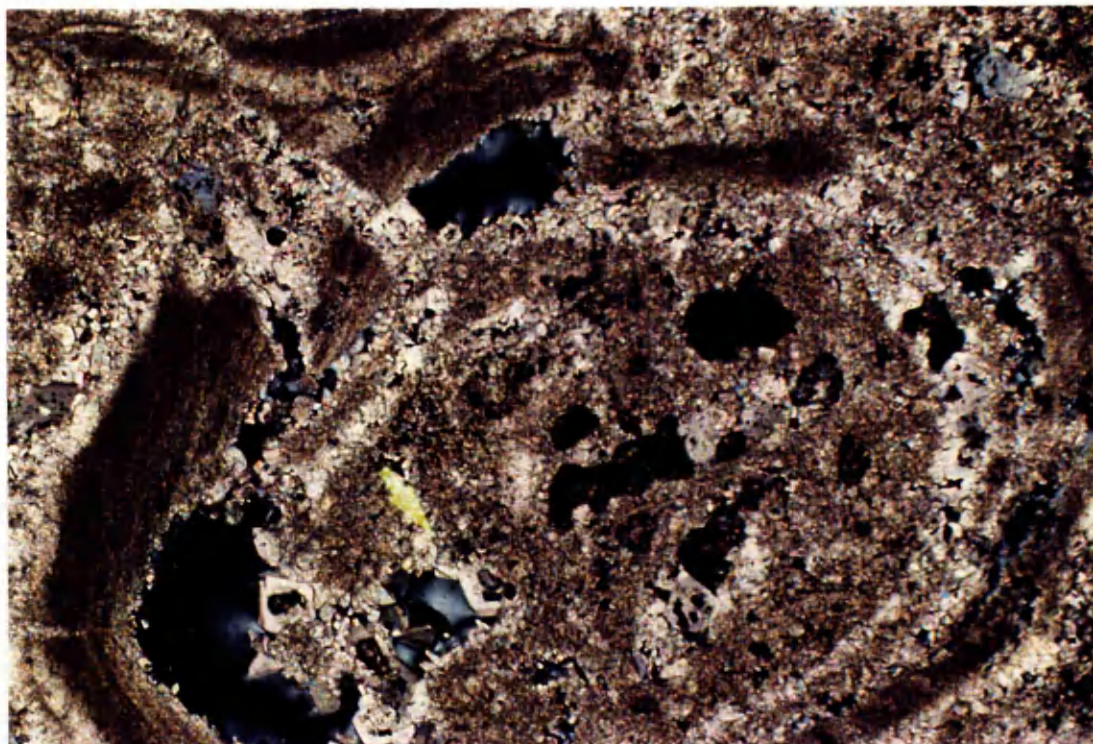
Plate (4.42) Showing destructive fabric of red algae by dolomite crystals (Arrow) to fine cellular structure which have been infilled by calcite. Field of view = 1.3 mm, (XPL).
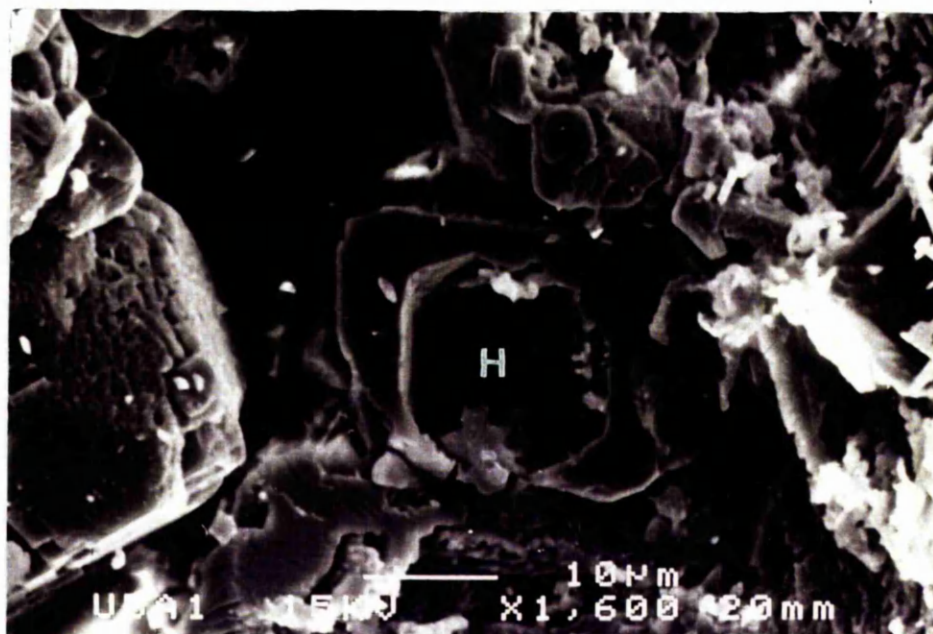
Plate (4.43) Scanning electron micrograph showing hollow (H) within dolomite rhombs (metastable center of dolomite dissolved leaving more stable stoichiometric rim), Ar Rajmah Formation (UBA1), Ar Rajmah Quarry.
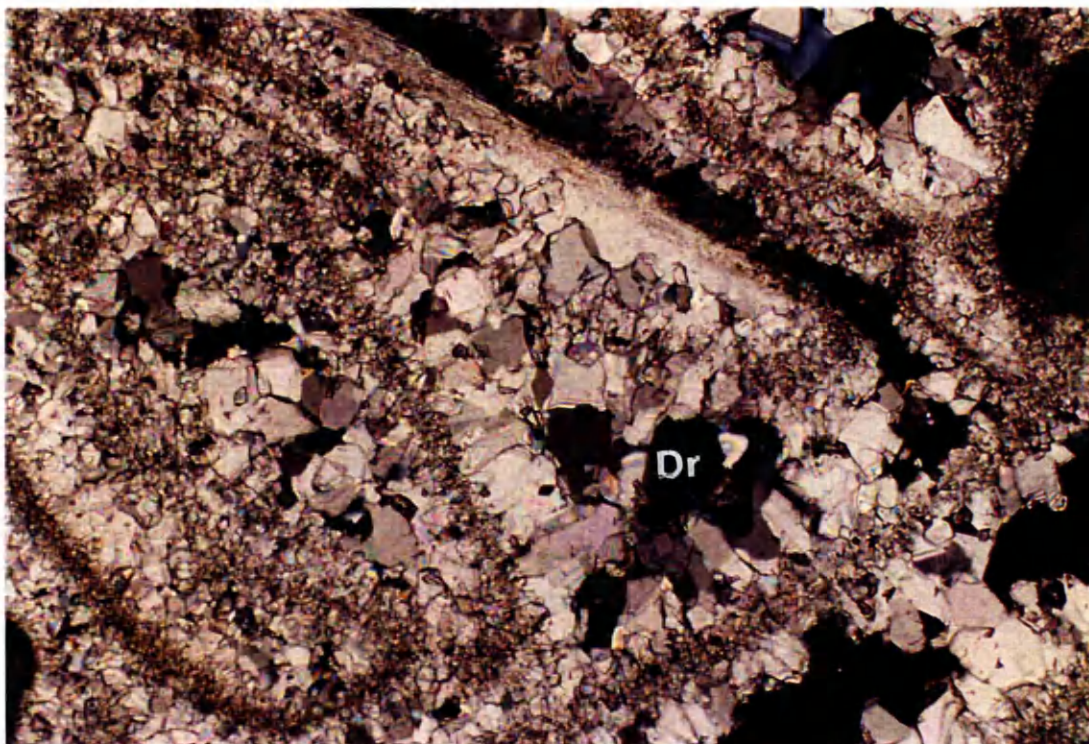
Plate (4.44) Showing drusy calcite spar (Dr), increasing in crystal size towards the cavity center, Ar Rajmah Formation (RQ3), Wadi Al Faj Quarry. Field of view = 1.3 mm, (XPL).
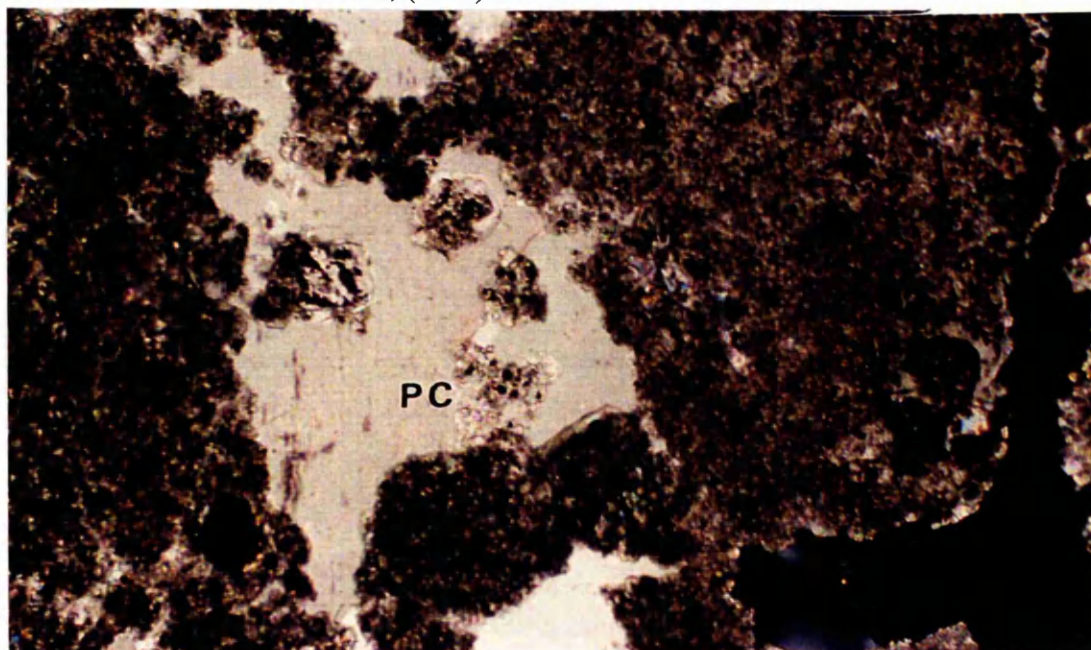
Plate (4.45) Showing poikilotopic calcite spar (Pc), large enveloping dolomite crystals, Ar Rajmah Formation (UBA1), Ar Rajmah Quarry. Field of view = 1.3 mm, (XPL).
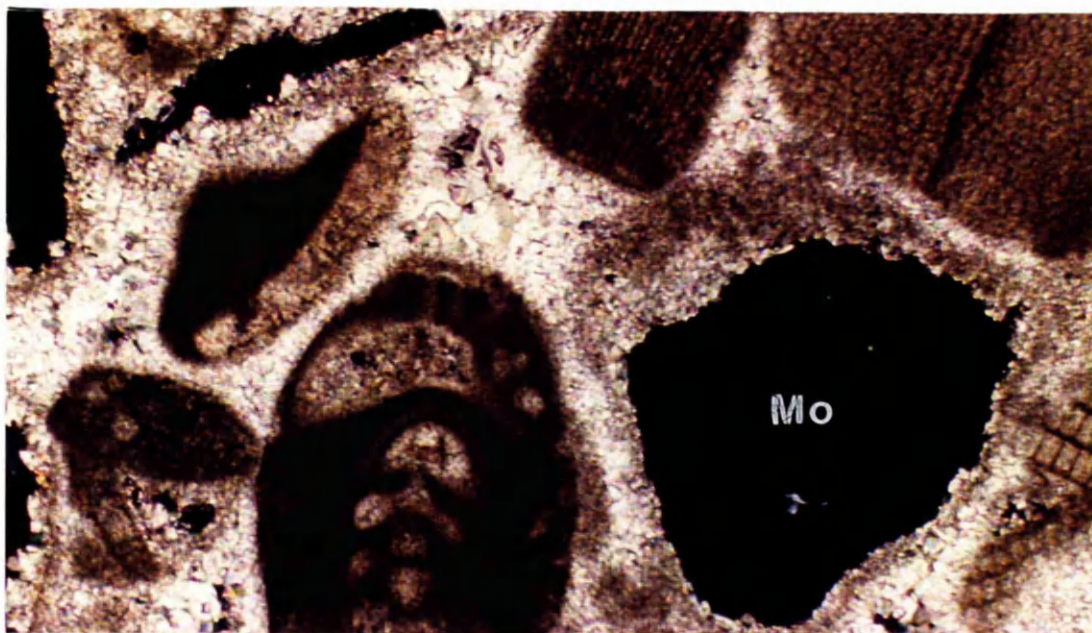
Plate (4.46) Showing mouldic porosity (Mo), Ar Rajmah Formation (RQ3), Wadi Al Faj Quarry. Field of view = 1.3 mm, (XPL).
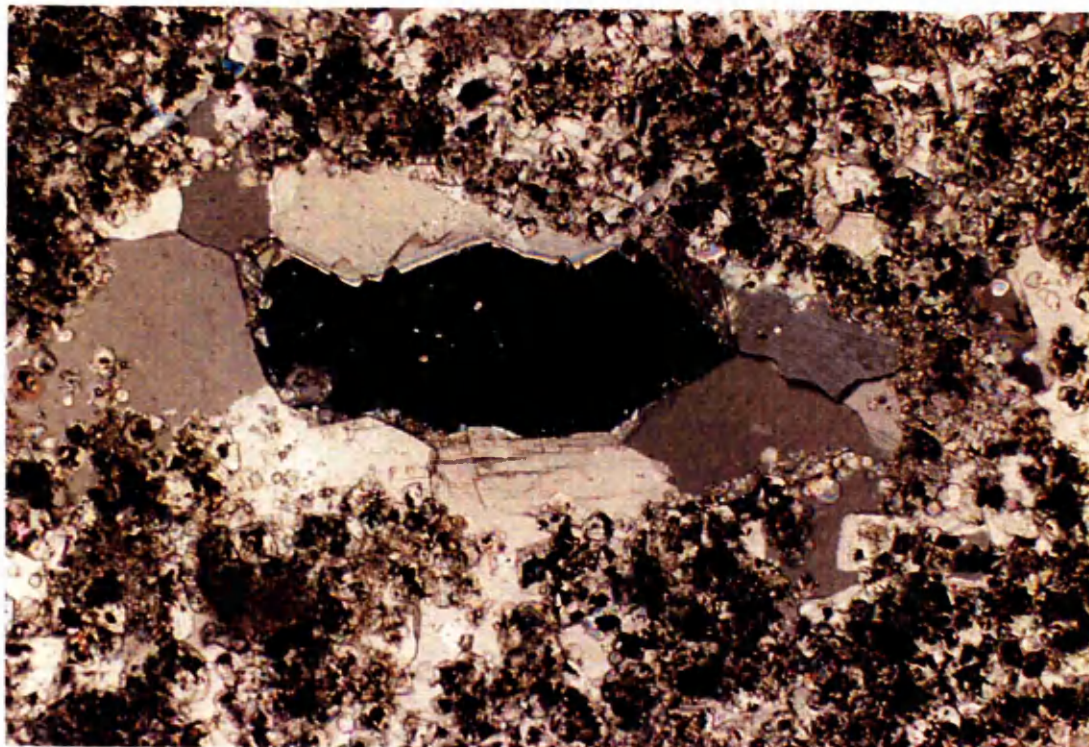
Plate (4.47) Showing pore partially filled by calcite spar (reduced porosity), Ar Rajmah Formation (UBA3L), Ar Rajmah Quarry. Field of view = 1.3 mm, (XPL).
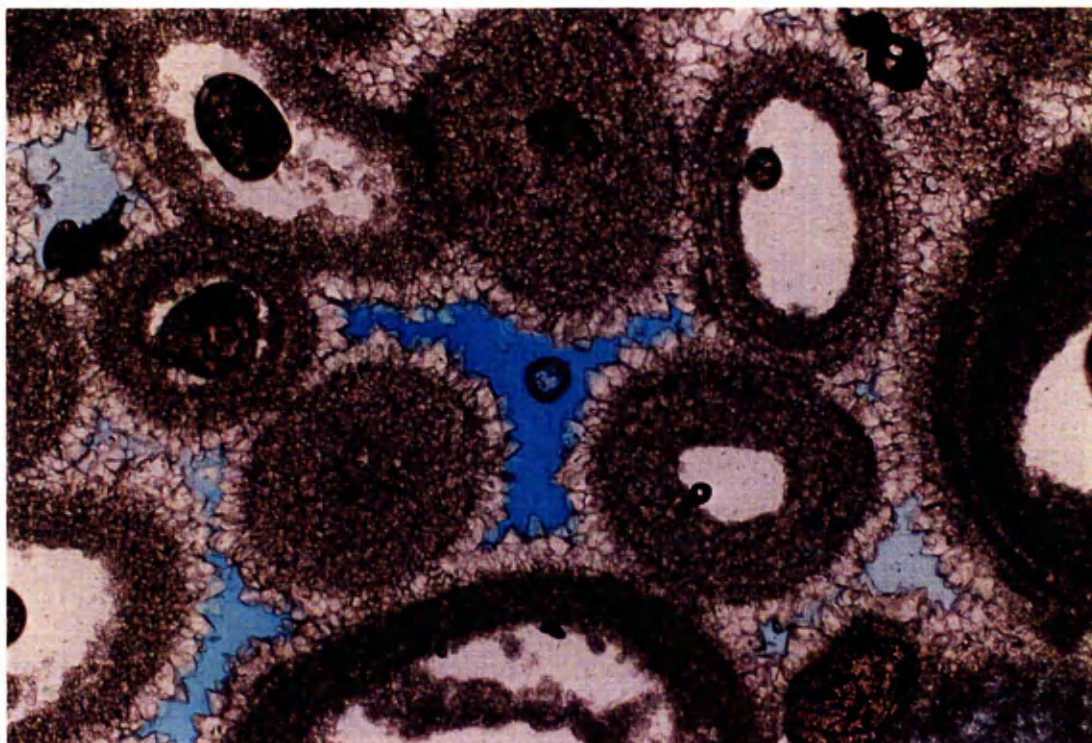
Plate (4.48) Ooid grainstone with isopachous cement (impregnated with blue-dye resin), Wadi Al Qattarah Member (QM1). Field of view = 1.3 mm, (PPL).
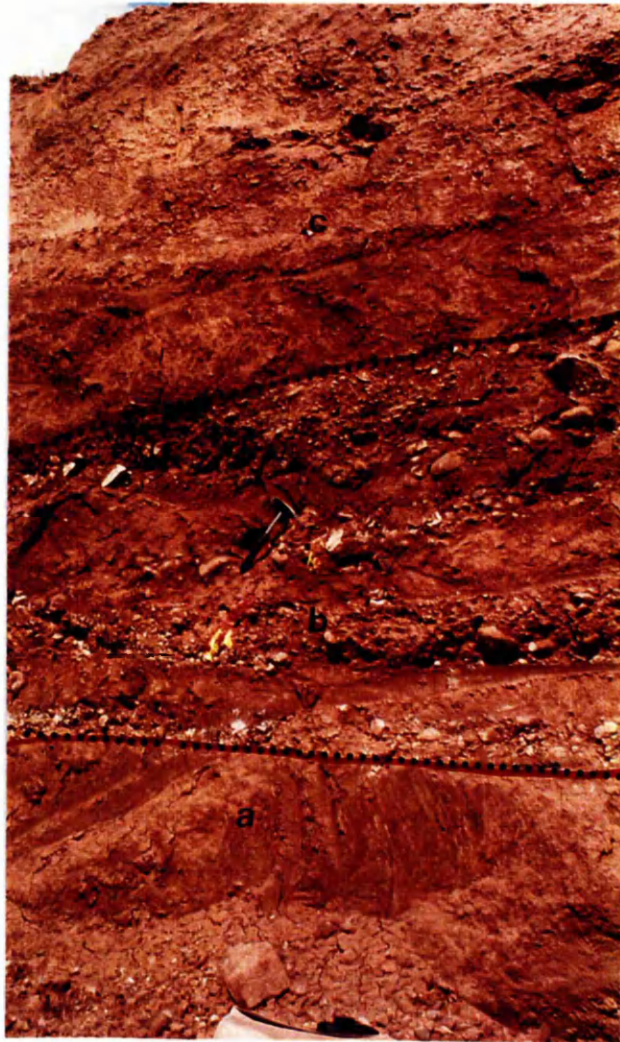
Plate (4.49) Terra rosa soil (overburden), with three layers (a; LB6, b; LB7, and c; LB8), Benghazi Cement Quarry.
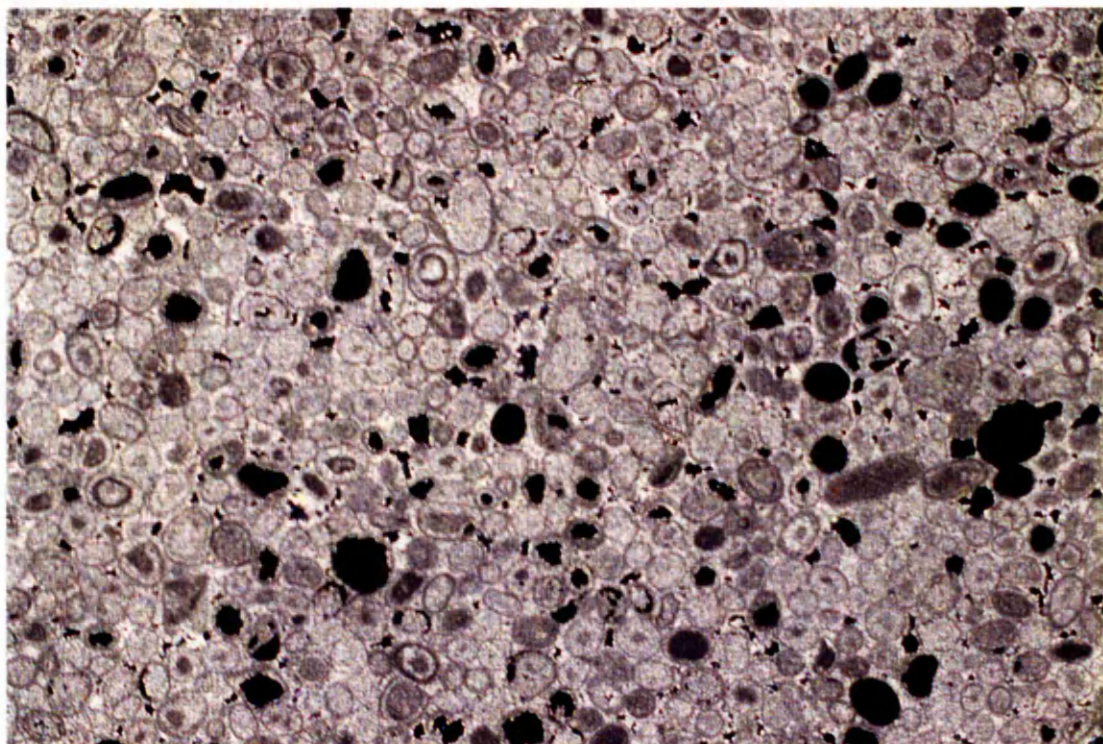
Plate (4.50) Grainstone with ooids, superficial ooids (LB7) and mouldic porosity, Benghazi Cement Quarry. Field of view = 6 mm, (XPL).

Chapter 5

LIMESTONE GEOCHEMISTRY

5.1 Introduction:

Limestone consists primarily of calcite ($CaCO_3$). It is commonly contaminated with other carbonate minerals which may be present, including dolomite $CaMg(CO_3)_2$, less commonly magnesite ($MgCO_3$), or siderite ($FeCO_3$), and / or non-carbonate minerals such as quartz, clay minerals and other silicates. Chemical analyses of the major oxides (SiO_2, Al_2O_3, Fe as Fe_2O_3, MgO, CaO, S, K_2O, TiO_2, MnO, P_2O_5), and 16 trace elements (Nb, Zr, Y, Sr, Rb, Zn, Cu, Ni, Cr, Ce, Nd, V, Ti, La, Ba, Sc), were carried out by X-ray fluorescence spectrometry (XRF), and are summarised in Table 5.1. Insoluble residue was determined with the classical chemical method as explained at the end of this chapter. Mineralogical identifications and analyses have been done, using electron probe microanalysis (EPMA), scanning electron microscopy (SEM), and X-ray diffractometry (XRD).

From a commercial viewpoint, the main impurities such as dolomite, quartz, and clay minerals (montmorillonite, kaolinite and glauconite) throughout the limestone deposits were found in some formations in variable amounts. Their distributions are very important factors in grade control for the production of very high or low quality limestone.

Harries (1979) classified the limestones according to purity as follows;

Categories of limestone	Composition % $CaCO_3$
Very high purity	>98.5
High purity	97.0-98.5
Medium purity	93.5-97.0
Low purity	85.0-93.5
Impure	<85.0

The formations in the study area vary from very high purity to impure limestones (Appendix A.5.1–A.5.9). Two different characteristics are the presence in some cases of a high strontium content (reflecting the formation of celestite and strontianite minerals), and dolomitic limestone to calcitic dolomite rocks (Tucker, 1991 classification). Both are observed in the Benghazi Member (lower Member) of the Ar Rajmah Formation.

Table (5.1) Summary data for major and trace elements in the rock types from study area (selected analyses: full data in Appendix A5)

Sample no.	Formations (Eocene to Miocene)								
Oxides	Apollonia	Darnah	Al Bayda		Al Abraq	Al Faidiyah		Ar Rajmah	
(wt. %)	(AH)	(DE4)	Shahhat Marl M.* (SMP)	Algal Lst.** M.* (Algal Lst. L.)	(A6)	Faidia Clay M.* (US)	Faidia Lst.** M.* (UF3)	Benghazi M.* (LB2)	Wadi Al Qattarah M.* (QM)
SiO_2	0.24	0.00	16.03	0.00	4.55	23.57	0.00	0.00	0.00
Al_2O_3	0.00	0.00	5.12	0.00	1.2	10.30	0.00	0.00	0.00
Fe_2O_3	0.00	0.00	1.12	0.01	0.87	5.10	0.00	0.00	0.00
$MgCO_3$	1.63	0.67	3.93	1.14	2.85	2.10	0.74	2.61	1.44
$CaCO_3$	98.67	100.20	72.86	99.37	90.43	56.1	100.07	97.7	99.41
S	0.00	0.00	0	0.00	0.00	0.00	0.00	0.02	0.00
K_2O	0.00	0.00	0.23	0.00	0.12	0.62	0.00	0.00	0.00
TiO_2	0.00	0.00	0.21	0.00	0.10	1.03	0.00	0.00	0.00
MnO	0.01	0.01	0	0.06	0.00	0.05	0.02	0.09	0.05
P_2O_5	0.01	0.01	0.08	0.01	0.01	0.02	0.04	0.00	0.00
Total	100.56	100.89	99.58	100.59	100.13	98.89	100.87	100.42	100.90
CaO	55.26	56.11	40.80	55.65	50.64	31.42	56.04	54.70	55.67
MgO	0.96	0.40	2.32	0.67	1.68	1.24	0.44	1.54	0.85
Trace elements (ppm)									
Nb	0	0	9	3	10	166	0	0	2
Zr	221	35	106	58	113	790	16	719	63
Y	38	42	52	41	45	144	39	34	37
Sr	2408	329	686	605	532	314	163	8042	726
Rb	41	42	54	43	49	177	44	41	42
Zn	0	0	31	0	12	254	4	0	0
Cu	9	17	13	5	10	40	29	6	12
Ni	0	0	0	0	0	110	0	0	0
Cr	21	28	89	24	64	449	0	0	0
Ce	27	0	54	73	20	410	15	26	12
Nd	0	0	15	0	0	174	3	0	0
V	12	3	51	18	73	435	3	14	0
La	0	15	9	0	15	173	11	4	21
Ba	0	0	0	0	0	21	0	0	17
Sc	97	76	66	87	74	53	107	79	101

*M.- Member
** Lst.-Limestone

The aims of this geochemical study are:

- To indicate the geochemistry of the dominant formations (Eocene, Oligocene, and Miocene), in the Jabal Al Akhdar area, and to show the variety in major and trace elements from one formation to another.

- To determine the percentage of insoluble residues of each Formation, and with geochemical data to classify the grade for production (very high or low quality).

- To check the petrographic investigations, by relating the major and trace elements to the original minerals.

The study is divided into two parts: 1) Whole rock geochemistry, and 2) Mineral chemistry and mineralogy.

Whole rock geochemistry:

5.2 Major element geochemistry:

According to Brownlow (1996) most carbonate rocks in the study area are either limestones with less than 3 % of MgO, or dolomites with more than 19 % MgO. The dolomites are present in most of the formations of Al Jabal Al Akhdar area, but in different amounts. The presence of impurities not only contributes colouring and grade impurities but may also significantly affect abrasiveness, for example causing excessive wear on papermaking machinery. Abrasiveness decreases as particle size decreases. The evaluation of natural calcium carbonates for some industries is based on an assessment of physical properties. Many carbonate rocks with very high chemical purity (>98.5 %) are unsuitable for filler applications, because of the colour contamination (Morgan, 1994). Many industrial consumers also specify constraints on the amounts of impurities such as SiO_2, MgO, and Fe_2O_3.

5.2.1 Apollonia & Darnah Formations (L. to M. Eocene & M. to U. Eocene):

The ternary system SiO_2-CaO-Al_2O_3 is used to interpret major element data and reference to Portland cement clinker phases. The major constituent in Portland cement clinker after heating is tricalcium silicate (Figure 5.1).

Plotting the data in the ternary system SiO_2–$CaCO_3$– $MgCO_3$ (Figure 5.2) also shows the very high purity of the limestone. Dolomite minerals are present with maximum amounts of 1.6 % of the whole rock volume for the Darnah Formation, and about 2.0 % in the Apollonia Formation. However, mining of high purity limestone will be difficult and uneconomic in the Apollonia Formation due to the presence of chert nodules.
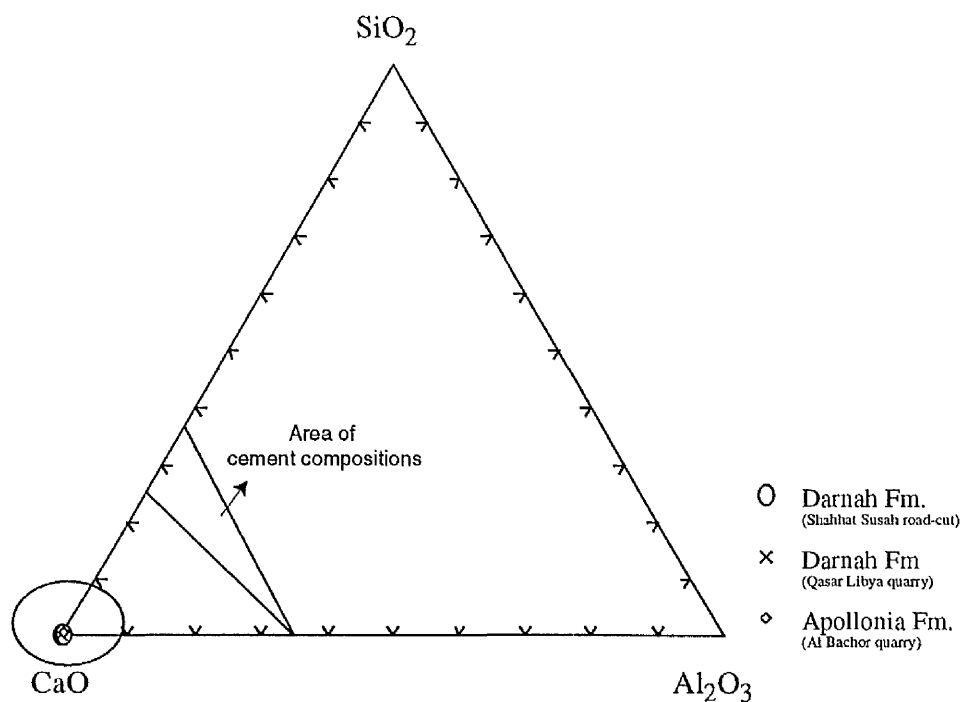
Figure (5.1) SiO_2-CaO-Al_2O_3 Ternary diagram (XRF analyses) of Apollonia, and Darnah Formations (wt. %). Cement compositions from Manning (1995).
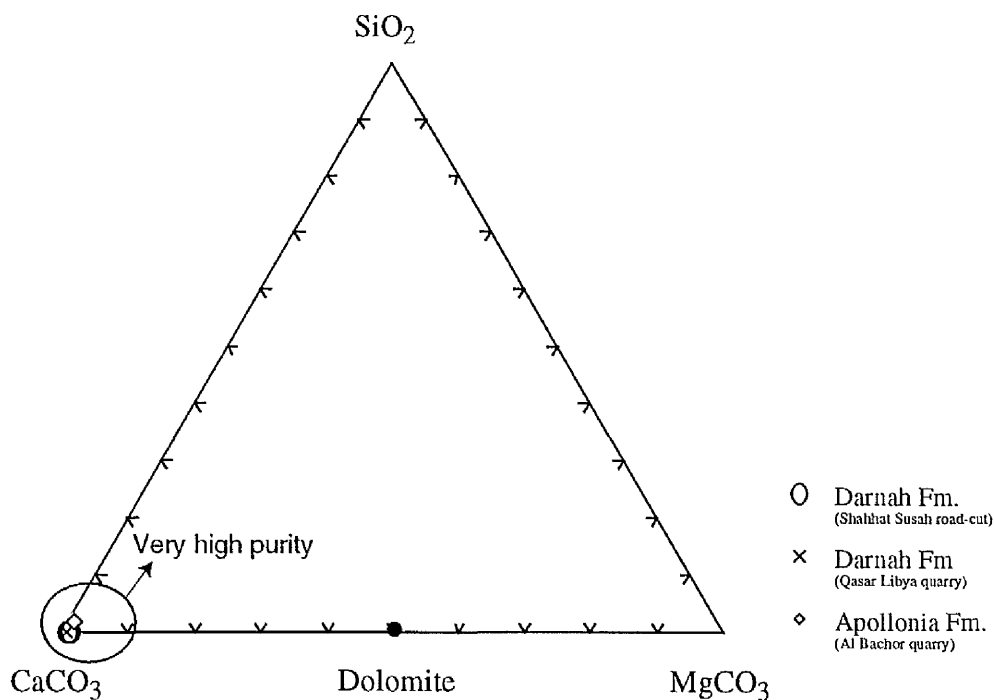
Figure (5.2) SiO_2-$CaCO_3$-$MgCO_3$ Ternary diagram (XRF analyses) of Apollonia, and Darnah Formations, at different localities (mol. %).

5.2.2 Al Bayda Formation (Lower Oligocene):

The Lower Member of the Al Bayda Formation (Shahhat Marl) is high in SiO_2 and Al_2O_3 contents (Figure 5.3). The Upper Member (Algal Limestone) of the Formation in the Shahhat Susah road-cut is higher in SiO_2 and Al_2O_3 contents than the Algal Limestone Member in the Deryanah Al Abyar road-cut. The reason for the higher amount of SiO_2 and Al_2O_3 of the Algal Limestone is due to contamination of the upper sample with the overlying Al Abraq Formation. Plotting in the ternary system SiO_2–$CaCO_3$–$MgCO_3$ (Figure 5.4) shows high Mg content due to the presence of dolomite minerals with 0.6-4.0 % of the whole rock volume. The Shahhat Member contains low purity limestone. The Algal Limestone Member in the Shahhat Susah road-cut contains medium purity, whereas the same Member in the Deryanah Al Abyar road-cut has high purity.

5.2.3 Al Abraq Formation (M. to U. Oligocene):

As observed from the ternary system SiO_2-CaO-Al_2O_3 (Figure 5.5), the Abraq Formation consists of limestone with high SiO_2 and Al_2O_3 contents.

The ternary system SiO_2–$CaCO_3$–$MgCO_3$ (Figure 5.6), shows high Mg content due to the presence of dolomite minerals ranging from 0.6-7.0 % of the whole rock volume.

5.2.4 Al Faidiyah Formation (U. Oligocene – L. Miocene):

The lower Member (Faidia Clay) of the Formation, from the Deryanah Al Abyar road-cut, consists of glauconitic marl with intercalated green clay (Figure 5.7). Plotted in the ternary system SiO_2-CaO-Al_2O_3, the data show highly variable SiO_2 and Al_2O_3 contents. The Al Fatayah and Umm Ar Razam quarries, which mainly consist of greenish calcareous clay, are similar and lie within the range for the formation. The Faidia Limestone Member (the upper part of Al Faidiyah Formation in Al Fatayah quarry) is characterised by very high purity. The equivalent Member in the Umm Ar Razam quarry has lower grade due to intercalations of glauconitic limestone (Figure 5.7).

The ternary system SiO_2–$CaCO_3$–$MgCO_3$ (Figure 5.8) shows high Mg content in both Members due to their dolomite contents, in variable amounts.
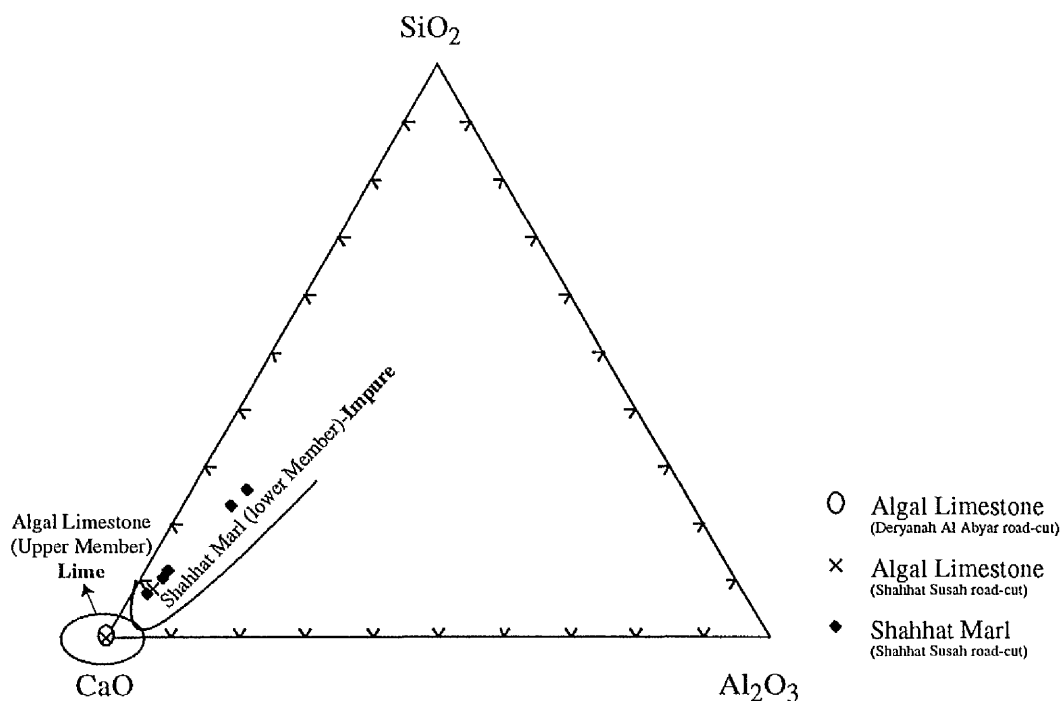
Figure (5.3) SiO_2-CaO-Al_2O_3 Ternary diagram (XRF analyses) of the Al Bayda Formation (wt. %), at different localities.
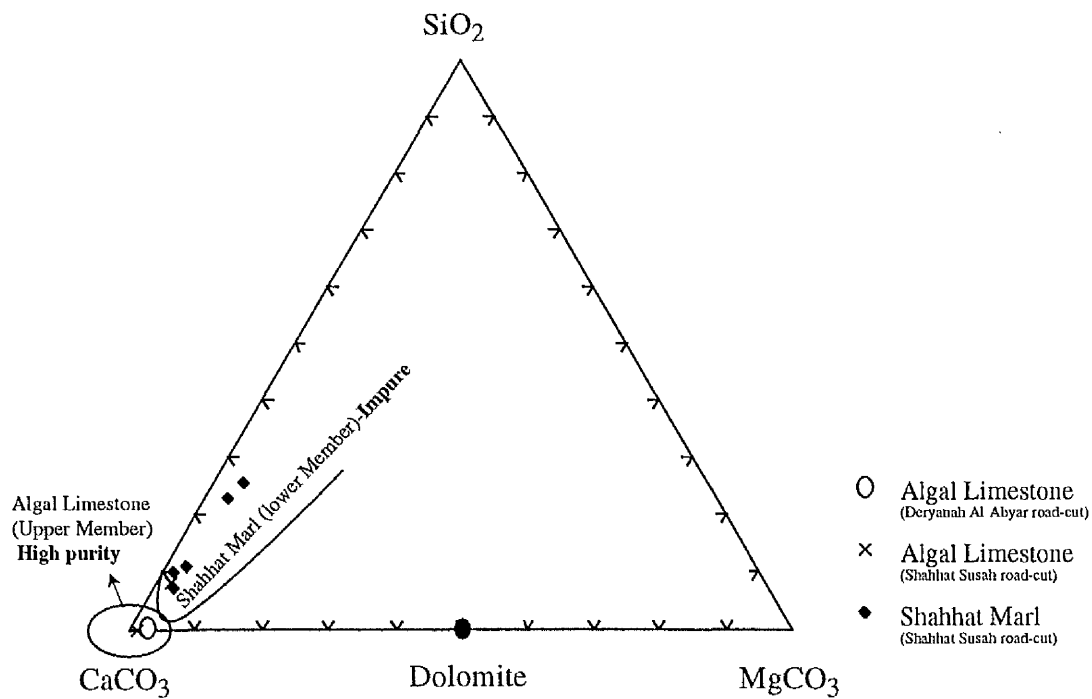
Figure (5.4) SiO_2-$CaCO_3$-$MgCO_3$ Ternary diagram of the Al Bayda Formation (mol. %), at different localities.

141
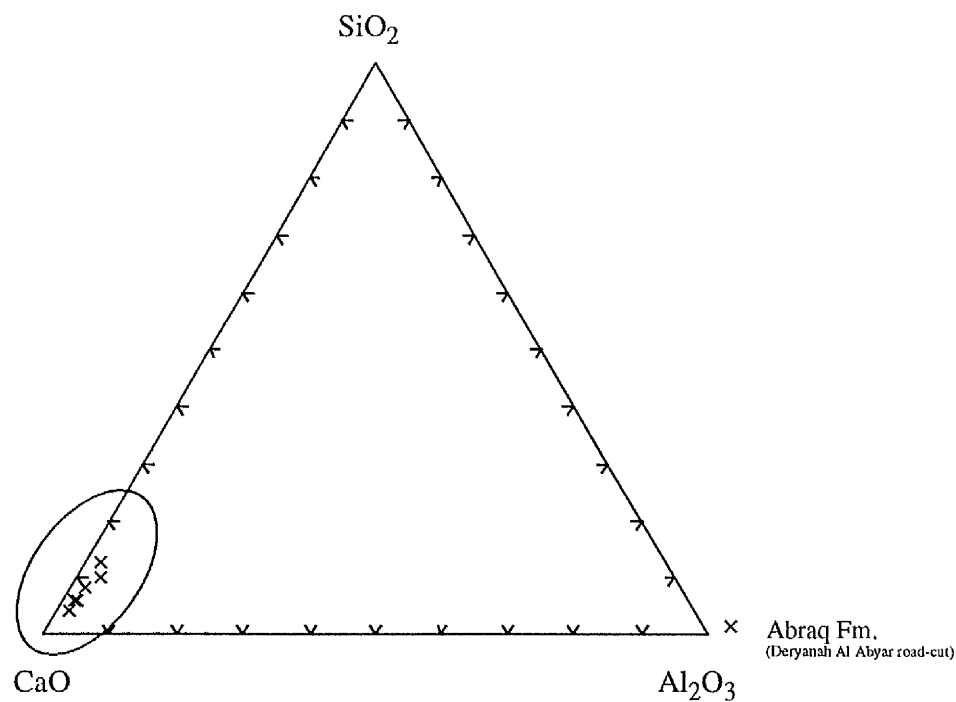
Figure (5.5) SiO_2-CaO-Al_2O_3 Ternary diagram (XRF analyses) of the Al Abraq
Formation (wt. %) (Deryanah-Al Abyar road-cut).
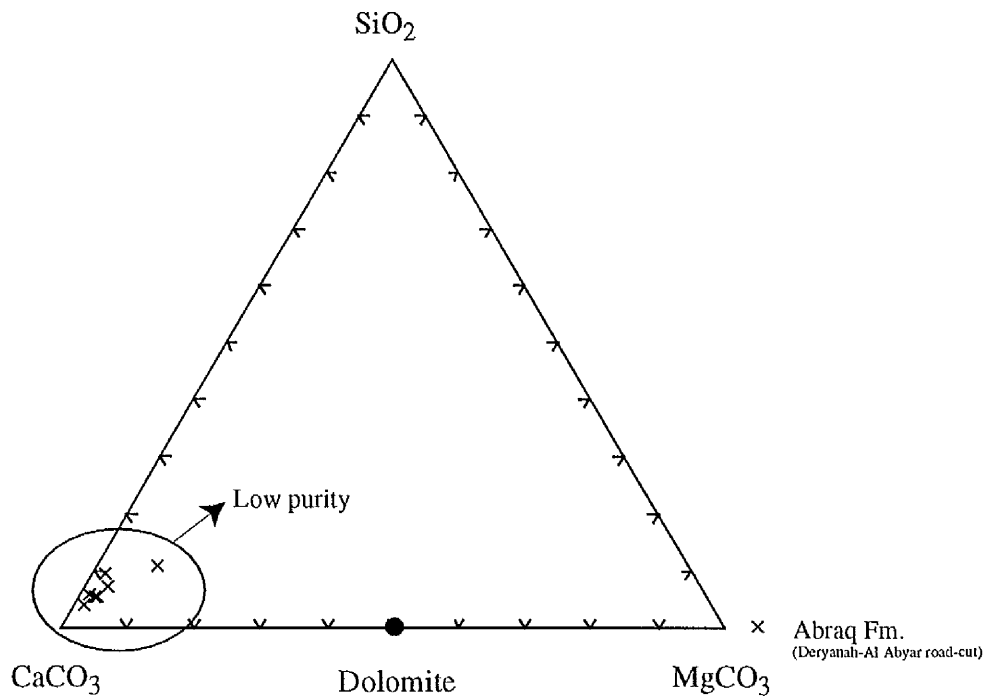
Figure (5.6) SiO_2-$CaCO_3$-$MgCO_3$ Ternary diagram (XRF analyses) of the Al Abraq
Formation (mol. %) (Deryanah-Al Abyar road-cut).
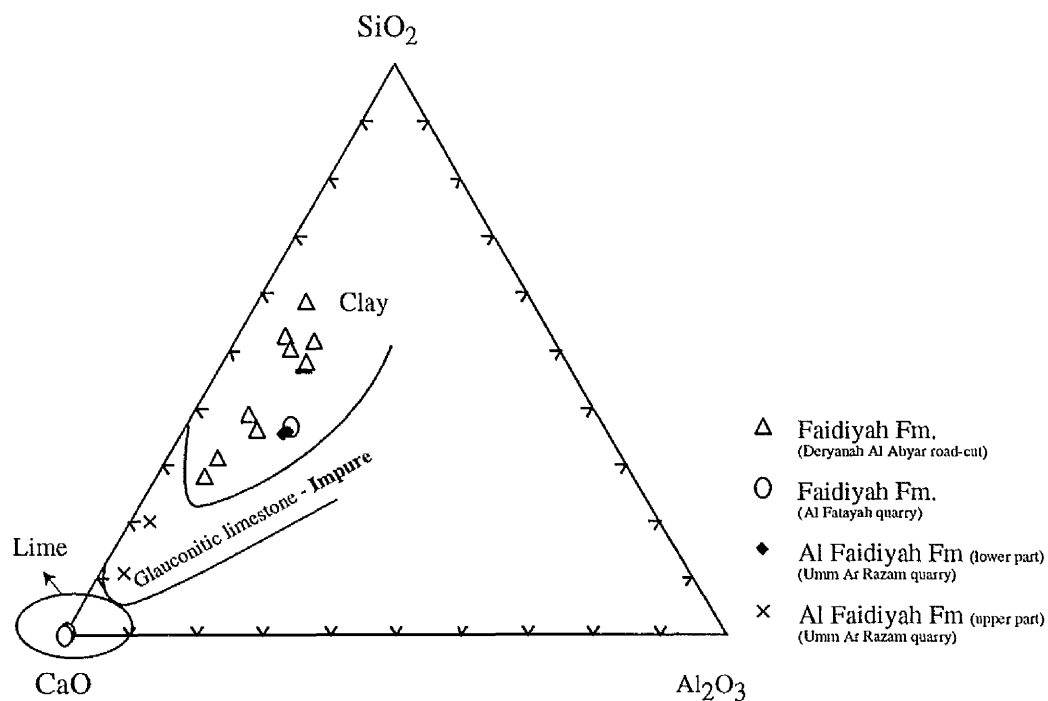
Figure (5.7) SiO_2-CaO-Al_2O_3 Ternary diagram (XRF analyses) of the Al Faidiyah Formation (wt. %) at different localities.
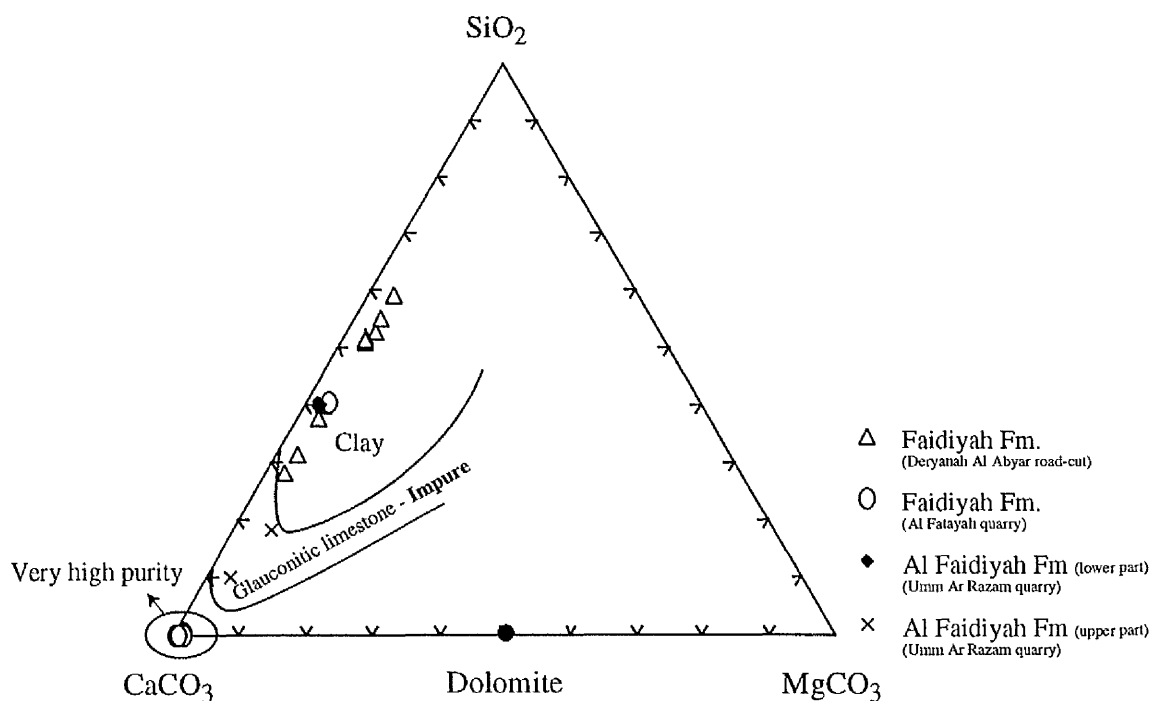
Figure (5.8) SiO_2-$CaCO_3$-$MgCO_3$ Ternary diagram (XRF analyses) of the Al Faidiyah Formation (mol. %) at different localities.

5.2.5 Ar Rajmah Formation (Middle Miocene):

The grade of the Benghazi Limestone Member (lower part of the Formation) varies, and is classified into three main facies according to Mg content (Figure 5.9).

Plotting the data in the ternary system SiO_2-CaO-Al_2O_3 (Figure 5.10), the data for the Ar Rajmah Formation show very low SiO_2 and Al_2O_3 contents.

In the ternary system SiO_2–$CaCO_3$–$MgCO_3$ (Figure 5.11), the data show the dolomitic limestone in the Benghazi Member (middle part) of the Ar Rajmah Formation, in Ar Rajmah quarry. Very high purity to high purity limestones occur in the Lower and the Upper parts of Benghazi Member (Wadi Al Faj and Benghazi quarries), and in the Wadi Al Qattarah Member, of the Ar Rajmah Formation.

CaO vs MgO and CaO vs SiO_2 + Al_2O_3

The source of SiO_2 + Al_2O_3 in the studied area is the clay minerals, and quartz grains, and varies from one formation to another. Plots of CaO vs MgO and CaO vs SiO_2 + Al_2O_3 (Figures 5.12-5.15) show a strong negative correlation. The lowest amounts of MgO, SiO_2 and Al_2O_3 in the formations reflect the grade and the purity of limestone.

5.3 Blending of raw materials: (e.g. Benghazi cement Quarry)

For cement making, the blended raw materials are mixtures of two types of rocks: limestone and clay and/or shale. In the Benghazi cement quarry the two raw materials, limestone and weathered clay, are in situ. Using the ternary diagram CaO-Al_2O_3-SiO_2 (Figure 5.16), the blend of both raw materials must plot within the C2S-C3A-C3S triangle. Chemical composition using X-ray fluorescence (XRF) analyses of the raw materials should be known, to get the correct ratio for blending of both raw materials (Manning, 1995).

5.3.1 Lime Saturation Factor (LSF): (Harris, 1979; Manning, 1995)

LSF is a measure of the ability of the blend to react leaving no free lime. LSF should be greater than 0.66 and less than 1.02. If LSF equals 1 that means the amount of lime is exactly the same as the amount of silica, alumina and ferric oxides. If LSF is greater than 1, free lime will be present within the produced clinker. LSF is calculated from chemical analysis of the raw materials as follow:

$$LSF = CaO - 0.7SO_3 / \ (2.8SiO_2 + 1.18Al_2O_3 + 0.65Fe_2O_3)$$
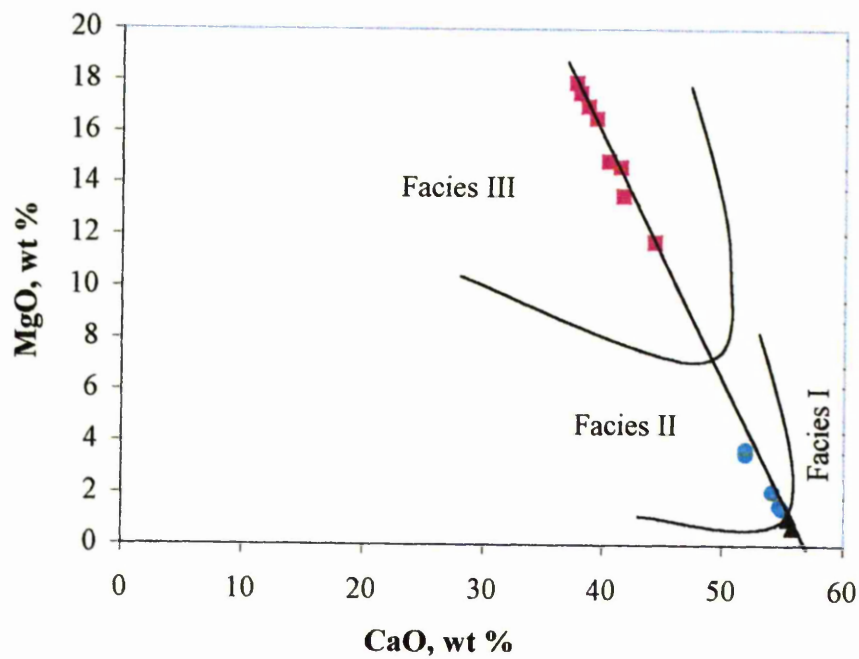
Figure (5.9) Plot of major oxides (wt. %) CaO vs MgO of the Benghazi Member of the Ar Rajmah Formation. Facies I: Wadi Al Faj quarry, Facies II: Benghazi cement quarry, and Facies III; Ar Rajmah quarry.
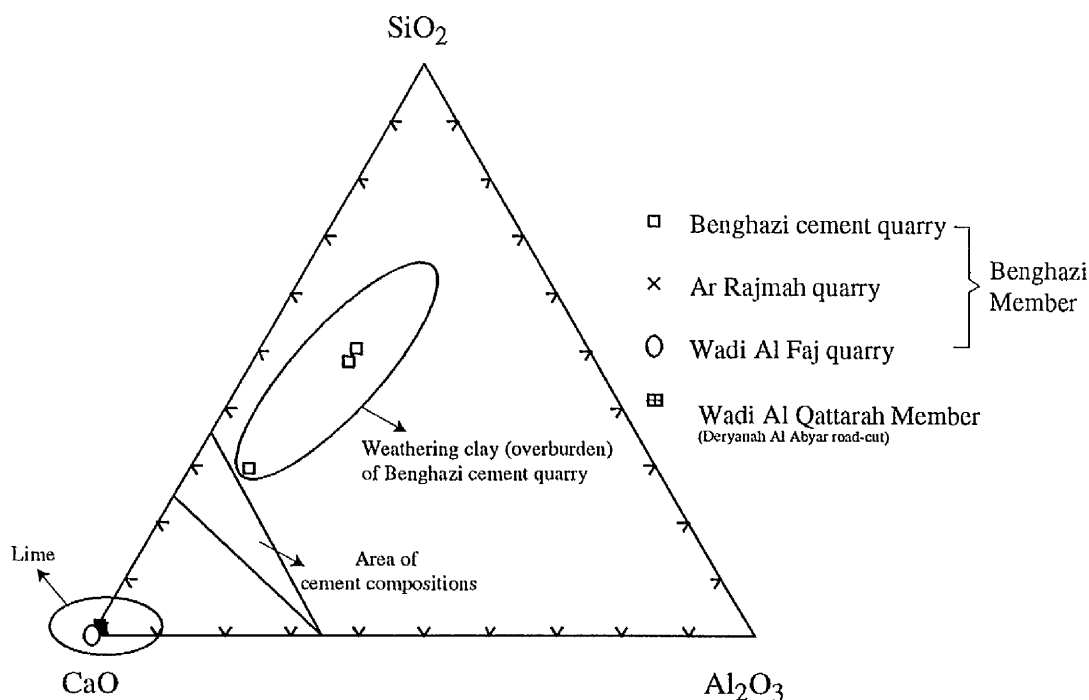
Figure (5.10) SiO_2-CaO-Al_2O_3 Ternary diagram (XRF analyses) of the three different quarries of the Benghazi Member (lower part), and Wadi Al Qattarah Member (upper part) of the Ar Rajmah Formation (wt. %). Cement compositions from Manning (1995).
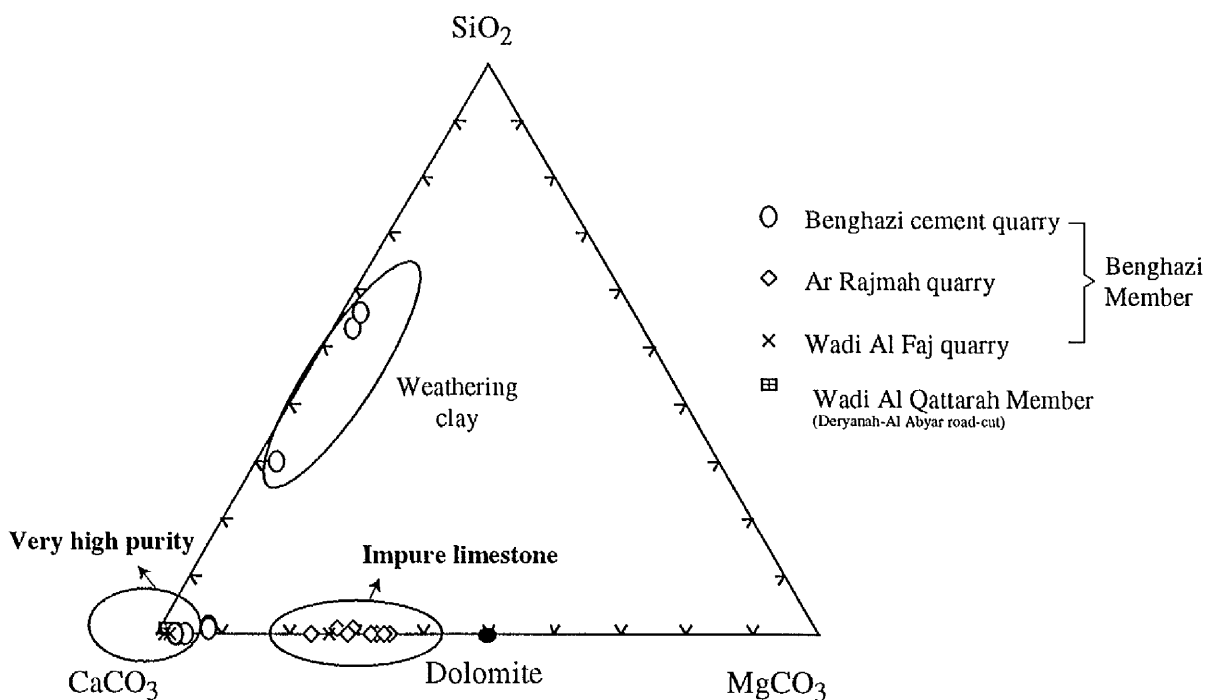
Figure (5.11) SiO_2-$CaCO_3$-$MgCO_3$ Ternary diagram (XRF analyses) of the Benghazi Member (lower part) and Wadi Al Qattarah Member (upper part) of the Ar Rajmah Formation (mol. %).

146
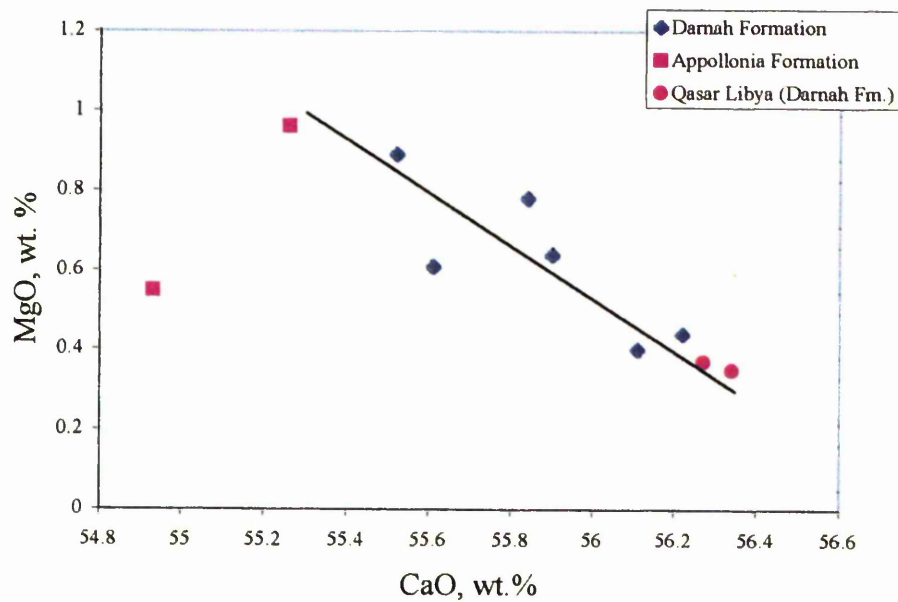
Figure (5.12) Plot of major oxides CaO vs MgO of the Darnah Formation. Shahhat-Susah road-cut & Qasar Libya quarry, and the Apollonia Formation, Bachor quarry.
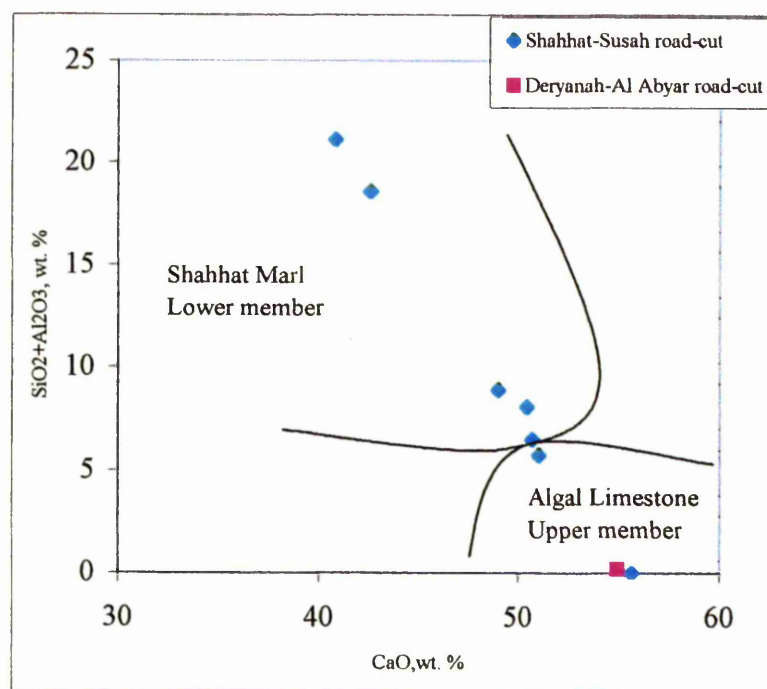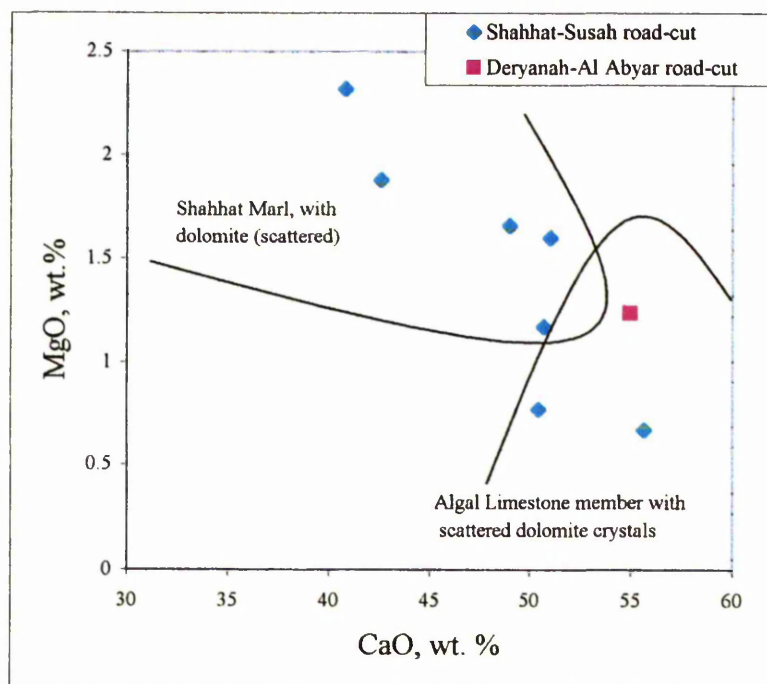
Figure (5.13) Plot of major oxides (wt. %) CaO vs MgO, and SiO_2 + Al_2O_3 vs CaO, in different localities of the Al Bayda Formation.
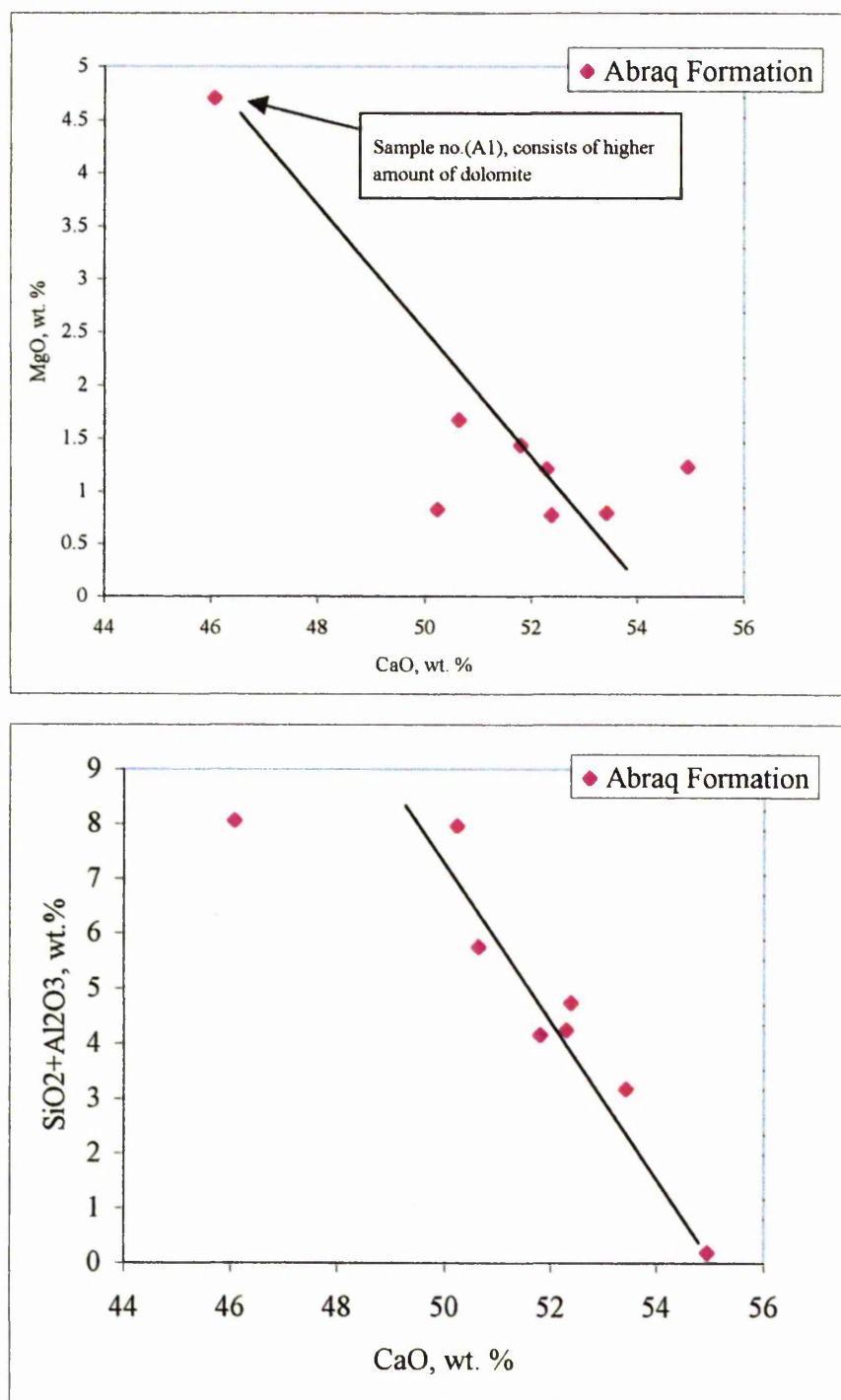
Figure (5.14) Plot of major oxides (wt. %), CaO vs MgO, and SiO_2 + Al_2O_3 vs CaO, of the Al Abraq Formation.
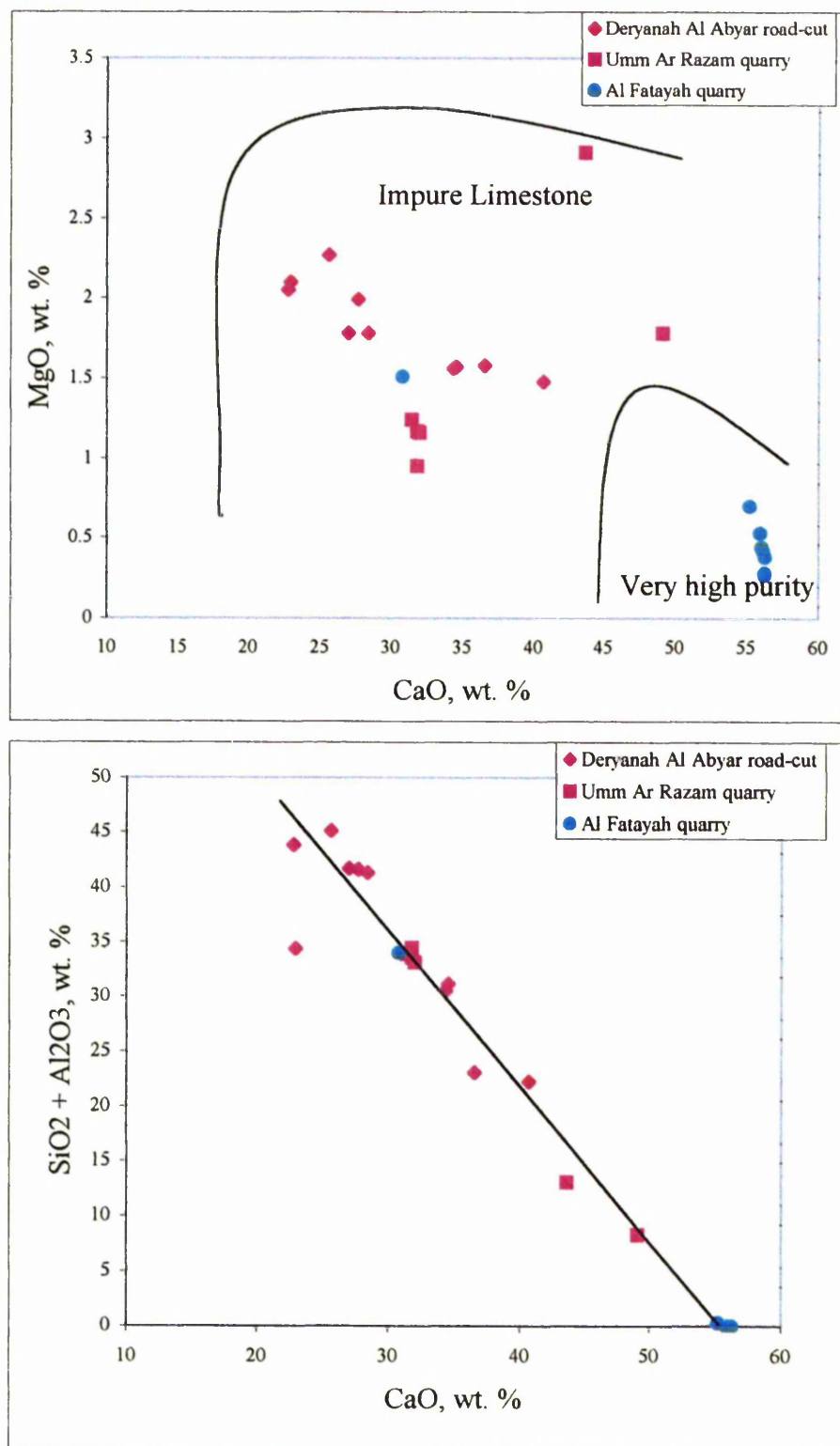
Figure (5.15) Plot of major oxides (wt. %) CaO vs MgO, and SiO_2 + Al_2O_3 vs CaO, of the Al Faidiyah Formation in different localities.

Most cement works in the U.K require their product to have an LSF over 0.9 and many operate at about 0.98. In the LSF equation, the symbols in *italics* refer to the percentage by weight of each oxide in the raw material. In practice materials are blended to give a value for the LSF typically of 0.96 (or 96%). The blending of raw materials should not contain more than 3.0-4.0 % MgO, and SO_3 < 3.0 %. Other controls on the raw materials include the ratio of silica to alumina and iron, $SiO_2:Al_2O_3+Fe_2O_3$, which is usually between 1.5 and 3, and the ratio $Al_2O_3:Fe_2O_3$ which is usually between 1.5 and 3.5.

5.3.2 Calculation of the proportion in blend: (Manning,1995)

Weathering clay for sample no. (LB6), and limestone sample no. (LB1) are used as an example (Figure 16). For sample LB6 the proportion of Si, Al and Fe oxides is given by the sum of (Appendix A5.10);

2.8 (SiO_2) + 1.18 (Al_2O_3) + 0.65 (Fe_2O_3), which in this case is:

94.67 + 11.93 + 2.31 = 108.94.

For a lime saturation factor of 0.96, the amount of lime required to saturate these oxides is 108.94 x 0.96 = 104.58 equivalent parts. The clay already contains 26 equivalent parts of CaO and so 78.58 are needed (104.58 – CaO in clay = 104.58 – 26 = 78.58)

Thus, in this example, for complete reaction, one unit of LB6, needs 78.58 equivalent parts of lime (CaO). Limestone (LB1) supplies 92.78 x 0.56 = 52 equivalent parts.

The 52 parts CaO, 2.76 parts are already compensated by the SiO_2, Al_2O_3 and Fe_2O_3 in the limestone. So 49.2 parts CaO are contributed by limestone. So, 1 unit of LB6 needs 78.58 units of LB1 = 1.6 units.

% LB6 = 100 x 1 / 2.6 = 38.5 %, and

% LB1 = 100 x 1.6 / 2.6 = 61.5 %

Results for this calculation for samples taken from the lower Benghazi Member are shown in Table 5.2A and 5.2B. Variations in limestone proportions are very small, and the proportions of clay (LB6, LB7, LB8) differ greatly. This reflects variation in the composition of the clay available to be used in cement manufacture, while the limestone may be consistent in composition.

Table(5.2) Shows the blend proportions (wt. %) for limestone (LB1-LB5), and weathering clay (LB6, LB7, and LB8), of the lower Benghazi Member of the Ar Rajmah Formation in Benghazi cement quarry

% Limestone	LB6	LB7	LB8	% Clay	LB6	LB7	LB8
LB1	61.5	27.5	63.0	LB1	38.5	72.5	37.0
LB2	59.0	25.4	61.5	LB2	41.0	74.6	38.5
LB3	60.0	25.9	61.5	LB3	40.0	74.1	38.5
LB4	58.8	25.4	61.5	LB4	41.2	74.6	38.5
LB5	61.5	28.6	63.0	LB5	38.5	71.4	37.0

Table (5.2B) Chemical analysis for major elements, Benghazi Member of the Ar Rajmah Formation (M. Miocene) at Benghazi Cement Quarry.

Oxides (wt. %) → / Sample no. ↓	SiO_2	Al_2O_3	Fe_2O_3	MgO	CaO	S	K_2O	TiO_2	MnO	P_2O_5	Total
LB1	0.87	0.25	0.09	3.52	51.90	0.00	0.04	0.01	0.00	0.03	100.04
LB6	33.82	10.11	3.55	1.47	25.96	0.00	1.77	0.70	0.05	0.07	98.91
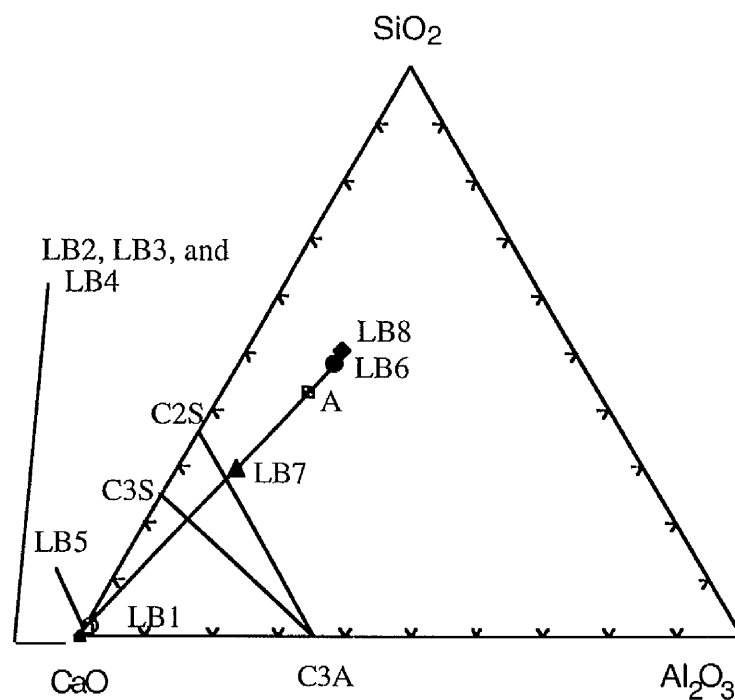
Figure (5.16) SiO_2-CaO-Al_2O_3 (wt. %). Ternary diagram of the Benghazi Cement Quarry, the lower part of the Benghazi Member of the Ar Rajmah Formation (A: the average clay composition).

5.4 Trace element geochemistry:

The study of trace elements is classified into two groups. The first group includes Fe, Ni, V and Cr, which relate mainly to clastic constituents within carbonate deposits. The migration possibilities of this group are determined by tectonic and climatic conditions (Peryt *et al.*, 1980). The other group consists of Mn, Sr and Cu which are related to the chemical precipitation of carbonate (and coprecipitated) deposits which are migrating in solutions.

Ce vs Nd & La and V vs Ni & Cr & Cu, Ce & Zr and Rb & Zn

The correlation coefficient matrix (Table 5.3) may or may not conceal important geological correlations and can produce misleading results. Correlation between two major oxides may have arisen through the closure process from an actual correlation between two other oxides (Rollinson, 1993). From these points the trace elements were considered and the results were as follows: there are strong positive correlations between Ce against Nd and La (Figure 5.17), and also between V against Ni, Cr and Cu, Ce and Zr and Rb and Zn. The distribution of V and Ni is controlled to a great extent by the content of clay materials. The very high purity of limestone relates to the decrease in V, Ni, Cr and Cu (Peryt *et al.*, 1980, Figure 5.18). Sr varies from 161 – 8042 ppm and shows no correlation with other trace elements, or with CaO.

5.5 Mineral geochemistry:

Principal mineral components have been determined by X-ray diffraction (XRD) which indicates impurities present within the formations of Al Jabal Al Akhdar area. Also chemical analyses were carried out using EPMA and SEM techniques. Mineralogical studies focused in the Benghazi Member of the Ar Rajmah Formation, characterised first by high strontium content, due to the presence of celestite and strontianite minerals, and secondly by the presence of dolomites in high amounts, especially in the middle part of the Benghazi Member of the Ar Rajmah Formation.

5.5.1 Mineralogy of the Benghazi Member (dolomite) using XRD:

X-ray diffraction has been used to study carbonate sediments, limestones, and dolomites. Using XRD data, indirect information can be obtained about the chemical composition of carbonate minerals (Ca or Mg excess of dolomite). Also XRD can be used to determine the ordering of dolomite crystals, and to determine Ca / Mg ratios. In Ca-rich dolomites the excess Ca substitutes for Mg in Mg-Layers (or vice versa in Ca-poor dolomites). Ca ions are larger in size than Mg, therefore the substitution will create a certain amount of lattice strain. This could be minimised if the Ca ions were distributed within the lattice plane (regular), rather than
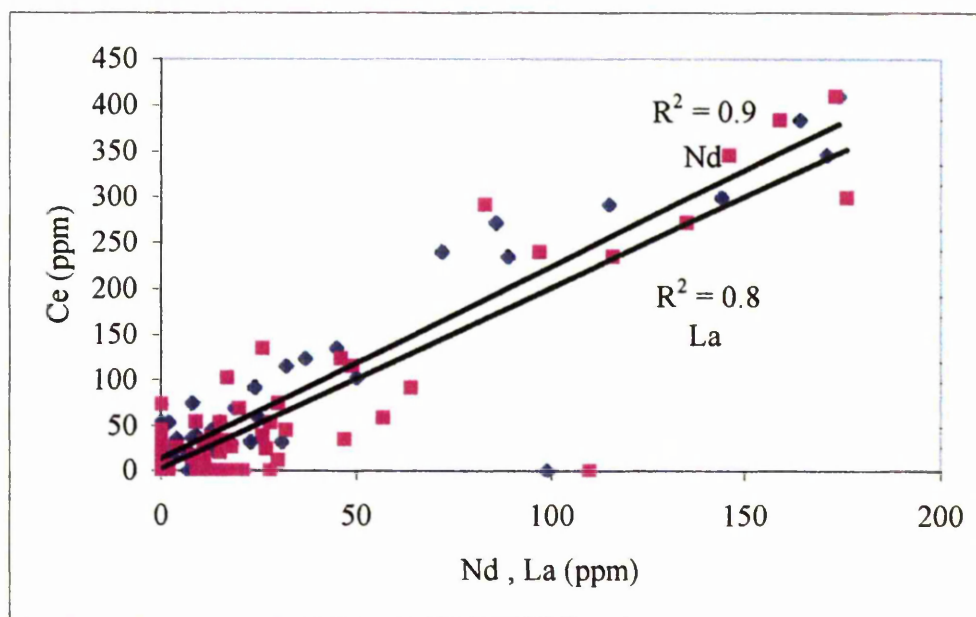
Figure (5.17) Plot showing the variation between Ce (ppm) against Nd and La (ppm) in the study area
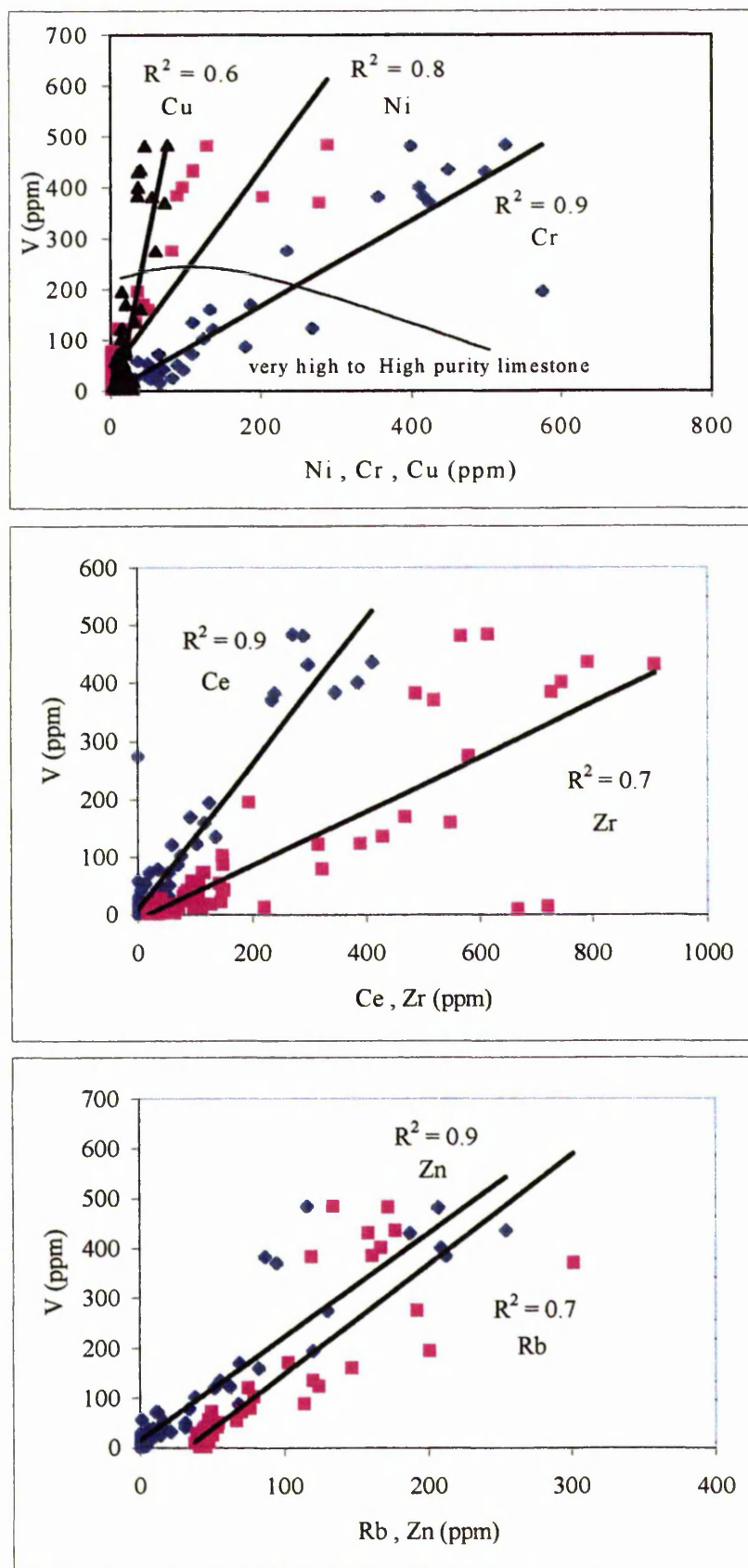
Figure (5.18) Plot showing the variation between V (ppm) against Ni, Cr & Cu, Ce & Zr and Rb & Zn (ppm) in the study area

Table (5.3) Correlation coefficient matrix for trace elements in carbonate rocks in the study area

Oxides (wt %)	SiO_2	Al_2O_3	Fe_2O_3	$MgCO_3$	$CaCO_3$	S	K_2O	TiO_2	MnO	P_2O_5	CaO	MgO	Nb	Zr	Y	Sr	Rb	Zn	Cu	Ni	Cr	Ce	Nd	V	La	Ti	Ba	Sc
SiO_2	1.00																											
Al_2O_3	0.91	1.00																										
Fe_2O_3	0.76	0.67	1.00																									
$MgCO_3$	-0.21	-0.22	-0.17	1.00																								
$CaCO_3$	-0.88	-0.82	-0.74	-0.26	1.00																							
S	0.02	0.01	-0.04	0.19	-0.10	1.00																						
K_2O	0.79	0.60	0.91	-0.14	-0.74	-0.04	1.00																					
TiO_2	0.82	0.96	0.65	-0.20	-0.75	-0.06	0.49	1.00																				
MnO	-0.02	0.12	0.07	-0.35	0.14	-0.14	-0.02	0.20	1.00																			
P_2O_5	-0.03	-0.12	0.00	0.63	-0.26	0.28	0.07	-0.14	-0.40	1.00																		
CaO	-0.89	-0.83	-0.74	-0.22	0.99	-0.08	-0.75	-0.76	0.12	-0.25	1.00																	
MgO	-0.21	-0.22	-0.17	1.00	-0.26	0.19	-0.14	-0.20	-0.35	0.63	-0.22	1.00																
Trace element (ppm)																												
Nb	0.62	0.71	0.42	-0.16	-0.55	-0.09	0.29	0.75	0.10	-0.12	-0.56	-0.16	1.00															
Zr	0.63	0.74	0.48	-0.23	-0.55	-0.08	0.37	0.79	0.33	-0.20	-0.55	-0.23	0.77	1.00														
Y	0.48	0.71	0.44	-0.16	-0.46	-0.07	0.22	0.82	0.27	-0.10	-0.47	-0.16	0.77	0.76	1.00													
Sr	-0.10	-0.12	-0.15	-0.08	0.15	0.04	-0.12	-0.13	0.29	-0.14	0.15	-0.08	0.00	0.38	-0.16	1.00												
Rb	0.74	0.72	0.69	-0.18	-0.67	-0.10	0.63	0.73	0.10	-0.03	-0.68	-0.18	0.78	0.73	0.72	-0.08	1.00											
Zn	0.66	0.81	0.67	-0.20	-0.62	-0.07	0.46	0.89	0.22	-0.13	-0.63	-0.20	0.83	0.82	0.93	-0.11	0.84	1.00										
Cu	0.48	0.52	0.25	-0.12	-0.41	-0.12	0.23	0.52	0.06	-0.08	-0.43	-0.12	0.81	0.59	0.62	-0.10	0.75	0.65	1.00									
Ni	0.57	0.57	0.34	-0.14	-0.49	-0.10	0.30	0.58	0.02	-0.06	-0.49	-0.14	0.94	0.66	0.60	0.05	0.79	0.68	0.88	1.00								
Cr	0.73	0.75	0.77	-0.19	-0.68	-0.07	0.62	0.77	0.11	-0.08	-0.69	-0.19	0.87	0.75	0.76	-0.08	0.89	0.90	0.70	0.80	1.00							
Ce	0.67	0.81	0.59	-0.17	-0.63	-0.10	0.40	0.88	0.23	-0.14	-0.63	-0.17	0.90	0.80	0.87	-0.04	0.77	0.92	0.65	0.76	0.88	1.00						
Nd	0.58	0.74	0.53	-0.16	-0.54	-0.12	0.33	0.84	0.19	-0.09	-0.55	-0.16	0.86	0.81	0.95	-0.09	0.80	0.96	0.68	0.71	0.85	0.93	1.00					
V	0.69	0.79	0.58	-0.18	-0.63	-0.09	0.42	0.84	0.15	-0.11	-0.63	-0.18	0.95	0.83	0.86	-0.05	0.86	0.93	0.80	0.88	0.93	0.93	0.92	1.00				
La	0.61	0.75	0.49	-0.19	-0.55	-0.10	0.32	0.82	0.19	-0.17	-0.56	-0.19	0.91	0.83	0.89	-0.06	0.81	0.92	0.74	0.79	0.87	0.89	0.93	0.96	1.00			
Ti	0.66	0.79	0.48	-0.16	-0.60	-0.09	0.32	0.84	0.15	-0.12	-0.61	-0.16	0.98	0.80	0.82	-0.02	0.77	0.87	0.77	0.88	0.87	0.95	0.89	0.96	0.91	1.00		
Ba	0.44	0.35	0.12	-0.12	-0.33	-0.08	0.25	0.27	-0.08	0.00	-0.34	-0.12	0.67	0.48	0.31	0.09	0.63	0.38	0.84	0.85	0.54	0.41	0.41	0.62	0.52	0.58	1.00	
Sc	-0.73	-0.68	-0.62	-0.27	0.86	-0.02	-0.59	-0.65	0.16	-0.26	0.85	-0.27	-0.63	-0.59	-0.50	0.08	-0.68	-0.63	-0.51	-0.61	-0.72	-0.62	-0.59	-0.70	-0.59	-0.64	-0.49	1.00

This type of correlation is not appropriate for major elements, because of the closure problem (Rollinson, 1993)

clumped (irregular). The order ratio is defined as the ratio I_{015}/I_{110}, where I_{hkl} represents the intensity of a specific *hkl* reflection. The Mg/Ca ratio of dolomite is generally interpreted to reflect environmental factors such as fluid temperature and chemistry (Mattes *et al.*, 1980; Machel *et al.*, 1986). The homogeneous values of Mg/Ca may be interpreted to reflect dolomitization within a stable diagenetic environment, or complete dolomite recrystallization in a homogeneous fluid regime. The percentages of the various minerals in the mixture can be estimated from X-ray peaks. The main peaks of the common carbonate minerals, calcite, aragonite and dolomite are given in Table (5.4).

Table (5.4) Dominant X-ray diffraction peaks of the common carbonate minerals, from JCPDS, (1986).

	$d(A°)$	3.396	1.977	3.273	2.700	2.372	2.481
Aragonite	I/I_l	100	65	52	46	38	33
	hkl	111	221	021	012	112	200
	$d(A°)$	3.035	2.285	2.095	1.013	1.875	2.495
Calcite	I/I_l	100	18	18	17	17	14
	hkl	104	113	202	108	116	110
	$d(A°)$	2.886	2.192	1.786	1.804	2.015	1.389
Dolomite	I/I_l	100	30	30	20	15	15
	hkl	104	113	009	018	202	030

The Ca excess can be calculated by Lumsden's equation (1979), relating mol. % $CaCO_3$ (N_{CaCO3}) to the $d104$ spacing measured in angstrom units (d): $N_{CaCO3} = Md_{104} + B$, where M is 333.33 and B is (-911.99). Dolomite in the Benghazi Member is not stoichiometric and has an excess of Ca^{+2}, with an average Ca:Mg of 54:45. All XRD data are given in Table (5.5) and illustrated in Figure (5.19).

Table (5.5) X-ray diffraction data for the Benghazi Member of the Ar Rajmah Formation.

Location	Sample no.	Order ratio *015/110*	Mol. % $CaCO_3$ in dolomite	d_{104}	Ca:Mg ratio
Benghazi Cement Quarry	LB1	0.46	54.1	2.8983	54:46
	LB2	0.00	54.7	2.9000	55:45
	LB3	0.00	54.0	2.8980	54:46
	LB4	0.00	56.0	2.9040	56:44
	LB5	0.72	56.1	2.9044	56:44
Ar Rajmah Quarry	UBA1	0.38	53.8	2.8973	54:46
	UBA2	0.49	53.0	2.8951	53:47
	UBA3L	0.36	52.5	2.8949	53:47
	UBA3U	0.30	51.6	2.8909	52:48
	UBB1	0.32	52.7	2.8940	53:47
	UBB2L	0.30	54.2	2.8985	54:46
	UBB2U	0.44	52.5	2.8934	52:48
	UBBMUP	0.63	52.8	2.8945	53:47
Wadi Al Faj Quarry	RQ1L	0.46	52.9	2.8946	53:47

Dolomite from Ar Rajmah quarry is less rich in Ca^{2+} ions than the lower and upper parts of the Formation where the Ca^{2+} decreases to Ca:Mg 52:48. Wadi Al Faj quarry contains mainly calcite except the lower part of the quarry, which represents the upper most part of Ar Rajmah quarry (sample no.RQ.1), with dolomite having a Ca:Mg of 53:47. The upper part of the quarry is the lower margin of the dolomite body.
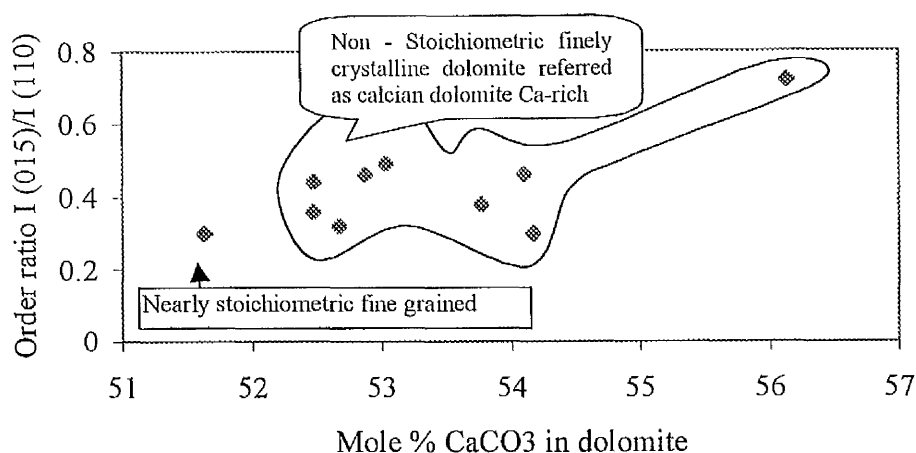
Figure (5.19) XRD-data from Middle Miocene dolomites from the Benghazi Member of the Ar Rajmah Formation showing stoichiometry (as mole % CaCO₃) plotted against ordering.

In Figure (5.19), calciam dolomite reflects the general change in pore-water composition to progressively lower Mg/Ca ratios. This suggests freshening of the groundwater as a result of a falling sea level (Ward *et al.*, 1985). Limpid euhedral dolomite is evidence of precipitation of dolomite in mixed water with relatively low Mg/Ca ratios (Weaver, 1975). Dolomite in the Benghazi Member of the Ar Rajmah Formation is characterised by the presence of limpid euhedral crystals.

5.5.2 Mineral chemistry of the Benghazi Member using EPMA:

Bulk X-ray diffraction results showed that calcite is the main carbonate mineral present in the Ar Rajmah Formation. Dolomite is present in significant amounts, and the highest amounts are in the Ar Rajmah Quarry of the Benghazi Member. An electron probe microanalysis (EPMA) traverse across dolomite crystals of sample no. UUB2MUP is illustrated in Figure (5.20). The shape of the crystal is a well formed rhomb (euhedral), and the size of the crystal is 40 – 50 μm. The analytical results of 12 spots from the centre to the rim (Table 5.6), confirmed that the crystal centre is Mg-rich. The outer rim of the crystal is relatively enriched in Ca (more calciam rich) and depleted in both Fe and Mn contents corresponding to those expected from early near-surface dolomitization. The low concentrations of these elements indicate that dolomitization occurred under oxidising conditions. The centre of the crystal has Mg:Ca:Fe ratios ranging from 52:48:0 to 51:49:0, and the rim has Mg:Ca:Fe ratios of 45:54:0.1. The core and rim are both non-ferroan

where the mol % of $FeCO_3$ is nil, reaching 0.066 mol % $FeCO_3$, in the margin (spot no.12). The Mn concentration is invariant between the core (range from 0-340 ppm, mean 90 ppm) and rim (range from 0-120 ppm, mean 70 ppm), whereas strontium (Sr) concentration varies within the dolomite crystal. The average values are 445 ppm. XRD results for the same sample showed that the main (d_{104}) dolomite reflection is sharp, with a value of 2.8945 $\overset{o}{A}$, suggesting that the mineral is relatively well crystallised, and that it deviates little from the value expected (2.886 $\overset{o}{A}$). Chemical analyses for the strontianite (sample no. LB2) and dolomite minerals in the Benghazi Member have been taken (Appendix A.5.15).

Table (5.6) Electron microprobe traverse of 12 spots from the core to the rim across dolomite crystal of sample no.UBB2MUP of Benghazi Member of the Ar Rajmah Formation.

Oxides (Wt %)	1 Core	2	3	4	5	6	7	8	9	10	11	12 Rim
CaO	28.83	30.89	32.60	33.01	26.02	38.38	38.96	39.64	37.82	39.01	39.11	42.49
SiO_2	0.00	0.00	0.00	0.00	0.00	0.00	0.00	0.02	0.00	0.02	0.01	0.00
SrO	0.04	0.05	0.04	0.01	0.01	0.02	0.04	0.01	0.00	0.01	0.00	0.01
MgO	22.70	26.27	24.38	25.89	30.35	25.13	25.33	29.55	25.67	28.52	31.00	25.34
FeO	0.00	0.00	0.00	0.00	0.00	0.00	0.00	0.00	0.00	0.00	0.00	0.07
MnO	0.00	0.03	0.02	0.00	0.00	0.00	0.01	0.00	0.01	0.01	0.01	0.00
SO_3	0.03	0.02	0.00	0.00	0.00	0.12	0.00	0.00	0.00	0.00	0.03	0.08
Al_2O_3	0.00	0.00	0.00	0.00	0.00	0.00	0.00	0.00	0.00	0.00	0.00	0.00
K_2O	0	0.07	0.02	0.00	0.00	0.00	0.01	0.05	0.06	0.05	0.03	0.00
Na_2O	0	0.00	0.00	0.00	0.00	0.00	0.00	0.00	0.00	0.00	0.00	0.00
Total	51.65	57.34	57.07	58.93	56.42	63.65	64.35	69.27	63.57	67.63	70.20	67.99
Number of Cations on basis of 2 (O) Oxygen excluding CO_2												
Ca	0.880	0.920	0.980	0.960	0.760	1.050	1.050	0.980	1.030	0.990	0.950	1.090
Si	0.000	0.000	0.000	0.000	0.000	0.000	0.000	0.000	0.000	0.000	0.000	0.000
Sr	0.000	0.000	0.000	0.000	0.000	0.000	0.000	0.000	0.000	0.000	0.000	0.000
Mg	1.120	1.080	1.020	1.040	1.240	0.950	0.950	1.020	0.970	1.010	1.050	0.900
Fe	0.000	0.000	0.000	0.000	0.000	0.000	0.000	0.000	0.000	0.000	0.000	0.000
Mn	0.000	0.000	0.000	0.000	0.000	0.000	0.000	0.00	0.000	0.000	0.000	0.000
S	0.000	0.000	0.000	0.000	0.000	0.004	0.000	0.000	0.000	0.000	0.000	0.000
Al	0.000	0.000	0.000	0.000	0.000	0.000	0.000	0.000	0.000	0.000	0.000	0.000
K	0.000	0.000	0.000	0.000	0.000	0.000	0.000	0.000	0.000	0.000	0.000	0.000
Na	0.000	0.000	0.000	0.000	0.000	0.000	0.000	0.000	0.000	0.000	0.000	0.000
Total	2.000	1.990	2.000	2.000	2.000	2.004	2.000	2.000	2.000	2.000	2.000	2.000
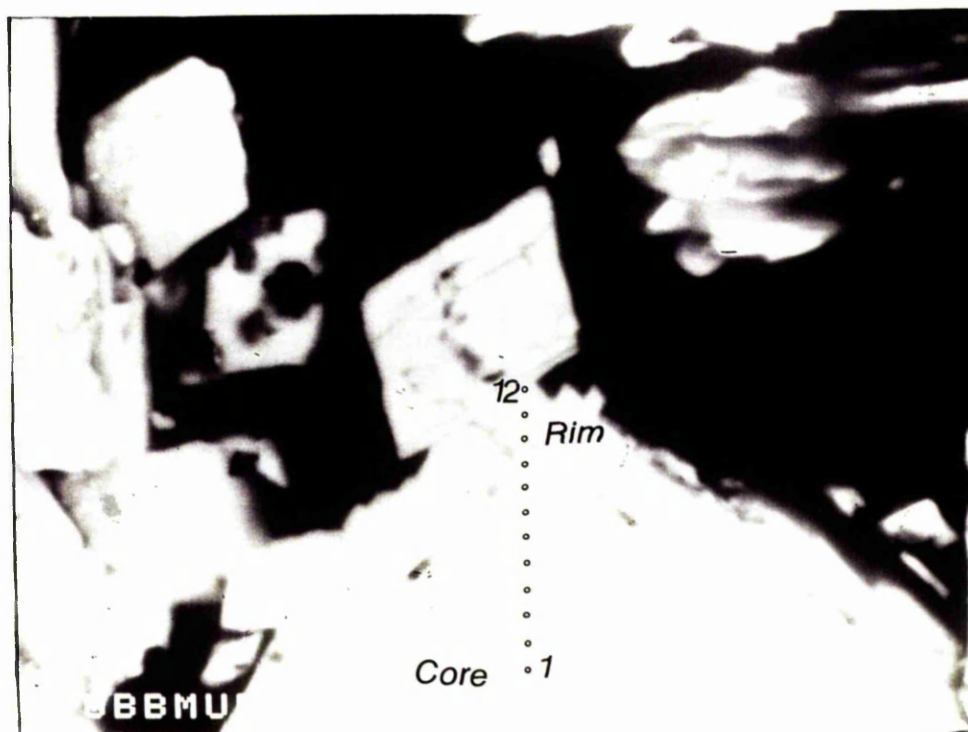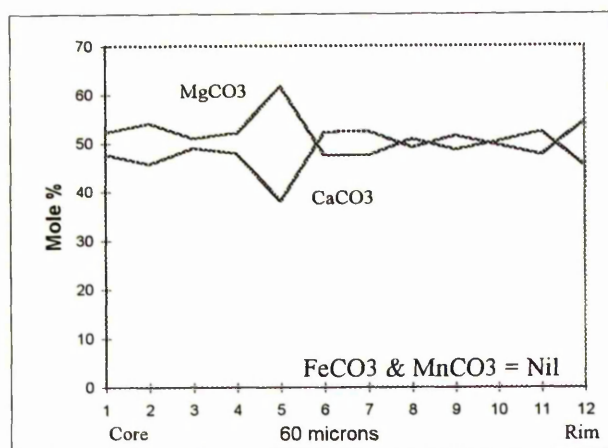
Figure (5.20) Showing electron microprobe traverse across dolomite crystal from sample no. UBB2MUP (60 μm in sized) of the Benghazi Member (middle part) of the Ar Rajmah Formation (Ar Rajmah quarry), from Ward & Halley, 1985.

162

5.5.3 Mineral chemistry of the Benghazi Member using SEM:

Chemical analyses were determined using SEM (BSE) techniques for the Benghazi Member of the Ar Rajmah Formation (see Appendix A.5.16). This Member contains impure, low purity and very high purity limestones. The resulting mineral analyses are illustrated in the $FeCO_3$-$CaCO_3$-$MgCO_3$ ternary plot (Figure 5.21). This shows the presence of pure calcite in the pure limestone and dolomite in the impure limestones with some intermediate mineral compositions.

5.6 Insoluble Residues of limestones, Jabal Al Akhdar Area:

In addition to calcite the limestone contains other carbonates such as dolomite and non-carbonates such as clay minerals, quartz and other silicates. Eighteen samples were chosen from different formations for investigation of the insoluble residues (Robinson, 1980).

5.6.1 Experimental:

One gram of dry powdered sample was weighed into a 100-ml Pyrex beaker. Fifty of ml 1 *M* HCl at room temperature was added, and the mixture was stirred over a period of 2 hours. The solutions were filtered through number 5 filter papers and washed with deionized water. The filter papers with the wet residues were dried at about 50 °C for 2 hours and weighed, and the mass of the residues calculated. The mineralogy of the insoluble residues as determined by X-ray diffractometry (XRD).

5.6.2 Insoluble residues:

The insoluble residues of the Darnah Formation and the Faidia Limestone Member of the Al Faidiyah Formation (Al Fatayah quarry) are extremely low, with values of 1.9-2.0 %. From Table 5.8 it is observed that the softer beds have higher values than the other hard ones, e.g the Apollonia Formation consists of intercalated soft (AS) and hard (AH) layers where the soft bed has a value 7.07 %, whereas the hard layer contains 3.64 %, and both together have an average value of 5.4 %. The lower Member of the Al Faidiyah Formation in Deryanah- Al Abyar road-cut (soft layer), has the highest value as illustrated in Table 5.8 of about 57 %. The residues were examined by X-ray diffractometry (XRD), and contain quartz, dolomite (incompletely dissolved), smectite, glauconite and kaolinite (Table 5.7). Clay minerals and quartz were found in all four samples, and occur as trace components, except in sample no.4 of the Al Faidiyah Formation, which contains very high values of residue.
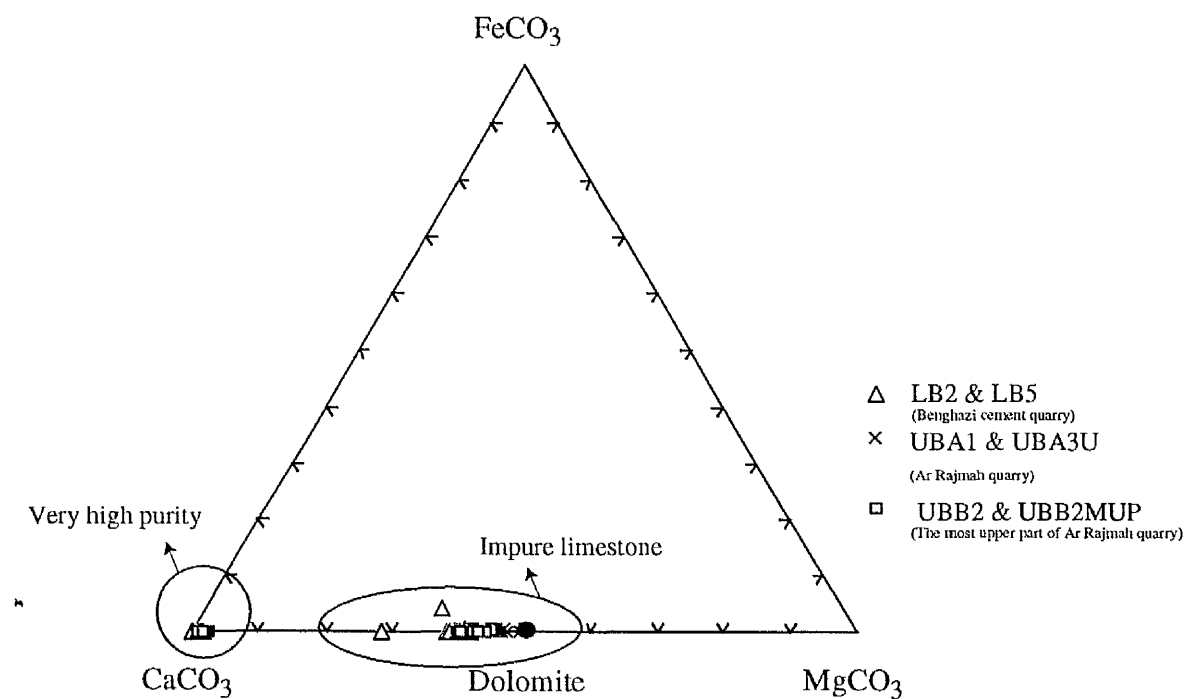
Figure (5.21) $FeCO_3$-$CaCO_3$-$MgCO_3$ Ternary diagram by SEM analyses (90 spots), of the Benghazi Member, Ar Rajmah Formation (mole. %).

Table (5.7) Showing samples containing different minerals (/), determined using XRD.

Minerals	Algal Lst. U	A4	4	ULst.1
Quartz	/	/	/	/
Dolomite	/	-	/	/
Smectite	/	/	-	/
Glauconite	-	-	/	/
Kaolinite	/	/	-	-

Table (5.8) Insoluble residues (%) of the studied area

Item	Formation	Member	Sample no.	Insoluble residue (%)	% CaCO$_3$	Remarks
1	Ar Rajmah (M. Miocene)	Benghazi	LB4	1.27	98.11	Benghazi cement Quarry
			UBA2	2.87	72.03	Ar Rajmah
			UBB2(U)	2.33	78.98	Quarry: dolomite
			RQ.2	2.87	99.03	Wadi Al Faj Quarry
		Wadi al Qattarah	Q.M	2.12	99.41	Deryanah - Al Abyar road-cut
2	Al Faidiyah (U. Oligo.-L. Mio.)	Faidia Clay	4	57.23*	40.63	Deryanah - Al Abyar road-cut
		Faidia Limestone	UF1	1.5	100.48	Al Fatayah cement Quarry
			UF6	2.55	100.30	
			ULst.1	16.2*	87.73	Near the contact of Faidia Clay member Umm Ar Razam Quarry
3	Al Abraq (M. to U. Oligo.)	-	A4	9.01*	89.71	Deryanah - Al Abyar road-cut
4	Al Bayda (L. Oligo.)	Shahhat Marl	SUP	5.79	91.12	Shahhat – Susah Road-cut
		Algal Limestone	Algal Lst (U)	7.08*	90.53	
			Algal Lst (L)	1.84	99.37	
			Bayda.1	2.07	98.13	Deryanah - Al Abyar road-cut
5	Darnah (M. to U. Eo.)	-	DE1	1.7	100.40	
			DE5	2.11	99.14	Shahhat – Susah Road-cut
6	Apollonia (L. to M. Eo.)	-	AS	7.07	98.09	Bachor
			AH	3.64	98.67	Quarry

* XRD result were obtained

5.7 Brucite in limestones:

The mineral brucite, Mg $(OH)_2$, has been found in the skeletons of red algae (Schmalz, 1965; Weber and Kaufman, 1965). Lowenstam (1964) suggested that Mg is commonly present in some form such as a separate mineral phase. The presence of such separate phases is very difficult to establish due to very small amounts of the mineral relative to the calcite or aragonite constituting most of the specimen. In some skeletons separate mineral phases may be present not as a biochemical precipitate but as impurities that were entrapped within the skeleton during calcification. Separate mineral phases may be common as diagenetic replacements in fossils e.g. the dolomite and hematite inclusions commonly noted in fossils (Zenger, 1967; Dodd, 1967). The concentration of $MgCO_3$ greater than 25 mole percent may give an indication of the presence of brucite in the skeleton (Milliman, 1974; Blatt *et al.*, 1980). The presence of brucite in red algae was from the Ar Rajmah Formation (Middle Miocene) suspected on the basis of the discrepancy between the Mg/Ca ratio in the crystal lattice. Electron probe microanalysis (Table A.9.1) of coralline algae in the Ar Rajmah Formation, shows that brucite may be concentrated in certain areas of the skeleton structure, where the magnesium content of the skeletal carbonate ranges from 27.75 to 43.74 mole percent $MgCO_3$ (Figure 5.22).
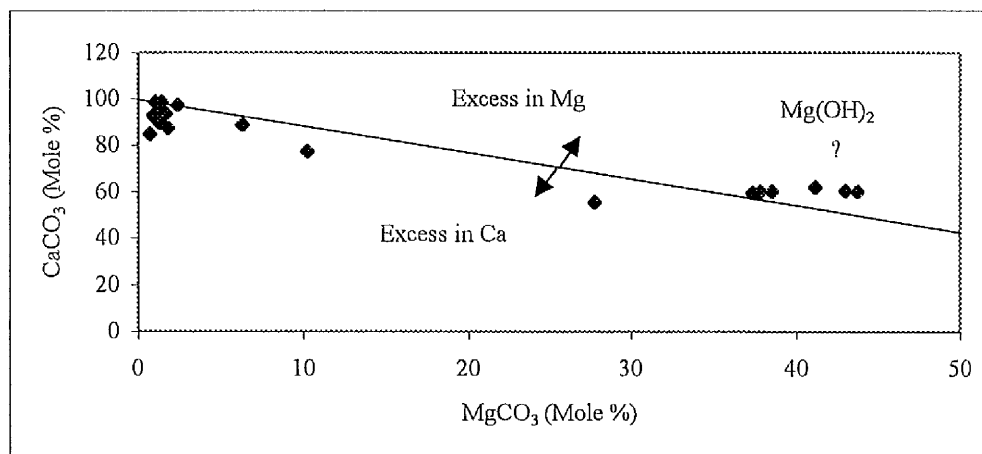
Figure (5.22) Relation between $MgCO_3$ vs $CaCO_3$ (Mole %). EPMA analyses show excess in magnesium in coralline algae, in the Ar Rajmah Formation (Middle Miocene).

BSE-SEM and EPMA (Plate 5.1) shows the lattice-like structure and the differences in magnesium-calcium concentration of the skeletal material. Brucite is expected to be present in the dark area of high magnesium concentration.
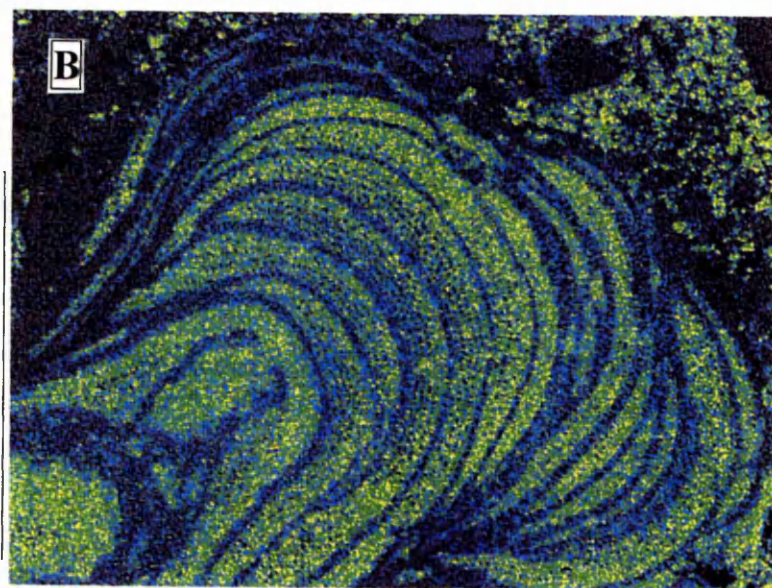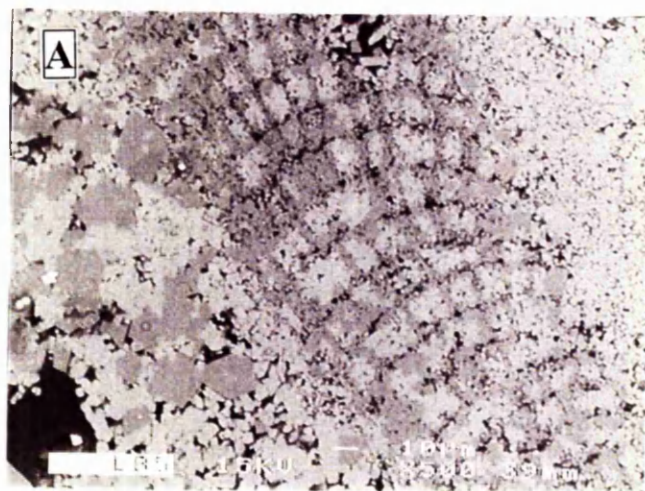
Plate (5.1) A- BSE-SEM image of coralline algae showing dark areas of high magnesium concentration and calcium-rich cells in white areas. B- X-ray element distribution mapping for Ca and Mg; blue = Mg and Yellow = Ca. In the Ar Rajmah Formation (Middle Miocene).

The presence of brucite in the coralline algae of the Ar Rajmah Formation was confirmed by infrared absorption studies (Figure 5.23), where magnesium hydroxide has a sharp absorption band at a wavelength close to 2.7 μ. XRD also indicated the presence of brucite. The position of

the strongest peak, $2\theta = 50.830°$, corresponds to d-spacing $= 1.7948$ $\overset{o}{A}$. NMR shows a narrow line (Figure 5.24). Narrow lines are observed in solid-state NMR if either the molecules are mobile or if the protons are isolated from each other. The explanation for relatively narrow lines in sample no. LB1 of the Ar Rajmah Formation is from isolated hydroxyl (OH) groups. In a case like this NMR is not recommended to give a good result due to the presence of brucite in small amounts (personal communication; Dr. F. Heatley – see Chapter 3). The coralline algae studied is not a homogeneous single phase, but it is a mixture of different crystalline phases.
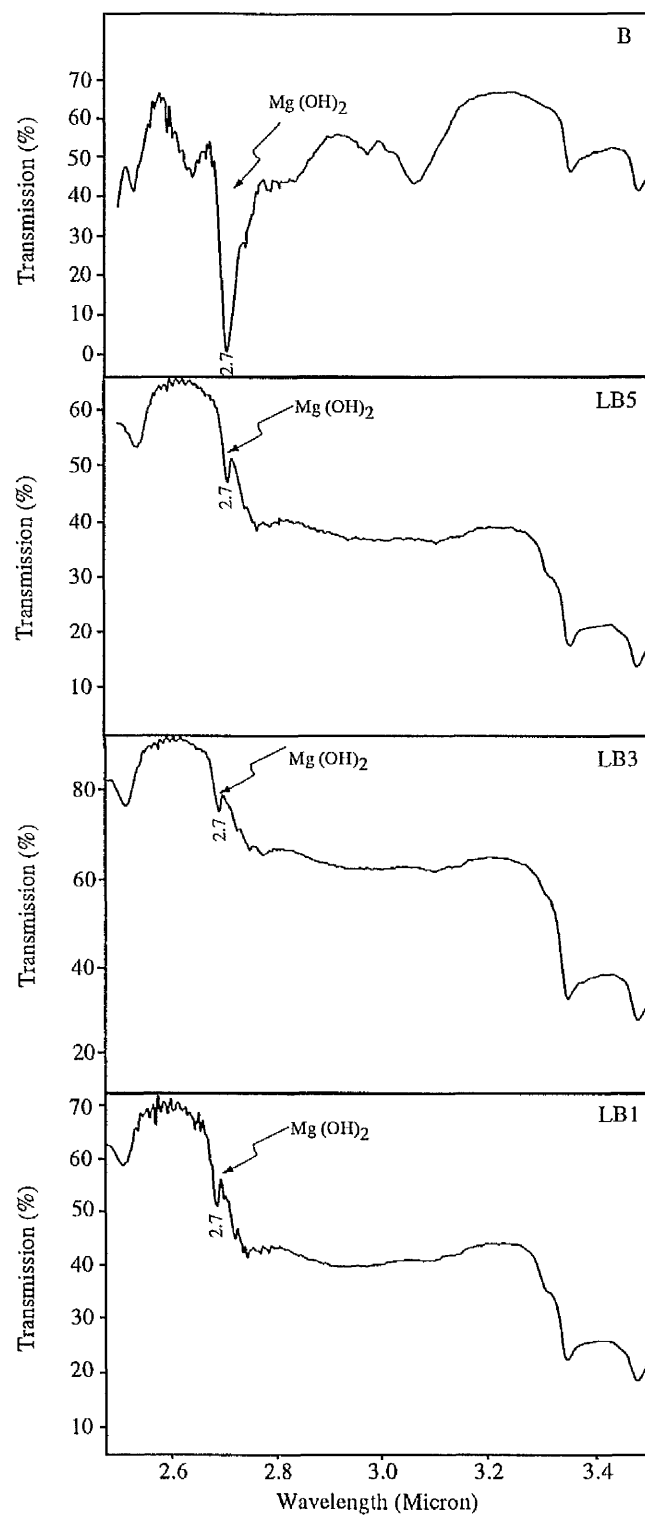
Figure (5.23) Infrared absorption spectra of carbonate
samples of the Benghazi Member of the
Ar Rajmah Formation compared with the
standard brucite mineral (B).
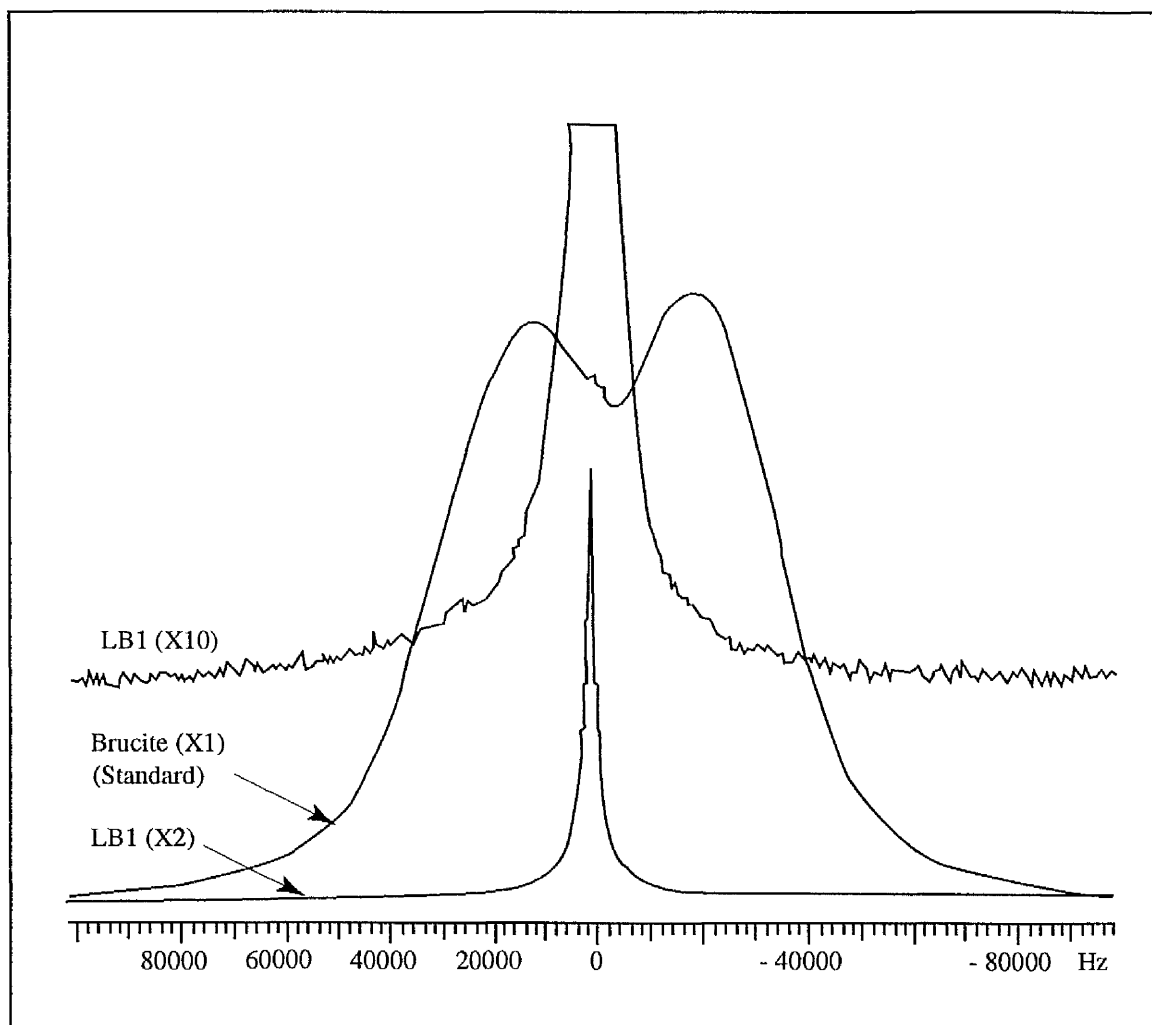
Figure (5.24) ^{1}H NMR spectrum of brucite mineral (standard) and sample no. LB1, Benghazi Member of the Ar Rajmah Formation (Middle Miocene).

5.8 Differential scanning calorimetry:

Carbonate and sulphate reactions, which are accompanied by heat effects detected in thermal analysis include: 1- loss of absorbed or crystal water; 2- crystallographic inversions; 3- decomposition of sulphates and carbonates; and 4- fusion points (Gruver, 1950). Carbonates and sulphates have heat effects occurring in the range of temperatures at which they are used in ceramics, cements (gypsum for example is used as a retarder for setting in portland cement) and glasses. Thermogravimetric and differential scanning calorimetric (TG-DSC) provide a means of studying the chemical and physical changes that take place in a sample when it is heated, and these changes can be used to characterise the material. Thermal analysis has found wide application in such areas as ceramics, polymer sciences, metallurgy and gravimetry (Robinson, 1982). Carbonate and sulphate minerals were subjected to air and CO_2 atmospheres and heated to 1200°C. Additional heating was used to 1500°C for the celestite of the Ar Rajmah Formation, with a heating rate of about 10°C per minute. A summary of the thermal characteristics of carbonate and sulphate minerals in this study is tabulated in Table 5.9 (see Chapter 9).

Table (5.9) Temperatures of thermal effects given by various minerals of the Ar Rajmah Formation and other standards.

Mineral	Formula	Observed weight losses (%)		Temperature (°C)			
				Endothermic		Exothermic	
		air	CO_2	air	CO_2	air	CO_2
Calcite-dolomite Mixed (7 %)	$CaMg(CO_3)_2$ (Benghazi Cement Quarry)	43.60	43.70	750 800	741 910		
	$CaCO_3$ (Benghazi Cement Quarry)			847	932		
Brucite	$Mg(OH)_2$ (Standard)	34.50	34.68	442 820	464 941		
Gypsum	$CaSO_4.2H_2O$ (Ar Rajmah Village)	19.22	19.81	144 163	141 157 938 972	366	359
Gypsum	$CaSO_4.2H_2O$ (Deryanah Al Abyar road-cut)	19.26	19.80	145 164 763	143 161 940 1036	364	361

5.8.1 TG-DSC curves of calcite and dolomite:

Calcite in facies LB1 of the Benghazi Member of the Ar Rajmah Formation is mixed with 7 % dolomite (the percent was determined by using point counting). The three steps in the TGA curves result from weight losses. Observed weight losses were 2.2 %, 5 % and 35.97 %. The 5 %

weight loss corresponds to peak 1 at 750 °C. The first endothermic peak which accompanies the loss of CO_2 by the $MgCO_3$ in dolomite is at about 750 °C and before the peak is completed it is interrupted by an endothermic deflection accompanying the loss of CO_2 by $CaCO_3$ at about 800 °C. Directly, and before the peak 800 °C is completed, there is another endothermic deflection in the same peak accompanying the loss of CO_2 by $CaCO_3$ but this time from calcite, with a observed weight loss of about 35.97 % at about 847 °C. When the same material is heated in an atmosphere of CO_2, the $MgCO_3$ endothermic peak was recorded at about 741 °C (lower in temperature). The $CaCO_3$ part of dolomite does not start to breakdown until 910 °C. The loss of CO_2 by $CaCO_3$ was recorded at 932 °C (Figure 5.25)

5.8.2 TG-DSC curves of brucite (standard):

Brucite (from Wakefield, Quebec in Canada) has a layered structure with two sheets of OH parallel to the basal plane with a sheet of Mg ions between them, each Mg lying between six OH. Kauffman and Dilling (1950) demonstrated that brucite dehydrates to perclase at about 480 °C. Brucite analyses confirms that brucite contains about 31 % water (Deer *et al.*, 1962). The thermal curves for brucite $Mg(OH)_2$ in air and CO_2 atmospheres are given in Figure 5.26. There are two endothermic peaks with associated weight losses. In air, the first of these, at 442 °C, is associated with a sample weight loss of 17.33 %. The second showed a 16.97 % increase at about 820 °C. The observed total weight loss is 34.3 %. The initial loss of 17.33 % observed by TG-DSC corresponds to dehydration of the brucite taking place at 442 °C. The remaining loss, 16.97 %, reflects a second stage of dehydration of brucite with further heating, and is complete by about 820 °C The presence of the talc as an impurity is confirmed by XRD analysis with peaks developed clearly at 18.98 °C 2θ (4.67 Å d-spacing) and at 48.56 (1.87 Å d-spacing). This may have affected the TG-DSC results, but as talc contains only 4 % water the effects will be very small, as described by Barlow *et al.* 1997) and Brindley and Chang (1974). Murray *et al.* (1951) conclude from DTA studies that there is some suggestion that carbonation of magnesium hydroxide can occur. From the DTA curves, there is no evidence of the presence of brucite in sample LB1, due to the absence of the peak of the loss of hydroxyl water at the range of about 440 °C to 470 °C. In CO_2, peaks shift to higher temperatures (464 °C and 941 °C). Heating in air is significantly different from heating in CO_2.

$$Mg(OH)_2 \Leftrightarrow MgO + H_2O$$
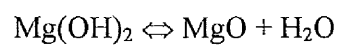
$$58 \Leftrightarrow 40 + 18$$

Predict weight loss $\quad = 18/58 \quad = 31\ \%$

Observed weight loss $= 34.5\ \%$ (Approximately 35 %; talc contains 4 % of water)
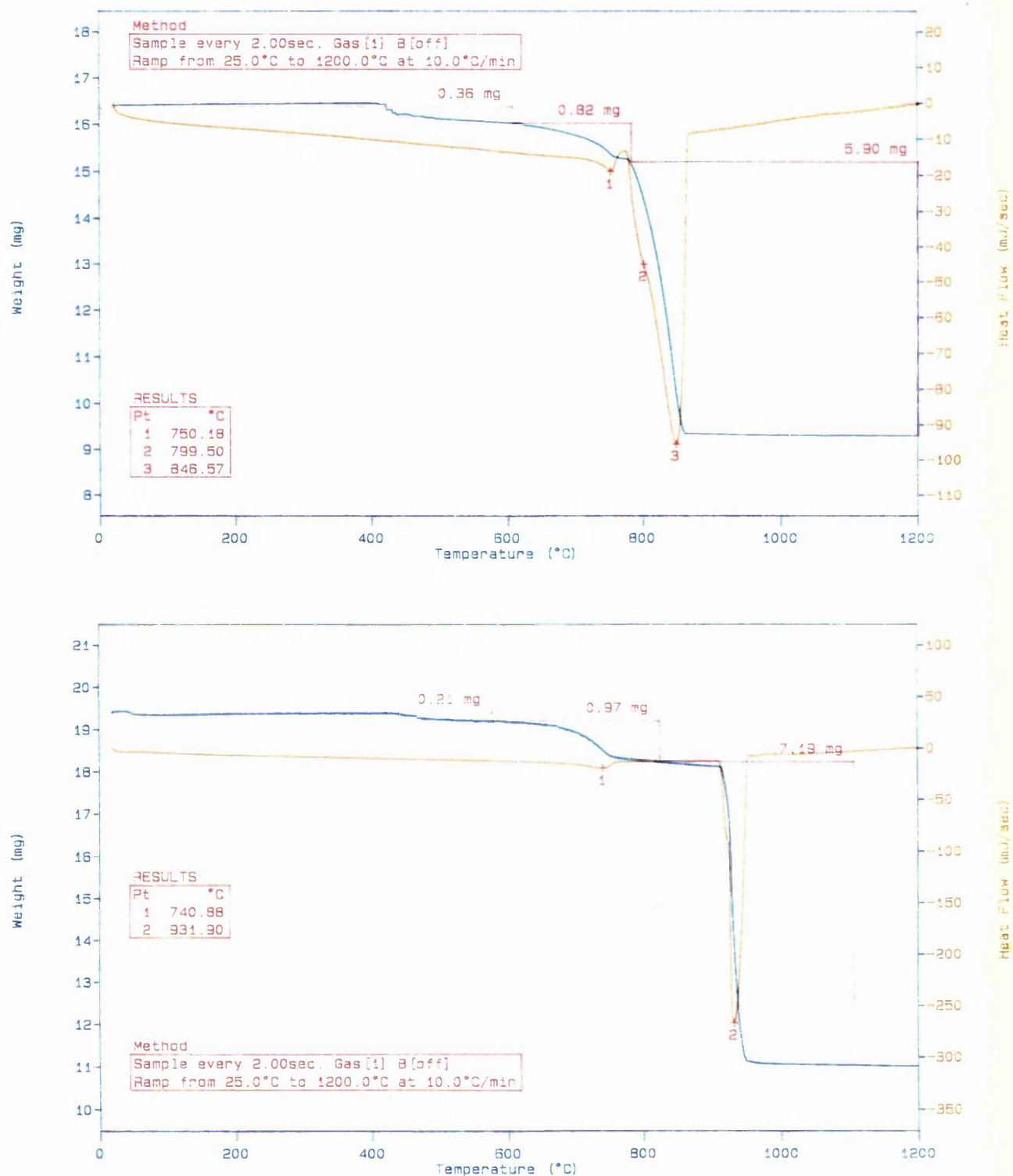
Figure (5.25) TG-DSC curves of calcite (LB1), of the Ar Rajmah Formation (Middle Miocene), in air (sample size = 16.2 mg) and CO_2 (sample size = 19.2 mg) atmospheres.
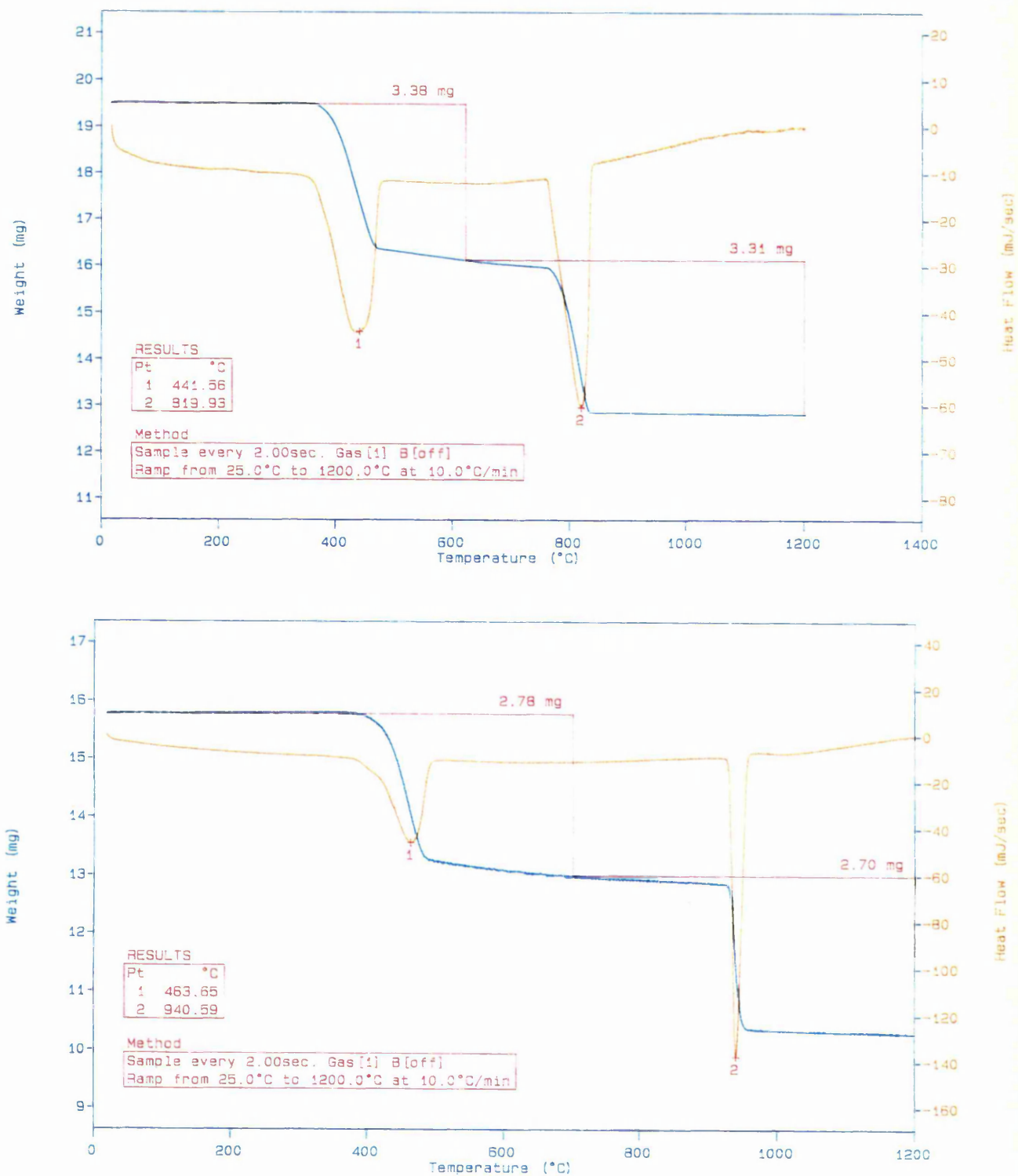
Figure (5.26) TG-DSC curves of brucite (standard), in air (sample size = 19.5 mg) and CO_2 (sample size = 15.8 mg) atmospheres.

5.8.3 TG-DSC curves of gypsum:

The DTA curves were obtained for the gypsum samples from two different locations in the study area (Deryanah Al Abyar road-cut and Ar Rajmah village) of the Wadi Al Qattarah Member of the Ar Rajmah Formation. In both locations, dehydration (hemihydrate $CaSO_4.1/2$ H_2O) began at < 200 °C. The two locations have one step in the TGA (Figure 5.27 and 5.28) resulting from weight losses. They correspond to peaks 1 and 2. The first location (Deryanah Al Abyar road-cut), with 19.3 % at peaks 145 °C and 164 °C, and the second location (Ar Rajmah village) with 19.4 % at about 144 °C and 163 °C. The possible cause for the small exothermic event at 364 °C and 366 °C for both locations is due to transformation of partly dehydrated gypsum (which preserves the structure of the hemihydrate), where the structure of anhydrite forms (polymorphic transition). The small endothermic peak at about 763 °C was observed in the first location only (Deryanah Al Abyar road-cut). It might be due to the presence of some foreign material (a trace of dolomite). In CO_2, the first endothermic peaks in both samples shift to lower temperatures of about 143 °C and 161 °C in the first location and 141 °C and 157 °C in the second location of the Ar Rajmah village. Gypsum at the first location Deryanah Al Abyar road-cut;

$$CaSO_4.2H_2O \Leftrightarrow Ca.SO_4 + 2H_2O$$
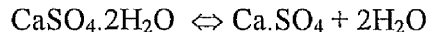
$$172.184 \qquad \Leftrightarrow 136.144 + 36.04$$

Predict weight loss   = 36.04/172.184 = 20.93 %

Observed weight loss = 19.30 %
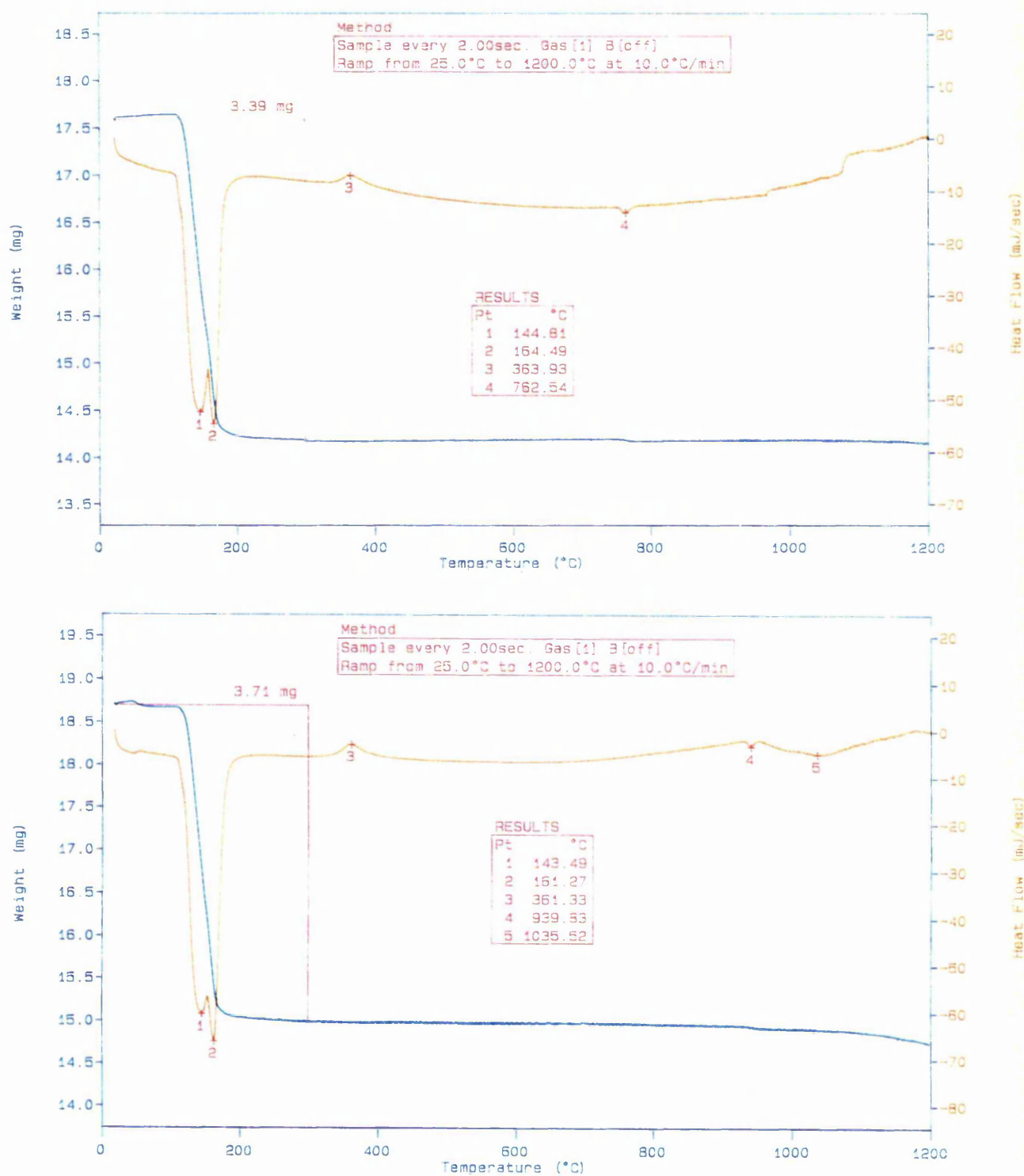
Figure (5.27) TG-DSC curves of gypsum, of the Ar Rajmah Formation (Middle Miocene), in air (sample size = 17.6 mg) and CO_2 (sample size = 18.75 mg) atmospheres, at Deryanah Al Abyar road-cut.
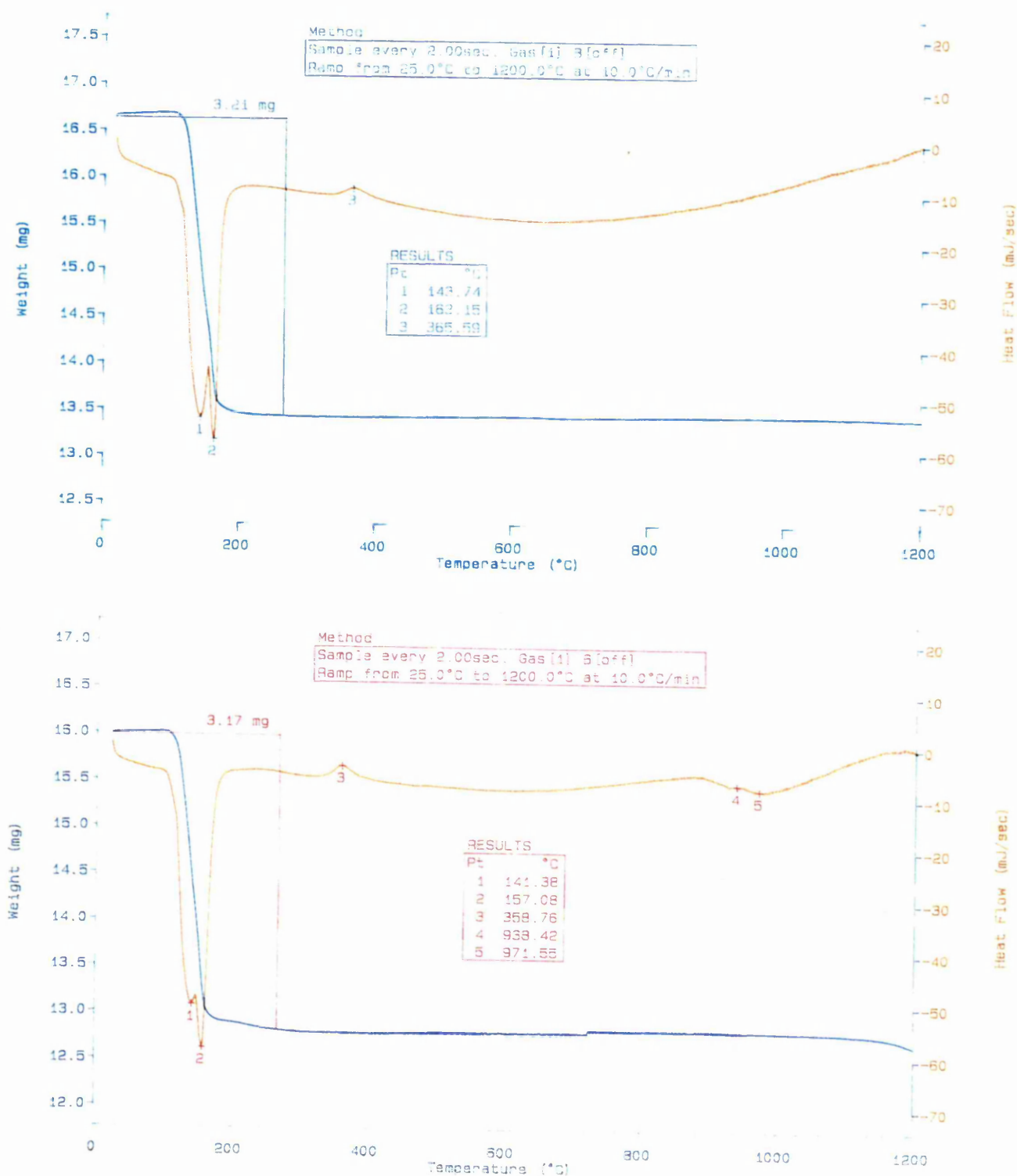
Figure (5.28) TG-DSC curves of gypsum, of the Ar Rajmah Formation (Middle Miocene), in air (sample size = 16.7 mg) and CO_2 (sample size = 16 mg) atmospheres, at Ar Rajmah village.

178

5.9 Conclusion:

- The region contains very high to high purity limestones except when dolomitised or contaminated by silicates of clastic origin (clays and glauconite) or diagenetic origin (chert).

- For cement manufacture, limestone of the Benghazi Member at Benghazi Cement Quarry has a consistent quality, but clays appear to be more variable.

- Sr minerals occur locally giving high Sr contents, the lack of correlation with other elements is consistent with the presence of high purity celestite ($SrSO_4$) and strontianite ($SrCO_3$).

- Coralline algae of the Ar Rajmah Formation comprise a mixture of high and low magnesium calcite and probably brucite $Mg(OH)_2$ is present and concentrated in the high magnesium calcite areas.

Chapter 6

LIMESTONE INDUSTRIAL POTENTIAL

6.1 Introduction:

Limestone is probably the most important industrial rock or mineral used by man. Limestone is a sedimentary rock, which contains 50 % or more of carbonate minerals, calcite or aragonite ($CaCO_3$) and dolomite $CaMg(CO_3)_2$. Aragonite (orthorhombic) is predominant in recent deposits. In dolomites (dolostones) the mineral dolomite is the major carbonate. There is a complete gradation from impure to very high purity limestone (< 85.0 % - > 98.5 % $CaCO_3$). High purity dolomites are defined as carrying > 87 % to 94 % of the mineral dolomite $CaMg(CO_3)_2$, or 40 to 43 % $MgCO_3$ (Harben and Bates, 1990). Modern carbonate sediments are composed of aragonite, high magnesium calcite (HMC) and low magnesium calcite (LMC). Ancient limestones are composed of low magnesium calcite (< 4 mole % $MgCO_3$) formed through diagenetic replacement of aragonite grains and loss of Mg from originally high Mg calcite (typically ranging between 11 and 19 mole % $MgCO_3$). Other diagenetic changes include dolomitization. This replacement process may greatly increase the porosity and silicification (Tucker, 1991). The texture of limestone reflects its sedimentary and compaction history and can be an important factor for economic purposes. For example limestone formed of loosely compacted shell fragments may break down easily on calcining and be unsuitable for use in certain kilns, whereas a compacted calcite mudstone of similar chemical composition may be perfectly satisfactory for calcining. Changes in texture can occur both laterally and vertically throughout some limestone deposits. Four components occur in the majority of limestones; non-skeletal grains (e.g. ooids and pisoids); skeletal grains; micrite and cement (sparite). Common non-carbonate minerals (impurities) in limestones are quartz, clay, pyrite, hematite, chert and organic matter. Evaporite minerals, in particular gypsum and anhydrite, may be closely associated with limestone rocks. Limestones possess a wide range of colour, grain size and bed thickness. All these features can have an influence on their utilisation. Overburden (soil or waste stone) is generally present and must be stripped off; its nature and thickness can greatly affect the economics of the operation. Structurally, joints and fault patterns must be determined as this will guide engineers in planning the method of extraction. Joints frequently occur at right angles to each other and well-jointed rocks are more easily extracted. If a high purity product is required a considerable amount of drilling and core analysis will be necessary. Limestones have widespread availability at relatively low cost. However, the main economic factor governing the

location of a quarry is probably the cost of transport to the place of consumption (Hull and Thomas, 1974).

Limestone calcination:

In the calcination of limestone using a rotary kiln or shaft kiln to produce lime (quicklime), the basic chemical reaction is as follows:

$$CaCO_3 \text{ (limestone)} + Heat \rightarrow CaO \text{ (quicklime)} + CO_2 \text{ (carbon dioxide gas)}$$
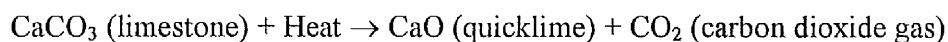
The temperature required is (1000 °C – 1300 °C). Pure limestone loses 44 % of its weight in the process (Harben and Bates, 1990). If quicklime is allowed to adsorb moisture from the air or combines with water with the evolution of heat, it is converted to the more stable form of lime known as hydrated lime (slaked lime).

$$CaO \text{ (quicklime)} + H_2O \text{ (water)} \rightarrow Ca \text{ (OH)}_2 \text{ (slaked or hydrated lime)}$$
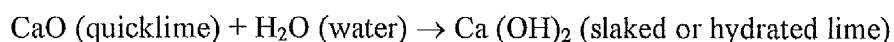
In excess of water, a little of the hydroxide dissolves, but the bulk remains in suspension, giving milk of lime also known as whitewash (O'Driscoll, 1988), the form in which limestone products are used for many industrial operations. Calcined dolomite is produced in a similar way and is commonly known as dolime. The purity of lime is dictated by the purity of limestone and secondarily by its manufacture. The major impurities are silica, iron, alumina and sulphur, and these range in importance depending on the lime's end use. Uncalcined limestone particles may remain as core in the individual lime pieces. Impurities and unreacted cores also affect the hydration reaction. If the source rock contains dolomite, this will also inhibit the hydration reaction, as dolomite's hydration may be nearly three orders of magnitude slower than that of calcium oxide. Typical analyses of pure quicklime and hydrated lime are illustrated in Tables 6.1 and 6.2.

Table (6.1) Typical analysis of pure quicklime suitable for industrial purposes

Constituents	% Dry
CaO	97.14
$CaCO_3$	0.71
$CaSO_4$	0.49
MgO	0.41
Fe_2O_3	0.31
Al_2O_3	0.18
SiO_2	1.01

Source: Stowell, 1963

Table (6.2) Typical analysis of pure hydrated lime suitable for industrial purposes

Constituents	% Dry
$Ca(OH)_2$	96.92
$CaCO_3$	0.93
$CaSO_4$	0.30
$Mg(OH)_2$	0.45
Fe_2O_3	0.07
Al_2O_3	0.14
SiO_2	0.53
H_2O	0.62

Source: Stowell, 1963

6.2 USES AND SPECIFICATIONS

The physical, mineralogical and chemical properties of carbonate rocks are widely utilised in many sectors of industry. The primary use of carbonate rocks is in construction, as aggregates (e.g. in road construction, railway ballast, concrete aggregate), or in the production of cement. These are also used in steelmaking, in the chemical industry (e.g. glass industry) and in many other uses. Limestone or lime may have non-construction uses as fillers and extenders or pigment. Diverse uses have diverse quality requirements. A brief summary of the major end uses of limestone is given in Figure 6.1.

6.2.1 CONSTRUCTION USES

Most limestones are hard and durable and useful for construction. The most common material used in construction is aggregate. Limestones are common rock types and usually occur in thick beds, which are structurally simple and easy to quarry, and are widely extracted for aggregate materials, as well as for the cement industry (limestone only; Harrison, 1993). Aggregates are also used in industrial building construction and in most public work projects such as roads, cement concrete, highways, bridges, railroad beds, dams and tunnels. The widespread use of limestone aggregate results not only from its general availability, but also from economic considerations. Natural aggregate varies widely in quality, mainly depending on the source of rocks. Suitable aggregate consists of clean, uncoated particles of proper size and gradation, shape, physical soundness, hardness, strength, and chemical properties. Aggregate containing deleterious ingredients can be a primary or secondary cause of problems such as crumbling driveways and bridges or cracks in sidewalks and building (Langer and Glanzman, 1993). Some limestone rocks are too soft and friable to yield high quality aggregate. Sandstones and impure sandstones or gravels are all commonly used as aggregate materials, where their strength and durability directly depends on the degree of cementation (Harrison and Bloodworth, 1994). A brief summary of the major uses of aggregates with an indication of typical specification requirements is given below.
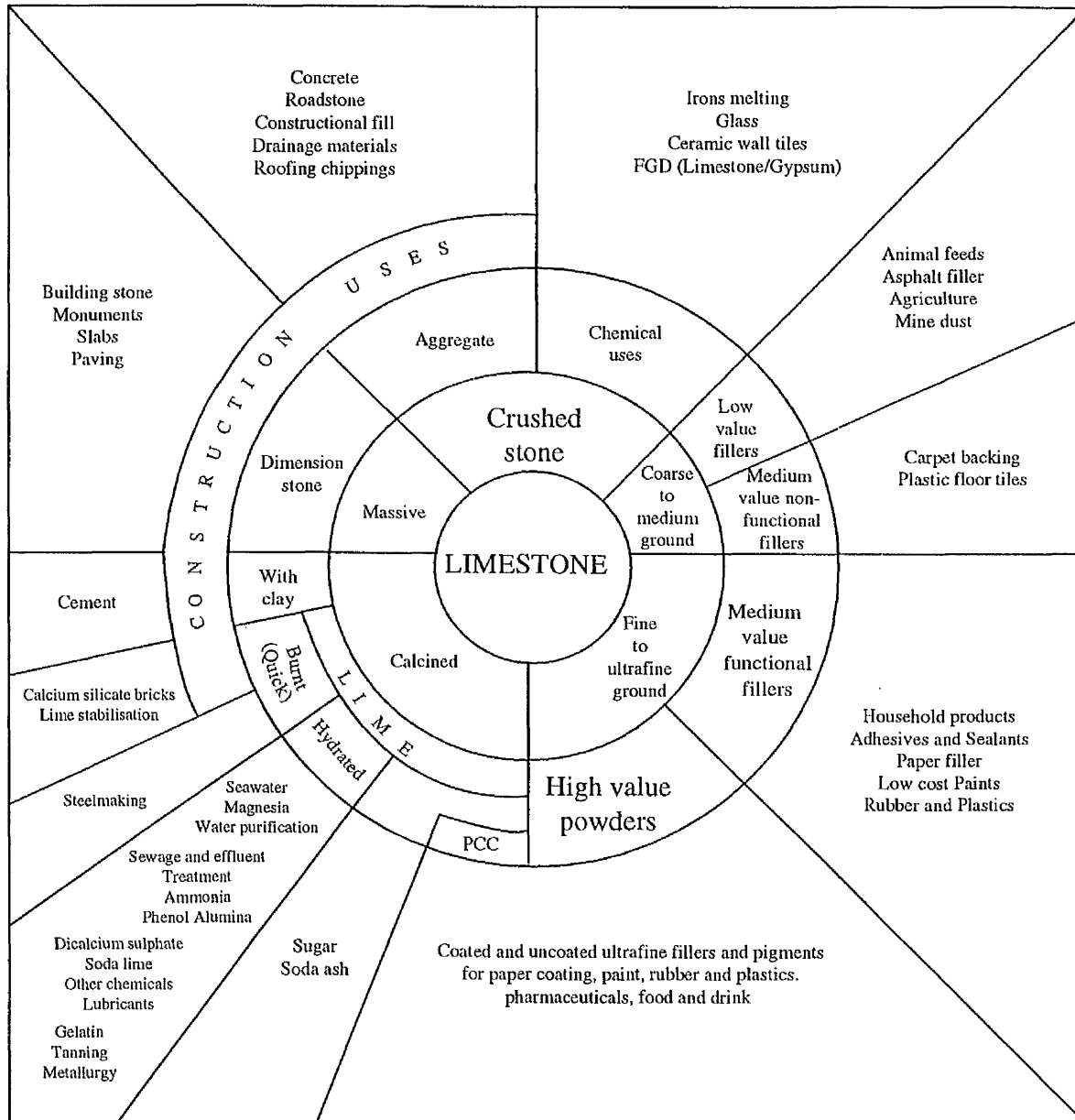
Figure (6.1) Processing and major uses of limestone, after Harrison (1993).

6.2.1.1 Roadstone:

Coarse, hard aggregate used in highway construction is called roadstone. Roadstone aggregates are commonly produced from all three groups of rocks at the Earth's surface: igneous, sedimentary and metamorphic. Crushed rock aggregates, natural gravels and sands are used in road pavement construction. Modern flexible road pavements consist of a series of layers with different properties is shown in Figure (6.2).

Wearing course	10 – 40 mm
Basecourse	40 – 75 mm
Roadbase	100 – 200 mm
Sub-base	(varies in thickness)
Capping layer	(if required)
Bedrock (Sub-grade)	

Figure (6.2) Cross-section of typical road pavement construction layers, after Harrison and Bloodworth, 1994.

The 'sub-base' consists of unbound crushed rock aggregate mainly 6-38 mm in size, which distributes the load onto the subsoil (sub-grade), and forms a working platform for construction. Clays are undesirable, but fine grained crushed rock is acceptable. It is overlain by the 'roadbase', which is the main load-bearing layer and consists of aggregate bound by bitumen (aggregate must bond well with bitumen binder and they must not shrink or swell, crack or react in use). The surfacing layers consist of a 'basecourse' and a thin 'wearing course'. Limestone aggregates are most commonly used in the sub-base and roadbase layers where they are required to be clean and strong with low porosity. The wearing course provides the texture of the road surface. It is made from rolled asphalt containing up to 30 % coarse aggregate, and is covered

by a layer of bitumen-coated chippings which come into contact with vehicle tyres. The performance of an aggregate layer in a pavement depends on the mineralogical, physical and mechanical properties of the stone, particle shape and grading and the method of laying the pavement. Aggregates that are used in pavement surface must being sounded, strong and durable. In addition they must be resistant to polishing and show resistance to stripping (Harris, 1979; Manning, 1995; Harrison, 1993; Harrison and Bloodworth, 1994). Some typical specification requirements for road stone aggregate are given in Table 6.3.

Table 6.3 Typical specification requirements for roadstone aggregate

Particle density (specific gravity)	generally >2.65
Water absorption (an indicator of porosity)	<2%
Flakiness index (shape factor)	<25 (for wearing course)
	<35 (for general purpose)
Aggregate crushing value (ACV strength test)	generally <24 or <30
Aggregate impact value (AIV strength test)	generally <25
10% fines value (strength test)	>160 KN
Aggregate abrasion value (AAV surface wear test)	<14 for lightly trafficked sites or <10 for potentially dangerous sites
Los Angeles abrasion value (LAAV attrition test)	<40 (for wearing course) <50 (for base course)
Polished stone value (PSV)	37-39
Sulphate soundness test (disintegration by weathering test)	<18% magnesium sulphate loss

Note: This table shows specifications relating to British and American standards. Where test value limits are not specified, then guideline values are shown, (Harrison and Bloodworth, 1994).

The chief causes of failure of a bituminous road or surface dressing are as follow;

- Actual wear of the surface.

- Fretting or working loose of individual particles or pieces of stone. Once such fretting has started, complete disintegration can often follow very rapidly. If the adhesion between the stone and the binder used is poor and insufficient, there is nothing to stop two adjacent stones from separating.

- Flattening up, or bleeding of binder, resulting in a slippery road.

- Displacement of the surface under the weight of traffic, causing rapid disintegration; where the stones become loose in the structure of the surfacing by movement under traffic.

6.2.1.2 Concrete aggregates:

Concrete is usually made from mixtures of cement, coarse and fine aggregate (sand) in the approximate weight ratio 1:3:2. Crushed limestone and other hard rocks are used for coarse aggregate. Sand and fine crushed limestone are used as fine aggregate. Aggregate is the major constituent of concrete (60 % - 80 % by volume). The type of aggregate influences the mix proportions and performance of the concrete. The important specifications required for concrete aggregates are density, strength, durability, thermal conductivity, the amount of deleterious materials (includes clay, mica, shale and other laminated materials), and shrinkage and creep. The shape and surface textures of the aggregate particles, their grading (distribution of particle sizes) and reactivity (aggregate should not react with cement pore waters) are important factors influencing the workability and strength of the concrete. Generally, crushed rock aggregates consists of angular particles, which have higher strength compared with similar mixes made from gravel. Crushed rock aggregates are essential for the production of very high strength concrete. Aggregates should not contain sufficient impurities that would have an adverse effect on the setting properties of the cement or the durability of the concrete. Physical and mechanical properties for concrete aggregates and some special requirements for coarse aggregate in concrete are given in Table 6.4 and 6.5.

Table 6.4 Physical and mechanical properties of concrete aggregates

Particle size and grading	BS gives grading limits
Particle shape (flakiness index)	<50 (gravel) and < 40 (crushed rock) – BS 882
Particle density	Not usually limited, except for concrete used in dams and marine protection
Water absorption (porosity)	Not usually limited, but recommended max. value of 2.5 % is sometimes specified
Soundness (magnesium sulphate)	< 18 for coarse aggregate and < 15 for fine aggregate – ASTM C33

Source: Harrison and Bloodworth, 1994

Table 6.5 Limits upon fines content in concrete aggregates (BS 882)

Aggregate type	Quantity of clay, silt, dust (%)
Gravel	2
Crushed rock	4
Sand	4
Crushed rock sand	16

Source: Harrison and Bloodworth, 1994

Concrete aggregates should be resistant to attack by alkaline cement pore fluids. The alkali – silica reaction (ASR) is a phenomenon in which alkalis derived from the cement and transported by the concrete pore fluids react with siliceous aggregates to form a calcium silicate gel which adsorbs water, expanding, cracking and weakening the concrete. For ASR to occur there must be a combination of three criteria; 1) a significant quantity of reactive silica, 2) sufficiently alkaline cement pore fluids (above the critical level), 3) sufficient moisture. ASR can be inhibited by restriction of any or all of these criteria (Manning, 1995). A list of undesirable constituents is given in Table 6.6. A further type of alkali-aggregate reactivity is the alkali-carbonate reaction (ACR), which occurs when certain carbonates react with alkalis to cause expansion and cracking (Gillot and Swenson, 1969).

Table 6.6 Deleterious minerals in concreting aggregates

ASR minerals	Opal (vein material, vug fillings, cementing materials)
	Tridymite and cristobalite (minor constituent of some acid and intermediate volcanic rocks)
	Chalcedony (some cherts and flints, vein material, cementing material etc.)
	Microcrystalline quartz (chert and flint, groundmass of some igneous and metamorphic rocks, cementing material etc.)
	Strained quartz (metamorphic rocks)
	Volcanic glass (some acid to basic volcanic rocks)
	Zeolites (particularly natrolite and heulandite)
ACR minerals	Dolomitic carbonates
Swelling minerals	Smectite, mixed-layer clays, kaolinite, zeolites
Iron minerals and metallic oxides	Pyrite, lead and zinc oxides
Chlorides	Common salt
Sulphates	Gypsum, magnesium and sodium sulphates
Organic matter	Coal, lignite, sugars, humus
Mica	Can be present in granites, gneisses and sandstones

Source: Harrison and Bloodworth, 1994

6.2.1.3 Aggregate for mortar:

From the French 'mortier', out of the Latin 'mortarium', consisting of a binding agent, mortar is mix of natural sand (or other fine aggregate) and lime and/or cement with water (pasty material) to provide a level of durability to match the bricks. It is used in bonding masonry (bonds the bricks together). The principal constituent of mortar is sand and the quality of the mortar is dependent on the particle size and shape of the sand as well as any impurities within the sand. Sands for mortars are often referred as; 'builder's sand', 'brick layer's sand', or 'mortar sand'. Also soft sands should not be used for mortars, as these contain fine silt and clay particles, which lead to unacceptable shrinkage and may interfere with the strength development in the mortar (Harding and Smith, 1986).

Properties of a good mortar are (Lynch, 1994):

- Adequate strength. Mortar should have strength compatible with bricks. It should never be harder than the bricks.

- Durability. When fully set is should be resistant to extremes of weather and pollution.

- Porosity. It should be similar to the bricks

- Workability. A good mortar is 'fatty', holding together when being worked and stiffens slowly.

- Aesthetically pleasing. As mortar represents between 15 – 25 % of a wall face, it affects the appearance of the overall brickwork. Therefore, consistency of colour and joint finish is essential. Typical grading requirements for mortar sand used in bricklaying are given in Table 6.7.

Table 6.7 Grading specifications for mortar sands for laying bricks

Sieve sizes	Percentage by weight passing sieve			
	UK (type S)	Japan	USA	Belgium
5.00 mm	98-100	100	100	100
2.36 mm	90-100	90-100	95-100	100
1.18 mm	70-100	70-100	70-100	100
100 μm	40-100	40-100	40-75	80-100
300 μm	7-70	5-75	10-35	40-85
150 μm	0-15	0-25	2-35	10-25
75 μm	0-5	0-10	-	0-7

Source: Harrison and Bloodworth, 1994

6.2.1.4 Railway ballast:

Railway ballast is specified largely on the basis of its resistance to abrasion when wet, a property in which igneous rocks generally, and some quartzites, have a significant advantage over limestones. Igneous rocks (e.g. granite and basalt) are generally preferred. Aggregates should be strong, angular, and with high resistance to abrasion. The material is usually expected to lie within a specified size range (often between 70-20 mm) and should be free of organic impurities, marl and clay.

6.2.1.5 Aggregate filters:

Aggregates are widely used as drainage filters in earthworks, in water filtration and in effluent treatment. Aggregates used as filters are required to be strong and durable, with a specified grading and particle shape. The filter layer will need to be structurally stable, highly permeable and durable with a low susceptibility to physical and chemical decay. Guidelines for acceptable materials in filters are given in Table 6.8, (Harrison, 1994).

Table 6.8 Typical specification requirements for filter aggregates

Grading	< 10 % fines
Flakiness index	< 30
Relative density	> 2.5
Water absorption	<3 %
Aggregate impact value	< 30
Los Angeles value	< 40
Soundness (MgSO$_4$)	< 12 % loss

Source: Harrison and Bloodworth (1994)

Although the total volume of filter aggregates is relatively small, they are used in a wide range of applications (Table 6.9).

Table 6.9 Aggregates for filter applications

Water supply	Well filters and envelopes
Purification works	Fine and coarse filter beds
Land drainage	Trench fills, pipe envelopes
Structural drainage	Foundation drainage, roadbed drainage, dam and slope drainage
Stabilisation works	Pressure relief, saturation control

Source: Harrison and Bloodworth (1994)

6.2.1.6 Dimension stone:

The term dimension stone is used for a rock that can be cut and worked to a size or shape for use in building. It is must be free from fractures, durable and devoid of minerals which may break down chemically or by weathering. Hard limestones and marbles are popular in building or ornamental stones. The durability of limestone is a function of its pore size. In particular a stone with high microporosity is susceptible to the crystallisation of salts. Fine micritic limestones are less durable than coarse spar-cemented limestones. Petrographic studies of limestones have shown that several parameters, including cement type and grain size, directly affect building stone durability (Price, 1986; Sedman and Barlow, 1989; Harrison and Bloodworth, 1994).

6.2.1.7 Cement:

Cement is made by calcining (at about 1500 °C) a mixture of about 75 % limestone and 25 % clay to form a calcium silicate clinker, which is then ground and mixed with a small amount of gypsum which acts as a setting retardant (Figure 6.3). The main impurities in the raw materials which may effect the quality of cement are magnesium (harmful because it forms periclase in the cement, which can survive until long after concrete has hardened, hydrated and causing expansion and disruption), fluorine (usually present in the raw materials as fluorite, and in excess of 0.1 % causes reduction in the strength of the cement), phosphates (in excess of 0.5 %), zinc, lead, alkalis (can affect the cement making process, they can volatilise and condense in inconvenient parts of the plant as alkali sulphates) and sulphides (form calcium sulphate in the kiln and in the presence of alkalis form alkali sulphates). Specifications for ordinary Portland cement (OPC) require that the cement should not contain more than 6 % MgO (< 3 % in the limestone), SO_3 and P_2O_5 (<1 %) and the total alkalis to be less than 0.6 %. For special cement types, such as sulphate-resisting cement, oil-well cement and white cement other constraints apply (< 0.01 % Fe_2O_3). Iron can also be a problem if it is present as pyrite, which will create SO_2 during heating. Loss on ignition should be < 3% in temperate climates or 4 % in tropical climates. Cement production requires crushing and grinding the raw material to make a fine grained powder followed by gradually increasing temperature, and then cooling rapidly. The raw material can be introduced as a dry power or wet, as slurry. Dry processing is preferred because it requires less energy. Heating the mixture is carried
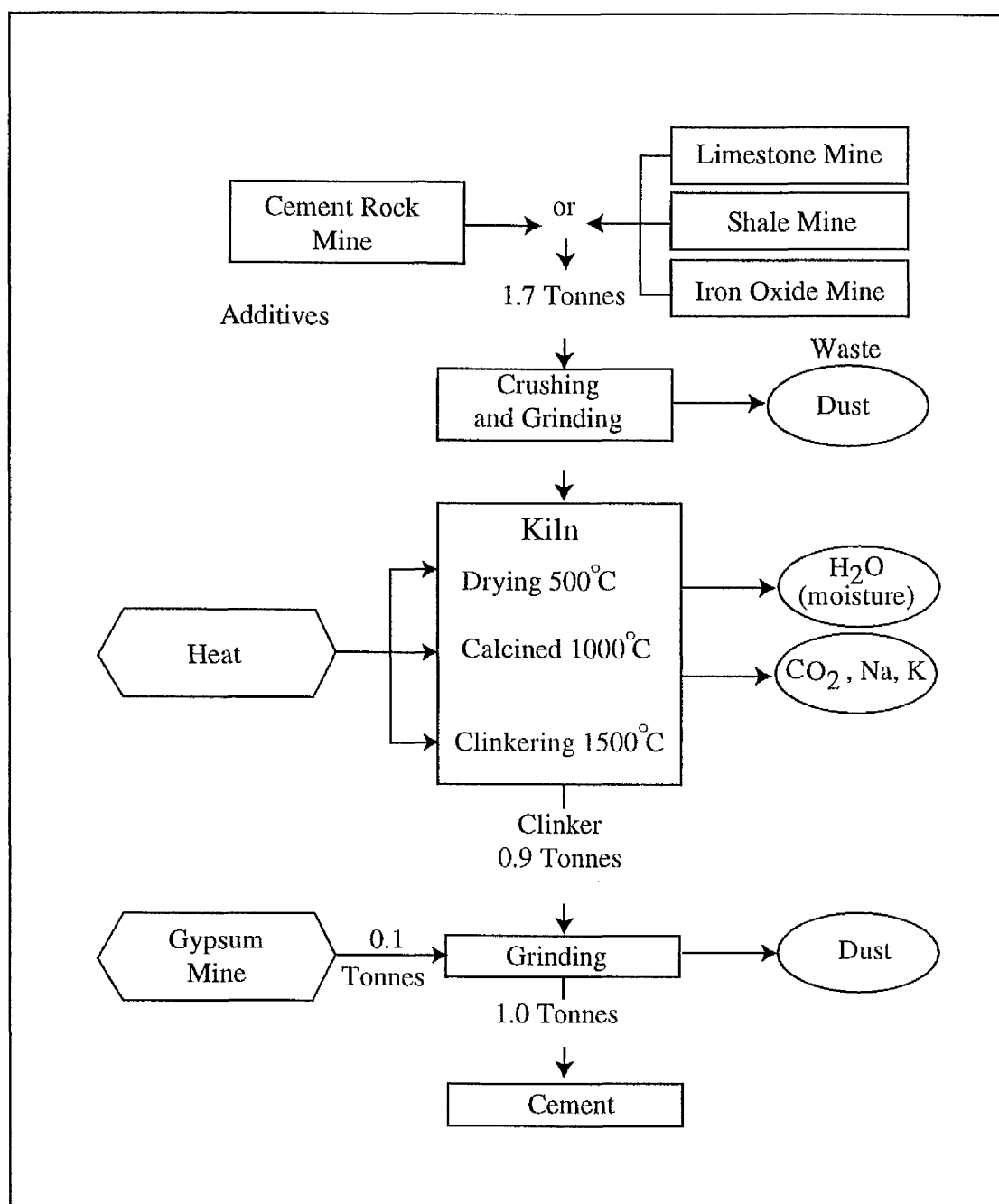
Figure (6.3) Schematic illustration of cement-producing progress, after Kesler (1994)

out in a rotating cylinder known as a rotary kiln. The process involves evaporation of any water, thermal decomposition of clay minerals (300 °C – 650 °C), and decomposition of calcite (> 800°C). At about 1500 °C the clinker is formed and then cooled and removed from the kiln for grinding into powder to make cement. Gypsum is usually added to the clinker to control the rate at which the cement sets, when it is mixed with water (Moore, 1976; Harris, 1979; Harrison and Bloodworth, 1994; Manning, 1995).

6.2.1.8 Calcium silicate bricks and lime plasters:

Lime is widely used in the building industry in the manufacture of calcium silicate bricks, lightweight concrete blocks, mortar, plaster and limewash. Calcium silicate bricks are manufactured from a mixture of lime and sand, which may contain other aggregates such as gravel or crushed rocks together with pigments. The bricks are moulded to the same size as clay brick and hardened in a steam press over a period of 4 – 15 hours, depending on the steam pressure used. Specifications for the lime required are not rigorous, but in general a good quality commercial quicklime for this use would be expected to contain 90 – 95 % CaO, and material containing less than 80 % CaO would be unsuitable. Lime is also used in the production of aerated concrete blocks by the reaction of a slurry of lime and sand with powdered aluminium or zinc. This results in the production of hydrogen gas and a cellular structure within the cured block. Limewashes, produced by adding water to lime or hydrated lime, are used for wall decoration and surface stabilisation. Plaster materials are designed to provide a durable, flat, smooth and easily decorated finish to the internal walls (Harrison, 1993; Taylor, 1994).

6.2.2 NON-CONSTRUCTION USES

Fillers and Pigments:

Any crushed carbonate rocks could be used as white carbonate fillers (white minerals) in a vast range of industrial uses. Material used as fillers varies, and depends on availabilities, costs, technologic trends and advancements and other factors. The white carbonate fillers industry uses includes ground limestone, chalk, marble or dolomite along with synthetically produced precipitated calcium carbonate (PCC). The important mineral fillers also include commodities such as talc, baryte, clay (China clay), mica, quartz and wollastonite. These minerals are predominantly used in the paint, plastic and paper industries. They must have high brightness and they can vary in particle size from industry to industry. Filler and pigment definitions depend more on their use than on physical or chemical properties (Dickson, 1987; Vidal, 1994; Parikh, 1998).

Ground carbonate and precipitated calcium carbonate (PCC):

There are two forms of carbonate fillers: carbonates ground to fine powder from naturally occurring rock (GCC), and precipitated calcium carbonate (PCC). PCC is a manufactured carbonate which is most commonly made by reacting quicklime (CaO) with water to form slaked lime or hydrated lime or milk of lime $Ca(OH)_2$. Then through recarbonation of the milk of lime with carbon dioxide a product forms that is aragonite (needle-like) or calcitic (hexagonal rhombic);

$$Ca\ (OH)_2\ (slaked\ lime) + CO_2\ (carbon\ dioxide) \rightarrow CaCO_3\ (PCC)$$
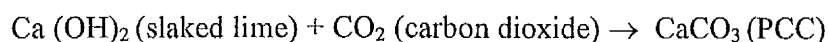
The limestone starting material for burnt lime must have a good chemical purity (minerals such as manganese and iron which lead to less bright precipitates must be avoided at all costs). Production of natural ground carbonates involves careful processing to obtain high-grade products. Particle size is one of the most critical physical properties of carbonate fillers. Generally, mean particle sizes in the < 2 micron range are designated as ultrafine and those in the 2-10 micron range as fine (McConnell, 1988; O'Driscoll, 1990; Sims, 1997; Harben, 1998). Brightness, chemical purity and oil absorption are also important properties but different end use applications will have different priority requirements e.g. a high brightness of > 85 %

will be required for a paper coating grade, but the same property would be unnecessary for a carpet backing adhesive (O'Driscoll, 1990). Many high volume uses of limestone powders do not require pure limestone (including asphalt, coal mine dust). Powders used in pharmaceuticals and food are required to be of very high purity and generally use PCC. Specifications for limestone powders used as fillers in paper, plastics and paints are typically based on a number of factors including particle shape, particle size distribution, high brightness values, specific gravity, surface area, reactivity, low absorptivity, refractive index and good rheological properties.

Limestone powders are classified according to particle size into the following (Harrison, 1993):

Coarse fillers (low value)	75 µm to several millimetres	Used for agriculture, animal feedstuffs fertilisers, asphalt filler and mine dust
Medium fillers (medium value)	< 50 µm	Used for carpet backing, floortiles, sealants, adhesives and putties
Fine fillers (medium value)	Max. particle size 50 µm, 50 % less than 2 µm	Used for paper fillers, rubbers and cheaper paints
Pigments and very fine fillers (high value)	Max. particle size 10 µm, 90 % < 2 µm	Used in paper coatings, paints, rubber and plastics

Source: Harrison (1993)

6.2.2.1 Use in Paper:

A paper made from fibres will be strong but is likely to be porous and have a rough surface, making it unsuitable for quality printing. The fillers and pigment materials, especially minerals, have been found to reduce porosity and roughness, and to fill irregularities of the paper surface and improve the printability of printing and writing papers. The most important raw material in paper production is wood pulp (the greatest cost). So any mineral that can replace the fibre and enhance the properties of the end product is going to be used as much as is technically possible. An amount of mineral fillers is beneficial since it improves the paper properties and reduces the total raw material costs. Mineral filler functions in paper are summarised as follows:

- Increased opacity

- Improved texture

- Improved printability

- Added brightness and whiteness

- Better formation and sheet structure through improved fibre distribution and the fill in of void areas

- Increased bulk

- Added cost savings proportional to fibre and TiO_2 replacement.

Mineral properties and their effect on paper: (Keegan, 1997)

Brightness. The brightness of a mineral increases in importance as the quality of paper increases. For high quality printing paper the brightness requirement increases to > 90 %. In general a minimum brightness of 80 % is required for filler clays and 85 % for coating. **Particle size and morphology.** Paper is composed of a network of cellulose fibres and filler minerals used to replace the expensive pulp and fill the spaces in between. Completely filling this space is not the desired effect; air still needs to be retained in the pore spaces to help with ink receptivity in the final printing stage. Therefore an important requirement of a mineral is its particle size and distribution. **Viscosity.** This property is not as important for filler minerals as it is for those used in coating, and the viscosity is a function of particle size and morphology. An increase in the size range will improve the viscosity of the mineral. **Glossing and opacifying effects.** The higher the refractive index (RI) of a mineral the greater the opacifying effects. (e.g. TiO_2 with RI of 2.5 is considered the foremost opacifier compared with talc and kaolin which have RIs of around 1.56). **Surface area.** This is particularly important when producing lightweight coated paper as an adequate coating can be attained using less mineral, therefore giving a lighter weight product. **Abrasivity.** It is important that any mineral used in paper should have a low abrasion factor, because it causes excess wear on the papermaking machine, wire and printing plates.

Paper was made under acidic conditions and around 90 % of filler used in the acidic processing techniques was kaolin. The switch to alkaline papermaking from acid took off in the 1980's and saw the demand for carbonate increase at the expense of minerals such as kaolin and talc. Currently, more calcium carbonate than kaolin is used in filler applications. Calcium carbonate slurries typically also have a higher solids content as opposed to kaolin slurries, which makes the slurry easier to apply

and reduces the amount of water that needs to be driven off in the drying process, resulting in additional cost savings to the paper mill. Calcium carbonate has also a higher brightness compared to kaolin. Calcium carbonates tend to increase the paper's brightness and opacity. For high finish carbonates for paper coating, the particles are less than 0.1 micron in size. The brightness of calcium carbonate is generally in the range of 93-98 %. In 1972, PCC was only used in some coating formulations as well as filler of some speciality paper. Initially, ground calcium carbonate (GCC) replaced PCC in coating formulations. PCC became the third largest filler pigment after kaolin and GCC (Decker, 1997). In the majority of cases, the replacement of kaolin by calcium carbonate has brought about the following advantages (Vidal, 1994):

- Reduction in costs due to increase in production.
- Reduction in costs due to the lower cost price of calcium carbonate slurry.
- Improvement in the whiteness of the coating layer.
- Improvement in the porosity of high speed printing paper without losing the shine of the printing dyes.

Foaming of the coating mixture is a frequent source of trouble to the coating mill chemist. Foam is of two types, coarse and fine. Coarse foam, commonly called froth, collects easily from the top of the coating mixture and ordinarily is not troublesome. Fine foam remains dispersed throughout the body of the coating mixture. It is usually very difficult to remove. Agitation greatly increases foam, and excessive agitation should be avoided as much as possible. Anti-foaming materials are used such as sulphonated oil, amyl or other high molecular weight alcohol, skim milk, ether, kerosene and tributyl phosphates (Casey, 1952; Casey, 1961).

6.2.2.2 Use in Paint:

Paints are surface coatings, and may be used for one or more of the following purposes (Taylor, 1994):

- To protect the underlying surface by exclusion of the atmosphere, moisture, fungi and insects.
- To provide a decorative easily maintained surface.
- To provide light and heat reflecting properties.

There are three stages in a painting system: 1) *primer* to provide protection against corrosion and to provide a good key for remaining coats, 2) *under coat* to provide good opacity together with a smooth surface, which provides a good key for finishing

coat, and 3) *finishing coat* must provide a durable layer of the required colour and texture.

Calcium carbonates are used in paint of which the most important uses are:

- As a pigment.

- As a diluent, reducing the need for other pigments.

- As a primer especially for gilding.

- In the production of putty.

In each case calcium carbonate should be perfectly white, of low density and of great fineness (Table 6.10).

Table 6.10 British Standard (BS1795) for calcium carbonate and dolomite extenders in paint

Physical specification								
		Residue on sieve (max.%)			*Particle size distribution (min.%)*			
Extender	*Grade*	*125µ m*	*63µ m*	*45µ m*	*<20µ m*	*<10µ m*	*<5µ m*	*<2µ m*
No.3	a	0.5	6.0	15.0	-	-	-	-
	b	0.01	0.5	2.0	85	65	45	20
	c	-	0.05	0.5	90	80	55	25
	d	-	-	0.01	97	95	70	35
No.4	a	0.01	1.0	5.0	70	40	25	10
	b	0.01	0.5	1.5	80	45	30	10
	c	-	0.01	0.1	95	65	35	15
	d	-	-	0.01	-	98	70	25
No.5	a	0.1	0.25	0.5	90	70	40	-
	b	0.1	0.25	0.5	-	90	70	20
No.6	a	0.01	1.0	5.0	70	40	25	10
	b	0.01	0.5	1.5	80	45	30	10
	c	-	0.01	0.1	95	65	35	15
	d	-	-	0.01	-	95	70	25

Chemical specification	*No.3*	*No.4*	*No.5*	*No.6*
%$CaCO_3$	96-99	98	97-100	-
%$CaMg(CO_3)_2$	-	-	-	97
Volatile matter 105°C	0.3	0.3	1.0	0.3
LOI	42-44	42-44.5	43.5-44.5	46-48
Matter soluble in water	0.15	0.15	0.3	0.2
pH of aqueous solution	8-9.5	8-10	8-10.5	8-10.5

Source: IM Pigments, Fillers & Extenders (1988)
Extender No.3: Whiting (grades a, b, c, d). Calcium carbonate, naturally occurring Cretaceous chalk, primarily $CaCO_3$ of microcrystalline forms (essentially remains of coccoliths and formaminifera)
Extender No.4: Calcium carbonate, crystalline (grades a, b, c, d). Limestone, Iceland spar, natural calcium carbonate, other than in No.3.
Extender No.5: Calcium carbonate, precipitated (grades a, b).
Extender No. 6: Dolomite (grades a, b, c, d). Calcium magnesium carbonate. Approximately equimolar proportions of calcium and magnesium carbonates.

6.2.2.3 Use in Plastic:

Calcium carbonate filler is by far the most widely used mineral filler in plastics, accounting for nearly 60 % of the total volume. Traditionally, calcium carbonate was a cheap bulk filler, merely used to reduce the overall price of the plastic component, since the filler is considerably cheaper than the plastic resin. More recently all fillers are required to impart useful properties and the role has changed from one of a cheap bulk material to a functional filler that imparts desirable properties to the system as a whole. Still, cost is the major factor, but calcium carbonate with the other fillers available must add to the properties of the finished composite. PVC is the principal plastic in which ground calcium carbonate is used in applications such as PVC rigid/flexible pipes (rate up to 15 %), PVC sheet (5 %) and PVC window profiles (7 %). Finer materials (ultrafine) and coated grades are now used to give less abrasion and better synergy with plastic systems. Polypropylene (PP) ranks second in calcium carbonate consumption. Calcium carbonates (often stearate coated) are principally used for garden furniture and household items. Combinations of talc and calcium carbonate are occasionally used where the plate-like talc particle provides good rigidity through its high aspect ratio, and calcium carbonate ensures that this is not coupled with the loss of too much impact strength ('IM' Pigments, Filler and Extenders, 1988; Jones, 1997; Decker, 1997; Parikh, 1998). Other examples of calcium carbonate consumption in smaller amounts include polyesters, engineering plastics, phenolics, polyurethane (PU), foam or low-density polyethylene (LDPE) and epoxy resins. Summaries of applications for calcium carbonate as a filler, and also selected minerals used in plastics, are given in Tables 6.11 and 6.12.

Table 6.11 Summary of applications for calcium carbonate filler in plastics

Polymer	Filler level (phr)*	Particle size microns	Remarks
Flexible PVC	20-60	3	Compared with coarser grades fine filler causes less of a decrease in physical properties and provides better performance in thinner calendered films and coating
PVC plastisols and organisols	20-100	wide range	Coarse grades for carpet backings to ultra fine precipitated grades and coated chalk whiting for thixotropic viscosity control. Coarse particles lead to lower viscosity in plastisols.
Rigid PVC	1-5	2-3	Application in plastics for potable water pipe
	40	1-3	Other pipe and conduit applications. Stearate-coated grades improve melt rheology and smoothness of extrusion; uncoated grades serve as antiplate-outagents.
PVC floor tile	8-400	small	Finest grind is about 12 microns, size distribution is wide, colour varies with feedstock.
Sheet moulding compound	200	3-6	Used in low viscosity one and two component resins. Moisture content must be kept below 0.1% for controlled thickening during maturing.
Bulk moulding compound	250	3-6	Loading is usually 250 phr for BMC, 100-150 phr for premix, preform, and mat-over 400 phr is possible. Size, distribution, and purity are selected to provide low uniform viscosity polyester.
Marine polyester	175-200	3-5	Meets standard requirements for this application of 0.15% maximum water absorption during a (1) hour immersion.
Polypropylene	43-67	1-3	For both polypropylene homopolymer and copolymers.

*Part per hundred of resin
Source: IM Pigments, Fillers & Extenders (1988)

Table 6.12 Minerals used in plastics

Mineral	Major resin	Function
Mica	Polypropylene	Flexural strength
Kaolin, surface treated	Nylon	Dimensional stability
Wollastonite	Nylon	Reinforcement stability
Alumina hydrate	Polyester	flame retardance
PCC	PVC	Impact strength
Kaolin,calcined	PVC	Electerical resistance
Talc	Polypropylene	Stifiness
Silica, ground	Epoxy	Dimensional stability
Calcium carbonate ground	PVC	Cost reduction
Kaolin, air-floated	Polyester	thixotropy

Source: IM Pigments, Filler & Extender (1988)

6.2.2.4 Use in pharmaceuticals: (Russell, 1988)

The pharmaceutical industry is very highly regulated with stringent control to govern laboratory practice, clinical trials, manufacture, product labelling and marketing. This of course also includes exacting requirements on the raw materials used. The pharmaceutical industry is a very low volume specialised market for minerals, which carries strict specifications for the supplier. In many cases a close relationship is developed between a pharmaceutical company and its supplier, which understands the nature of the business and is rewarded by the premium prices paid for pharmaceutical grade materials. Testing and batch verification must be carried out. The mineral suppliers have to ensure that the material supplied has consistent physical as well as chemical properties. Likewise minerals supplied to the pharmaceutical manufacturer must meet pharmacopoeia standards and do not require further processing. Some of the main international pharmacopoeias used and specifications are given in Table 6.13 and 6.14.

Table 6.13 Some of the main international pharmacopoeias used

Pharmacopoeia	*Abbreviations*
British pharmacopoeia	BP
German pharmacopoeia	DAB
European pharmacopoeia	PH. Eur/EP
The pharmacopoeia of the USA	USP
Japanese pharmacopoeia	JP
United State National Formulary	NF

Source:Alison Russell (1988)

Table 6.14 Pure Carbonate and USP specifications

Chemical properties	*USP*	*Pure Carb.*
$CaCO_3$	98.8% min.	99.78%
Loss on drying	2.0% max.	0.19%
Acid insoluble substances	0.2% max.	0.10%
Flouride	0.0005% max.	0.001%
Arsenic	3.0 ppm max.	2.0 ppm
Barium	no green colour	no green colour
Lead	3.0 ppm max.	>3.0 ppm
Iron	0.05% max.	>0.05%
Mercury	0.5 ppm max.	>0.05 ppm
Heavy metals	0.002% max.	>0.002%
Magnesium & alkali salts	1.0% max.	0.02%

Physical properties of Pure Carb.	
SG	2.70 g/cc
Hardness	3.0
Dry brightness (green filter)	95.0%
Oil absorption (100 grams)	20.0 g
Mean particle size	2.4 microns
Top cut	10.0 microns

Source:Mike O'Driscoll (1990)

6.2.2.5 Use in Adhesives and Sealants: (O'Driscoll, 1990)

Carbonate fillers are one of the most widely used fillers in adhesive and sealant compounds. Extremely tight specifications are required of fillers in high performance adhesives and sealants, which usually use coated grades of ground carbonates and PCC. Chalk and limestone fillers are also used where colour (i.e., whiteness) is not a priority. When colour is required (e.g. sealant material used to grout ceramic tiles), the more expensive calcite is selected. Calcite, which is superior in quality to limestone and chalk whiting is found in high performance sealants such as silicones. For the sealant to remain stable during storage the filler must have a very low moisture content (< 0.2 %).

6.2.2.6 Use in Mine dusting:

Limestone dust is used to limit of coal mine roadways to prevent the propagation of explosion flames. Limestone is used because it is free from silica and so does not cause a respiratory disease known as silicosis. Limestone dust requires that the material should contain less than 3 % free silica and have a size distribution in which 90 % is finer than 250 μm. The dust should be easily dispersed in air and free from any tendency towards caking (Harris, 1979).

6.2.3 CHEMICAL USES

6.2.3.1 Use in Glass manufacture:

Glass is the material from which windows, bottles, jars, light bulbs and a whole host of other products are made. Limestone is the third most important industrial raw material in glass after silica sand (around 70 % of the total) and soda ash (22 %). Limestone and dolomite are added to the glass batch to contribute the correct ratio of CaO and MgO required for the manufacture of the common soda-lime-silica glass.

Glass manufacture:

Soda-lime-silica glass manufacture involves melting of the mixed raw materials at 1600 °C. The two most common bulk additions to silica in glass are soda ash (sodium carbonate Na_2CO_3) and limestone. In the resultant glass the elements sodium and calcium are present as the oxides, soda and lime, and hence the name

soda-lime-silica glass. These three components are the basis for over 90 % of all glass melted. Lowering the temperature of initial formation of the glass, the presence of soda and lime also lowers the viscosity sufficiently to allow working at temperatures as low as 600 °C. In Libya the most common composition of a soda-lime-silica glass is approximately 70 % silica, 13-15 % soda ash, 9-10 % lime (CaO), 1-2 % MgO, 9-10 % limestone, 2 % feldspar and 1 % barite or gypsum. For sheet glass (flat type), MgO increases to 4 % and CaO decrease to 7 %, with the addition of 25-30 % cullet (Al Aziziyah glass factory). The international composition of soda-lime-silica glass is approximately 70 % silica, 15 % soda ash (higher amounts of soda ash produce water glass) and 5-10 % lime. There are four basic stages common to the manufacture of all glass products. **Melting** of the raw materials; **refining** to achieve homogeneity of the molten glass; **working** to form the glass into the desired shape; and **annealing** to relieve internal stress developed during the working stage. The raw materials are mixed before entered the furnace and waste glass known as cullet (of the same type) is also added. Cullet melts before any other constituents and reaction takes place in the region 600 °C –900 °C, releasing carbon dioxide and other gases which form bubbles. To remove these bubbles, the temperature is raised to about 1600 °C. Refining agents such as sodium sulphate (which are added to the original batch), become most active in their role of aiding the release of bubbles and preventing the formation of a scum on the surface of the molten glass. The melt is cooled to about 600 °C to obtain the required viscosity for working to begin. Limestone in glass manufacture is required twice:once to produce soda ash section 7.2.3.4 and as an ingredient to produce glass. The chief impurities to be avoided are iron (varies from < 0.05 % to 0.02 % depending on the type of glass), as minute amounts of this will colour the glass into green to brown. MgO has to be known; the presence of magnesia in small quantities assists the melting rate as well as increasing the chemical resistance of the finished glass. The presence of lithium will reduce the temperature required to melt the glass. Chromium, cobalt or nickel must be very low as minor amounts might have an affect on the glass colour. Generally, very high purity limestones (>98.5 % $CaCO_3$ or 55.2 % CaO) are required for this application (Hull and Thomas, 1974; Harben, 1988; Prentice, 1990; Kendall, 1993; Manning, 1995).

6.2.3.2 Use in Iron and Steel:

Limestone or lime is added to the furnace as a flux, to extract iron (pig iron) from iron ore pellets. This is usually done in a blast furnace, a large vertical cylinder that is charged with a mixture of metal ore, coke, and limestone (Figure 6.4). Air is 'blasted' in from the bottom to promote combustion of the coke to carbon monoxide, and the waste minerals (impurities such as silica and alumina), react with limestone to form slag. Pig iron liquid, accumulates at the bottom of the furnace. Therefore, slag will float on the surface of the metallic melt. It can then be removed from the furnace before pouring off the purified metal. The slag from iron and steelmaking in USA is recovered and sold as construction aggregate. For steelmaking processess, pig iron is converted to steel. This process is carried out in steel furnaces. Highly purity limestone (or dolomite) with low sulphur and phosphorus contents are generally specified for this process. Specifications for lime or calcined dolomite for steel fluxes demand high-purity material with low silica (< 5% to 2 %) and sulphur (< 0.1 %). Particle size, surface area and density of the lime are also important (Harrison, 1993; Kesler, 1994).
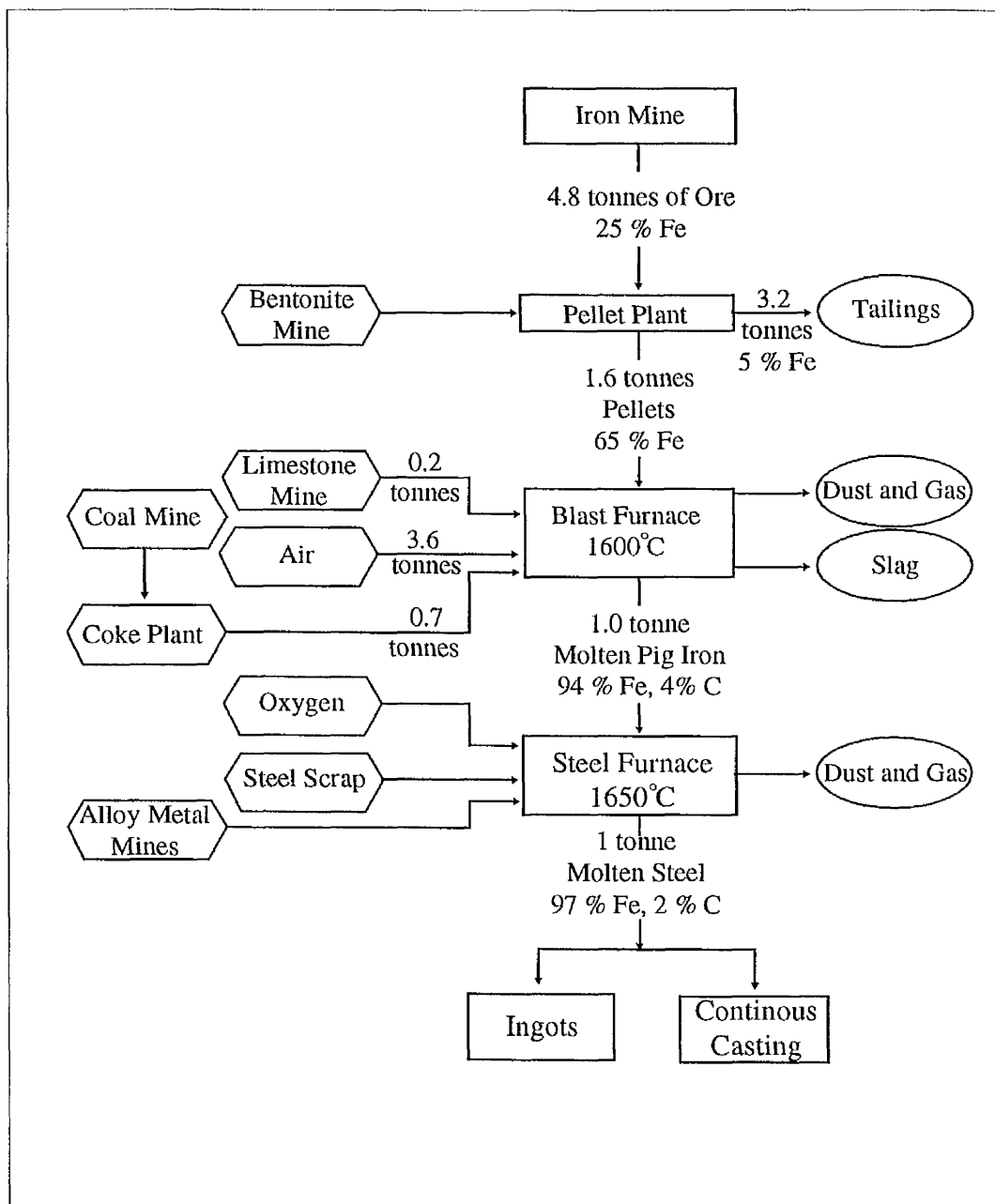
Figure (6.4) Schematic illustration of the pig iron and steel production process, after, Kesler (1994).

6.2.3.3 Use in Agriculture:

Limestone and dolomitic limestone furnish the important elements of calcium and magnesium necessary for the correction of acidity of the soil and for the promotion of plant life. The main functions of limestone are to reduce soil acidity, to separate the particles of dense clay and open up the soil, thereby making it easier to dig or the plant roots to penetrate it. The soil becomes more porous and better aerated, improving soil structure and preventing the development of harmful organisms, thereby correcting sourness and faciliating plant growth. As soon as soils become acid bacterial action is largely suspended and in their place moulds and other micro-fungi become predominant. For agricultural use the calcium carbonate should be in the form of a fine powder. It should pass completely through a 60-mesh sieve and not leave more than 10 % on a 100-mesh sieve. Also calcium is essential for the development of healthy bones and teeth, but is also vital for lactation and in chickens it provides eggshell strength. Limestone is the most prolific of all minerals used in animal feed, but consumption is highest in cattle and chickens. Limestone is added in the form of powder or granules, with inclusion levels varying from 1-2 % in cattle feeds to 7-8 % in chicken feeds. However, excess calcium can affect the absorption of other essential minerals (Harris, 1979; Loughbrough, 1993).

6.2.3.4 Use in Soda ash manufacture:

Sodium carbonate (soda ash) is an important raw material for the chemical industry (such as glass, soap, textiles and in drilling fluid to treat total hardness), and involves the reaction of carbon dioxide with a solution of brine and ammonia to produce ammonium chloride and a sodium bicarbonate precipitate. The precipitate is recovered and heated to produce sodium carbonate and the solution is treated with lime to release ammonia for recycling. The lime and carbon dioxide consumed in the process are obtained by calcining limestone, which should be of high purity (> 98.5 % $CaCO_3$) (Harrison, 1993).

6.2.3.5 Use in Sugar Refining:

Both limestone and lime are used in the sugar industry as part of the purification process. In the processing of sugar beet, the vegetable is cut into slivers from which the soluble constituents are extracted by leaching with water. The resulting solution is then treated with milk of lime which is used to adjust pH and to

assist in precipitation of impurities. Carbon dioxide is then blown into the sugar juice to precipitate the original lime as calcium carbonate. Subsequent filtration gives a clear solution from which the sugar can be crystallised after evaporation. The settled material, which contains significant amounts of nitrogen, phosphorus and magnesium, is eventually sold for agriculture purposes. High-grade limestone containing at least 96 % calcium carbonate with low silica content is normally required (< 1 % SiO_2) and < 0.35 % Al_2O_3 and < 0.3 % Fe_2O_3 is usually specified (Harris, 1979).

6.2.3.6 Use in Flue gas desulphurisation (FGD): (Harris, 1979)

Limestone and lime are used to remove sulphur dioxide from flue gases of coal-fired plants. The limestone-gypsum process involves passing the flue gases through circulating slurry of limestone and water. Sulphur dioxide dissolves and reacts with the limestone to form calcium sulphite that is then oxidised to gypsum. The gypsum may be a useful by-product. High quality limestone is used, with over 95 % $CaCO_3$ and small amounts of SiO_2 (<0.65 %), Al_2O_3 (< 1 %), and Fe_2O_3 (< 0.25 %).

FGD processes using lime:

Wet scrubbing:

Lime or limestone is added to the slurry to neutralise the acidic SO_2 and convert to a solid. Most of the neutralised slurry is returned to the scrubber to absorb more SO_2. A portion of the slurry is fed to a dewatering system that produces a wet cake for disposal.

Dry scrubbing:

Slaked lime slurry is sprayed directly into the flue gas. SO_2 is captured by the lime and the slurry is dried by the heat of the gas. The dry solid containing captured SO_2 is then disposed. Advantages over the wet process include lower operating costs, and disadvantages are the dry process is limited to coals containing < 2.5 % S. As sulphur content increases lime utilisation decreases.

6.2.3.7 Use in calcium carbide (CaC_2) manufacture:

Calcium carbide is a primary heavy chemical and it is an intermediate material in the manufacture of cyanamid ($CaCN_2$) and acetylene. It is made by heating a

mixture of lime and coke together in a furnace (usually electrical) at 2000 °C. The reactions which take place are represented by the equation:

$$CaO + 3C \rightarrow CaC_2 + CO \uparrow$$
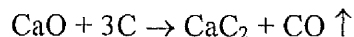
About one tonne of lime is required for each tonne of carbide (Thompson, 1977; Harris, 1979).

6.2.3.8 Use in seawater magnesia manufacture:

Dolime (slaked calcined dolomite) or hydrated lime is used to precipitate the available magnesium in seawater as magnesium hydroxide. The latter is calcined to give magnesia (MgO) which is used in a wide variety of industries including agriculture, animal feedstuffs and mainly in the manufacture of refractories. Dead burned magnesia (double burned form of dolomitic quicklime) is used extensively for metallurgical, cement and glassmaking refractories, and is employed primarily as a refractory for lining open-hearth steel furnaces. Typical specifications demand low $SiO_2 < 0.15\ \%$, $Al_2O_3 < 0.05\ \%$ and $Fe_2O_3 < 0.15\ \%$ (Thompson, 1977).

6.2.3.9 Use in water treatment (potable water):

Hydrated lime is used in the treatment of drinking water to adjust the pH and removing impurities. Acidic water would be corrosive to the distribution system. In these circumstances the hydrated lime is used by water supply authorities to bring the pH to 7 before water is distributed. Chemical and physical constraints on the type of limestone used to produce the lime are not usually specified (Thompson, 1977).

6.2.3.10 Use in drilling fluids:

Calcium carbonate and lime are used in oil drilling wells. Calcium carbonate (at least 97 % $CaCO_3$) is an acid soluble weighting material designed to increase the density of non-damaging workover and completion fluids. It also acts as a bridging material reducing the fluid loss and in combination with polymers forming a tough impermeable filtercake. This filtercake can be treated by acidizing with HCl (high return permeability). Slaked lime is used in water base drilling fluids as a pH-regulator and bicarbonate and carbonate precipitant. The product is also used in invert emulsion systems to form calcium-based emulsifiers. If there is no slaked lime in oil

based mud the emulsifiers does not work. Hydrated lime in oil based mud makes alkali water in oil to control corrosion (the system contains of about 20 % water and 80 % oil). Hydrated lime should have a purity of at least 95 % (Jowfe product data sheets).

6.2.3.11 Use in carpet backing:

In Libya limestone is used in carpet backing, as a part of the raw materials for latex compound (Table 6.15). High-grade limestone used in this mixture contains at least 96 % $CaCO_3$.

Table 6.15 Raw material for latex compound

Latex (S.B.R*)	23.2 %
Limestone	69.8 %
Thickener; polyacrylate	1.9 %
Anti-foam agent	0.72 %
Sequestering agent	0.5 %
water	4.6 %

* Styrene Butadine Rubber   Source: Textile industry Benghazi-Libya

Chapter 7

CLAY MINERALOGY AND GEOCHEMISTRY

7.1 Introduction:

The Al Faidiyah Formation is the youngest unit in the Umm Ar Razam area, and the Faidia Clay Member is the lower part of the Al Faidiyah Formation. The lower boundary of the Formation is sharp and unconformable with the underlying Al Abraq Formation. Many workers (Alami and Salem, 1981; PRC, 1987; Sassi, 1991; Abdalla and Mahmoud, 1991; Waston and Rahuma, 1992; Lat and Zamarsky, 1992) have extensively studied the clay of Umm Ar Razam Quarry of the Faidia Clay Member because of its economic potential. The descriptions, identification and analyses of clay minerals in this chapter are based on the work of many authors (Grim, 1968; Carrol, 1970; Berner, 1971; Tucker, 1988 and 1991; Deer *et al.*, 1992; Velde, 1992; Moore and Reynolds, 1997). A number of mineralogical, chemical and physico-chemical laboratory assessments have been used to identified the grade and quality of the Faidia Clay Member of Umm Ar Razam and Al Fatayah Quarries, and to compare these clays with other commercial clays. The Faidia Clay Member has been studied from the point of view of its application as a chemical additive (bentonite) in drilling oil wells and specially for deep hole drilling, where high pressure and temperature occur. Smectite clays used for drilling muds must meet the American Petroleum Institute (A.P.I.), or the Oil Companies Materials Association (O.C.M.A.) standards. Only certain natural Na and Na-exchanged Ca smectites have the potential for meeting the A.P.I. and/or O.C.M.A. specifications.

The main functions of bentonite – based drilling mud are to (Benzabanta *et al.*, 1986)

- Lift cuttings.
- Control subsurface pressure.
- Stabilise the hole (Filter cake).
- Clean the hole by taking the cuttings to the surface.
- Suspend cuttings when the mud is not circulating.
- Control corrosion (e.g. H_2S).
- Cool and lubricate bit and drill strings.
- Support drill strings and casing.

The Umm Ar Razam clay has very high filtrate values if compared with other standards below.

	O.C.M.A.	Wyoming	Bulgarian	Algerian	Libyan Umm Ar Razam clay
Filtrate ml/30 mm	15 max.	11.75	12.31	15	>50

Source: Abdalla and Mahmoud (1991)

The successive fluid loss of Umm Ar Razam clay will generate problems in oil drilling wells such as: increase in filter cake thickness, leading to potentially stuck pipes, poor performance of electric logs, an unstable well bore with the possibility of caving, formation damage resulting in low production from the pay zone and loss of fluid and expensive chemicals into the formations (Tony, 1991).

Faidia Clay Member: (U. Oligo. – L. Mio.)

The Faidia Clay is the Lower Member of the Al Faidiyah Formation. Pietersz (1968) subdivided this Formation into two members: Faidia Clay Member and Faidia Limestone Member. The Lower Member consists of dark green clay becoming yellowish green to brown when weathered and near the land surface. The yellowish brown coloration, observed especially in sample no. US, is due to oxidation of iron near the surface. It forms a very plastic sticky mass, with soap like textures. Thickness varies from a few meters up to a maximum recorded thickness of 25 m in some places (according to 20 bore holes drilled in Umm Ar Razam Quarry; Abdalla and Mahmoud, 1991). The clay of the Faidia Clay Member is composed of montmorillonite, kaolinite and chlorite. Of these montmorillonite constitutes by far the highest percentage. Also, it contains a variable proportion of other minerals (a heterogeneous mixture of non-clay minerals) such as fine quartz grains (< 50μm), calcite, ilmenite, dolomite, gypsum, K- feldspar, anatase and hematite. These impurities detract from the commercial performance of the Faidia clay.

Laboratory evaluations of the Faidia Clay Member:

The laboratory assessment of bentonites involves a variety of mineralogical, chemical and physico-chemical techniques. These are used to characterise the clay and to assess grade and quality.

7.2 Mineralogical and chemical evaluations:

A number of mineralogical identifications and chemical analyses have been done to characterise the clay of the Faidia Member using X-ray diffraction (XRD), scanning electron microscopy (SEM), X-ray fluorescence (XRF), differential scanning calorimetry (DSC) and optical microscopy.

7.2.1 X- ray Identification of Faidia clay minerals:

X-ray diffraction is a basic tool in the mineralogical analysis of sediments. XRD provides information on the mineralogical composition of clay and non-clay constituents. Oriented mounts were produced on glass slides using Wilson's method (Wilson, 1987) and the < 2.0 μm - > 0.5 μm and < 0.5 μm fractions were used. Faidia clay samples were run on the X-ray diffractometer four times: untreated (air dried), glycolated and allowed to remain overnight, heated to 350 °C and at the higher temperature of 550 °C for one hour. XRD patterns were recorded from 65 to 2° 2θ. JCPDS powder diffraction cards were used to identify the type of clay minerals and the use of the computer was very helpful for XRD pattern interpretations.

7.2.1.1 Smectite:

Smectite is easily identified by comparing diffraction traces of untreated oriented smectite samples with glycolated samples. The advantages of using ethylene glycol or glycerol complexes is to increase basal intensities and to give higher and strong basal spacing order reflections (Brindley, 1966; Theng, 1974; Srodon, 1980). The XRD patterns of smectite (Figures 7.1-7.5) showed a broad basal peak with the ethylene glycol complex and produced a very strong 001 reflection at about 17.0-17.55 Å, compared with 14.0-15.41 Å for untreated (air dried) conditions. Heat
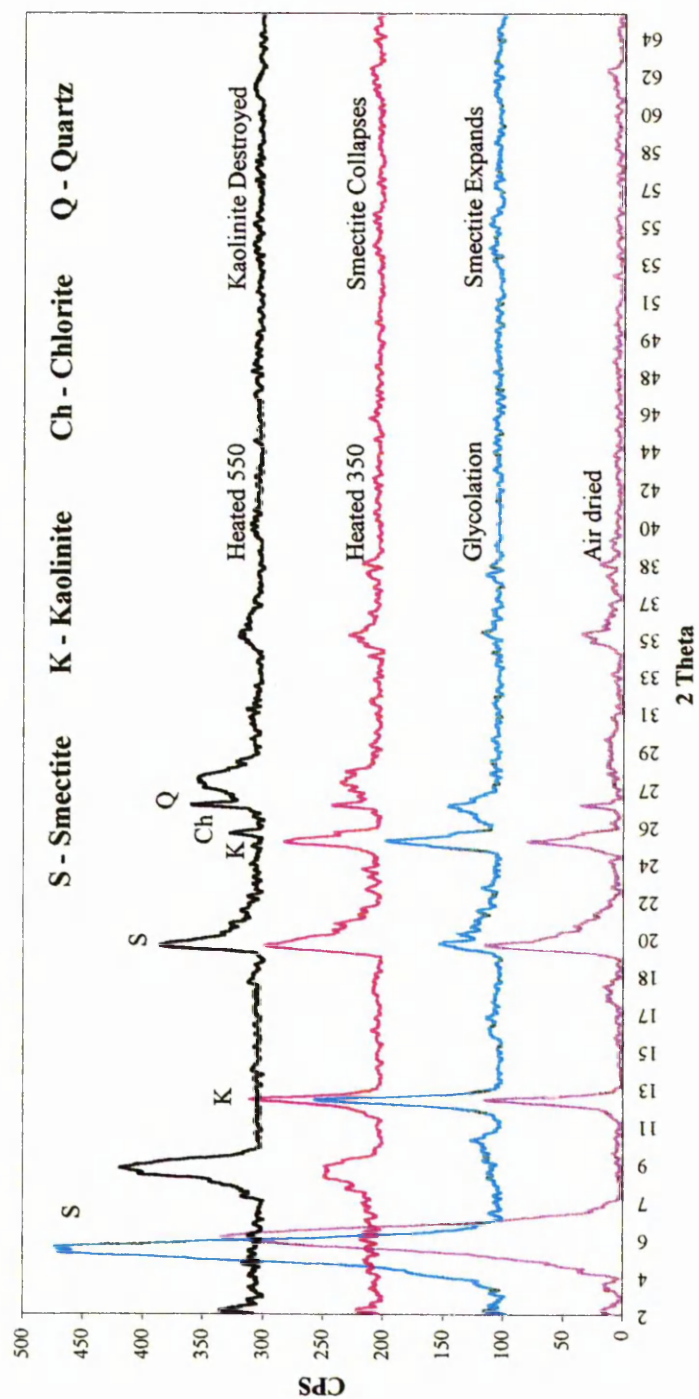
Figure (7.1) XRD pattern of sample no. LF1 (<2μm - > 0.5 μm) of the Al Faidiyah Formation (Al Fatayah cement – Quarry). Showing (S) Smectite, (K) Kaolinite, (Ch) Chlorite, (Q) Quartz. Untreated (Air dried), and treated (Glycolation and Heated to 350 °C & 550 °C).
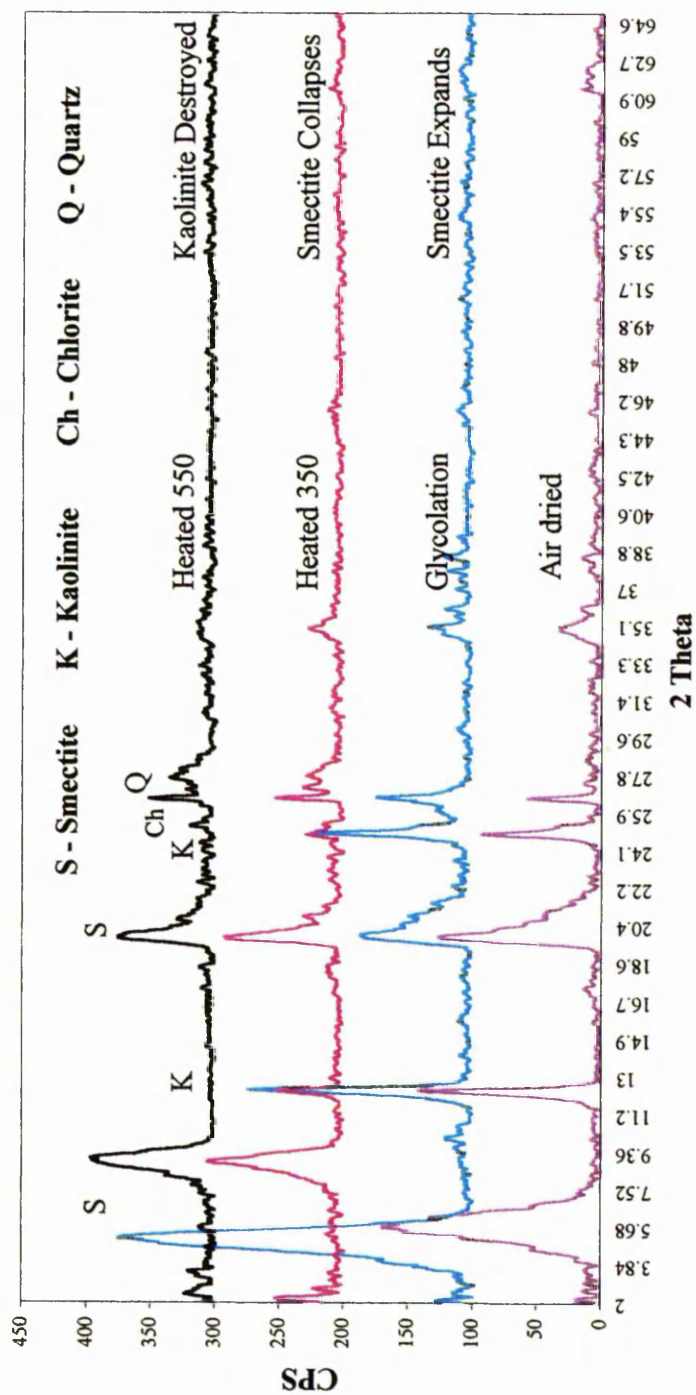
Figure (7.2) XRD pattern of sample no. US (< 2 μm - > 0.5 μm) of the Al Faidiyah Formation (Umm Ar Razam – Quarry). Showing (S) Smectite, (K) Kaolinite, (Ch) Chlorite, (Q) Quartz. Untreated (Air dried), and treated (Glycolation and Heated to 350 °C & 550 °C).
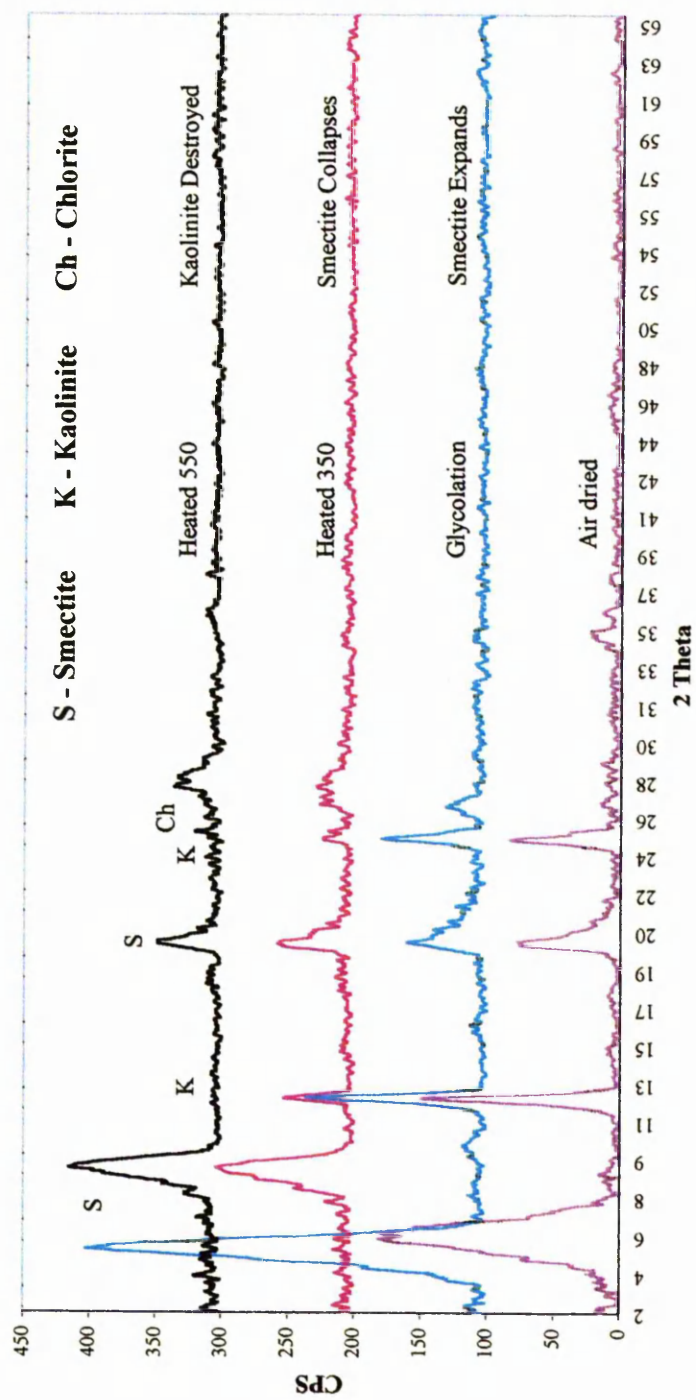
Figure (7.3) XRD pattern of sample no. US (< 0.5 μm) of the Al Faidiyah Formation (Umm Ar Razam quarry) showing (S) Smectite, (K) Kaolinite, (Ch) Chlorite. Untreated (Air dried) and treated (Glycolation and Heated to 350 °C & 550 °C).
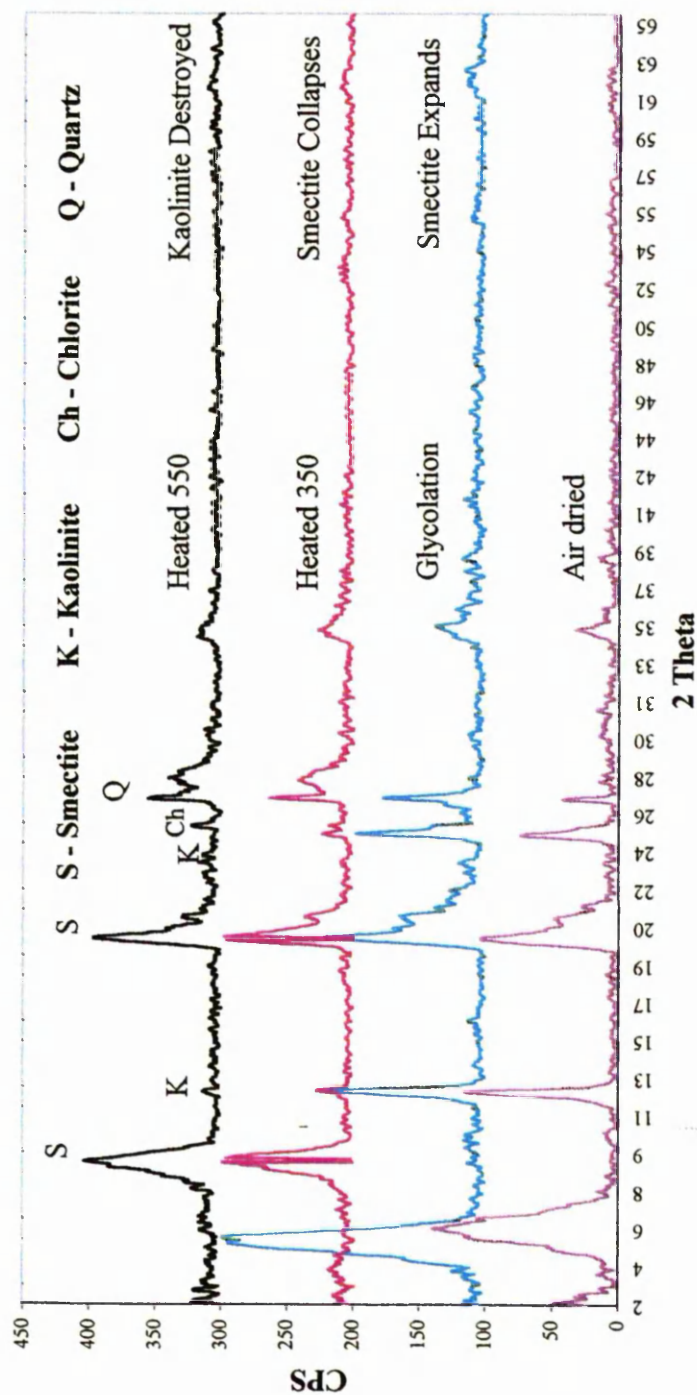
Figure (7.4) XRD pattern of sample no. UM (< 2 μm- > 0.5 μm) of the Al Faidiyah Formation (Umm Ar Razam quarry) showing (S) Smectite, (K) Kaolinite, (Ch) Chlorite, (Q) Quartz. Untreated (Air dried), and treated (Glycolation and Heated to 350 °C & 550 °C).
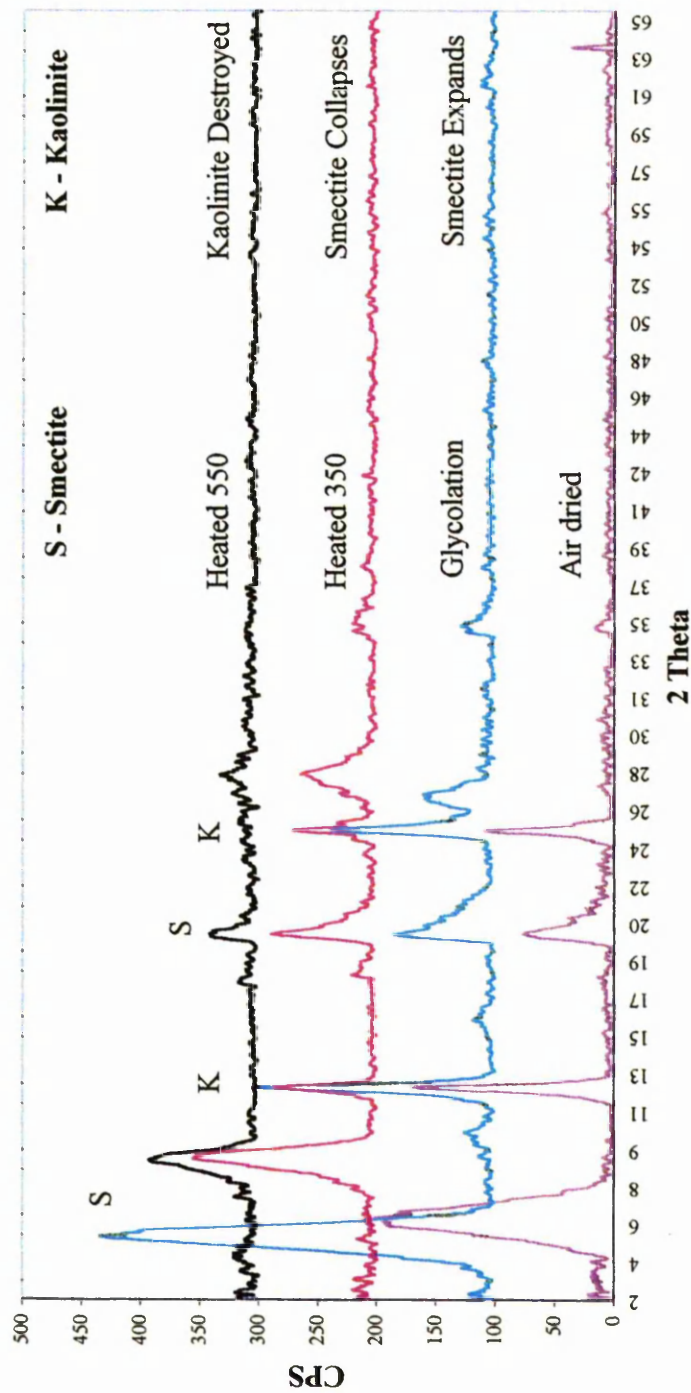
Figure (7.5) XRD pattern of sample no. UM (> 0.5 μm) of the Al Faidiyah Formation (Umm Ar Razam quarry) showing (S) Smectite, (K) Kaolinite. Untreated (Air dried), and treated (Glycolation and Heated to 350 °C & 550 °C).

treatment of smectite to 550°C caused collapse and the basal spacings of the samples were shifted to 9.80-10.06 Å , producing diffraction patterns similar to that of illite.

7.2.1.2 Kaolinite and Chlorite:

There are differences in structure and geological occurrences between these two minerals, but they can occur in mutual mixtures as described by Moore and Reynolds (1997). Table 7.1, Appendix 8.4 and Figures 7.1-7.5 illustrate the problem. Sometimes it is very difficult to distinguish the two types of minerals, because the kaolinites have the 002 peak at 24.89° 2θ and chlorites have their 004 reflection at 25.20° 2θ . The only way found to distinguish these minerals from each other is by heat treatment. Kaolinite reflections after glycolation are not affected. Heat treatment shows an important affect on the kaolinite where at temperatures of 350°C reflections were not very great and peaks remained in the same position. In the case of heating up to the temperatures of 550°C reflections are completely destroyed or disappear. Chlorite is not destroyed by heating to 550°C.

7.2.1.3 Bulk samples:

XRD analysis of the Faidia clay bulk samples also revealed the presence of quartz, calcite, gypsum, dolomite and other minor minerals such as ilmenite and anatase. The presence of these impurities leads to poor rheological and binding properties of the Faidia clay. XRD patterns for the Faidia Clay Member (crude) and reference clay standards are shown graphically in Figures 7.6 and 7.7.
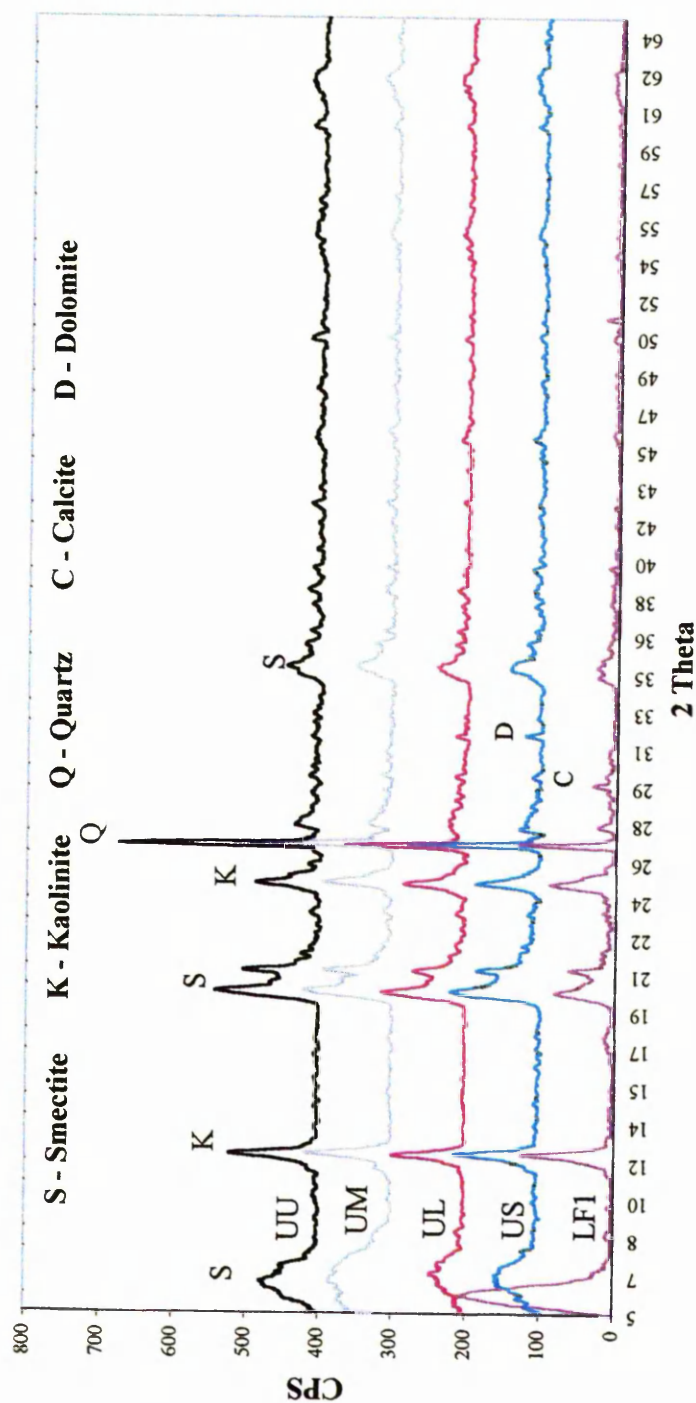
Figure (7.6) XRD pattern of clay samples (crude) of the Al Faidiyah Formation (Al Fatayah cement quarry & Umm – Ar Razam quarry) showing (S) Smectite, (K) Kaolinite, (Q) Quartz, (C) Calcite, (D) Dolomite.

221
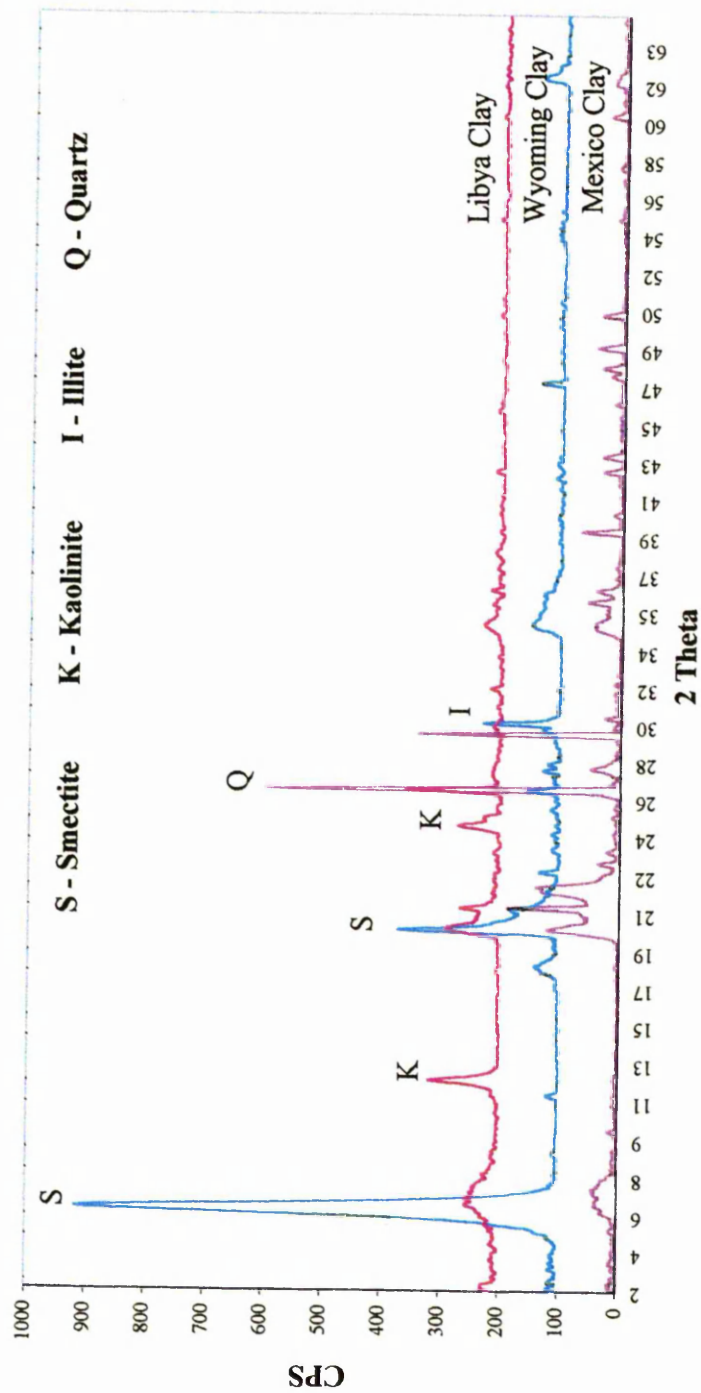
Figure (7.7) XRD pattern comparison for crude clay samples (Libya, Wyoming, and Mexico). for (S) – Smectite, (K) Kaolinite, (I) Illite, (Q) Quartz.

Table (7.1) Clay minerals of the Faidia Clay Member, Al Faidiyah Formation (U. Oligocene-L. Miocene), full data in Appendix 8.4.

Sample no. (μm)	Untreated	Glyco.	Heated 350°C	Heated 550°C	Clay & non-clay minerals
UU (< 2.0 to > 0.5)	/	/	/	/	Smectite
	/	/	/	-	Kaolinite
	/	-	/	/	Chlorite
UU (< 0.5)	/	/	/	/	Smectite
	/	/	/	-	Kaolinite
	-	-	/	/	Chlorite
UM (< 2.0 to > 0.5)	/	/	/	/	Smectite
	/	/	/	-	Kaolinite
	-	/	/	/	Chlorite
UM (< 0.5)	/	/	/	/	Smectite
					Kaolinite
	-	-	/	-	Chlorite
UL (< 2.0 to > 0.5)	/	/	/	/	Smectite
	/	/	/	-	Kaolinite
	-	-	-	/	Chlorite
UL (< 0.5)	/	/	/	/	Smectite
	/	/	/	-	Kaolinite
	-	-	/	/	Chlorite
US (< 2.0 to > 0.5)	/	/	/	/	Smectite
	/	/	/	-	Kaolinite
	/	-	/	-	Chlorite
US (< 0.5)	/	/	/	/	Smectite
	/	/	/	-	Kaolinite
	-	-	-	/	Chlorite
LF1 (< 2.0 to > 0.5)	/	/	/	/	Smectite
	/	/	/	-	Kaolinite
	/	/	/	/	Chlorite
LF1 (< 0.5)	/	/	/	/	Smectite
	/	/	/	-	Kaolinite
	/	/	/	/	Chlorite

/ = present
- = absent

7.2.2 Scanning electron microscopy (SEM):

SEM has been used extensively to provide additional useful information about the textural relationships between the smectite and associated minerals. Chemical analyses of clay minerals from the Faidia Clay Member were determined using SEM (BSE) technique and energy dispersive analysis. Table (7.2) shows detailed quantitative analyses obtained using this technique. BSE- imaging of the clay mineral in the studied area also revealed other important petrographic features not apparent from the optical microscope, for example, in the identification the other non-clay minerals (impurities) such as ilmenite, calcite, dolomite, anatase and orthoclase (Plates 7.1and 7.2 and Table 7.3). Quartz, gypsum and hematite were only observed under the optical microscope. The common clay minerals in Faidia Clay Member are montmorillonite, kaolinite and chlorite.

7.2.2.1 The alteration of ilmenite:

Altered ilmenite is a product of the natural alteration of the mineral ilmenite, which results in the formation of co-existing different phases. The alteration is accompanied by changes in the chemical, physical and optical properties of the ilmenite mineral. Chemically, the main results of the alteration are an increase in TiO_2, Fe_2O_3 and a decrease in FeO. When the ilmenite is oxidised at a certain temperature the structure breaks down into rutile/anatase and hematite. With increasing degrees of alteration ilmenite disappears and the ratio of $TiO_2:Fe_2O_3$ increases until the altered grain becomes rutile/anatase. Temple (1966) mentioned that there is a close connection between the water and altered ilmenite with the iron oxide hydrated during the alteration process and removed as a mobile hydroxide (the presence of water contributes to the removal of iron from the ilmenite mineral).

7.2.2.2 The Source of Hematite and Anatase in Faidia Clay Member:

Hematite was found in the sample no. US only. In thin section hematite was recognised by its red colour in reflected light (Plate 7.3), filling pore spaces and fractures of part of the Faidia Clay Member of the Al Faidiyah Formation. Hematite and anatase have been analysed using the SEM (BSE), which show the hematite mineral filling fractures and pore spaces (Plates 7.4, 7.5, 7.6 and Figure 7.8). A porous anatase mineral was observed with pores filled by clay minerals (Table 7.3 and Plate 7.1B). The weathering of ilmenite in the Faidia clay is considerable, because this

mineral is the major source of the high Ti and high iron content in the Faidia Clay Member (Table 7.4). The alteration of ilmenite is responsible for the formation of the hematite and anatase minerals. This explanation is based on Flinter (1959), Temple (1966), Cambell (1973), Grey and Reid (1975), Anand and Gilkes (1984), Deer *et al.*, 1992 and Babu *et al.* (1994), as follows:

The alteration of ilmenite in the Faidia Clay Member took place in a two-stage process. First, all of the iron oxidizes and some diffuses from the ilmenite leaving pseudorutile in which closely packed oxygen layers remain intact. This stage represented by the following reaction:

$$Fe^{2+} TiO_3 \; \rightarrow \; Fe_2^{3+} Ti_3O_9$$

$$\text{(Ilmenite)} \qquad \text{(Pseudorutile)}$$
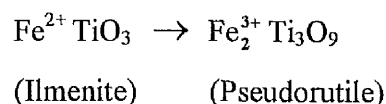
In the second stage of the alteration pseudorutile dissolves. Iron is removed by solution, and both rutile/anatase (TiO_2) and hematite Fe_2O_3 precipitate, according to the following reaction:

$$Fe_2^{3+} Ti_3O_9 \; \rightarrow \; TiO_2 \quad + \quad Fe_2O_3$$

$$\text{Rutile/Anatase} \qquad \text{Hematite}$$
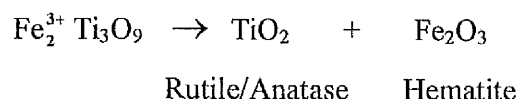
The alteration of ilmenite in the study area could be also due to the presence of water, where iron is hydrated during the alteration process and is removed as a mobile hydroxide (based on Temple, 1966). This is supported by the presence of perched aquifers at different levels in the Faidia Member due to the affects of major faults and joints and is suggested by the presence of remnants of hematite. Anatase and not rutile was the final alteration product because of the following reasons. (a) Anatase is commonly distributed in bands, as seen using BSE, which contain variable traces of ilmenite or isolated ilmenite minerals (Plate 7.1B). (b) It has a highly porous structure with the loss of iron and this is evident in the SEM-BSE photograph and EDX data (based on morphology and chemistry, Plate 7.1B and Table 7.3). The high porosity of the anatase grains appears to have enabled clay minerals to crystallise from soil solutions within the pores. In this case the anatase should be lighter than the rutile mineral. This porous property is absent from the rutile mineral. (c) In altered ilmenite Si and Al increase with decreasing Fe. Si and Al are nil or minor constituents in ilmenite and rutile, but both are abundant in anatase compared with the other two

minerals (ilmenite and anatase) due to the presence of the clay minerals as a patches within the porous anatase grains. (d) XRD data of bulk samples indicate the presence of anatase minerals in the Faidia Clay Member. A proportion of anatase present was located in the greater than 10 μm fraction.
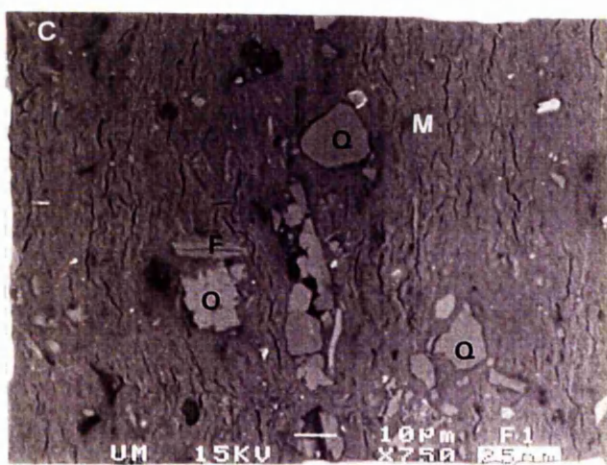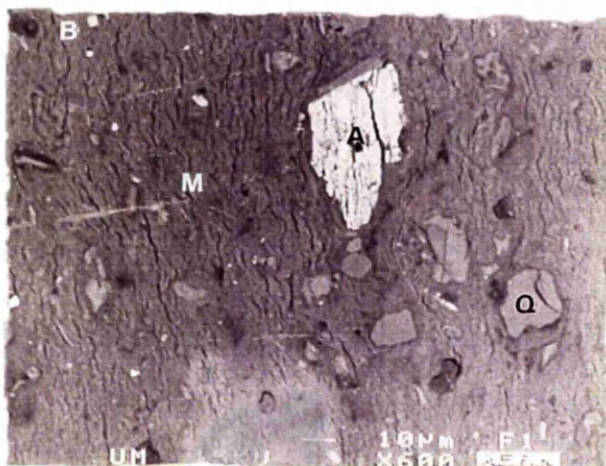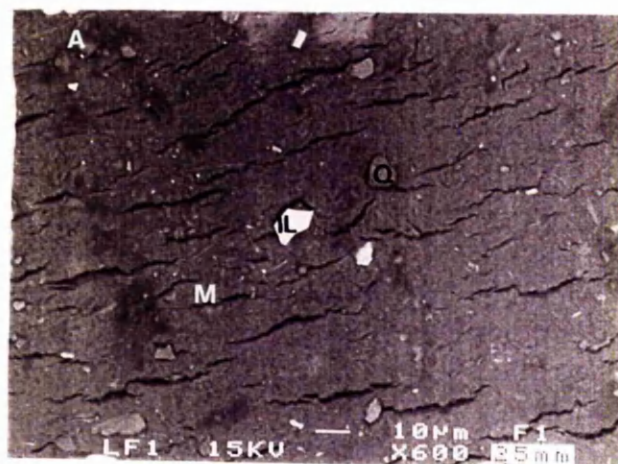
Plate (7.1) Scanning electron micrograph (BSE) showing (A) Quartz grains (Q) and Ilmenite (IL); (B) Anatase (commonly distributed by parallel bands) (A); (C) Orthoclase (O). All were embedded in montmorillonite clay (M). In Al Fatayah and Umm Ar Razam Quarries.
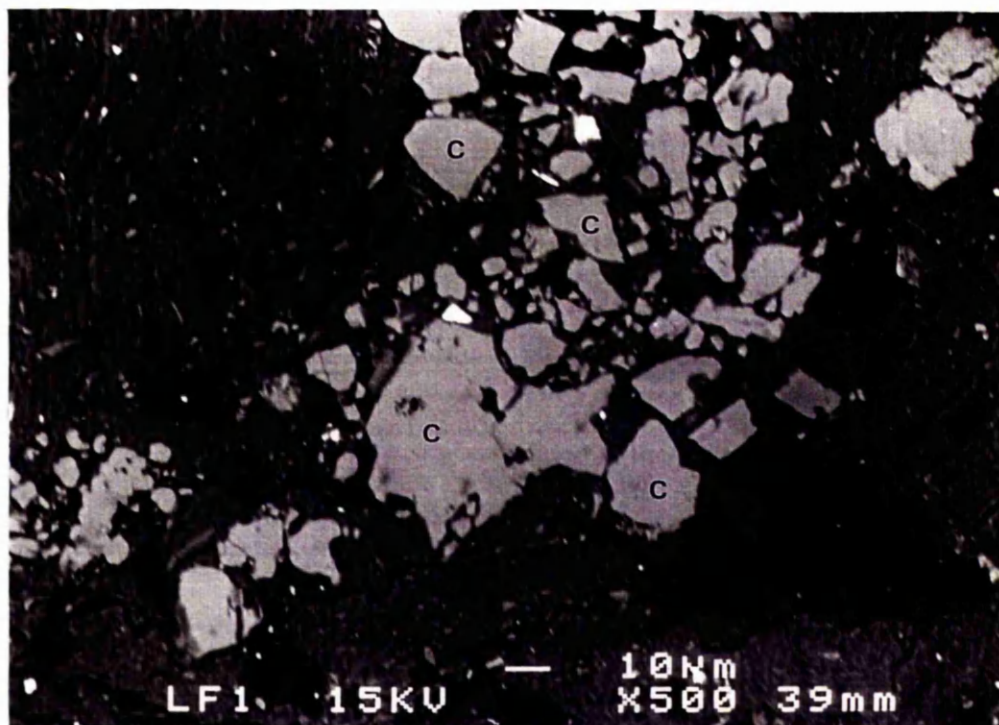
Plate (7.2) Scanning electron micrograph (BSE) shows calcite cement (C), filling pore spaces. Sample no. LF1 of the Faidia Clay Member, Al Fatayah Quarry

Plate (7.3) Hematite filling fractures (sample no. US), Faidia Clay Member, Al Faidiyah Formation, in Umm Ar Razam Quarry. Field of view = 6 mm, (XPL).
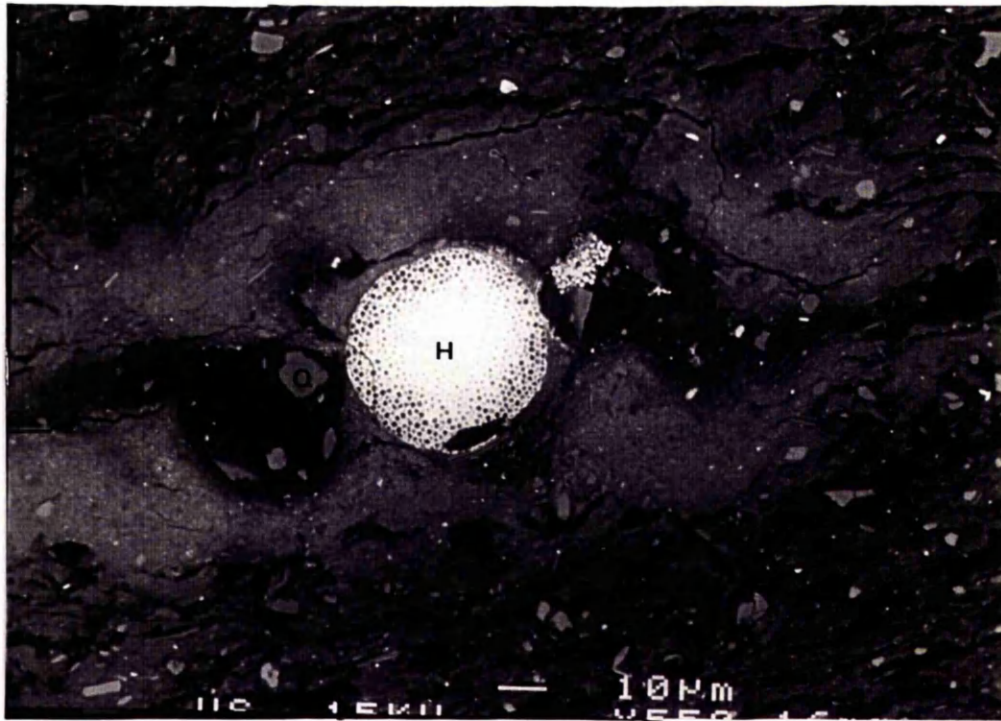
Plate (7.4) Scanning electron micrograph (BSE) showing hematite (H) filling pore spaces, and remnant of hematite (RH). Sample no. US of the Faidia Clay Member, in Umm Ar Razam Quarry.
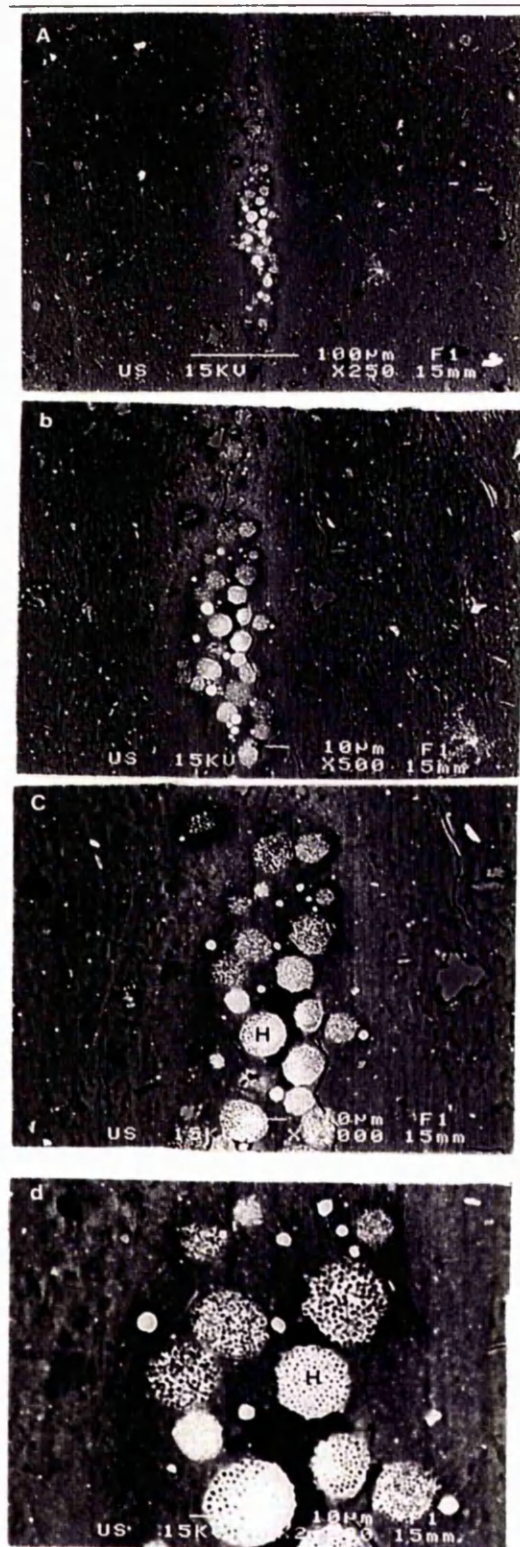
Plate (7.5) SEM (BSE) – View of hematites (H), b, c and d are close up views of A showing hematite filling pore spaces (Sample no. US). In Umm Ar Razam Quarry.
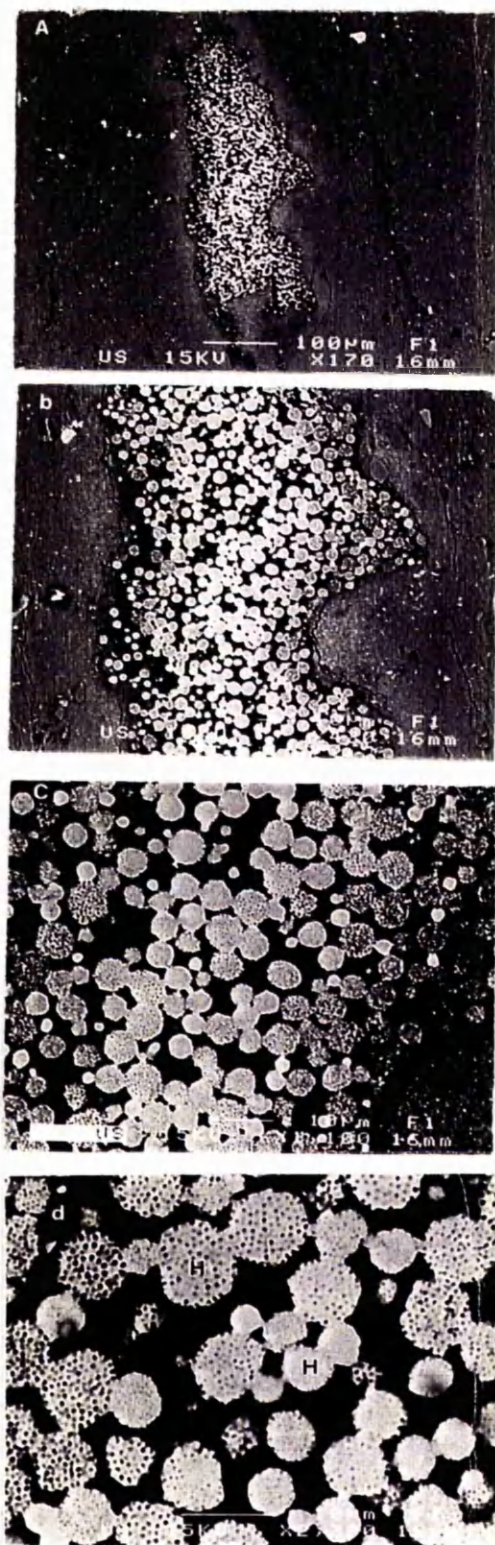
Plate (7.6) SEM (BSE) – Another view of hematites (H), b, c and d are close up views of A showing hematite filling pore spaces (Sample no. US). In Umm Ar Razam Quarry.

Counts (x10³)

8 —

```
Mineral: Hematite
Work distance: 39 mm
Probe current = 1.5 nA
Accelerating voltage = 15kV
magnification = 800
```

7 —

6 —

5 —

Fe

4 —

3 —

2 —

1 —

0 —

0   2   4   6   8   10

Range (keV)

o
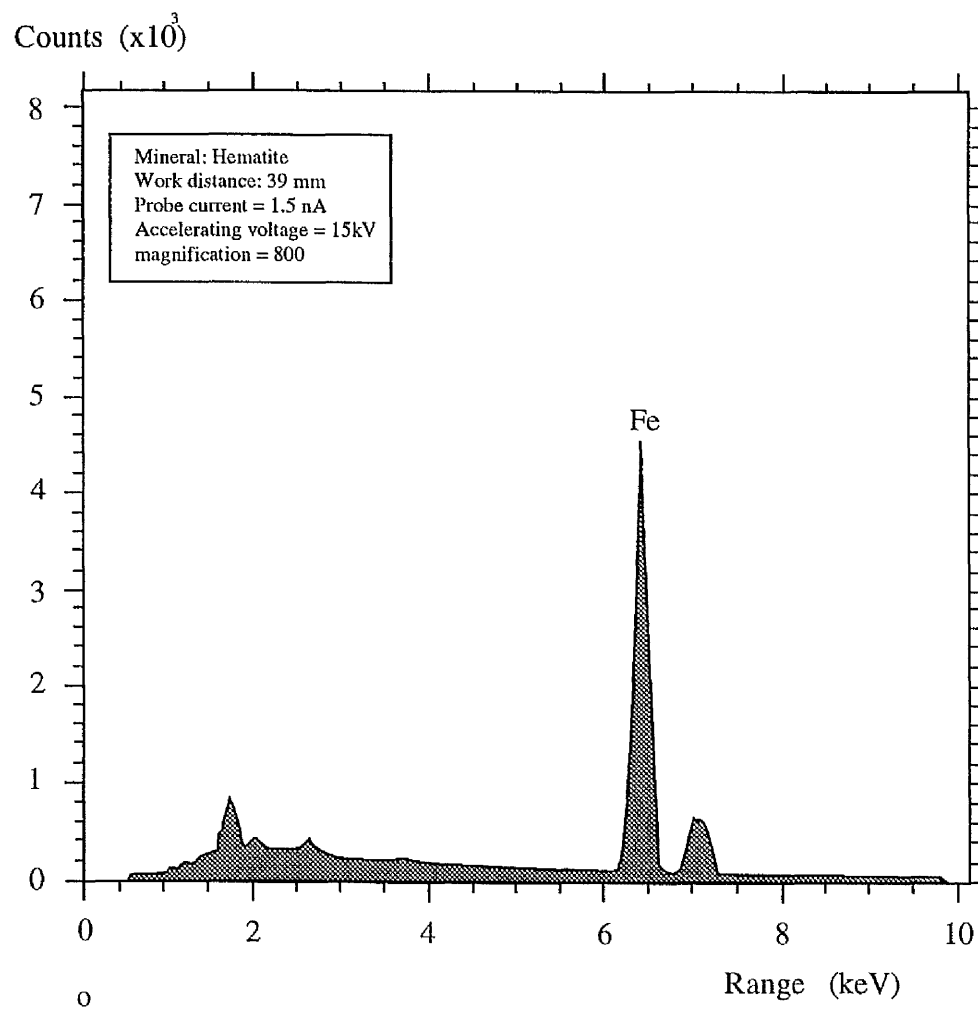
Figure (7.8) SEM-EDX spectrum for hematite in the Faidia Clay Member (US), of the Al Faidiyah Formation.

233

Table (7.2) Representative table of montmorillonite analyses of the Faidia Clay Member

Oxides	Al Fatayah Quarry	Umm Ar Razam Quarry			
	LF1	US	UL	UM	UU
FeO	8.31	7.32	7.93	5.01	6.78
MgO	2.37	2.19	2.52	1.62	2.40
CaO	0.62	0.22	0.37	0.21	0.51
SiO_2	49.44	45.80	42.89	39.75	45.54
Al_2O_3	19.42	18.45	16.40	14.69	18.49
K_2O	1.53	1.61	1.91	1.58	1.82
Na_2O	0.56	0.27	-	0.34	0.63
SO_3	0.32	0.64	0.33	0.32	0.40
TiO_2	0.86	0.62	1.23	0.83	0.48
Total	83.43	77.25	73.58	64.35	77.05
Number of ions on basis of 22 (O) excluding H_2O					
Formula					
Fe	1.034	0.979	1.126	0.807	0.910
Mg	0.525	0.522	0.639	0.466	0.574
Ca	0.099	0.037	0.067	0.044	0.089
Si	7.355	7.327	7.282	7.663	7.314
Al	3.405	3.479	3.281	3.339	3.500
K	0.289	0.329	0.413	0.387	0.373
Na	0.161	0.082	-	0.128	0.196
S	0.036	0.077	0.042	0.010	0.049
Ti	0.097	0.074	0.157	0.046	0.057
Tetrahedral	$Si_{7.377}$ $Al_{0.623}$	$Si_{7.327}$ $Al_{0.673}$	$Si_{7.282}$ $Al_{0.718}$	$Si_{7.663}$ $Al_{0.337}$	$Si_{7.314}$ $Al_{0.686}$
Octahedral	$Al_{2.76}$ $Fe_{1.034}$ $Ti_{0.097}$ $Mg_{0.525}$	$Al_{2.806}$ $Fe_{0.979}$ $Ti_{0.074}$ $Mg_{0.522}$	$Al_{2.282}$ $Fe_{1.126}$ $Ti_{0.157}$ $Mg_{0.639}$	$Al_{3.003}$ $Fe_{0.807}$ $Ti_{0.046}$ $Mg_{0.466}$	$Al_{2.814}$ $Fe_{0.910}$ $Ti_{0.057}$ $Mg_{0.574}$
Interlayer	$Ca_{0.099}Na_{0.161}K_{0.289}$	$Ca_{0.037}Na_{0.082}K_{0.329}$	$Ca_{0.067}Na_{0.00}K_{0.413}$	$Ca_{0.044}Na_{0.128}K_{0.387}$	$Ca_{0.089}Na_{0.196}K_{0.373}$
Group (Layer charge)	Smectite 0.648	Smectite 0.485	Smectite 0.547	Smectite 0.604	Smectite 0.747
Species of clay mineral	Montmorillonite	Montmorillonite	Montmorillonite	Montmorillonite	Montmorillonite

Table (7.3) Analyses of non-clay minerals found in the Faidia Clay Member

Oxides	Quartz	Ilmenite	Calcite	Hematite	Anatase	Orthoclase	Rutile (Standard)*	Anatase (Standard)**
FeO	-	35.29	-	63.20	1.57	-	0.41	5.0
MnO	-	1.11	-	0.31	-	-	-	-
MgO	0.15	0.19	-	1.03	0.17	-	0.06	-
CaO	-	-	62.58	0.22	0.37	-	-	-
SiO$_2$	100.1	0.36	-	4.82	3.67	63.31	-	0.6
Al$_2$O$_3$	0.26	-	-	0.85	1.76	17.63	0.05	2.1
K$_2$O	-	-	0.13	-	-	15.83	-	-
Na$_2$O	0.21	0.32	-	0.88	0.27	0.40	-	-
SO$_3$	-	-	-	0.37	-	-	-	-
TiO$_2$	-	55.93	-	-	83.88	-	99	88.6
Total	100.72	93.20	62.71	71.68	91.69	97.17	99.52	96.30

* Deer *et al.* (1992).

** Anand and Gilkes (1984).

Table (7.4) Chemical analyses (XRF) for major and trace elements of the Faidia Clay

Member (U. Oligo.-L. Mio.)

Sample no.	LF1	US	UL	UM	UU	Wyoming
Oxides (wt. %)						
SiO$_2$	23.80	23.57	23.45	23.22	23.86	54.63
Al$_2$O$_3$	10.17	10.30	10.09	9.87	10.55	16.71
Fe$_2$O$_3$	5.50	5.10	4.94	5.05	4.44	3.59
MgCO$_3$	2.56	2.10	1.98	1.97	1.61	4.45
CaCO$_3$	54.97	56.1	56.77	57.12	56.76	2.43
S	0.00	0.00	0.00	0.00	0.00	-
K$_2$O	0.59	0.62	0.64	0.63	0.63	0.53
TiO$_2$	1.14	1.03	1.04	1.02	1.08	-
MnO	0.05	0.05	0.03	0.04	0.05	-
P$_2$O$_5$	0.02	0.02	0.02	0.01	0.02	-
Total	98.80	98.89	98.96	98.93	99.00	82.34
CaO	30.78	31.42	31.79	31.99	31.79	1.36
MgO	1.51	1.24	1.17	1.16	0.95	2.13

7.3 Differential Scanning Calorimetry (DSC):

DSC curves record the differential heat input to the sample (expressed as a heating rate dh/dt; James, 1987). Thermal events in the sample thus appear as deviations from the DSC baseline in either an endothermic or exothermic direction, depending upon whether more or less energy has to be supplied to the sample relative to the reference material (Brown, 1988). Samples of the Faidia Clay Member and other standards were run using the DSC technique. The samples were heated continuously at a regular rate from 25°C to 1200°C at 10°C/min. Curves for the various clay minerals obtained by DSC (Figure 7.9) are typically as expected for montmorillonite. When smectite clays are heated two forms of water are lost, adsorbed and crystalline. The adsorbed water loss, most of which is interlayer water, occurs at low temperatures between 100 - 200°C (Odom, 1984). The curves of various smectites show wide variation of temperature for the loss of OH lattice water comparing the Umm Ar Razam clay and the clay standards. The Umm Ar Razam clay shows an endothermic reaction due to loss of OH lattice water, beginning at about 450°C and ending at about 600°C, with the endotherm peak at about 500°C. For the other standards such as Wyoming bentonite the peak is at about 683°C and for calcium montmorillonite (standard) at about 682°C. The variation of Umm Ar Razam clay from the other two standards can be explained by reference to Mackenzie, (1957) and Grim (1968) as follows:

- Replacement of aluminium by Fe and Ca causes a reduction in the temperature of the reaction. The clay of the Faidia Member is characterised by high Fe_2O_3 = 5.01 % and CaO = 31.55 % contents compared with the standard (Table 7.4).

- Presence of small amounts of kaolinite as impurities. Kaolinite was observed in all Faidia Clay Member samples and gives a mixed clay. In the other two standards the kaolinite mineral is absent (Figure 7.7).

- Particle size might be important in influencing the temperature of the loss of hydroxyl, since the dehydration temperature decreases with decreasing particle size.

- Defect structures or variation in crystallinity, where the poorly crystalline material loses its hydroxyl water somewhat more readily than well-crystallised clay mineral.

- Dehydroxylation of smectite depends on the nature of the exchangeable cation.
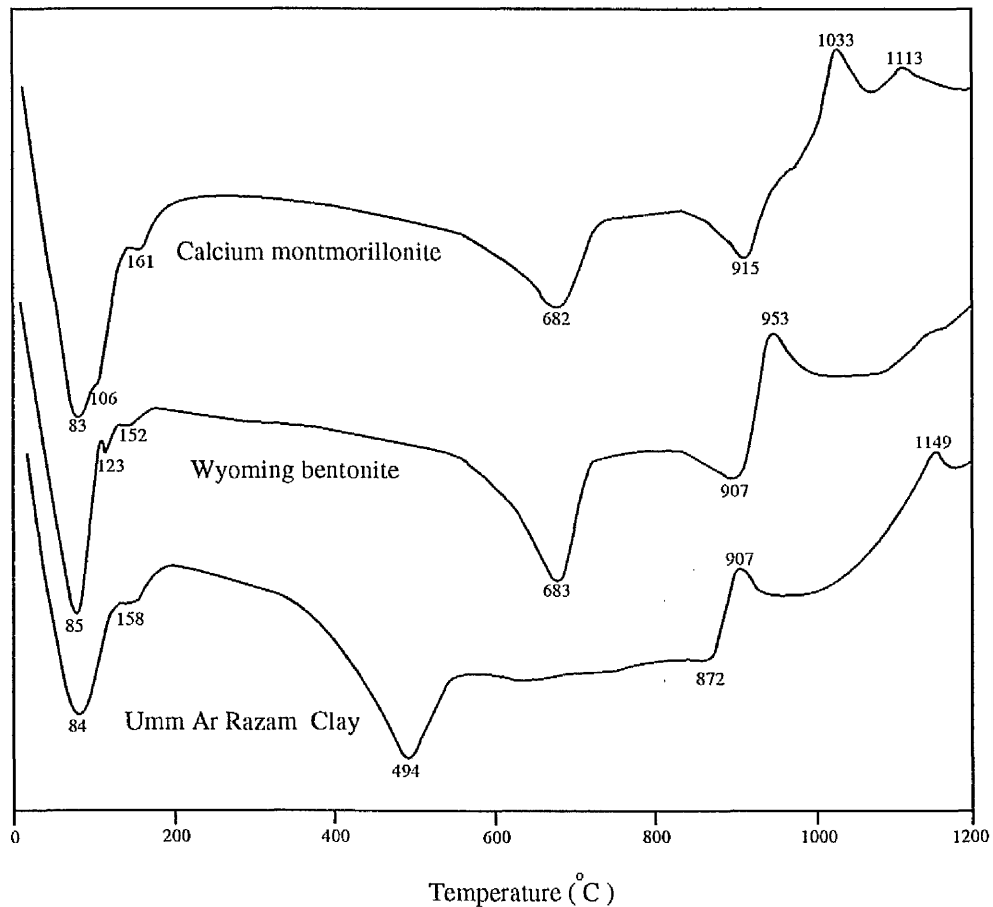
Figure (7.9) DSC curves of Umm Ar Razam Clay showing different dehyd-
roxylation behaviour compared with Wyoming bentonite and C-
alcium montmorillonite (Standard). Note the well-defined shoulder
< 200°C on the low temperature endotherm.

237

7.4 Estimation of organic matter + H₂O content by loss on ignition (LOI):

A standard method with ignition at 1000 °C was used (Gale and Hoare, 1991). XRD was also run to examine the sample's patterns after heating to 1000°C. Heat treatment of the Faidia Clay Member at this temperature caused collapse and most of the reflections of the clay minerals were destroyed (Figure 7.10). The Faidia Clay Member, when fired at 1000 °C, has a brown-red colour. The results of this experiment are as follows:

	Al Fatayah Quarry	Umm Ar Razam Quarry				USA
	LF1	US	UL	UM	UU	Wyoming
Loss at 1000°C	20.1 %	17.1 %	19.9 %	19.7 %	19.2 %	17.64 %

7.5 Physico-chemical tests:

The physico-chemical tests are used to determine the **Grade**, which is defined as the smectite content of the clay. This is determined using a surface area measuring technique. **Quality** is related to the industrial performance of the material in its different applications whether in its natural or modified form. Quality depends on clay properties, crystal structure of the clay minerals and the nature and the amount of impurities present. Smectites are particularly valued for their remarkable physical and chemical properties, which make them suitable for many industrial applications. The most important properties are exchange capacity, swelling capacity, surface area, impermeability and rheological properties (Inglethorpe *et al.*, 1993).

7.5.1   Grade of the Faidia Clay Member:

7.5.1.1   2-ethoxyethanol [ethylene glycol monoethyl ether (EGME)] surface area test:

Total surface area is a fundamental property of layer silicates and it has been used as a criterion for identification. This method has been used to determine the total surface area of Faidia clay samples. To determine the retention of EGME the procedure followed Carter *et al.*, (1965). One point one gram samples of each clay mineral were placed in shallow aluminium dishes and dried with 70 g of P₂O₅ in an evacuated desiccator.
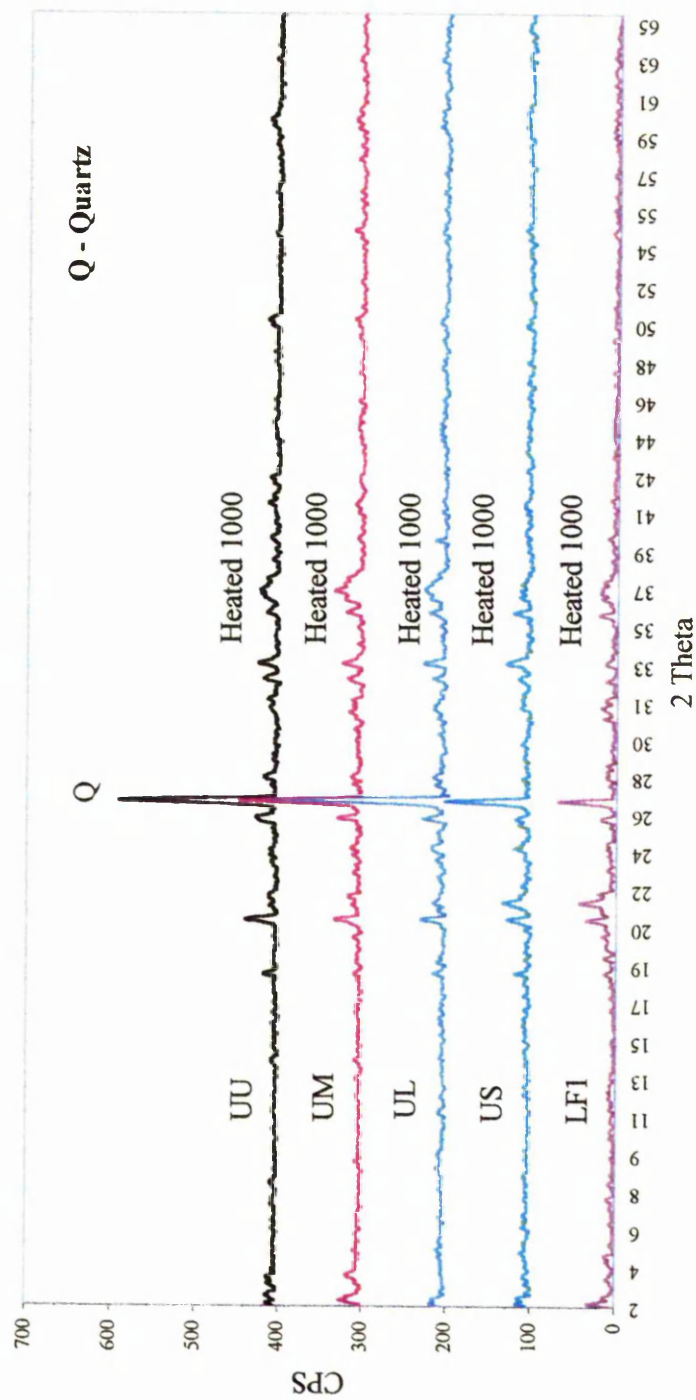
Figure (7.10) XRD pattern of clay samples (crude) of the Al Faidiyah Formation (Al Fatayah cement quarry & Umm – Ar Razam quarry) for (Q) Quartz heated to 1000 °C.

Approximately 3 ml of reagent grade EGME was added to each dried sample to form a mineral-adsorbate slurry. The slurry was allowed to equilibrate for at least 1 hour (see Appendix 7.1). Pure smectites have surface areas of 800 m^2/g, other clay mineral such as kaolin < 40 m^2/g and non-clay mineral (including quartz) < 5 m^2/g (Moorlock and Highley, 1991; Inglethorpe *et al.*, 1993). Sorption of EGME on montmorillonite is highly dependent on the exchangeable cation (Kellomaki *et al.*, 1987). The surface area values of the Faidia Clay Member compared with other clay standards are illustrated in Table 7.5. Grade can be estimated by taking the ratio of the observed surface area to 800 m^2/g, and is expressed as % smectite.

Table (7.5) EGME surface area values for the Faidia Clay Member and control (Ca-montmorillonite) using 2-ethoxyethanol method:

Sample No.	Surface Area (Crude) (m^2/g)	Surface Area (<2µm to >0.5µm) (m^2/g)	% Smectite (Crude)	% Smectite (<2µm to >0.5µm)
UU	333	490	42	61
UM	389	490	49	61
UL	389	559	49	70
US	428	559	54	70
LF1	420	524	53	66
Control Sample (Ca-montmorillonite)	661	–	83	–

7.5.2 Quality of Faidia Clay:

7.5.2.1 Swelling test:

This is a measure of the swelling efficiency of the raw material (Christidis and Scott, 1993). Natural smectite clays range from strongly swelling to non-swelling depending on the smectite clay species and on the ratio of exchangeable calcium and magnesium present. The majority of naturally occurring smectite clays has Ca and Mg as the predominant exchangeable cations and is essentially non-swelling. Because swelling bentonites are much less common than the non-swelling bentonites, it is

usual in industry to convert the non-swelling to swelling clay by treatment with soda ash (sodium carbonate, Morgan, 1994). The main objectives of activation are to increase hydration and swelling of the Faidia Clay Member. An amount of sodium carbonate between 1 and 6 % by weight was mixed with Faidia clay samples (< 125 μm fraction size), the mixture slurried, gently dried, crushed and dropped slowly into a 10 ml. measuring cylinder of water (see Appendix 7.2). A moderately swelling bentonite will swell to a volume of 15-20 ml., and a good bentonite to about 25 ml. An excellent grade will swell to 30 ml. or more (Inglethorpe *et al.*, 1993). The Faidia clay showed unchanged swelling power. Table 7.6 shows the results for the Faidia clay, in comparison with other clay standards.

Table (7.6) Swelling test values for the Faidia Clay Member, Wyoming and Mexico clays with addition 1 to 6 % sodium carbonate.

Type	before 24 hrs.	After 24 hrs.	Swelling volume (ml.)
Umm Ar Razam Quarry(Libya)	4.60	4.60	Nil
Al Fatayah Quarry (Libya)	2.50	2.50	Nil
Wyoming (U.S.A.)	2.50	4.00	15
Chihuahua (Mexico)	1.80	2.30	5

7.5.2.2 Cation exchange capacity (CEC):

CEC can be measured by a variety of methods and to some extent the result obtained is dependent on the method used. The differences in cation-exchange capacity of smectite qualities are essential to their structure and give them important chemical properties with industrial applications (Moore and Reynolds, 1997). The composition of the exchangeable cation assemblage is also a prime criterion of suitability for most major applications (Odom, 1984; Inglethorpe *et al.*, 1993). The cation exchange capacity and the loss in the CEC of montmorillonite, were both linearly dependent on the Al-content of hydroxy-Al interlayered montmorillonite,

where the CEC decreased as the Al-content of the clay mineral increased (Helmy *et al.*, 1994). The values for cation exchange increased with decreasing pH. The cation exchange capacity of relatively pure smectite clays ranges between 70 to 130 meq/100g (Odom, 1984). The $BaCl_2/MgSO_4$ method for measurement of CEC was used (see Appendix 7.3). Table 7.7 gives the results for the Faidia clay compared with Wyoming bentonite.

Table (7.7) CEC values of Faidia Clay Member of the Al Faidiyah Formation and Wyoming bentonite

Sample no.	LF1	US	US/A*	UL	UM	UU	Wyoming
CEC values (meq/100 g)	50	55	56	63	52	60	70

* US/A: US repeated   Note: pH value of 8.1 was obtained

7.6 Conclusions:

- The Faidia Clay is composed of montmorillonite (the highest percentage), kaolinite and chlorite.

- The Faidia Clay contains non-clay minerals such as fine quartz, calcite, ilmenite, dolomite, gypsum, K- feldspar, anatase and hematite. The presence of these impurities leads to poor rheological and binding properties.

- Ilmenite from the Faidia Clay contains 56 % TiO_2 and 35 % Fe.

- The Faidia Clay has relatively high amounts of Fe_2O_3 and CaO, whereas the SiO_2, Al_2O_3 and MgO are low compared with Wyoming bentonite.

- The Faidia Clay is a non-swelling clay, with surface area 385 – 420 m^2/g and C.E.C. 50 – 57 meq/100 gms.

Chapter 8

CLAY INDUSTRIAL POTENTIAL

8.1 Introduction:

Clay minerals are extremely fine-grained materials ($<2\mu m$). They are hydrous aluminum silicates in which Mg or Fe may substitute totally or partly for aluminum and with alkalies as essential constituents. Clay deposits become an important part of many industrial applications, consisting of one or more clay minerals, with varying proportions of non clay minerals, the most common being, quartz, feldspar, carbonate minerals, gypsum and organic material. The different uses of clay minerals in industrial applications depend upon the special properties of the clay minerals. For commercial utilisation the most important clay minerals are kaolinite and montmorillonite (smectite) (Evans, 1993). Attapulgite, sepiolite and hectorite are also used. Illite, the most abundant clay mineral in nature, is important in ceramic clays.

Bentonite and Fuller's earth:

The most commonly occurring smectite clay mineral is montmorillonite, which has many variants but several properties in common such as medium to high surface area and sorptive properties (Evans, 1993). The smectite group is characterised by a unique combination of properties on which their economic importance is based, and it is unstable with increasing age and depth (Moorlock and Highley, 1991). The general term for commercial smectite clays which is most commonly applied is bentonite, after the Cretaceous Benton Group of Wyoming (Na-montmorillonite), USA (Harben and Bates, 1990). The two most important smectites are the sodium-montmorillonite and the calcium montmorillonite. Sodium-montmorillonite swells when immersed in water, is often known as swelling bentonite and is in great demand, even being produced synthetically from calcium-montmorillonite (which does not have swelling properties) by the addition of sodium carbonate (soda ash) (Harben and Bates, 1990; Moorlook and Highley, 1991). Calcium-montmorillonite in Britain is known as Fuller's Earth. Outside Britain, the term non-swelling bentonite is used. The Faidia Clay Member consists mainly of smectite (montmorillonite), and for convenience it is described as bentonite throughout this study.

Kaolinitic clays:

This group includes those clays composed of kaolinite with more or less illite, montmorillonite, quartz and other non-kaolinite material (Harben and Bates, 1990). The most common important commercial varieties are kaolin, ball clay and refractory clay (fire clay).

8.2 Kaolin:

The term being derived from ''Kauling'' a hill near Jauchau Fu, China, from which clay was extracted to make porcelain (Harben and Bates, 1990). The kaolin extracted from the commercial deposits contains kaolinite as the major component together with ancillary minerals such as quartz, mica and sometimes anatase. Commercial deposits contain 10 – 95 % kaolinite (Evans, 1993). Kaolin deposits (in situ) are white and soft, with low to moderate plasticity. Clay with a low iron content and well-ordered kaolinite is known as China clay (Harben and Bates, 1990; Evans, 1993; Bloodworth *et al.*, 1993; Manning, 1995). The kaolin deposit depends on the nature of the parent rock and the type and degree of alteration.

8.2.1 Properties and uses:

The shape and size distribution of kaolin particles is important in commercial uses, particularly in paper filling and paper coating. Industrially, particle size measurements below 0.15 μm are best made with a centrifuge and the <2 μm value is often used as a control in production (Jepson, 1984). The mineralogy of primary kaolin varies with particle size. The finer fraction has the greater kaolinite content and the smaller amount of ancillary minerals. Kaolin is used in the manufacture of porcelain and other ceramics. Today the principal use of kaolin is in the filling and coating of paper, making this industry the largest user (75 %). It is also used in lesser extent as a filler in paint, rubber and plastics (75 %) and in ceramics (10 %). The most important properties of kaolin used in filling paper are brightness, particle size, percent grit, and it is distinguished from other clays by its whiteness, and fine controllable particle size.

8.2.2 Use in paper:

The shape and size distribution of kaolin is important, because it effects the mechanical, optical and printing properties of the finished sheet of paper. Kaolin is used as a filler and as a coating pigment in the production of paper. Calcium carbonate recently is largely used for these applications. As a filler, kaolin is incorporated into the paper to provide opacity, reduce cost by replacing expensive wood pulp and improve printing characteristics. The most important properties of kaolin used in filling paper are brightness, particle size, percent grit, and abrasion number (Murray, 1984). For coating purposes the major factors that influence coating performance and determine the desirable properties are the shape and size distribution of the pigment and the mass of the coat that can be applied (Jepson, 1984; Bloodworth *et al.*, 1993). Gloss, brightness, opacity and smoothness all generally improve with increasing coat mass and with decreasing particle size. Sometimes very finely sized kaolin causes problems. For example the amount of adhesive needed to bond the platelets to themselves and to the base sheet increases with increasing fineness (Jepson, 1984). Coating grades are much finer (Table 8.1), and demand a higher price than filler grades. A measure of the mass of coat that can be applied is given by the viscosity concentration. This is the amount of solid in a suspension that gives a specific viscosity (5 poise) at 22 °C.

Table (8.1) Typical properties of kaolin (filler and coating) in paper

	Filler clays	Coating clays
Raw ISO* brightness %	76 - 82	81.5 – 90.5
Yellowness %	5.7 - 8	4 – 6.5
% < 2μm	25 - 60	75 – 95
% > 10 μm	6 - 25	0 – 6
% > 53 μm	0.05 max.	0.02 max.
Viscosity concentration (% solids with 5 poise at 22°C)	61.2 - 71.5	64.2 - 74.5

* International Standards Organisation (ISO)   Source: (Bloodworth *et al.*, 1993)

The quantity and quality of the kaolin can be improved by many processing methods. Firstly non-kaolin minerals (impurities) are removed using different settling velocities associated with particle size, then flotation is used to remove the remaining iron and titanium minerals, and magnetic separation completes this process to remove micas. Chemical leaching is used to increase the whiteness and brightness of the kaolin, and delamination to break down any kaolinite into individual platelets. Calcining above 400 °C improves optical properties and hardness (Evans, 1993; Bloodworth *et al.*, 1993).

8.2.3 Use in ceramics:

Kaolin is a major component in most ceramic bodies. Initially, the clay is mixed with water to obtain a plastic state. This allows the moulding and shaping of the clay into different forms by the producer. After that the clay is dried and it loses water by the drying process, but structural water is still present. At high temperature the clay becomes amorphous and loses structural water. The temperature range of 600 – 1000°C is mostly used in the manufacture of clay-based ceramics and this temperature is very important in transforming the dried clay into a new more rigid substance. Significant shrinkage occurs as this stage, and is treated and modified by addition of sufficient non-clay materials (sands and alkali feldspar are used) called temper. For high quality ceramics kaolin is used. Other material must be added to produce a portion of fused material to hold the ceramic together such as calcium oxide and quartz or feldspar. The highest quality ceramics (porcelain) require pure kaolinite, quartz sand and alkali feldspar (Velde, 1992). A low iron content (< 0.9 %) is necessary. The absence of tourmaline and iron-bearing minerals such as biotite is also important to prevent specking on the surface of the fired product (Bloodworth *et al.*, 1993).

8.2.4 Use as an extender and filler:

Hydrous and calcined grades of kaolin are used as functional fillers and extenders in the paint, rubber and plastic industries. Clay is used for both to reduce the cost and enhance the properties of the final product.

Paint. Kaolin in paint is used as a suspension aid, preventing pigment settling in the can. It improves the brightness and opacity, and allows this material to replace part of

the expensive TiO_2 pigment. Calcined grades are also produced to give greater durability to the paint. The requirements of kaolin grades used in paint are comparable to those used for paper coating (Jepson, 1984).

Rubber. Kaolin is used as a filler. The control parameters are particle shape, particle size distribution and surface properties. Surface finish may be improved by fine well dispersed fillers (Bloodworth *et al.*, 1993).

Plastics. Kaolin in plastics is commonly used in PVC flooring compounds. Electrical properties are enhanced by calcined clays, where high electrical resistance is required. Quality requirements for the polymer industries are comparable to those used for paper filling (Bloodworth *et al.*, 1993).

8.2.5 Other uses:

Kaolin is used for many other applications for which quality requirements are normally not so demanding, the notable exception being in pharmaceutical products. Kaolin is used as anti-caking agents in the manufacture of fertiliser, and as a carrier for pesticides. In the manufacture of white cement and in the production of glass fibre, kaolin with low iron contents is used (Bloodworth *et al.*, 1993).

8.3 Ball Clays:

This is an old English term that refers back to the days when these clays were rolled into balls for transporting (Evans, 1993). Ball clays are moderate to high plasticity dominated by kaolinite (about 70 %), as poorly ordered particles usually finer grained than in kaolin. Varying amounts of quartz, illite, chlorite, carbonaceous material and occasionally traces of smectite occur. Ball clay occurs as secondary, non-marine sedimentary deposits formed from transported sediments derived from a number of primary sources (Manning, 1995). Ball clays are highly regarded in the ceramics industry to provide strength and malleability to a ceramic body prior to firing. Also during firing at temperatures 1150 - 1200°C they have a white or near white colour and act as a cement binding together with the refractory, non-shrinking components of the ceramic body (Blyth and deFreitas, 1984; Manning, 1995). Plastic clays of lower grade are used in heavy products such as pipes, bricks and tiles. There are also used in refractories, as anti-caking agents in animal feedstuffs, and as fillers in plastics and rubber.

8.4 Refractory Clays:

Refractory clay, also known as fire clay, is a sedimentary deposit, composed chiefly of kaolinite, structurally disordered, and very plastic, with some mica or illite and quartz. Alumina content ranges from 20 or 25 % to 45.9 % (Dickson, 1986). For refractories (fire clay), clay must have a low content of mica and iron compounds. Refractory clay is also used in pottery, vitrified clay pipes.

8.5 Bentonite:

Bentonite is a fine-grained clay made up almost entirely of smectite group minerals, commonly montmorillonite. It was given its name at the end of the last century (1898) by W.C. Knight in describing rocks of Cretaceous age in the Benton shale near Fort Benton area, Montana, USA (Christidis and Scott, 1993; Baxter, 1997). Smectite minerals are tri-layered aluminosilicates. Where smectite consists of an octahedral alumina layer sandwiched between two tetrahedral silica layers the mineral is known as a montmorillonite. Where the smectite consists of an octahedral magnesium-oxygen layer sandwiched between two tetrahedral silica layers the mineral is known as saponite. Hectorites are modified saponites where some of the magnesium ions have been replaced by lithium and some of the hydroxyls by fluoride (Baxter, 1997). A particular feature of smectite clay is the substitution of Si^{4+} and Al^{3+} by lower valency cations. Smectite clays have a unique combination of physico-chemical properties leading to very varied industrial applications. These include small crystal size, high plasticity, high sorption and cation-exchange capacity, large chemically active surface area, swelling characteristics and important rheological, water sealing and bonding properties (Highley, 1990). The most important bentonites commercially are those that are predominantly composed of montmorillonite. It can be principally classified into sodium bentonite (swelling bentonite), and calcium bentonite (non-swelling bentonite), depending on the dominant exchangeable cations present in the clay and the nature and number of these substitutions (Inglethorpe *et al.*, 1993). There are several names for bentonite products and materials, some of which may be used differently in different countries (Table 8.2).

The uses of bentonite are extensive and diverse, but this chapter will cover the main commodity sectors of the market.

Table (8.2) Terminology of bentonites and related material

Dominant mineral	Geographical term	Synonymous term
Smectites		
Sodium montmorillonite	Wyoming bentonite (USA) Western bentonite (USA) bentonite	sodium bentonite swelling bentonite sodium-activated bentonite* sodium-exchanged bentonite* synthetic bentonite* engineered bentonite*
Calcium montmorillonite	Mississippi bentonite (USA) Southern bentonite (USA) Texas bentonite (USA) fuller's earth (UK)	calcium bentonite sub-bentonite non-swelling bentonite
Magnesium montmorillonite		saponite armargosite
Potassium montmorillonite		metabentonite potassium bentonite
Lithium montmorillonite		hectorite
non-smectites		
attapulgite		palygorskite
sepiolite		meerschaum (lumps)
sodium sepiolite		loughlinite

* Artificially produced by Na for Ca exchange of calcium montmorillonite   Source: (Manning, 1995)

8.5.1 Geological Occurrence:

Bentonite deposits consist essentially of smectite clays usually (but not always) formed by alteration of fine-grained volcanic ash deposited over relatively large areas (Christidis and Scott, 1993; Inglethorpe *et al.*, 1993). This material may have been subsequently reworked and concentrated by sedimentary processes. This type of deposit may be found associated with shallow marine or non-marine deposits. Other bentonites formed by in situ hydrothermal alteration of coarser igneous rock (parent rock) can yield bentonic deposits of economic significance (Manning, 1995). Parent materials for some hydrothermal bentonite are given in Table (8.3). The most important economic deposits are of Cretaceous or younger age (e.g. Wyoming bentonite).

Table (8.3) Examples of hydrothermal bentonites

Location	Parent rock/environment of alteration	Primary product
Greece: Milos	Dacite and associated tuffs / alkaline at depth	Ca-bentonite (deeplevels) kaolinite (shallow levels)
Italy: Sardinia	Trachytic volcanic ash	Ca-bentonite
Japan: W. Honshu	rhyolitic ash and pumice/marine	Na-bentonite

Source: (Manning, 1995)

8.5.2 Types and properties of commercial bentonite:

There are essentially five types of bentonite for industrial and domestic uses. Two are natural and three are treated or activated product (O'Driscoll, 1988);

Natural bentonites	Activated bentonites
Sodium bentonite	Sodium exchanged bentonite
Calcium bentonite	Acid activated bentonite Organophyllic bentonite

Source: (O'Driscoll, 1988)

8.5.2.1 Natural bentonites:

The presence of sodium or calcium as exchangeable cations greatly influences the properties of bentonite. Sodium bentonite typically exhibits very high swelling capacities and forms gel-like masses when added to water. If the calcium is the more abundant exchangeable cation, the clay will have a much lower swelling capacity than sodium bentonite. Some calcium types swell little more than common clay. Bentonites have several properties such as medium to high surface area, sorptive, rheological and bonding properties. The main bentonite properties are summerised below.

Rheological properties. When added to water, finely ground sodium bentonite increases the viscosity, suspending power and thixotropy. On agitation, the weak electrical bonds are broken and the dispersion becomes fluid with a high viscosity (Highley, 1972).

Bonding properties. The second largest end use for bentonite is as a bonding or pelletising agent (Grim and Guven, 1978).

Sorptive properties. Bentonites have high adsorption, or the ability to attract and hold ions or molecules of gas or liquid. When calcined, all clays have a large pore volume and surface area, and can take up liquids rapidly to 200 % or more of their own weight (Haden and Schwint, 1967; Grim and Guven, 1978).

Crystal size, surface area and exchangeable ions. Crystal shape and aggregate characteristics can have an important influence on physical and rheological properties. The surface area of bentonite allows them to be used as a catalyst. The most unique property of smectite clays is the presence of exchangeable cations, and the most common of these exchangeable ions are Ca, Mg, Na and H, but small amounts of exchangeable K and Li occur in some smectites. The cation exchange capacity of relatively pure smectite clays ranges between 70 and 130 meq/100 g (Odom, 1984). Other properties adopted by industry include impermeability in lining waste sites and canals and ceramic bodies. These physico-chemical properties lead to very varied industrial applications.

8.5.2.2 Activated bentonites:

Natural bentonites can be treated to enhance certain properties and provide products with a wider range of application. Calcium-bentonites that are generally low swelling can be converted to sodium-bentonites by adding a few percent of sodium carbonate to enhance swelling characteristics. Reaction of bentonite with inorganic acids serves three purpose: it dissolves minerals such as calcite, replaces exchangeable divalent calcium ions with monovalent hydrogen ions, and leaches ferric, ferrous, aluminum and magnesium ions. These changes to the crystal structure result in increased specific surface area and porosity. Organophyllic bentonites are manufactured from Wyoming bentonite, which is wet-refined to remove coarse non-clay minerals. This gives a slurry of essentially pure montmorillonite with Na, Ca and Mg present as exchangeable ions. Addition of 90 – 110 meq/100 g of a quaternary ammonium salt leads to a rapid and essentially complete exchange of ions, and then the clay is filtered and dried. The exchangeable cations present on certain montmorillonites can be replaced by long-chain quaternary ammonium cations, and the resulting clays have the important property of being able to swell and disperse in a variety of organic solvents. Organophyllic clays have a wide range of industrial applications such as oil-drilling fluids, paints, plastics and grease (Jones, 1983; O'Driscoll, 1988).

8.5.3   Industrial applications:

Bentonites have a wide variety of uses in many different industries. Relationships between the physico-chemical properties of bentonites and commercial application are summarised in Table (8.4).

Table (8.4) Commercial applications of bentonite in relation to physico-chemical properties (after Highley, 1972).

Sorptive properties (may be increased by acid treatment) A: In suspension	Refining and bleaching of glyceride oils Clarification and purification of sugar solution Water purification, sewage and effluent treatment
B: In dry state (or paste)	Pharmaceutical and therapeutic preparations Absorbent
Surface area (may be increased by acid-activation)	Catalytic action, carrier for catalyst Carrier for insecticides and fungicides Mineral filler and extender
Rheological properties A: Viscosity and suspending powers	Drilling fluid Paints (oil and water-based) Fertilizer sprays Bitumen emulsions Formulation of ceramic glazes
B: Thixotropy	Wall support for boreholes Civil engineering (diaphragm wall construction) Non-drip paints
Impermeability, coating properties	Civil engineering (grouting, impermeable membrane) Drilling in permeable strata
Bonding properties	Bonding foundry moulding sands Pelletising iron ore concentrates Pelletising animal feedstuffs
plasticity	Formulation of mortars, putties, adhesives, some ceramic bodies

Source: (Inglethorpe *et al.*, 1993).

The most important bentonites commercially are those that are predominantly composed of montmorillonite, and these account for over 98 % of all bentonite production. The major use of smectite (bentonite in commercial terms) is in drilling muds (Baxter, 1997), and the main industrial applications are summarised below.

8.5.3.1 Drilling fluids:

Well drilling remains one of the largest volume markets for bentonite. The mud fluid is pumped down through the drill strings, emerging at the bottom through a nozzle in the bit. It rises to the surface in the annular space (between the drilling strings and walls of the hole) and flows into the shale shaker, mud cleaner and centrifuge for removal of cuttings, then to the mud tanks and is pumped again to the borehole to repeat the same cycle. The functions of the drilling fluid are, to prevent settling of cuttings during circulation, to stabilise the walls by forming mud cake, to lubricate and cool the drilling strings, to support the drilling strings and casing, and to control the hydrostatic pressure and prevent blow out by adding barite to increase the mud weight so that the hydrostatic pressure of the mud will be greater than the hydrostatic pressure of the formation. These requirements obviously demand a clay of a certain quality, that is drilling mud grade, which meets specifications set by the American Petroleum Institute (API) or the Oil Companies Material Association (OCMA); Grim and Guven, 1978; Clarke, 1985; Benzabanta *et al.*, 1986; Harben and Bates, 1990; Inglethorpe *et al.*, 1993.

Mud types: (Kendall, 1996)

Drilling fluid muds are classified into three basic types.

Water based muds (WBMs). Very widely used in shallow wells. Essentially comprise a bentonite, a suspension of baryte, and additives in water, based on fresh water, brines or an emulsion of oil dispersed in water. There are few restrictions on the disposal of WBMs, but they have a number of performance limitations, particularly at high temperatures (deep wells).

Oil based muds (OBMs). These consists of two main types: invert emulsions (in which water or brine is dispersed in oil) and purely oil based. OBMs are used where the use of WBMs would be dangerous. They have good lubricity assist drilling at high-angle (deviation wells), have no corrosion, and a higher rate of penetration (ROP). They are stable at high temperature and are reusable. Disadvantages of OBMs are the high cost.

They are dirty to work with, not suitable for use in loss of circulation areas (mixed-

with mica), and it is not possible to run resistivity logs (Benzabanta *et al.*, 1986; Kendall, 1996).

Synthetic based muds (SBMs). The newest mud system used in drilling. They are formulated to have the technical advantages of OBMs without the pollution problems, enhanced lubricity, better hole cleaning characteristics and faster rate of penetration (ROP).

8.5.3.2 Foundry moulding sands:

Moulding sands, one of the largest applications for bentonite (ideal bonding agent for sand), are used extensively in the metallurgical industry in shaping metal by the casting process. Sand is mixed with bentonite and a small amount of water called tempering water added to the mixture. This makes it plastic and cohesive so that it can be moulded around a pattern, and gives it sufficient strength to maintain the cavity after the pattern is removed. Hot metal is poured into the mould. Plasticity and cohesion vary greatly with the amount of tempering water. The clay provides bonding strength and plasticity to the sand-clay mixture. Both sodium and calcium bentonite are used in the foundry industry and about 5-10 % bentonite is mixed with sand and water. Clay bonded moulding sands are recycled many times with small addition of new silica and bentonite in the mould-making process (Grim and Guven, 1978). Natural sodium bentonites have a medium green strength and a high dry strength, which increases their resistance to molten metal. When molten metal is poured into a mould a certain percentage of the bentonite is heated above the temperature where OH ions are removed from the clay structure. The loss of OH from bentonite generally occurs in the range of 500 - 750°C. The higher temperature of OH loss the greater the durability of the smectite clay. Primarily, durability is related to the temperature of OH loss, and secondary influenced by the type of exchangeable ions. Calcium bentonites have lower durability than sodium bentonites, and this can be improved by sodium exchange or by using a blend of calcium and sodium bentonites to achieve the desired combination of properties. Calcium-bentonite itself produces moulds with a medium green strength and a low dry strength, and low resistance. For this reason calcium-bentonites are rarely used alone. Sodium bentonites also have a greater capacity for adsorbing water and thus have much higher liquid limits than calcium bentonites. If the bentonite is unable to hold any additional water, the mould

will lose its strength and fail. Bentonite from the northwest USA has liquid limits of 600 – 700 %. The Cast Metal Technology Centre of the UK has recommended a minimum liquid limit of 525 % for bentonites for use in steel casting. Thus, both green and dry strength are important properties of moulding sands. Flowability (related to clay mineral composition), hot strength and permeability (the particle size of the sand grains rather than the clay is the major influence on permeability) are also important characteristics of moulding sands (Grim and Guven, 1978; Odom, 1984; Inglethorpe *et al.*, 1993). Table (8.5) shows typical foundry moulding sand test values for a range of commercial bentonites.

Table (8.5) Typical test values for commercial bentonites used in foundry moulding sands

Type	Green strength (kN/m^2)	Dry strength (kN/m^2)	Shatter Index No.	Compactibility (%)	Liquid limit (%)
Natural Na-bentonite Wyoming, USA	41-49 (medium)	655-897 (high)	80 – 83	NA	600 – 620
Fully-activated Ca-bentonite Italy	55 (high)	482 (low)	79	NA	530
Na-treated Ca-bentonite UK	80 (high)	240 (low)	78	62.5	NA
Natural Ca-bentonite Mississippi, USA	41 (high)	448 (low)	78	NA	118

All figures based on a 5% addition of bentonite to a standard silica sand at 3.5% moisture content

Source: (Inglethorpe *et al.*, 1993).

8.5.3.3 Civil engineering:

Sodium bentonite has been used in civil engineering applications for many years in water and fluid retention. It forms an impermeable barrier, grouting the cracks and fissures in rocks (slurries containing 4 – 8 % bentonite are used). It is used to increase the plasticity of mortar, and to make concrete pliable as well as impermeable. It is also used to waterproof concrete walls and floors that are below grade, but in recent years bentonite has come into its own as a landfill sealant. Sodium bentonite is used as a soil sealant in landfills in order to isolate the leachate generated from the waste from groundwater. The characteristics of the sodium bentonite

important for this application are the particle size distribution, free swell, and the resistance to chemical impurities. It is the free swell of the sodium bentonite that effectively reacts with soil and forms the impermeable layer against the leachate (Kendall, 1996; Shah, 1997; Nebergall, 1998).

8.5.3.4 Animal feed:

Bentonite, apart from industrial uses, is used in the animal feed industry. Both calcium and sodium bentonites are used as fillers and pellet binders (to avoid the wastage associated with powder feeds). Bentonite helps to increase egg size and shell hardness. Halloran (1974) proved that egg production increased by 2 % with a bentonite inclusion rate of 5 % in feed. Another study proved that with an inclusion rate of 2.5-5 % egg production increased up to 5 % with slightly better feed efficiency (Ahmed Saeed, 1996). The required physical properties of bentonites are not well defined within this market (Nebergall, 1998).

8.5.3.5 Iron ore pelletising (IOP):

Bentonites are widely used to bind fine-grained iron ore into pellets before these are introduced into the blast furnace feed. The mixture of iron ore and bentonite is rolled to form pellets, which are sintered at about 1250°C to develop enough strength to avoid breakage during handling. The conventional binder (4 – 5 kg/tonne of pellets) is high swelling Wyoming bentonite, or sodium exchanged bentonites may also be used. A proportion of olivine is added to some pellets to improve their high temperature properties. Also some pelletising plants use alternative inorganic binders. These include hydrated dolomite and hydrated lime, but their use is not at all widespread. Bentonite usually decreases the iron content of the pellet by 0.8 % (Inglethorpe *et al.*, 1993; Kendall, 1996). The main functions of bentonite in pellets are as follow: (Inglethorpe *et al.*, 1993):

- To absorb excess water from the iron ore.
- To provide enough strength to the green pellet.
- To provide adequate dry strength.
- To reduce the quantity of fine particles produced, and to improve their mechanical properties.

8.5.3.6 Absorbents:

Bentonite is highly hygroscopic and when crushed and dried to 5 % moisture will adsorb additional moisture rapidly. Sodium and calcium bentonites are commonly used. Non-swelling clays have the advantage of maintaining granule strength even when wet and will not become slippery. Bentonites may be calcined to improve their mechanical strength when wet. They are extensively used for pet litter, for adsorbing oil and grease from the floor and as a carrier for certain types of agriculture insecticides. There are no rigid specifications, the requirements being for a high liquid and odour absorbency, freedom from dust and uniformity in size. Ca-bentonite tends to slake in oil and grease, producing a slippery surface, and attapulgite and sepiolite are preferred for use as oil absorbents on factory floors, where spillage is likely. Calcined Ca-bentonites are water stable and can be used as carriers for pesticides and herbicides (Santaren, 1993).

8.5.3.7 Miscellaneous uses:

There are so many miscellaneous small volume and speciality uses of bentonites that only a few can be briefly mentioned, Odom (1984).

Adhesives. Bentonites having high dispersion and suspension characteristics make them useful in some adhesives such as those made with latex and asphaltic material.

Ink. Organic-clad smectites are used in some inks to control consistency, penetration and misting during the printing operation.

Medicines, pharmaceuticals and cosmetics. There is increasing use of Na-bentonite in the preparation of medicines, pharmaceuticals and cosmetics. These uses generally require bentonites having a high brightness and in some uses the bentonite must also be rich in magnesium. Cuciureanu *et al.* (1972) report that the stability of some antibiotics is increased when they are incorporated in bentonite pastes.

Paint. The various types of clay used in paint (natural sodium bentonite, Na-exchanged calcium and organic clad bentonite) are not necessarily only inert fillers but may add valuable properties to both oil and water-based paints. In water-based paints, the bentonite acts as a suspending and thickening agent. It is also used as an emulsifying agent in water and oil-based paints. These clays are added to improve pigment suspensions, viscosity, brushability and thixotropy, and to reduce pigment penetration into porous surfaces.

Soaps. Bentonites are used in soaps as a partial replacement for the fatty-acid component, because of their emulsifying action and their detergent effect. The sodium bentonites have a beneficial water softening action. There are many cleaning and polishing formulations containing bentonite (Grim and Guven, 1978).

Ceramics. Bentonites are not used in large volume as ceramic raw materials, because of their high water of plasticity. However, bentonites with low iron content are added to ceramic bodies to impart strength and to give desired vitrification or colour properties. Sometimes bentonites are added to kaolin to improve its suspension characteristics and to increase plasticity required for extrusion.

Chapter 9

MINERALOGY AND MINERAL CHEMISTRY OF

CELESTITE-BEARING FORMATIONS

9.1 Introduction:

Both 'Celestite' and 'Celestine' refer to the mineral composed of strontium sulphate ($SrSO_4$). Celestine is derived from the latin Celestis, celestial, an allusion to the sky-blue colour (Chang *et al.*, 1996). It is the most important mineral and source of strontium. The other commercial source is strontianite (strontium carbonate, $SrCO_3$). Celestite has a hardness of 3 to 3.5 on Moh's scale, and high specific gravity of approximately 3.98. It is usually colourless (in thin section), white, pale blue, reddish, greenish and brown. The colours of celestite specimens are mostly caused by impurities, but the blue colour of celestite is probably produced by irradiation (Deer *et al.*, 1992). It is found usually as scattered crystal aggregates, as geodes and nodules and as beds in association with evaporite minerals, especially gypsum (de Brodtkorb, 1989). It may also occur in fissures and cavities in dolomites and dolomitic limestones (Deer *et al.*, 1992). The main substitution for strontium in celestite is barium. Leading celestite producers are Mexico, Spain, Turkey and Iran. Significant quantities of celestite are also produced in China, former USSR, Italy, Algeria and Pakistan (Gorden, 1995; Wei Hong, 1993). Strontianite occurs in a number of localities including Strontian, Argyllshire, from which it takes its name. The strontianite is distinctly secondary in its occurrence and is believed to have been formed as an alteration product of celestite (Thomas, 1973; Deer *et al.*, 1992). Strontianite in the study area was found associated with celestite in the lower part of the Benghazi Member (Benghazi Cement Quarry).

9.2 Occurrences and properties of Sr minerals:

Celestite occurs in the Benghazi Member (Facies II) of the Ar Rajmah Formation, which consists mainly of a massive limestone bed (<10 % dolomite). The colour of celestite is brownish, and it is formed of friable prismatic crystal aggregates infilling vuggy pores (Plate 9.1 and 9.2). XRD of a powdered specimen showed the presence of impurities such as relicts of anhydrite, gypsum, calcite and dolomite. The presence of anhydrite within the celestite crystals indicates that the origin might be anhydrite nodules later replaced by celestite, as described by Wood and Shaw (1976). Authigenic celestite occurs both as a cement (Plates 9.3 and 9.4) and as a replacement of other fracture filling minerals such as anhydrite.

Plate (9.1) Celestite mineral, sample taken at 4.5 m, and found as geodic nodules. Benghazi Member, of the Ar Rajmah Formation. In Benghazi Cement Quarry.
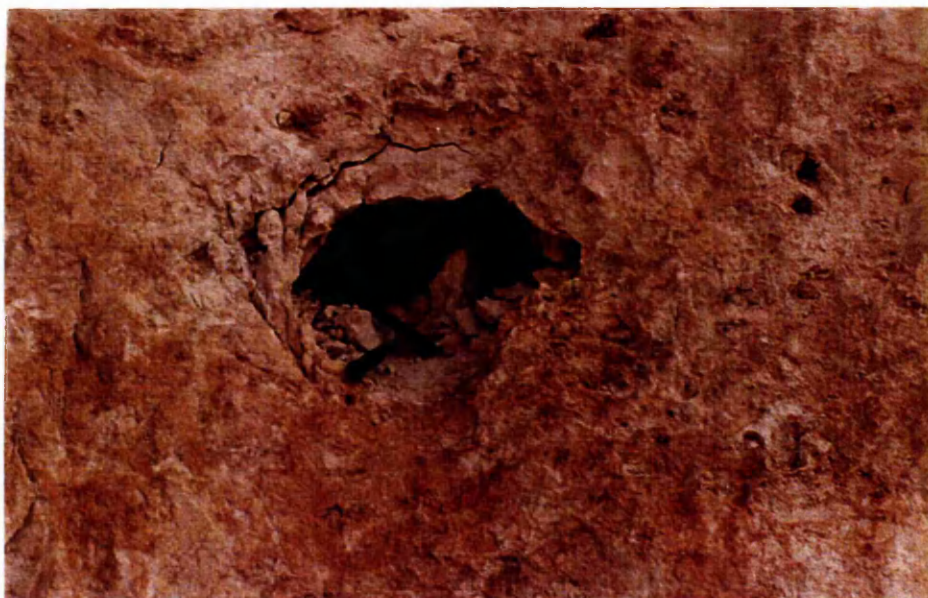
Plate (9.2) Celestite nest at 4.5 m, Benghazi Member, Ar Rajmah Formation. From Benghazi Cement Quarry.
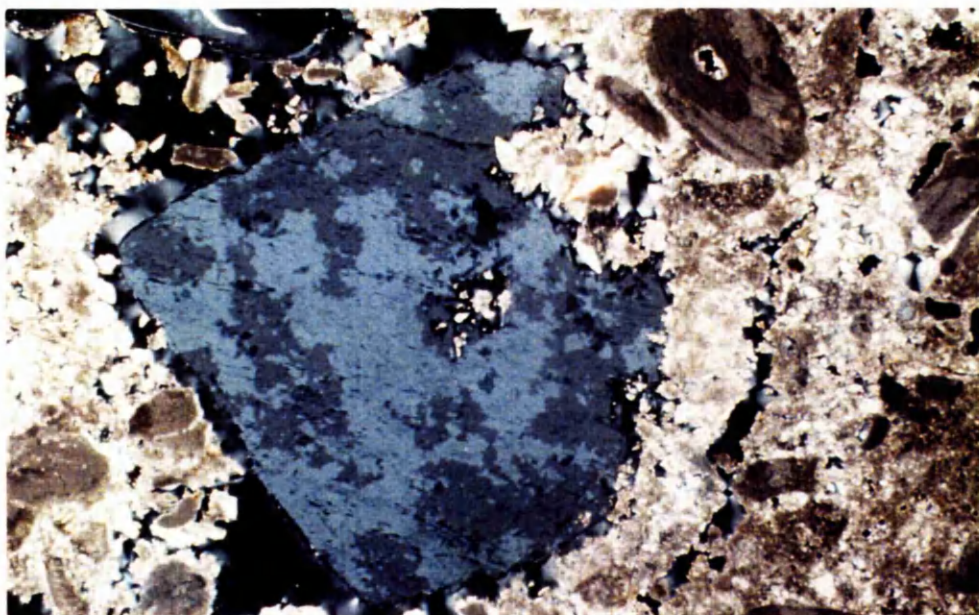
Plate (9.3) A photomicrograph (sample no. LB2) taken with crossed polars, showing celestite, etched (Arrows) by dolomite crystals, field of view = 6 mm.
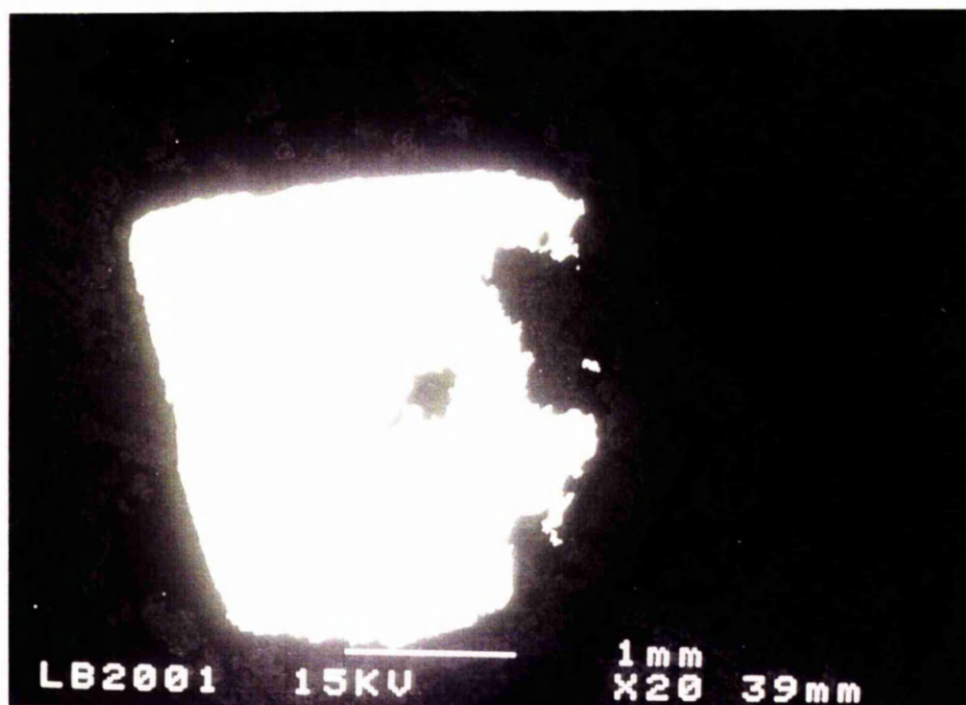
Plate (9.4) Scanning electron micrograph (BSE) of polished thin section of celestite mineral in Facies (II) of the Benghazi Member, Ar Rajmah Formation (sample no. LB2).

9.2.1 TG-DSC curve of strontianite (standard):

In air, strontianite ($SrCO_3$) has two steps in the TGA curve (Figure 9.1) which result from the weight losses of about 1.9 % and 27.6 %. The first weight loss corresponds to peaks 1 and 2 at about 868 °C and 918 °C and is associated with the rhombic $\Leftrightarrow$ trigonal inversion (polymorphic transition). The other two endothermic peaks at about 1065°C and 1108°C, with a 27.6 % weight loss, are due to decarbonation (Gruver, 1950). In CO_2 there is no change in weight loss until 1100°C at which point it decreases.

$$SrCO_3 \Leftrightarrow SrO + CO_2$$

$$147.6 \quad \Leftrightarrow \quad 103.6 + 44$$

$$\text{Predict weight loss} \quad = 44/147.6 \quad = 29.80\ \%$$

$$\text{Observed weight loss} = 1.9 + 27.6 = 29.50\ \%$$

9.2.2 TG-DSC curve of celestite:

In air, the TGA curve shows two steps resulting from weight losses. The first weight loss of 3.7 % is associated with the peaks 785 °C and 801 °C. The second showed a 0.37 % loss at about 1060 °C. The last endothermic peak is very sharp at about 1155 °C. The first and second peaks (Figure 9.2 and Table 9.1) represent traces of dolomite, confirmed by XRD analysis. The small peak at 1060 °C and the very sharp peak at 1155 °C are probably due to the presence of some foreign material such as impure strontianite. Anhydrite is expected to be found, but the anhydrite not effected by heating until inversion at 1230 °C (Kauffman and Dilling, 1950; Gruver, 1951). Kauffman and Dilling (1950) demonstrated that celestite does not show any significant peaks over the temperature range from 0 – 1100 °C. Gruver (1950) said that the celestite melts with decomposition near 1600 °C. Cocco (1952) suggested that the celestite from Catania in Italy has two endothermic peaks at 930 °C that represent possible polymorphic transitions, and melts at 1606 °C.

Celestite was heated at a range of temperatures (800°C, 1000°C, 1150°C, and 1500 °C; Figure 9.3). The only effects to be detected using XRD (approx. 0.5 mg) include a change in the sequence of peak intensities (Table 9.2). There is no change in mineralogical composition, but the degree of order changes, reducing at higher temperature.

$$SrSO_4 \Leftrightarrow SrSO_4 \quad (\text{no weight loss})$$
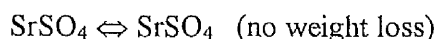
Table (9.1) Temperatures of thermal effects given by various minerals of the Ar Rajmah Formation and other standards.

Mineral	Formula	Observed weight losses (%)		Temperature (°C)			
				Endothermic		Exothermic	
		air	CO$_2$	air	CO$_2$	air	CO$_2$
Strontianite	SrCO$_3$ (Standard)	29.50	-	868	868	-	-
				918			
				1065	1031		
				1107	1101		
Celestite	SrSO$_4$ (Benghazi Cement Quarry)	0	0	785	757		
				801	967	-	-
		4.07 (impurities)	4.09 (impurities)	1060			
				1155	1121		

Table (9.2) Dominant X-ray diffraction peaks of celestite, in the Ar Rajmah Formation.

Age	Formation	Temperature (°C)	2 Theta	d-spacing d($\overset{\circ}{A}$)	Int. (%)	hkl
Middle Miocene	Ar Rajmah	untreated	30.095	2.967	100	211
			27.077	3.291	98.80	210
			28.093	3.174	77.27	102
			32.793	2.729	67.02	112
			44.321	2.042	62.38	113
		800	27.210	3.275	100	210
			30.217	2.995	93.08	211
			44.431	2.037	68.49	113
			32.908	2.720	65.56	112
			28.216	3.160	59.56	102
		1000	27.104	3.287	100	210
			30.121	2.965	98.99	211
			32.805	2.728	60.89	112
			28.103	3.173	58.16	102
			44.337	2.041	52.89	113
		1150	27.094	3.289	100	210
			30.107	2.966	97.57	211
			32.807	2.728	74.07	112
			28.107	3.172	60.83	102
			44.317	2.042	54.16	113
		1500	30.178	2.959	100	211
			27.147	3.282	82.88	210
			32.837	2.725	80.79	112
			33.485	2.674	53.89	020
			28.165	3.166	50.55	102
			44.358	2.041	39.33	113
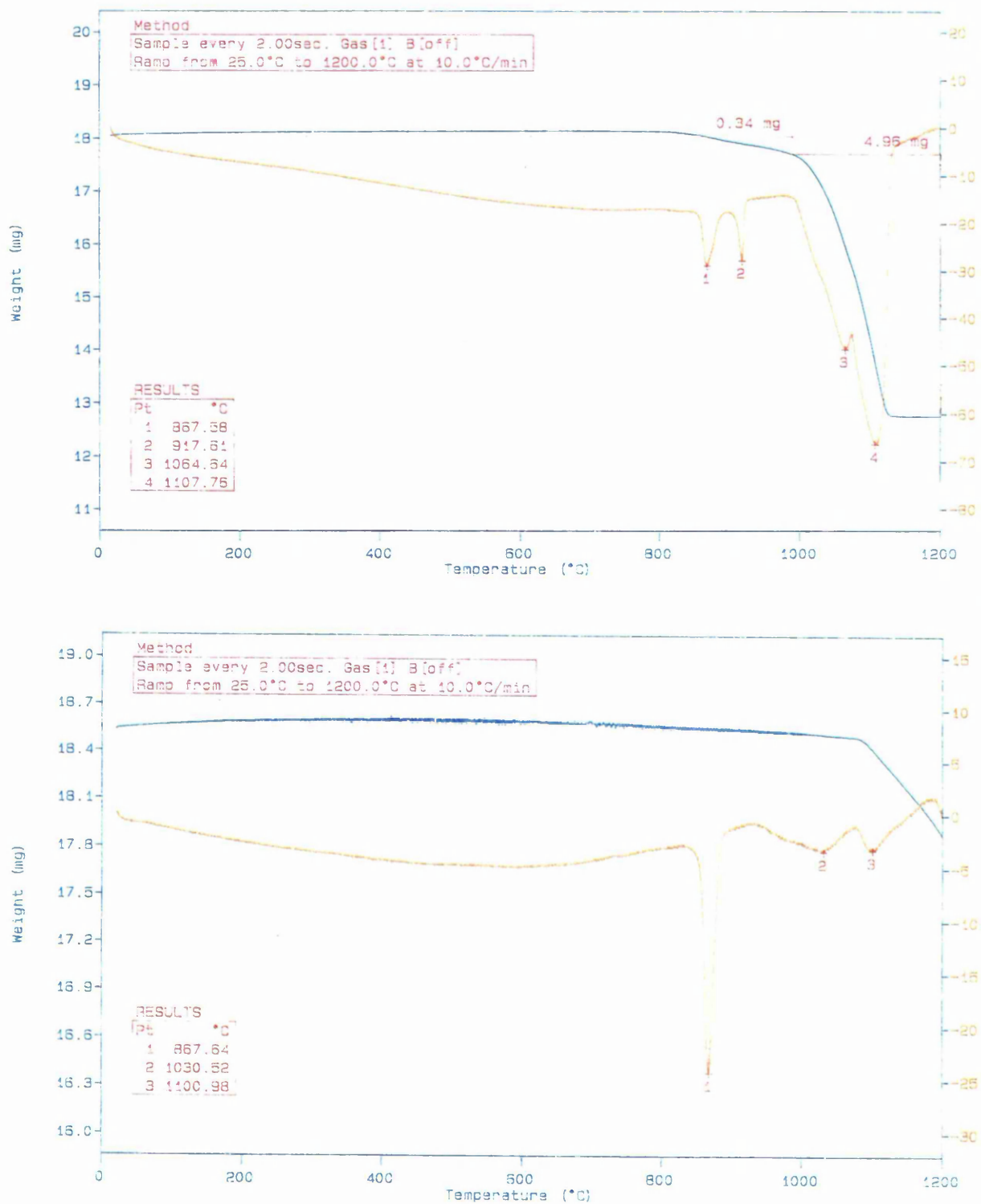
Figure (9.1) TG-DSC curves of strontianite (standard), in air (sample size = 18 mg) and CO_2 (sample size = 18.5 mg) atmospheres.
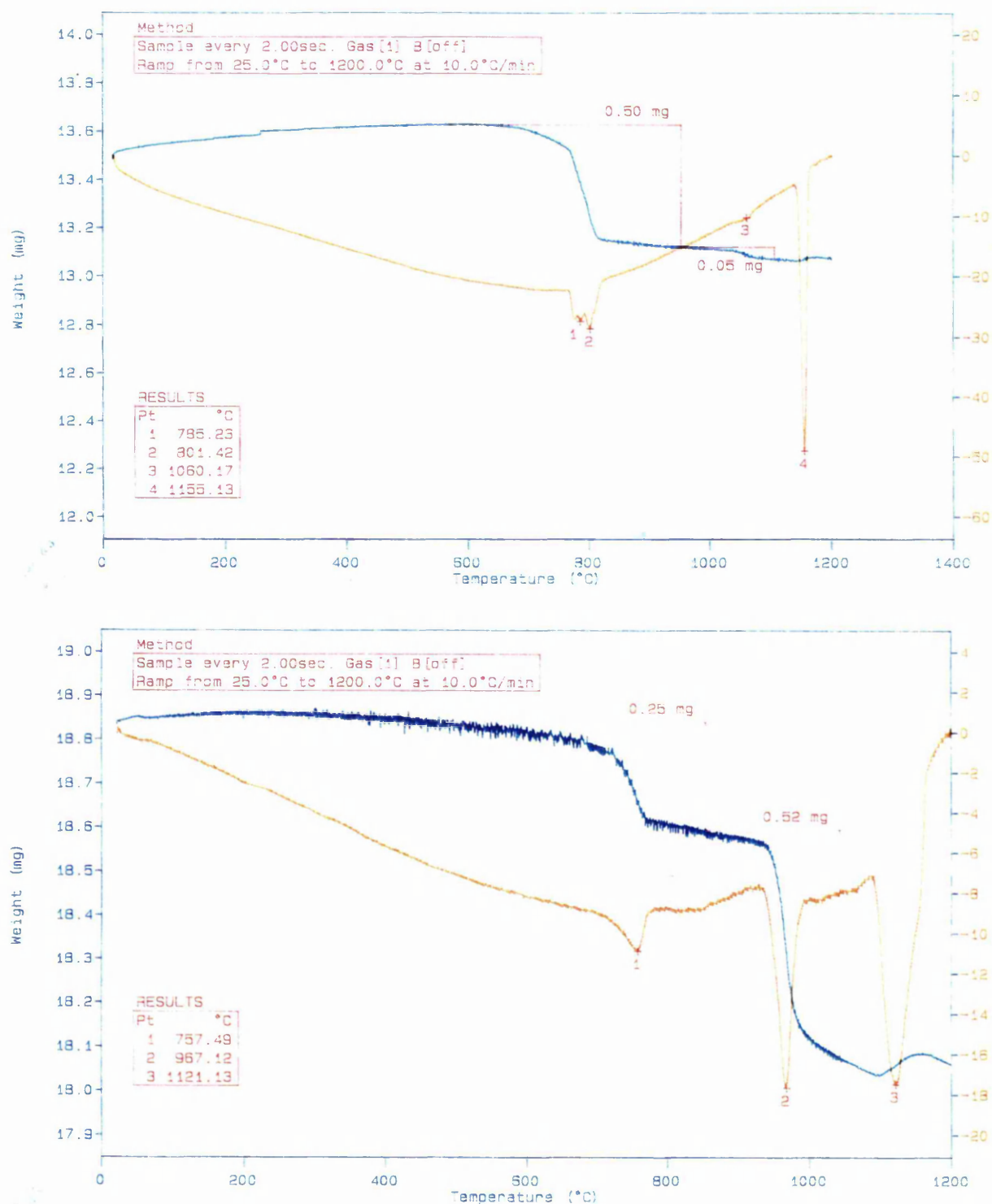
Figure (9.2) TG-DSC curves of celestite of the Ar Rajmah Formation (Facies, LB2), in air (sample size = 13.5 mg) and CO_2 (sample size = 18.82 mg) atmospheres, at Benghazi Cement Quarry.
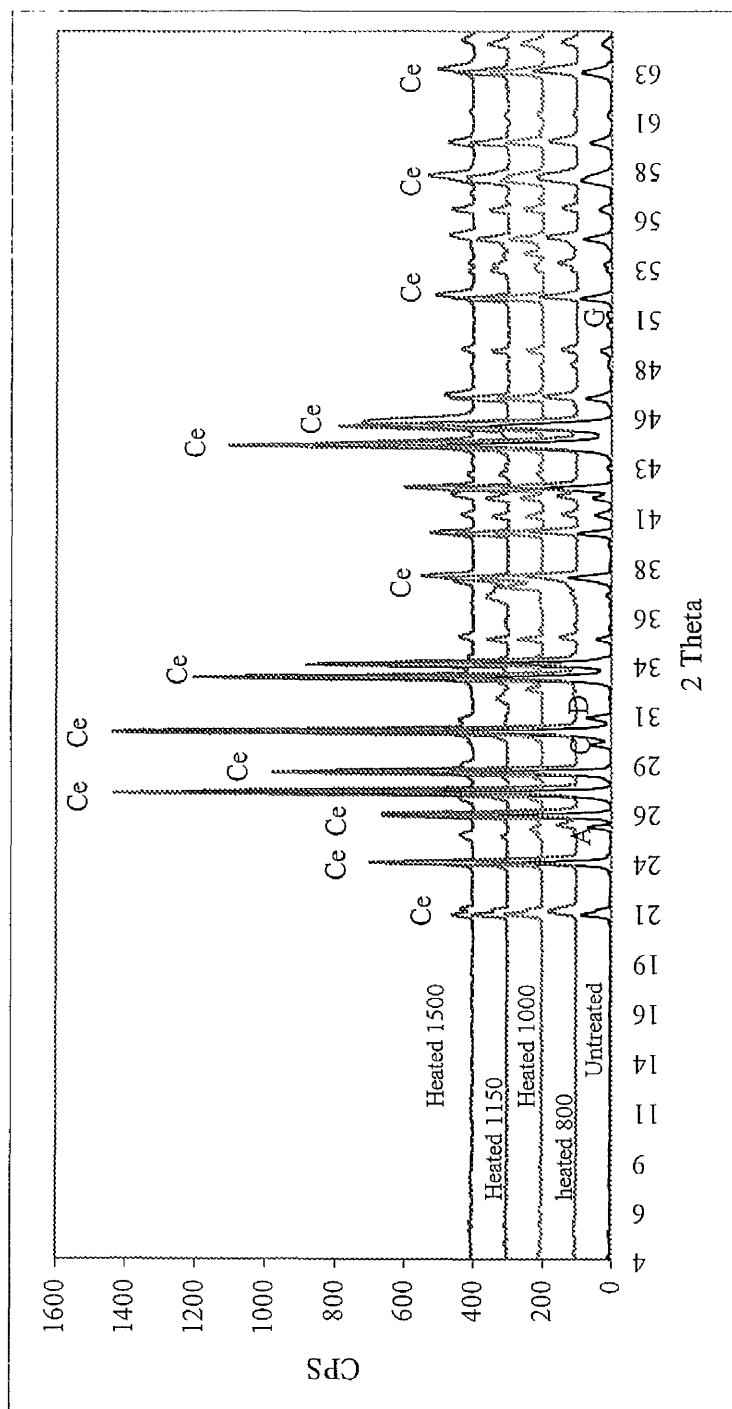
Figure (9.3) XRD pattern of celestite sample of the Ar Rajmah Formation (Benghazi quarry) showing (Ce) Celestite, (A) Anhydrite, (G) Gypsum, (D) Dolomite and (C) Calcite. Untreated (Air treated) and treated (heated to 800°C, 1000 °C, 1150°C, 1500°C).

9.3   Occurrence and distribution of Sr in other minerals:

9.3.1 Strontium in fossils:

The carbonate rocks (e.g. limestones) have many varieties, but all are essentially composed of $CaCO_3$. Most limestones in the study area contain skeletal material such as shells and coral skeletons. Calcite and magnesian calcite are the dominant minerals of carbonate skeletons. The distribution of strontium and magnesium in fossils has been studied for carbonate rocks of different ages (L. to M. Eocene to M. Miocene) in of the Apollonia, Darnah and Ar Rajmah Formations. Dodd (1967) has suggested that the concentration of magnesium and strontium in carbonate skeletons is controlled by four major factors: (1) water chemistry; (2) mineralogy (calcite is generally high in Mg and low in Sr relative to aragonite); (3) physiology of organisms (the distribution of Sr in a limestone fossil is complex and can be interpreted genetically); (4) and other enviromental factors (e.g. salinity and temperature). Kulp *et al.* (1952) and Turekian (1955) have postulated that the distribution of the strontium content in fossils depends on the salinity, composition of the original ocean environment, the ratio of aragonite to calcite in the original shell, and the subsequent recrystallization history. Maximum loss of strontium occurs during early diagenesis before major cementation, when aragonite allochems change to calcite. Factors of secondary importance in the loss of strontium may include changes by solid-state recrystallization and decomposition of organic material (Kahle, 1965). Solid-state recrystallization in carbonates requires an energy difference to drive the transformation. In many cases this is due to differences in strain caused by crystal growth or compaction. Often slow geological diagenetic processes are capable of reducing the strontium content with time. This loss can be related ordinarily to the change from aragonite to calcite in the original sediment mass. Recrystallization could be expected to result in at least partial transfer of Sr^{+2} from allochems into interstitial fluids or cement (Odum, 1957).

9.3.1.1 Apollonia Formation (Lower to Middle Eocene):

Generally, there is an extremely high value for the strontium content of the Apollonia relative to the Darnah and Ar Rajmah Formations (Tables A.9.2, A.6.4,and A.9.5). The high values were interpreted to be a result of the presence of acantharia-radiolarians, whose skeletons are composed of celestite. The skeleton of acantharia generally comprises 20 spines of $SrSO_4$ joined at one end (endoplasm), and the central capsule contains celestite (Pokorny, 1963; Brasier, 1980; Mann *et al.*, 1989). The Apollonia Formation contains chert nodules (see Chapter 2) and biogenic silica was largely supplied by radiolarians and diatoms. Most radiolaria and diatoms are dissolved relatively soon after burial and precipitate as chert nodules in carbonate host rocks

(Blatt *et al.*, 1980; Carter, 1990; Tucker, 1991). The geochemistry of chert formation differs somewhat from that of the formation of quartz overgrowths in sandstones, because the origin of most chert involves living organisms (Blatt *et al.*, 1980). Strontium sulphate is quite insoluble (solubility product of $SrSO_4$ is small) and precipitates from a solution in a manner not unlike that of silica.

The average value of Sr/Ca atom ratio x 1000 for coralline algae was 0.49. The coralline algae in the Apollonia Formation is lower in strontium than in other Formations. The range in strontium content is from 100 to 500 ppm. The range of $MgCO_3$ is 0.86 to 0.94 mole percent. The average value of Sr/Ca ratio for echinoderm fragments was 5.07. The range of $MgCO_3$ is 1.21 to 1.42 mole percent, and the range of strontium in parts per million was 2800 to 4400. Echinoderm fragments have the highest Sr/Ca values, which may be due to inclusion of high Sr/Ca ratios of insoluble argillaceous fractions as well as the carbonate in the porous parts of the skeleton. The average value for the Sr/Ca ratio within foraminifera was 4.15. The matrix has an average value of 2.60 of Sr/Ca ratio, and cement has an average of 3.93 for the Sr/Ca ratio and 1.19 for $MgCO_3$ (Figure 9.4).

The ratios between Sr^{+2} in ppm cement and matrix versus allochems are summarized in Table (9.3).

Table (9.3) Strontium content in parts per million of allochems versus cement and matrix of the Apollonia Formation.

Age	Formation	Mean of Sr^{++} content (ppm)					Approximate ratios Sr^{++} (ppm)						
		E	R	F	C	Mx	C:E	Mx:E	C:R	Mx:R	C:F	Mx:F	C:Mx
Lower To Middle Eocene	Apollonia	3375	333	3050	2900	1927	0.9:1	0.6:1	8.7:1	5.8:1	1:1	0.6:1	1.5:1

E = echindoderm fragments, R = coralline algae, F = foraminifera, C = cement, and Mx = matrix
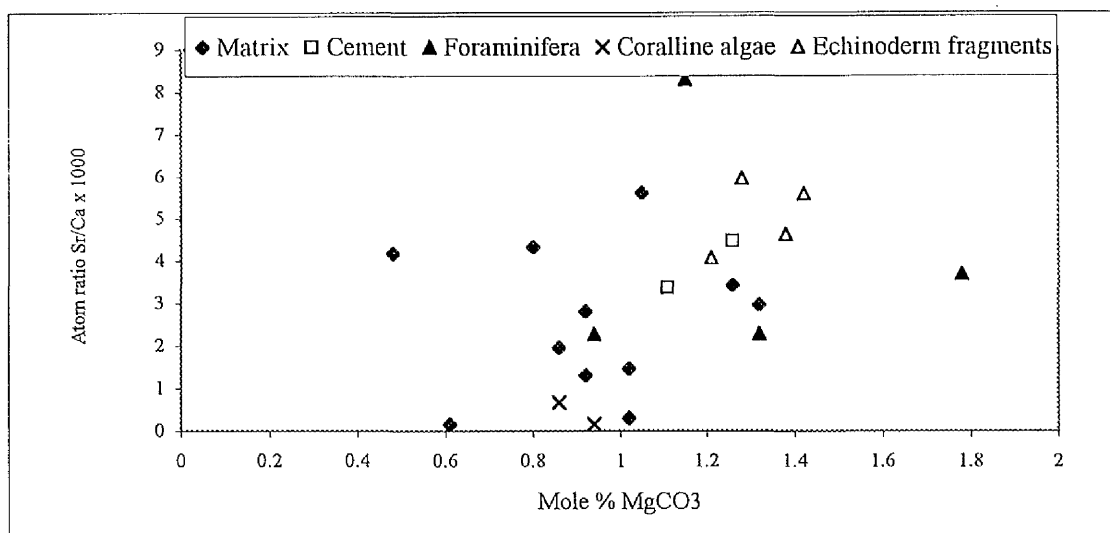
Figure (9.4) Scatter diagram of Sr/Ca x 1000 atom ratios vs MgCO₃ Mole %concentrations of the major components (coralline algae, echinoderm fragments, foraminifera, matrix and cement) in the Apollonia Formation (Lower to Middle Eocene).

9.3.1.2 Darnah Formation (Middle to Upper Eocene):

All average values of Sr/Ca ratio for coralline algae (0.2), echinoderm fragments (0.78), foraminifera (0.18), matrix (0.36) and cement (0.69) for the Darnah Formation are lower than for the Apollonia Formation (Tables A.9.3, A.6.6 - A.9.10 and Figure 9.5). Recrystallization (replacement) seems to have taken place in most carbonate rock of the Darnah Formation. This lowers the Sr/Ca ratio in varying amounts. The range of MgCO₃ in all samples is 0.12 to 6.11 mole percent.
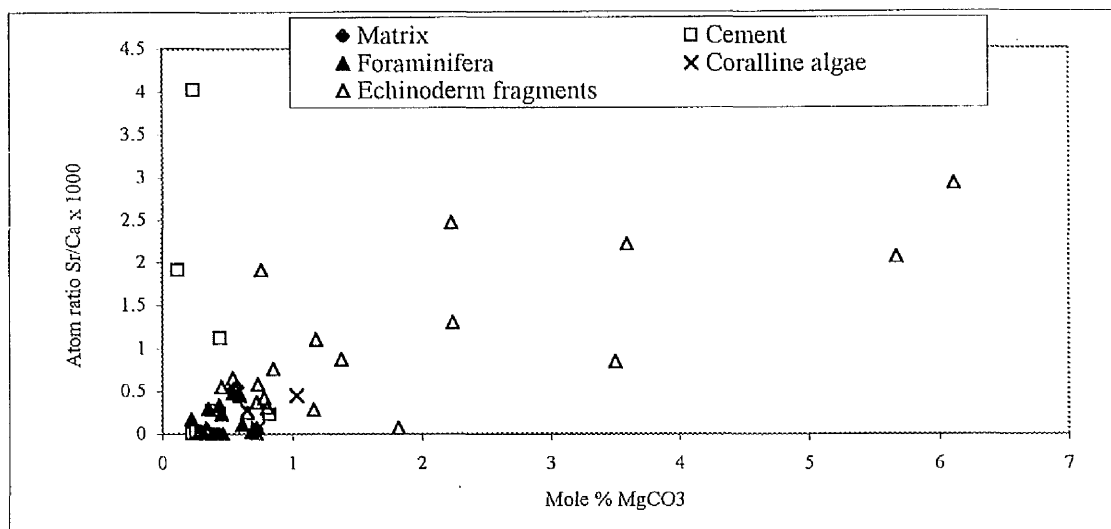
Figure (9.5) Scatter diagram of Sr/Ca x 1000 atom ratios vs MgCO₃ Mole % concentrations of the major components (coralline algae, echinoderm fragments, echinoid spines, foraminifera, matrix and cement), in the Darnah Formation (Middle to Upper Eocene)

The ratios between Sr^{++} in ppm in cement and matrix versus allochems of the Darnah Formation are illustrated in Table (9.4).

Table (9.4) Strontium content in parts per million of allochems versus cement and matrix of the Darnah Formation.

Age	Formation	Mean of Sr^{++} content (ppm)					Approximate ratios Sr^{++} (ppm)						
		E	R	F	C	Mx	C:E	Mx:E	C:R	Mx:R	C:F	Mx:F	C:Mx
Middle To Upper Eocene	Darnah	394	150	133	482	250	1.2:1	0.6:1	3.2:1	1.7:1	3.6:1	1.9:1	1.9:1

E = echindoderm fragments, R = coralline algae, F = foraminifera, C = cement, and Mx = matrix

9.3.1.3 Ar Rajmah Formation (Middle Miocene):

This Formation comprise celestite and dolomite. Where celestite is present, very high Sr/Ca ratios are expected. Dolomites have formed by replacement and the strontium carried away, and so very low Sr/Ca ratios were expected. The celestite associated with the dolomite deposits contains the strontium that was released from limestone in the formation of dolomite. The stontium-enriched solution precipitated celestite in the Lower Benghazi Member of the Ar Rajmah Formation (Benghazi Cement Quarry), where it rests on an impermeable clay layer.

Coralline algae contains a large amount of $MgCO_3$, sometimes more than 35 $MgCO_3$ mole percent. The distribution of high Mg-calcite (HMC) and low Mg-calcite (LMC) in coralline algae was observed and is illustrated in Figure 9.6.
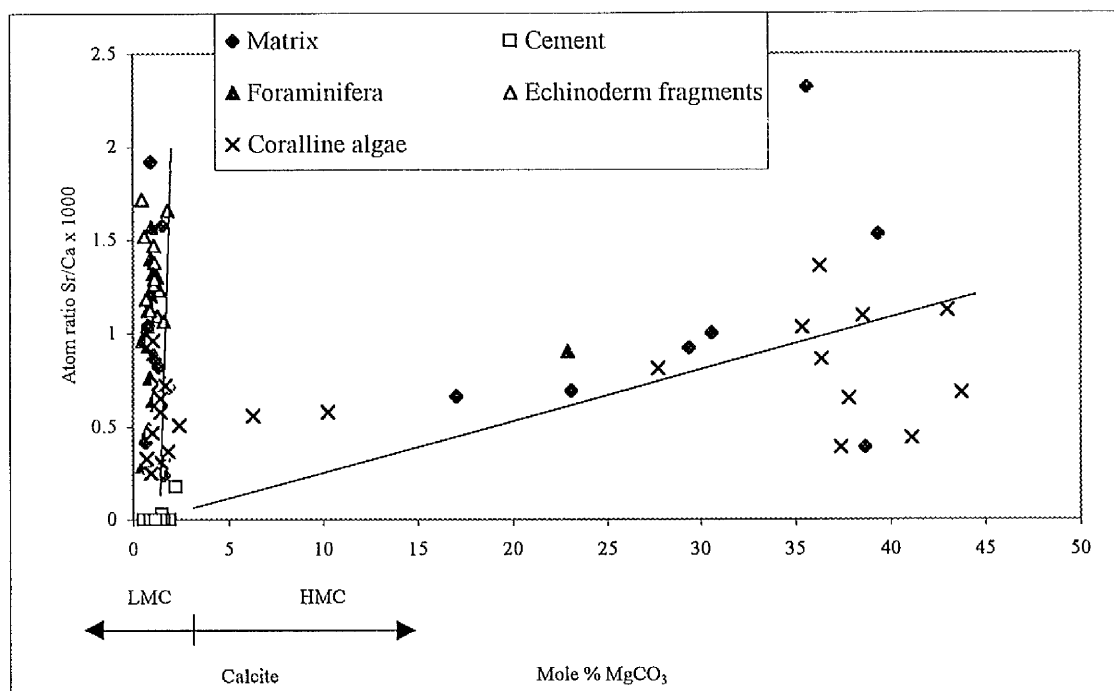
Figure (9.6) Scatter diagram of Sr/Ca x 1000 atom ratios vs Mole % $MgCO_3$ concentrations of the major components (coralline algae, echinoderm fragments, foraminifera, matrix and cement) in the Ar Rajmah Formation (Middle Miocene).

Low magnesium calcite has less than 4 mole percent $MgCO_3$ and high magnesium calcite greater than 4 mole percent (Chave *et al.*, 1964; Blatt *et al.*, 1980; Carter, 1990; Tucker, 1991). Because of their lower stability, carbonate skeletal materials with high magnesium calcite, such as coralline algae, are most likely to be replaced with metastable phases (e.g. brucite). However, carbonate skeletals have quite high $MgCO_3$ contents, reflecting sometimes the presence of dolomite and brucite minerals. The average Sr/Ca ratio of coralline algae is 0.65. Echinoderm fragments have the highest value (1.31) of Sr/Ca in the Ar Rajmah Formation. Echinoderm skeletal parts are calcitic generally, containing 0.47 to 1.8 mole percent $MgCO_3$ (Tables A.9.1 and A.9.11 – A.9.17). Echinoid spines contain higher strontium contents than other echinoderm fragments. Traverses have been taken by EPMA for two spines (Tables A.9.18 – A.9.19). However, the traverses showed near homogeneity in the strontium content (Figure 9.7)
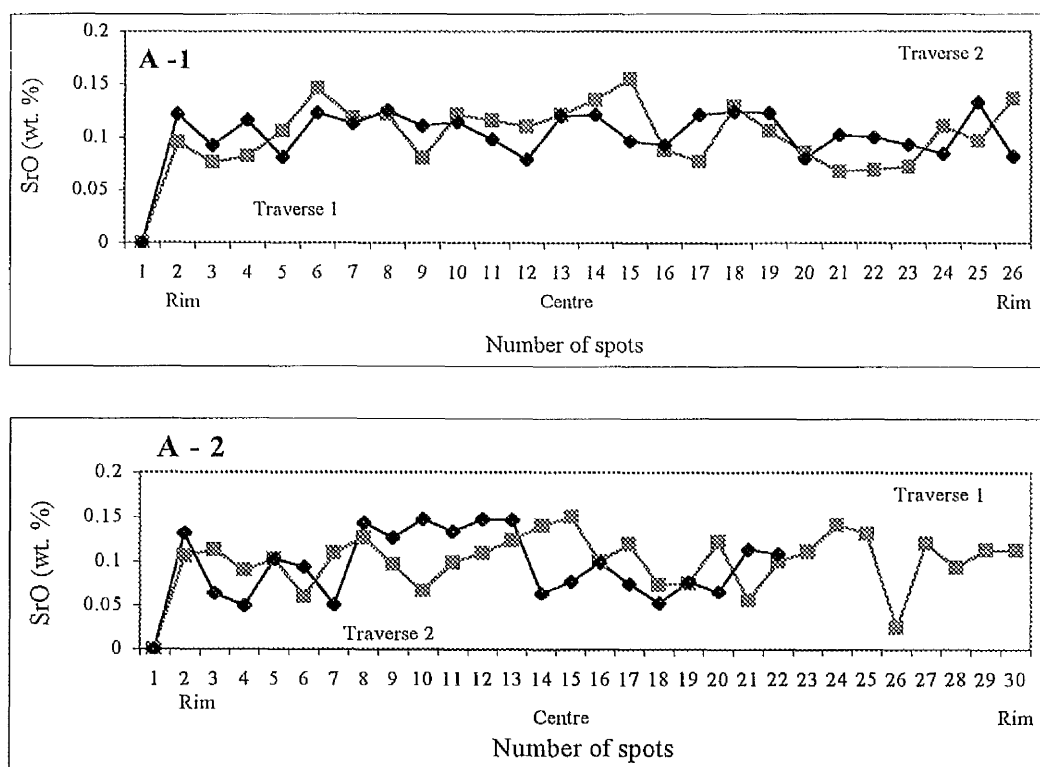
Figure (9.7) Electron microprobe traverses for echinoid spines (A-1 and A-2) in the Benghazi Member of the Ar Rajmah Formation (Middle Miocene).

Some bivalves are replaced totally by apatite and had very high absolute concentrations of strontium. The widespread distribution of strontium was confirmed by EPMA (Table A.9.16), Sr/Ca ratios in phosphate deposits have a range of values of about 2.50 to 4.46 atoms/1000 atoms. The lowest Sr/Ca value was found in the cement (0.01), and suggested that cement diagenetic processes may have occurred after the replacement of the carbonate skeletal materials. Matrix has an average ratio of Sr/Ca of about 0.78. The ratios between cement and matrix versus allochems are shown in Table (9.5).

Table (9.5) Strontium content in parts per million of allochems versus cement and matrix of the Ar Rajmah Formation.

Age	Formation	Mean of Sr^{++} content (ppm)					Approximate ratios Sr^{++} (ppm)						
		E	R	F	C	Mx	C:E	Mx:E	C:R	Mx:R	C:F	Mx:F	C:Mx
Middle Miocene	Ar Rajmah	973	363	639	24	545	0.02:1	0.6:1	0.07:1	1.5:1	0.04:1	0.9:1	0.04:1

E = echindoderm fragments, R = coralline algae, F = foraminifera, C = cement, and Mx = matrix

9.3.2 Strontium-bearing phosphate minerals and their origin:

Phosphorite is a mixed phosphate carbonate deposit. The source of phosphorous in the sea is marine organisms, particularly diatoms, in areas of high biological productivity. However, dissolution of fish debris and/or the presence of a phosphorous – bearing microbial mat on the seafloor may also be important in this regard. This suggests the formation of phosphorite deposits took place by the substitution of carbonate ions by phosphate ions in calcium carbonate in the sediments to form a replacement deposit (Cronan, 1992). Apatite formation depends on the availability of its constituent elements. Fragments of normal carbonate shell or material such as ooids, coral, forams and bivalves can be easily and quickly transformed into apatite and bacteria are responsible for this (Prevot and Lucas, 1986). The role of obligate bacteria is to liberate phosphate from the complex organic molecules in which it is trapped, allowing the previously organic phosphorous to be mineralized (Prevot and Lucas, 1986). Both BSE-SEM (Plate 9.5) and EPMA (Table A.9.16) show that apatite formed by replacing bivalve shell fragments in sample no. LB5 of the Ar Rajmah Formation. Apatite contains an average of 37.33 of P_2O_5 and 50.29 of CaO. The mineral is present as replacement of organic remains and the grain is completely cemented by calcium phosphate.
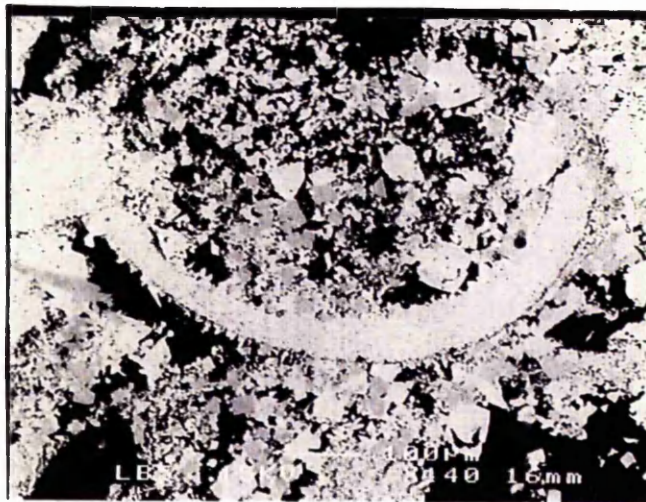
Plate (9.5) BSE-SEM image of bivalve totally replaced by apatite in the Ar Rajmah Formation (Middle Miocene).

The average amount of Sr content of apatite bivalve shells is 0.299 %. Apatite has the highest amount of strontium content in the study area (Table 9.6 and Appendix Table A.9.16).

Table (9.6) High resolution EPMA analyses of the bivalve

shell fragment in the Ar Rajmah Formation

(sample no. LB5).

Oxides (wt. %)	Sample no. LB5 (Benghazi Cement Quarry)		
P_2O_5	36.495	39.047	36.456
SO_2	1.061	0.327	1.041
TiO_2	0.002	0.016	0.016
MgO	0.149	0.140	0.154
CaO	50.470	50.305	50.105
MnO	0.000	0.000	0.004
FeO	0.185	0.321	0.195
NiO	0.000	0.007	0.000
CuO	0.000	0.000	0.002
SrO	0.226	0.161	0.299
BaO	0.000	0.000	0.034
Na_2O	1.120	1.024	1.100
K_2O	0.021	0.017	0.015
Total	89.729	91.365	89.421

9.3.3 Magnesium and strontium relationship:

The amount of strontium in the Lower Benghazi Member (Benghazi Cement Quarry) increases due to contamination of the limestone rocks with celestite minerals. The magnesium content decreases as the strontium content increases and reaches a maximum where the strontium content reaches a minimum. The high strontium – low magnesium content and low strontium – high magnesium content are related to the diagenesis, mineralogical nature of the sediments, and organic remains. The loss of Sr is connected with observed high dolomitization (e.g. at Ar Rajmah Quarry area; Table 9.7). Sr vs Mg % (Figure 9.8) show a decrease in Sr content with increasing dolomitisation and also show the Sr distribution and its relation to facies types.

Table (9.7) Strontium, magnesium, and calcium analyses (XRF) of sediments of traverses LB1 to LB5, UBA1 to UBB2MUP and RQ1L to RQ3, of the Ar Rajmah Formation

Location	Ca wt. %	Mg wt. %	Sr wt. %	Atom ratio Sr/Ca x1000 (Siegel, 1961)	Celestite & Strontianite + Facies
Benghazi Cement Quarry					
LB1	37.09	2.12	0.13	1.61	Present
LB2	39.09	0.93	0.13	1.54	+
LB3	38.66	1.27	0.12	1.45	dolomitic limestone
LB4	39.24	0.87	0.11	1.26	
LB5	37.09	2.24	0.11	1.39	
Ar Rajmah Quarry					
UBA1	28.31	10.81	0.03	0.45	
UBA2	29.98	8.97	0.03	0.42	
UBA3L	30.74	8.14	0.03	0.39	Absent
UBA3U	28.95	10.26	0.03	0.49	+
UBB1	30.6	8.83	0.02	0.34	calcitic dolomite to dolomite
UBB2L	29.36	9.97	0.03	0.45	
UBB2U	32.5	7.08	0.03	0.37	
UBB2MUP	28.5	10.57	0.04	0.60	
W. Al Faj Quarry					
RQ1L	33.16	7.97	0.07	1.00	Absent
RQ1U	39.22	0.66	0.07	0.79	+
RQ2	39.33	0.62	0.05	0.58	Partially dolomite
RQ3	39.5	0.42	0.06	0.71	
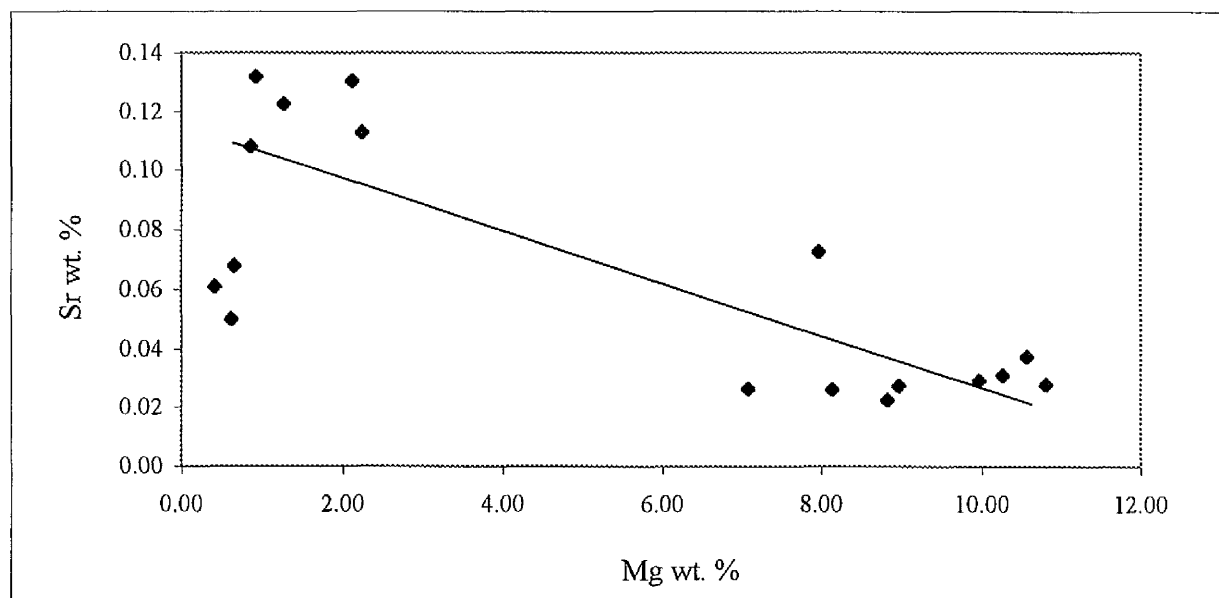
Figure (9.8) Sr (wt. %) vs Mg (wt. %) of the Benghazi Member, in the Ar Rajmah Formation (Middle Miocene).

9.4 Chemical compositions of celestite and gypsum:

To determine the bulk composition ICP-AES analyses was carried out on a solution of celestite and gypsum prepared as follows. Celestite in the Benghazi Member (Benghazi Cement Quarry) is a combination of strontium (40.41 %) and sulphate (47.89 %). Approximately 0.25g of celestite or gypsum were fused at 1000 °C with 1.25g of lithium metaborate (Johnson Matthey Spectroflux 100A) then made up to 250 ml with 2% HNO_3 in 18MΩ deionised water. Carbonate was determined with mixed known weight of HCl and known weight of celestite, the differences due to effervesce is CO_2. Analytical data for the two gypsum samples from various localities of the Wadi Qattarah Member of the Ar Rajmah Formation shows no strontium concentrations (Table 9.8).

Table (9.8) ICP-AES analyses of celestite and gypsum minerals in the Ar Rajmah Formation (Middle Miocene).

Symbol	Gypsum 1	Atomic proportion	Gypsum 2	Atomic proportion	Celestite	Atomic proportion
Sr	0.00	0.000	0.00	0.000	40.41	0.460
Al	0.06	0.002	0.08	0.003	0.01	0.000
Ca	28.24	0.700	26.98	0.670	2.60	0.060
Fe	0.01	0.000	0.04	0.001	0.02	0.000
K	0.06	0.002	0.00	0.000	0.01	0.000
Mg	0.01	0.000	0.00	0.000	0.52	0.020
Mn	0.00	0.000	0.00	0.000	0.00	0.000
Na	0.27	0.012	0.33	0.014	0.25	0.011
P	0.00	0.000	0.00	0.000	0.00	0.000
SO_4	71.45	0.744	73.30	0.763	47.89	0.499
Si	0.06	0.002	0.09	0.003	0.01	0.000
Ti	0.01	0.000	0.00	0.000	0.00	0.000
CO_3	0.00	0.000	0.00	0.000	10.10	0.168
Total	100.15		100.82		101.82	

Gypsum 1→ from Ar Rajmah village; Gypsum 2 → from Deryanah Al Abyar road-cut; and Celestite → from Benghazi Cement Quarry

9.5 Discussion:

9.5.1 Dolomite, anhydrite, celestite and replacement:

Celestite in the study area contains the strontium that was released from limestone in the formation of dolomite. Dolomite and celestite are often associated in the presence of evaporite deposits such as gypsum and/or anhydrite and the percolation within limestone by waters containing high sulphate. Such dolomites are extremely low in strontium content. Generally the composition of celestite in the Ar Rajmah Formation depends on three main factors: (1) the nature and intensity of diagenesis such as the chemical composition of interstitial waters, on their movement and renewal; (2) dolomitization; and (3) recrystallization as described by West (1964), Lloyd and Murray (1965), Jorgensen (1994), Purser (1998) and Rosell *et al.* (1998). The celestite occurs mostly as clear prismatic or tabular euhedral crystals and is coarse to extremely coarsely crystalline. Most of the replacement celestite occurs in nodular anhydrite; a complete replacement of isolated anhydrite nodules was occasionally observed. XRD analysis of the central portions of celestite nodules showed numerous relicts of anhydrite (Figure 9.9).
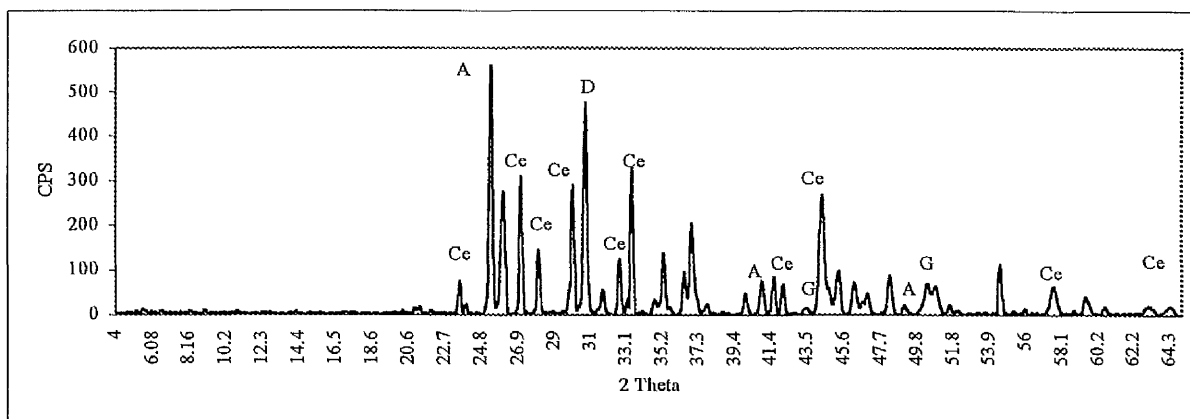
Figure (9.9) XRD pattern of sediment taken from celestite nest of the Ar Rajmah Formation (Benghazi Cement Quarry). Showing (Ce) Celestite, (A) Anhydrite, (D) Dolomite, and (G) Gypsum.

In Rhaetic limestones of southern England gypsum veins originating from the underlying Triassic strata have similarly been converted to celestite (West, 1964). Because of its low solubility in water, celestite could be also precipitated previously in association with dolomite (in high porosity), in Ar Rajmah Quarry, and after removal took place, celestite redeposited in the lower part of the Benghazi Member (Benghazi Cement Quarry). However, similar celestite nests have been observed in Ar Rajmah Quarry, but without celestite crystals. Dolomites always show very low strontium contents that are distinctly lower than those of limestones. This can be explained

by the complete metasomatic replacement of this carbonate rock. X-ray diffraction of the Ar Rajmah Formation has been carried out to obtain a more complete picture of the dolomite distribution in the different facies of this Formation. XRD traces show mainly calcite in Benghazi Cement Quarry with a small amount of dolomite (dolomitic limestone). XRD traces of sediment in Ar Rajmah Quarry show both calcite and dolomite (calcitic dolomite to dolomite). In Wadi Al Faj Quarry XRD traces of sediment show mainly calcite as the dominant mineral (Figures 9.10, 9.11 and 9.12).
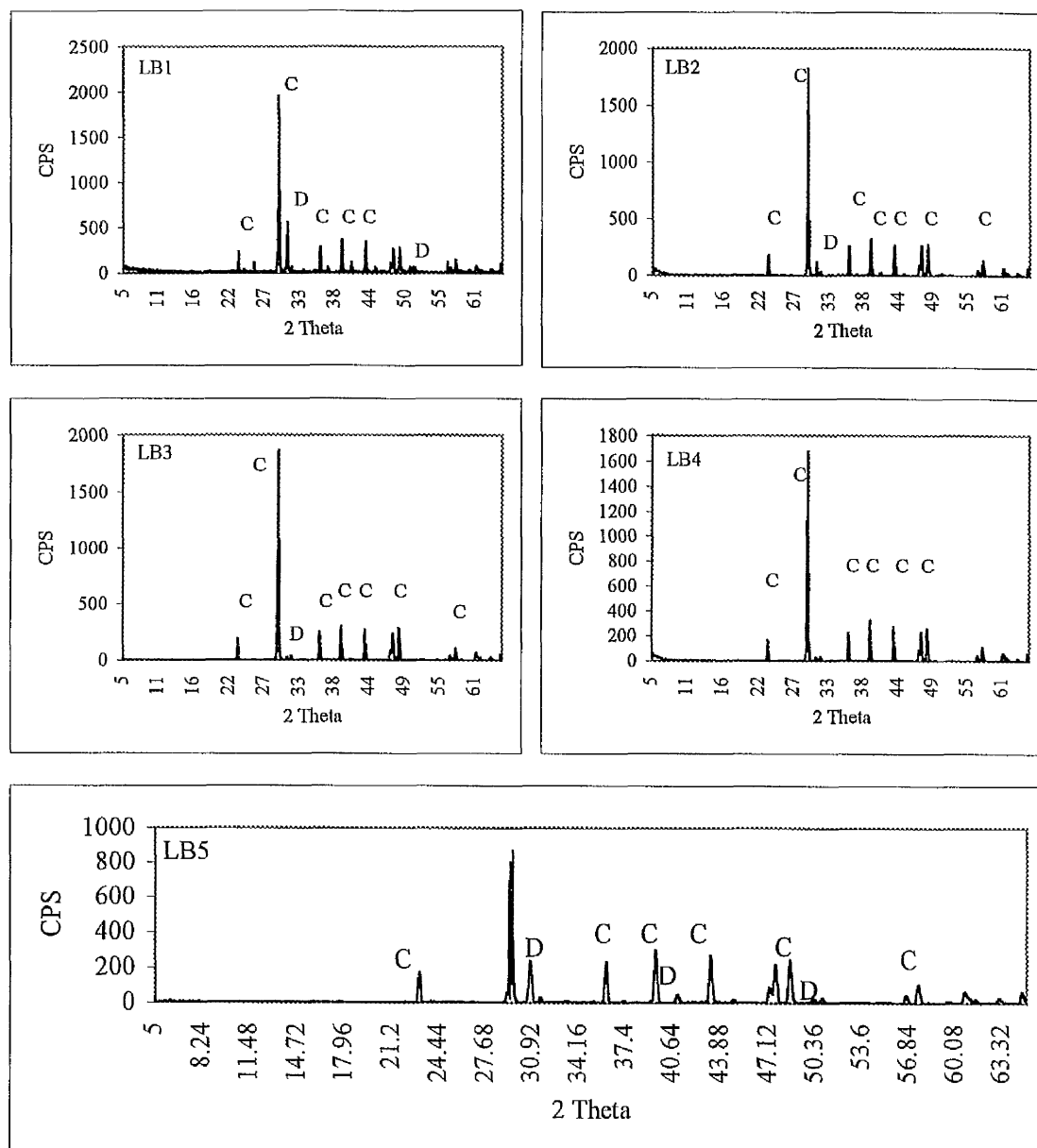
Figure (9.10) X-ray diffraction traces of bulk powdered specimens (air dried) for (C) Calcite, (D) Dolomite. Sample no. LB1, LB2, LB3, LB4, and LB5 are representates of the Benghazi cement Quarry (lower part), Benghazi Member of the Ar Rajmah Formation.
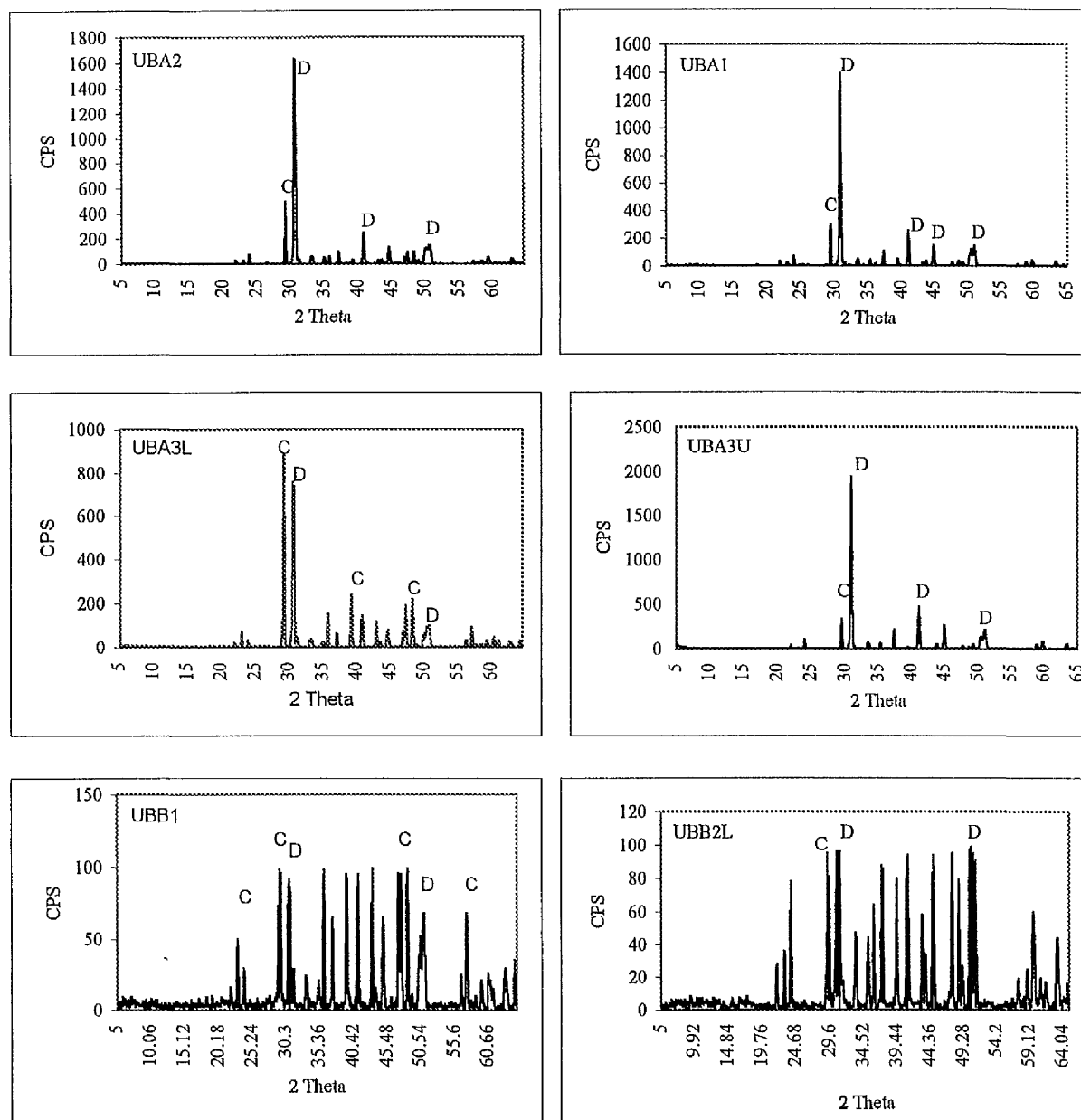
Figure (9.11) X-ray diffraction traces of bulk powdered specimens (air dried) for (D) Dolomite, (C) Calcite. Samples no. UBA1, UBA2, UBA3L, UBA3U, UBB1, and UBB3L are representatives of the Ar Rajmah Quarry (middle part), Benghazi member of the Ar Rajmah Formation.
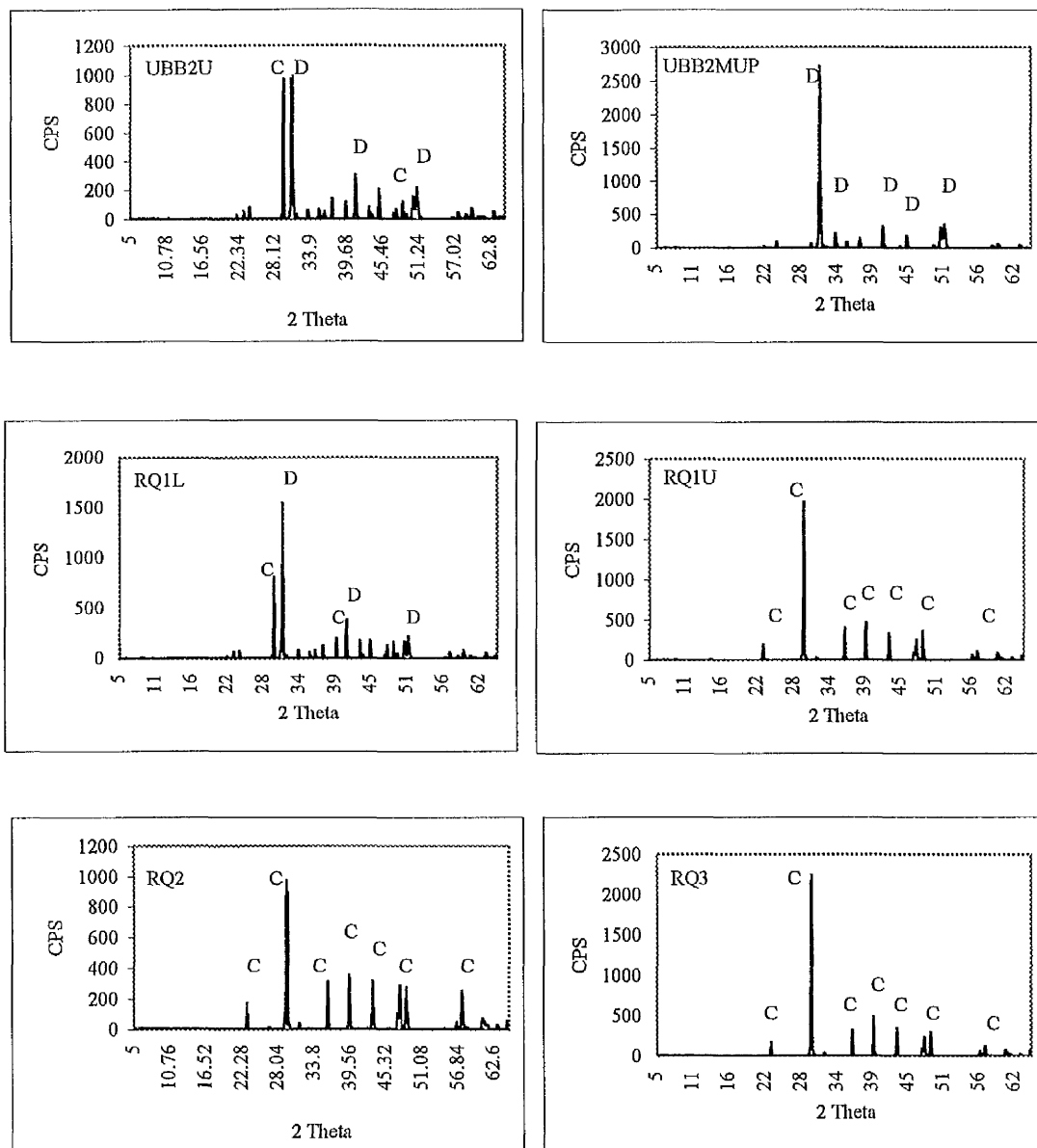
Figure (9.12) X-ray diffraction traces of bulk powdered specimens (air dried) for (D) Dolomite and (C) Calcite. Samples no. UBB2U, and UBB2MUP are representatives of the Ar Rajmah Quarry (middle part), and samples no. RQ1L, RQ1U, RQ2 and RQ3 are representatives of the Wadi Al Faj Quarry (upper part), Benghazi Member of the Ar Rajmah Formation.

9.5.2 Formation of Celestite:

Celestite has been formed from pore water enriched in both SO_4^{2-} and Sr^{+2} contents. For Sr^{+2} to precipitate as celestite, the activity product of Sr^{+2} and SO_4^{2-} must exceed the solubility product of celestite (Olaussen, 1981). A possible mechanism for concentration of strontium ions may be related to the loss of strontium by: (1) aragonite to calcite transformation (Dodd, 1967; Bathurst, 1975; Nicholas, 1978); and 2) intense dolomitization of aragonite mud. The Sr released during the replacement of aragonite (7000 —8000 ppm Sr) by dolomite (600 – 700 ppm Sr) is added to interstitial water and forms celestite (Kinsman, 1969; Garea and Braitwaite, 1996).

Nickless *et al.* (1976) concluded that sulphate is derived from anhydrite and gypsum, and suggested that the strontium became available when aragonite converted to calcite. Celestite is much less soluble than gypsum and anhydrite, and in most cases celestite is formed by the replacement of those two minerals (West, 1973). Gypsum or anhydrite both contain small amounts of strontium. More strontium can be accommodated in solid solution in anhydrite (up to 0.74 % = 7400 ppm) than in gypsum (up to 0.1 %; Dean and Tung, 1974). Therefore in the transformation from anhydrite to gypsum, Sr can be released to form celestite (de Brodtkorb, 1989). Olaussen (1981) presented three models to explain the formation of celestite in a subtidal to supratidal facies in the Wenlock of Norway: (1) early diagenetic dolomitization of aragonite mud releases Sr, which may react with the brine to form celestite; (2) Sr enrichment of the interstitial fluid produced by transformation of aragonite into calcite; and (3) late diagenetic dolomitization in which the Sr released may precipitate as late-stage authigenic celestite in geodes and veins.

In the study area, the Wadi Al Qattarah Member (upper part of Ar Rajmah Formation-Middle Miocene) consists of white, porous oolitic limestone with gypsum (Klen, 1974) (Plates 9.6 and 9.7). Fresh water infiltrating through the gypsum may have dissolved calcium sulphates of the Wadi Al Qattarah Member, resulting in the ground water being enriched with SO_4. The Benghazi Member has high porosity (secondary porosity), due to dolomitization and dissolving aragonite fossils, giving a high Sr content in the interstitial water. Here Sr reacted with SO_4 within downward percolating solutions and formed celestite in pore structures of the lower part of Facies II of the Benghazi Member (Figure 9.13; based on Olaussen, 1981). Elsewhere in Libya larger celestite deposits occur. In the Katla area, near the Bayda oil field, two main types have been found:
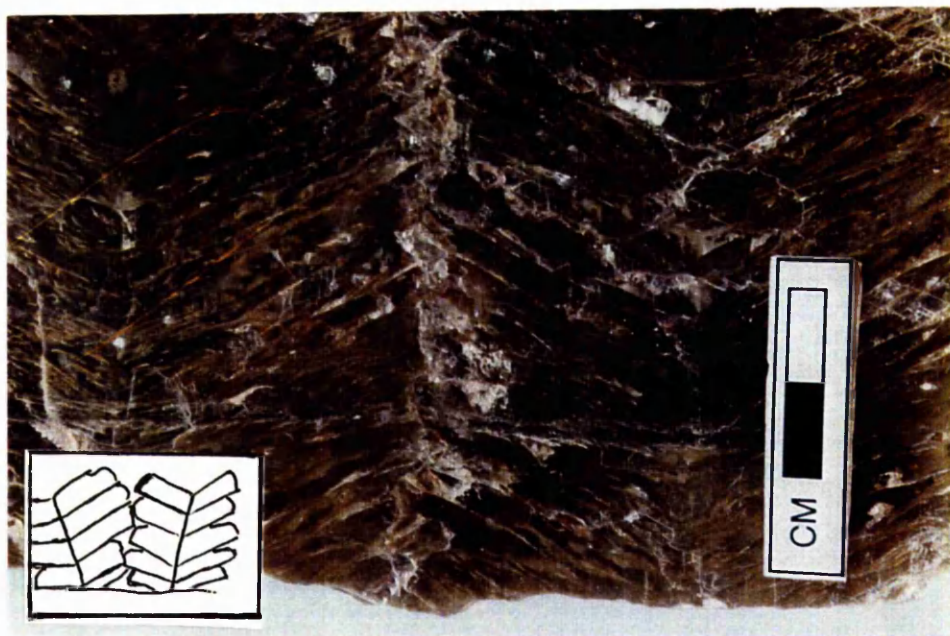
Plate (9.6) Gypsum (fibrous), yellow to brown in colour, of the Wadi Al Qattarah Member, Ar Rajmah Formation. Gypsum Quarry NE of Ar Rajmah village.

Plate (9.7) Gypsum of the Wadi Al Qattarah Member, Ar Rajmah Formation (M. Miocene). Deryanah Al Abyar road – cut.
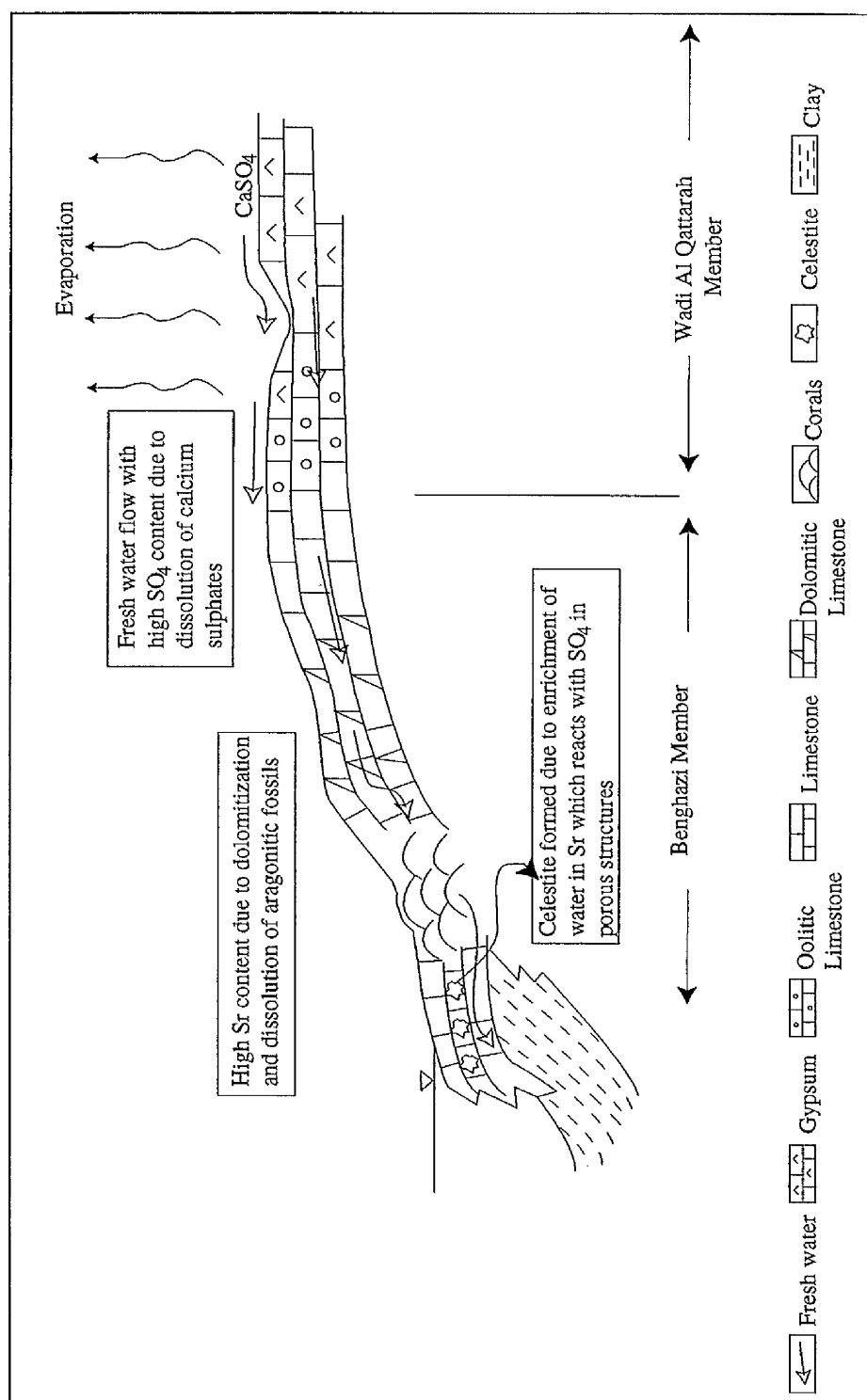
Figure (9.13) A schematic model for the formation of celestite in the lower part of the Benghazi Member of the Ar Rajmah Formation, based on Olaussen, (1981).

- Bedded celestite (stratiform deposits), white, with very high purity 98.6 % $SrSO_4$.

- Nodular celestite (nest-like), colourless, with 85 % $SrSO_4$.

The first type is higher in purity than the Iranian celestite (purity of about 96 % $SrSO_4$; Abdalla, 1991).

9.6 Conclusion:

- Celestite occurs mainly in sedimentary beds of the Ar Rajmah Formation, adjacent to evaporitic environment (anhydrite / gypsum), and near sites of intense dolomitization.

- The high strontium content of the bulk sample (LB2) examined by XRF, is due to contamination by celestite relicts.

- The various gypsum lithofacies studied in Deryanah Al Abyar road-cut and Ar Rajmah village show no elevated strontium contents.

- Significant variations in their strontium contents commonly accompany the transition from one facies to the another, influenced mainly by diagenetic processes such as aragonite transform into calcite and dolomitization.

- Where the strontium content is low, the magnesium content is correspondingly high.

- No chemical and mineralogical trend with age or fossil type appears, and the strontium content can not be used in the study area as an index of initial conditions. In general, it appears that the strontium content of limestone is not in itself a reliable guide to its original mineralogical composition. Fossils from low permeability/porosity sediments such as shale or claystones (close system) may be better indicators of the amount of strontium present originally within the fossil than in highly porous and permeable limestones (open system).

- The fossil echinoderm fragments reported in the literature are low in strontium content, but in the study area the echinoderm fragments have commonly the highest Sr/Ca values of all allochems in the Apollonia, Darnah and Ar Rajmah Formations (see text).

- The Apollonia Formation has the highest amounts of strontium content compared to the other two Formations (Darnah and Ar Rajmah) (Figure 9.14).
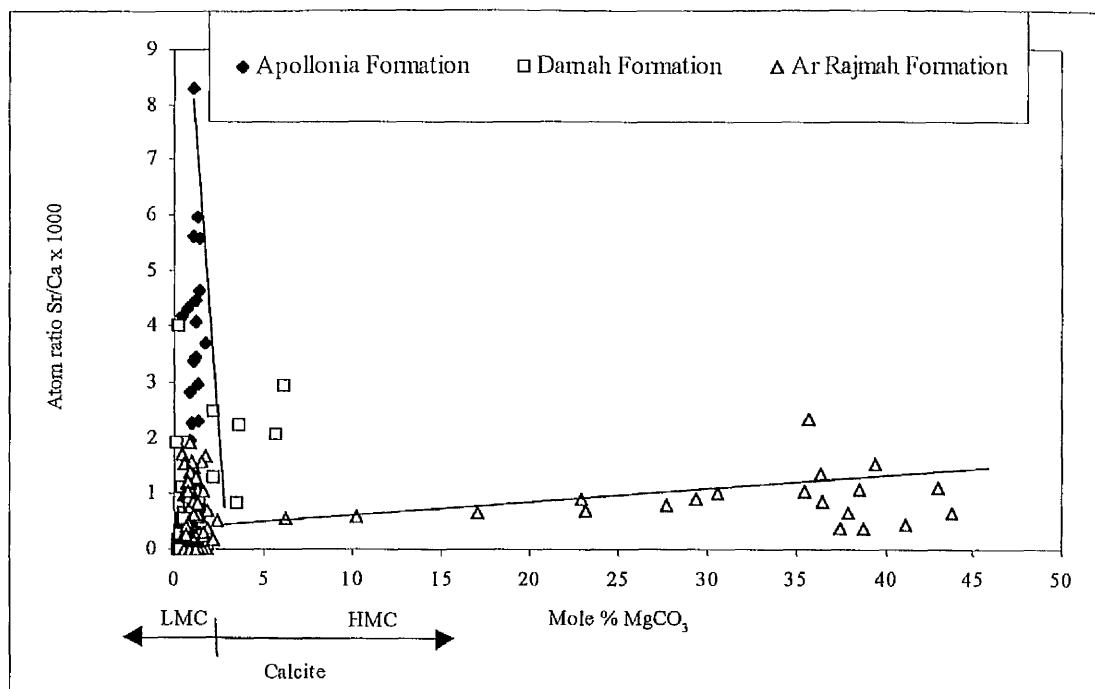
Figure (9.14) Scatter diagram of Sr/Ca x 1000 atom ratios vs Mole % MgCO₃ concentration of whole carbonate components in the Apollonia, Darnah and Ar Rajmah Formations (Lower to Middle Eocene to Middle Miocene)

- In the study area for the bulk sample analyses, any Sr/Ca values between 0.3 – 0.6 are considered to be calcitic dolomite to dolomite deposits. From 0.6 – 1.7 is limestone to dolomitic limestone, and greater than 1.7 to have a high ratio of evaporation and the presence of a Sr^{++} source such as celestite and/or strontianite.

Age	Formation	Atom ratio Sr/Ca x 1000	Environment
Middle Miocene	Ar Rajmah	0.3 – 0.6	Calcitic dolomite to dolomite
		0.6 – 1.7	Limestone to dolomitic limestone
		> 1.7	Presence of Sr source and associated with evaporitic deposits

Chapter 10

CELESTITE INDUSTRIAL POTENTIAL

10.1 Economic Factors

10.1.1 Introduction:

Celestite $SrSO_4$ is a member of the barite group of minerals and is the principal mineral source of strontium. Celestite is used in the manufacture of strontium compounds. Strontium compounds have many vital applications. Approximately 50 – 80 % of all strontium is used in carbonate form for special glasses primarily in manufacture of colour TV tubes. Strontium bearing-glasses absorbs the gamma radiation resulting from the high cathode potentials used to produce a bright picture. Strontium is used also in ferrite magnets, fireworks, flares and pyrotechnics. Celestite is used as an intermediate chemical source of strontium (Sr), and as a filler for white and coloured paints (Deer *et al.*, 1992; Ober, 1994; Chang *et al.*, 1996; Industrial Minerals, 1999).

10.1.2 Uses and applications:

Only two minerals, celestite and strontianite, are the principal source of strontium, and these minerals are found in sedimentary rocks. Apart from their main applications in television and computer screens, strontium compounds are also used in pyrotechnics, special glasses, ceramic, desensitising toothpaste, as a filler in anti-corrosive paint, fluorescent lighting, luminescent and phosphorescent paints. Celestite is also used for the production of strontium nitrate (Ober, 1994; Industrial Minerals, 1999). Quality requirements for purchase specification are greater than 95 % strontium sulphate content, with less than 1.5 % calcium sulphate and less than 2% barium sulphate (Gordon, 1995). The physical properties of strontium minerals are listed in Table (10.1) where they are compared with those of barite.

Table (10.1) Some physical properties of strontium minerals

Property	Celestite	Strontianite	Barite
Cleavage	Perfect basal and prismatic	Imperfect prismatic	Perfect basal
Colour	Colourless, white, pale blue, orange, reddish, yellow, yellow to brown	Typically colourless, or white	White, yellow brown, gray, pale green, pale blue, red and brown
Hardness	3 – 3 ½	3 ½	2 ½ - 3 ½
Specific gravity	≈ 3.98	3.72	≈ 4.5

10.1.2.1 Glass:

Strontium compounds in glass reduce the risk to the viewer from secondary X-ray emission. All colour televisions and other devices containing colour cathode-ray tubes are required by law to contain strontium in the faceplate glass of the picture tube. Strontium blocks X-rays better than barium, which was previously used. Major manufacturers of television picture tube glass incorporate about 8 % strontium oxide, by weight. Strontium compounds are also used in the production of several types of glass, for example, computer screens, iridescent and special optical glasses (Thomas, 1973; Joyce, 1992; Ober, 1994; Industrial Minerals, 1999).

10.1.2.2 Ceramic ferrite magnets:

Another large end use for strontium compounds is in the form of strontium ferrite. Ten to 15 % of $Sr\ CO_3$ mixed with iron oxide and crystal growth inhibitors are calcined to form strontium (hexa) ferrite ($SrO.6Fe_2O_3$). This has a high coercive force and is used primarily as magnetic closures for refrigerator doors. Because they have high coercive force, high thermal and electrical resistivity and are chemically inert, strontium ferrites are also used in ceramic magnets (Joyce, 1992; Ober, 1994).

10.1.2.3 Pyrotechnics:

One of the most important and continuing applications for strontium has been in pyrotechnic devices. Strontium burns with a brilliant red flame, and no other material has been found to be better in this application. A number of strontium salts (including strontium chromate, strontium chlorate, strontium carbonate, strontium oxalate, strontium nitrate and strontium sulphate), can be used in pyrotechnic applications. Strontium nitrate is used in significantly larger quantities than any other salt. Pyrotechnic devices are also used in military and warning devices, in marine distress signals and fireworks (Thomas, 1973; Joyce, 1992; Ober, 1994; Gordon, 1995; Ind. Mineral, 1999).

10.1.2.4 Paints:

Celestite has been used as a filler in rubber, plastics and in paint as a brightening and whitening agent. The addition of strontium chromate (anti-corrosive) to paint creates a coating that is resistant to corrosion. The nitrate and chloride content of strontium chromate paint pigment is very strictly controlled to prevent corrosion. Strontium sulphide has been used as the phosphorescent pigment in luminous paints (Thomas, 1973; Joyce, 1992; Ober, 1994).

10.1.2.5 Oil well drilling mud:

Ground barite is used as a weighting agent in oil and gas drilling fluid, due to its high specific gravity, to increase the density of the mud, and to kill any gas coming from the formations. The amounts added depend on well depth, size of casing and specific gravity needed in the mud, and it is not needed in all wells. Ground celestite is also used to substitute the barite as a weighting agent in oil-well drilling fluid (DeMille, 1947). The weight of the barite or celestite suppresses blowouts thus preventing well fires. The heavier mud also protects the well bore from collapse and provides more efficient transport of cuttings to the surface (Jowfe data sheets; Alatorre *et al.*, 1998).

10.1.2.6 Other uses:

Strontium hydroxide and sulphide are used as depilatories and strontium chloride is consumed in de-sensitising toothpaste. Small amounts of strontium are added to molten aluminium to improve the castability of the metal, making it more suitable for casting items that have been traditionally made from steel. The addition of strontium to the melt improves the machinability of the casting (Joyce, 1992; Ober, 1994; Gordon, 1995). Ground strontianite is used for desulphurising and dephosphorising steel, acting as a flux without damage to the furnace lining. It increases fluidity of the slag without reducing its basic character (DeMille, 1947).

10.1.3 Prices:

The price of celestite, finely powdered, imported from Mexico, FOB US border (94 % of $SrSO_4$) is about \$ 55 – 65 per ton; from Spain FOB Motril (94 %), \$ 50 – 60; from Turkey, FOB Iskenderum (96 %), \$ 65 – 80; from Iran, FOB European port, \$ 60 – 70 (Ind. Mineral, 1999).

10.1.4 Market:

The prices of strontium carbonate and sulphate drop with increasing demand and over capacity. In glass and ceramic ferrite magnet applications (Figure10.1) have expected growth rates between 3 – 5 %. In faceplate glass (TV_S and computers) the expected demand is positive (Industrial Minerals, 1999).

10.1.5 Specification:

Commercial celestite normally contains a minimum of 95 percent $SrSO_4$, not more than about 2.0 percent each of barium ($BaSO_4$) and silica (SiO_2) and approximately 0.5 percent each

of calcium carbonate ($CaCO_3$) and iron oxide (Fe_2O_3). Celestite containing 97 percent $SrSO_4$ is used as a white extender in paint (Thomas, 1973; Gordon, 1995).
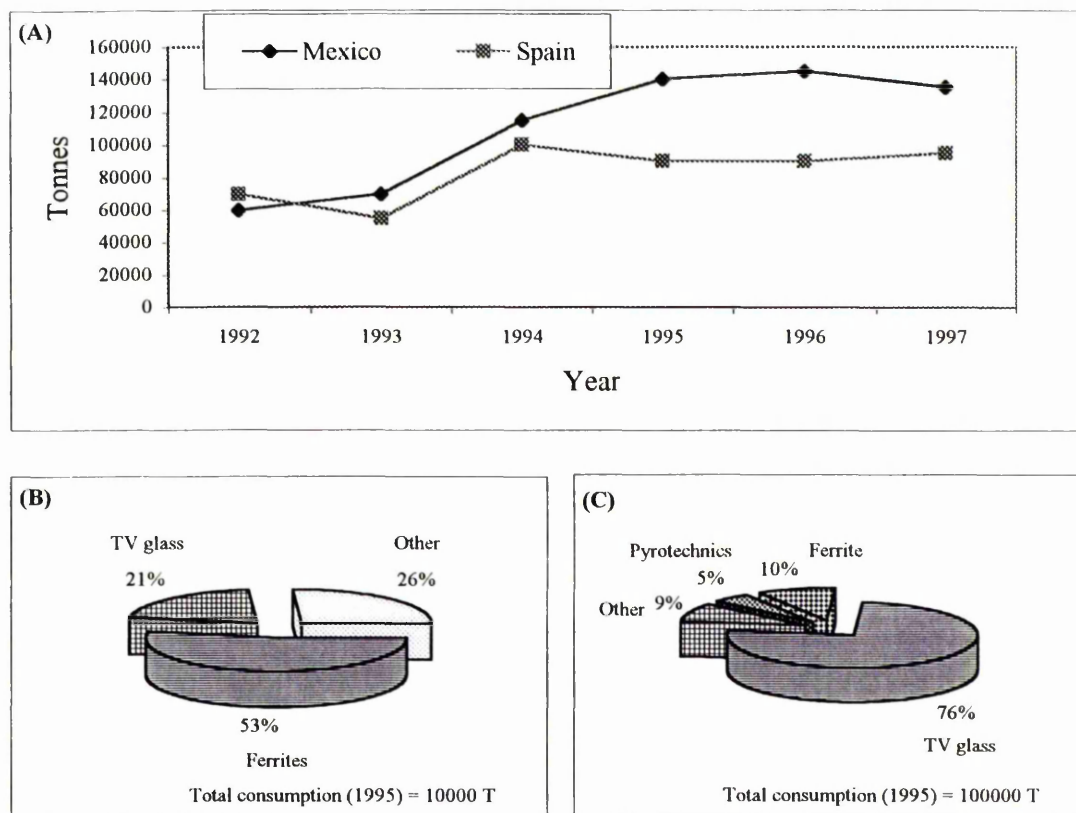
Figure (10.1) A- Celestite production in Mexico and Spain (the largest deposits and high grade; B- European consumption of the strontium compounds; C- USA consumption of the strontium compounds (Source: Stockwell *et al.* (1998), British Geological Survey, World Mineral Statistics 1992-1996).

10.1.6 Celestite in oil-well drilling fluid:

Strontium compounds are used in fluorescent lighting, luminescent and phosphorescent paints (Industrial Minerals, 1999). Because of this, the spectrofluorimetry experiment has been done to make sure if celestite has fluorescence or not. If celestite fluoresces, it can not be used in drilling fluid as a weighting agent near the zone of production, because it will interfere with the fluorescence of crude oil. Mud loggers (with no experience in the field) will not be able to differentiate between the crude oil and the celestite fluorescence under the U.V. box.

To investigate the fluorescence of celestite, its spectrum was measured as follows. A powder of celestite (0.5g) was heated to boiling in 20 ml of HCl. The same procedure was

repeated in water and after cooling the contents of the beaker were filtered through a No. 42 filter paper and the residue dried at 50 °C overnight. The filter papers were reweighed and the percentages of the residue were calculated as below:

The residue in water = 1.43 – 0.96 = 0.47g: solubility = 0.03 in 20 ml

The residue in acid (HCl) = 1.32 – 0.93 = 0.39g: solubility = 0.11 in 20 ml

Therefore, the celestite is slightly soluble in hot concentrated acid (HCl) and is less soluble in water. The HCl filtrate was more yellow in colour than water and these two solutions were used in the spectrofluorimetry experiment:

0.03g = 20 ml (for water)

0.03g/20ml = 0.002g per ml

Celestite mol. wt. = 183.68

mols = mass/mol. wt. = 0.002/183.68 = 1.09×10^{-5} mols/ml

$$= (1.09 \times 10^{-5}) \times 1000$$

Therefore the concentration = 0.011 mol/litre, and

For HCl;

0.11g = 20 ml

0.11g/20ml = 0.006g per ml

mols = mass/mol. wt. = 0.006/183.68 = 3.27×10^{-5} mols/ml

$$= (3.27 \times 10^{-5}) \times 1000$$

Therefore the concentration = 0.033 mol/litre

Beer-Lambert Law:

This empirical law is valid except when very high intensities of radiation are employed and a significant proportion of the molecules in a given region are in the excited state rather than the ground state at any one time. From the Beer Lambert Law:

$$A = \varepsilon CL \qquad\qquad \text{equation-1}$$

Where A = absorbance, C = Concentration of absorber, L = path length of radiation through the sample = 1 cm and ε = is a constant of proportionality known as the extinction coefficient.

$$\varepsilon = A/C \qquad\qquad \text{equation-2}$$

Figure (10.2) shows the events occurring during the excitation of the sample with a pulsed xenon source in the fluorescence mode. The fluorescence spectra (Figure 10.2B) of the celestite in solution with HCl, showed maximum emission at max. $\lambda_{ex.} = 348$ nm, max. $\lambda_{em.}$ At about 425 nm (blue in colour), the extinction coefficient is calculated (equation-2) from the emission spectra as follows:

A = 95, C = 0.033 mol/litre

Therefore, $\varepsilon = 2879$

The fluorescence spectrum (Figure 10.2C) of the celestite in solution with water, showed maximum emission at $\lambda_{ex.} = 348$ nm, max. $\lambda_{em.}$ at about 438 nm (blue in colour) and extinction coefficient $(\varepsilon) = 7917$.

The two sharp peaks in Figure 10.2B and 10.2C at about max. $\lambda_{em.} = 696$ nm are scattering bands, and have nothing to do with the actual sample. The higher the ε value the more stable excited state, where excited state is defined as follows: stable excited state produced by light absorption in light sensitive substances; unstable excited state, which returns to the initial condition with development of heat. A third case exists namely, an unstable excited state, which returns to the initial state with the emission of radiation. The return to the initial state can take place quickly or slowly. If the return is so rapid that when the illumination ceases the luminescence stops immediately, the process is called fluorescence. If the return to the initial state occurs after a time the process is called phosphorescence (Przibram and Caffyn, 1956).

The crude oil sample was dissolved in chloroform, excited at $\lambda_{ex.} = 350$ nm and the maximum emission at max. $\lambda_{em.} = 410$ nm. Therefore, the celestite in solution showed fluorescence as well as the crude oil, while the celestite in powder form showed no fluorescence under the U.V box (where $\lambda = 365$ nm, this long wavelength is used in the Mud Logging Unit during drilling operation). The references (water + HCl) were carried out (the background) and shows zero fluorescence. Celestite of the Ar Rajmah Formation (88.3% $SrSO_4$) is unsuitable in drilling muds for the petroleum industry as a weighting agent at high depth, with high temperatures and pressures. It could be used at shallower depths, where oil is not expected. Celestite of the Ar Rajmah Formation is undesireble for industrial applications, due to its fluorescence, as well as the presence of some impurities such as anhydrite, gypsum, calcite and dolomite.
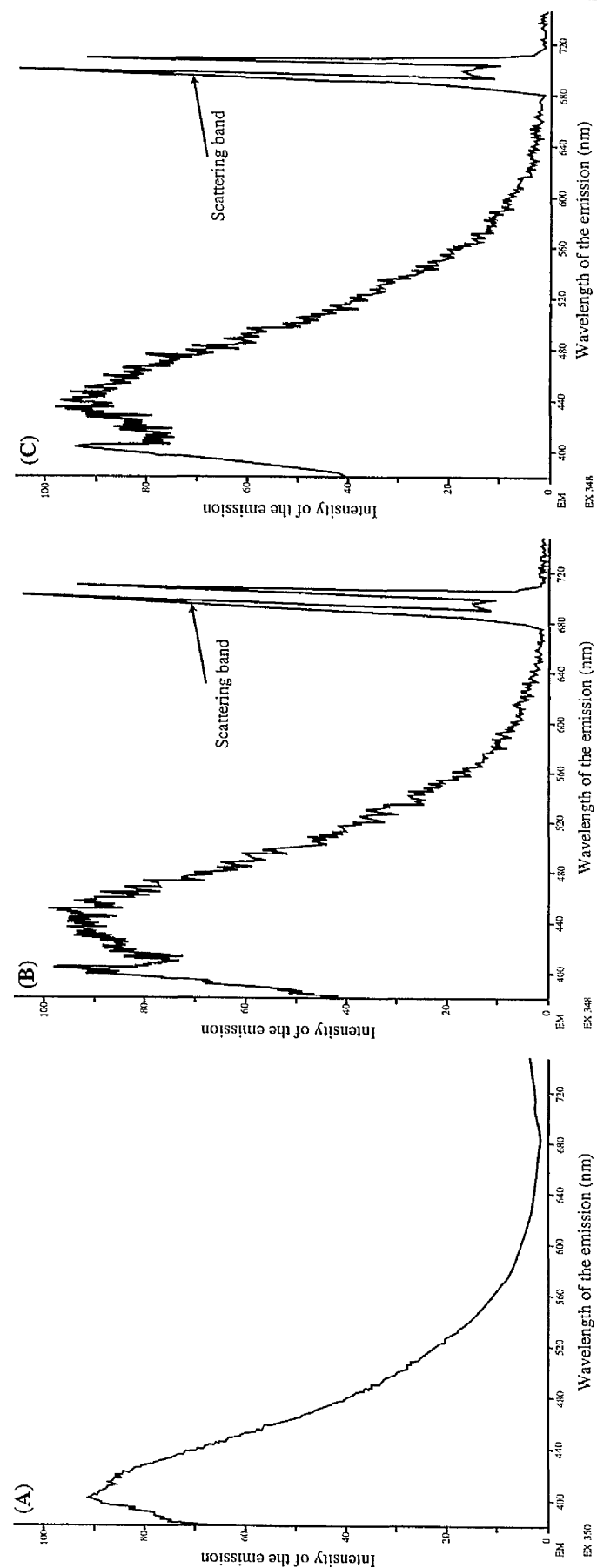
Figure (10.2) Schematic diagram of events occurring during the excitation of a celestite sample with a pulsed xenon source in the fluorescence mode: A- emission spectra of crude oil sample with chloroform; B- emission spectra of celestite sample in solution with acid (HCl); C- emission spectra of celestite sample in solution with water.

Chapter 11

CONCLUSION AND RECOMMENDATIONS

11.1 Introduction:

The study area comprises sedimentary carbonate rocks (Eocene to Miocene in age), represented by the Apollonia, Darnah, Al Bayda, Al Abraq, Al Faidiyah and Ar Rajmah Formations. In this chapter, the conclusions are divided into three main parts: limestone, clay and celestite.

11.2 Limestone:

- The Formations in the study area vary from very high purity limestones to impure limestones (Table 11.1);

Table (11.1) Classification of limestones in the study area according to purity.

Age →	Formations (Eocene to Miocene)					
Purity of limestone ↓	Apollonia	Darnah	Al Bayda	Al Abraq	Al Faidiyah	Ar Rajmah
Very high purity (VHP)	✓	✓	✓	-	✓	✓
High purity (HP)	✓	-	✓	-	-	✓
Medium purity (MP)	-	-	-	✓	-	✓
Low purity (LP)	-	-	✓	✓	✓*	✓
Impure (I)	-	-	✓	✓	✓*	✓

* Limestone in Deryanah Al Abyar road-cut and Umm Ar Razam Quarry

- In addition to calcite, limestone in the study area contains other carbonates such as dolomite, and non-carbonates such as quartz, smectite, kaolinite and glauconite minerals.
- Middle Miocene limestones are highly porous, due to dolomitization. However, the individual voids correspond to primary porosity, and to secondary porosity created by dissolution of aragonitic bioclasts.
- The presence of high strontium content (8042 ppm) in the Benghazi Member of the Ar Rajmah Formation reflects the occurrence of celestite.
- Most carbonate rocks in the study area are either limestones with less than 3 % MgO or dolomites with >19% MgO. Dolomites are present in most of the formations of the study area, but in different amounts.
- Dolomite is common in the Benghazi Member of the Ar Rajmah Formation, in varying amounts, between 10 – 80 %.
- Dolomite in the Benghazi Member is characterised by the presence of limpid euhedral crystals. It is not stoichiometric and has excess Ca^{2+} with average Ca:Mg ratios of 54:45. Ar Rajmah Quarry (middle part) is less rich in Ca^{2+} ions than the

lower and upper parts with an average Ca:Mg ratio of 52:48. Dolomite crystals (non-ferroan) are low in both Fe and Mn contents. The centre of the crystal has Mg:Ca:Fe ratios ranging from 52:48:0 to 51:49:0 and the rim has Mg:Ca:Fe of 45:54:0.1.

- Deposit homogeneity is important. Patches with different properties must either be discarded or blended to form a uniform product e.g. the mining in the Apollonia Formation for a very high purity limestone will be difficult and uneconomic due to the presence of chert nodules.

- > 65% of the total limestone production in Al Jabal Al Akhdar area is used in construction, cement, road and concrete aggregates.

- Due to heterogeneity, the Benghazi Member can be mined and used for different purposes. For example in Benghazi Cement Quarry it is used for cement manufacture, and at Ar Rajmah and Wadi Al Faj Quarries it is used in construction.

- The possible applications of limestone in the study area are summarised in Table 11.2 below;

Table (11.2) Possible uses of limestones in the study area

Age	Formation	Member/ (sample no.)	Location	Purity	Possible applications
M. to U. Eocene	Darnah	-	Shahhat Susah road-cut	VHP	Cement, animal feedstuffs, agriculture, construction as aggregates, glass, iron and steel, FGD, weighting material in drilling fluids
			Qasar Libya Quarry		
L. Oligocene	Al Bayda	Algal Limestone (Algal Lst L)	Shahhat Susah road-cut	VHP	Cement, animal feedstuffs, agriculture, construction as aggregates, glass, iron and steel, FGD, weighting material in drilling fluids
U. Oligocene to L. Miocene	Al Faidiyah	Faidia Limestone*	Al Fatayah Cement Quarry	VHP	Cement, animal feedstuffs, agriculture, construction as aggregates, glass, iron and steel, FGD, weighting material in drilling fluids, filler and pigment, paint, paper, carpet backing, plastic, soda ash
M. Miocene	Ar Rajmah	Benghazi Limestone	Wadi Al Faj Quarry	VHP	Construction (aggregates), glass, agriculture, animal feedstuffs, FGD, plaster, mortar, cement, weighting material in drilling fluid
			Ar Rajmah Quarry	I	Construction (aggregates), glass; mix with pure limestone (upper part) to manufacture sheet glass (flat type)
			Benghazi Cement Quarry	LP to HP	Cement, animal feedstuffs, agriculture, glass

* The highest grade and quality, VHP; very high purity limestone, HP; high purity limestone and I; Impure

11.3 Clay deposits:

Clay was found in the Faidia Clay Member of the Al Faidiyah Formation, at Umm Ar Razam Quarry and Al Fatayah Cement Quarry. The Faidia Clay Member of the Al Faidiyah Formation is summarised as follow;

- Faidia Clay is wet clay, consisting of dark green clay becoming yellowish green to brown when weathered. It forms a very plastic sticky mass with soap like textures.

- The Faidia Clay contains montmorillonite (the highest constituent), kaolinite and chlorite. It contains a variable proportion of other non-clay minerals such as fine quartz grains, calcite, ilmenite, dolomite, gypsum, K-feldspar, anatase and hematite. These impurities affect the rheological and physical properties and detract from the commercial performance of the Faidia Clay.

- The Faidia Clay has relatively high amounts of Fe_2O_3 and CaO, whereas the SiO_2, Al_2O_3, MgO and Na_2O are low compared with other commercial bentonites (Table 11.3).

Table (11.3) Comparison of chemical and physical properties of Faidia Clay Member (Umm Ar Razam and Al Fatayah Cement Quarries) and other commercial bentonites

Type of test		Umm Ar Razam		Al Fatayah		Wyoming Bentonite
Chemical Analysis	SiO_2	23.55		23.8		54.63
	Al_2O_3	10.2		10.17		16.71
	Fe_2O_3	4.9		5.5		3.59
	CaO	31.7		30.78		1.36
	MgO	1.13		1.51		2.13
	Na_2O	0.3		0.56		2.03
	K_2O	0.63		0.59		0.53
Loss at 1000 °C		18.98		20.1		17.64
Quality of Clay	Swelling test (ml)	0		0		15
Grade of Clay	C.E.C (meqs/100 gms)	57		50		70
Surface area m^2/g		Crude	< 2 μm - > 0.5 μm	Crude	< 2 μm - > 0.5 μm	800
		385	525	420	524	
		Smectite %		Smectite %		-
		48	65.6	52.5	65.5	

- The Faidia Clay is non-swelling clay, the swelling volume of crude samples and sample after treatment with addition of up to 6 % of Na_2CO_3, did not achieve the necessary specifications compared with standard bentonites.

- The Faidia Clay is unsuitable for drilling mud in oil field activities; its physical and chemical properties are very poor.

- Possible future uses are in foundry-moulding sands, floor decorations, bleaching and animal feed industries.

- Huge reserves are available for more suitable types of industries, where bentonite enrichment is not a critical parameter (use in low value applications).

11.4 Celestite deposits:

- The 288 specimens analysed in this study are sufficient to indicate the range of the strontium content of carbonate rocks (in Sr/Ca x 1000 atom ratio); matrix (0.020-4.040), cement (0.000-2.877) and fossils (0.000-5.969).

-- Most Middle Miocene rocks are highly porous, relating to the presence of dolomite. However, the individual voids generally correspond to primary and to secondary porosities created by dissolution of aragonitic bioclasts. As part of this process, Sr is released and reacts with pore water SO_4; the resulting product is celestite.

- The most likely source of the large Sr concentration in the Ar Rajmah Formation is due to dolomitisation of the limestone (Ar Rajmah Quarry), releasing Sr into solution.

- The presence of anhydrite relicts in the celestite and the geodic nature of the celestite nodules of the Ar Rajmah Formation indicate that the celestite is of secondary origin.

- Celestite is mainly precipitated in areas of intense dolomitisation and is commonly associated with evaporites such as gypsum and anhydrite.

- The high strontium content of the bulk sample (LB2; 8042 ppm), in the Ar Rajmah Formation, at Benghazi Cement Quarry, is due to contamination by celestite relicts.

- According to the literature (Carter, 1990; Blatt *et al.*, 1980; Milliman, 1974; Odum, 1957), the fossil echinoderm fragments are characteristically low in strontium content, but in the study area it was found that the echinoderm fragments commonly have the highest Sr/Ca values in the Apollonia, Darnah and Ar Rajmah Formations.

- Celestite (88 % of $SrSO_4$) of the Al Jabal Akhdar area is unsuitable for industrial applications due to the presence of impurities such as relicts of anhydrite, gypsum, calcite and dolomite.

- In the study area calcitic dolomite to dolomite samples have Sr/Ca ratios between 0.3 – 0.6, limestone to dolomitic limestone have Sr/Ca ratios between 0.6 – 1.7 and Sr/Ca ratios > 1.7 are associated with evaporitic deposits and strontium source deposits.

Age	Formation	Atom ratio Sr/Ca x 1000	Environment
Middle Miocene	Ar Rajmah	0.3 – 0.6	Calcitic dolomite to dolomite
		0.6 – 1.7	Limestone to dolomitic limestone
		> 1.7	Presence of Sr source and associated with evaporitic deposits

11.5 Recommendations:

- It is recommended that further research be carried out of each industrial end-use to obtain a higher quality end product.

- For aggregate evaluation the determination of mechanical properties should also be involved in addition to determination of mineralogy, chemistry and petrography. Aggregate should be free of clay and organic matter, which would have an adverse effect on concrete durability.

- If a high quality product is required a considerable amount of drilling and core analysis will be necessary.

- It is essential firstly that the properties of the material, before and after processing, match the specification for intended use and secondly that there are adequate reserves to meet the expected demand

- Feasibility studies should be made to any commercial source of raw material to prove its commercial viability.

- Rehabilitation is necessary; e.g. limestone in the Al Jabal Akhdar area has been worked for many years, initially for construction (building-stone and road-stone). The numbers of these quarries are increasing quickly and this will influence the natural processes of weathering and erosion. There is a need to balance the demand for extraction of limestone with the need to protect and conserve the natural beauty of the countryside through land use planning policies.

- From electron microprobe data, it was found that echinoderm fragments contained higher strontium contents than other fossils. This contrasts with the results of other workers. It is recommended that further work is carried out to investigate the relationship between high strontium contents and echinoderm fragments. One

reason may be due to the fact that echinoderm fragments have high porosity which has later become filled by carbonate mud, with a high strontium content.

REFERENCES

References

Abdalla, S. (1991) *Celestite in Maradah area* (unpublished). National Company for Oil Drilling Chemical and Equipments (Jowfe), Benghazi, Libya, 13pp.

Abdalla, S. and Mahmoud, A. (1991) *A final report on Umm Ar Razam bentonite project.* National Company for Drilling Chemicals and Equipments (Jowfe), National Oil Corporation, 60pp.

Adams, A. E., MacKenzie, W. S. and Guilford, C. (1984) *Atlas of sedimentary rocks under the microscope.* John Wiley and Sons, Inc., New York, 104pp.

Alami, M. R. and Salem, G. (1981) *Bentonitic clay of Al Jabal Al Akhdar.* Petrol. Res. Cent. (PRC), Tripoli, 33pp.

Alatorre, A. E., Barker, J. M. and Santini, K. (1998) Barytes-Mexican producers and Gulf markets. *Ind. Mineral,* **370**, 37-49.

Almond, D. C. (1986) Geological evaluation of the Afro-Arabian Dome. *Tectonophysics,* **131**, 301-332.

Anand, R. R. and Gilkes, R. J. (1984) Weathering of ilmenite in a lateritic pallid. *Clays and Clay Minerals,* **32**, 363-374.

Armstrong, A. K., Shavely, P. D. and Addicot, W. O. (1980) Porosity evaluation of Upper Miocene reefs, Almeria Province, southern Spain. *Am. Assoc. Petroleum Geologists Bull.,* **64**, 188-208.

Babu, D. S. S., Thomas, K. A., Mohan, P. N. and Damodaran, A. D. (1994) Alteration of ilmenite in the Manavalakurichi deposit, India. *Clays and Clay Minerals,* **42**, 567-571.

Barlow, S. G., Manning, D. A. C. and Hill, P. I. (1997) Influence of time and temperature on reactions and transformations of chlinochlore as a ceramic clay

mineral. *British Ceramic Transactions, The Institute of Materials*, **96**, No. 5, 195-198.

Barltrop J. A. and Coyle J. D. (1978) *Principles of photochemistry*. John Wiley and Sons, Chichester, 213pp.

Barr, F. T. (1968b) Upper Cretaceous stratigraphy of the Jabal Al Akhdar, northern Cyrenaica. In: *Geology and archaeology of northern Cyrenaica, Libya* (ed F. T. Barr). *Petrol. Explor. Soc. Libya*, 10th Annual Field Conf., 131-147.

Barr, F. T. (1972) Cretaceous stratigraphy and planktonic foraminifera of Libya. *Palaeont.*, **18**, 1-46.

Barr, F. T. and Berggen, W. A. (1981) Lower Tertiaty biostratigraphy and tectonics of northeastern Libya. In: *The Geology of Libya* (eds M. J. Salem and M. T. Busrewil). *Univ. Al Fateh.*, Tripoli, 163-191.

Barr, F. T. and Berggren, W. A. (1980) Lower Tertiary biostratigraphy and tectonics of northeastern Libya. In: *The Geology of Libya*. (eds M. J. Salem and M. T. Busrewil), Academic Press, London, **I**, 162-192.

Barr, F. T. and Hammuda, O. S. (1971) Biostratigraphy and planktonic zonation of the Upper Cretaceous Al Athrun limestone and Hilal shale, NE Libya. In: *Microfossils*. Proc. 2nd Int. Conf. Plankt. (ed A. Farinacci), 27-40.

Barr, F. T. and Weegar, A. A. (1972) *Stratigraphic nomenclature of the Sirte Basin, Libya*. Petroleum Exploration Society of Libya. Grafiche Trevisan Castle Franco, Italy, 179pp.

Bathurst, R. G. C. (1975) *Carbonate sediments and their diagenesis*. Developments in sedimentology 12. (Second edition), Elsevier Publishing Co., Amsterdam, 658pp.

Bathurst, R. G. C. (1975) *Developments in sedimentology (12)*. Carbonate sediments and their diagenesis. Second Edition, Elsevier, 658pp.

Baxter, P. (1997) European markets for US bentonites. *Ind. Minerals*, no. 362, 43-49.

Benzabanta, Vazgen, Scofield, M., Tony, G. and King, B. (1986) *Drilling mud course*. Bright star University, Brigha, Libya, 350pp.

Berner, R. A. (1971) Principles of chemical sedimentology. New York, 159-191.

Blatt, H., Middleton, G. and Murray, R. (1980) *Origin of sedimentary rocks*. Second Edition, New Jersey, 782pp.

Bloodworth, A. J., Highley, D. E. and Mitchell, (1993) *Kaolin*. Industrial minerals laboratory manual, British Geological Survey. Technical report WG/93/1, 76pp.

Blyth, F. G. H. and deFreitas, M. H. (1984) *A geology for engineers*. Seventh Edition, London, 325pp.

Brasier, M. D. (1980) *Microfossils*. George Allen and Unwin, London, 193pp.

Brindley, G. W. and Chang, T. S. (1974) Development of long basal spacings in chlorites by thermal treatment. *Am. Mineral.*, **59**, 152-158.

Brindley, G. W. (1966) Ethylene glycol and glycerol complexes of smectites and vermiculites. *Clay Miner.*, **6**, 237-259.

Brown, G. and Brindley, G. W. (1980) Procedures for clay mineral identification. In: *Crystal structures of clay minerals and their X-ray identification* (eds G. W. Brindley and Brown G.). Mineralogical Society monograph no. 5, London , 305-359.

Brown, M. E. (1988) *Introduction to thermal analysis techniques and applications*. Chapman and Hall, London, 211pp.

Brown, S. E., Fairhead, J. D. and Mohamed, I. I. (1985) Gravity study of the White Nile Rift, Sudan and its regional tectonic setting. *Tectonophysics*, **113**, 123-127.

Brownlow, A. H. (1996) *Geochemistry*. Second edition, Prentice Hall, Inc., 580pp.

Buchbinder, B. (1979) Facies and environments of Miocene reef limestones. *Jour. Sed. Petrology*, **49**, 1323-1344.

Buchbinder, B. (1996) Miocene carbonates of the eastern Mediterranean, the Red Sea and the Mesopotamian Basin: Geodynamic and eustatic controls. In: *Models for carbonate stratigraphy from Miocene reef complexes of Mediterranean regions* (eds K. F. Evan, C. W. William and M. R. Jean), *S.E.P.M.*, 89-96.

Burollet, P. F. (1960) *Lexique stratigraphique international 4*. Afrique Cong. Geol. Int. Comm. De Stratigraphic, 62pp.

Cambell, A. S. (1973) Anatase and rutile determination in soil clays. *Clay Miner.*, **10**, 57-58.

Carozzi, A. V. (1993) *Sedimentary petrography*. PTR Prentice Hall, 263pp.

Carroll, D. (1970) *Clay mineral: A guide to their X-ray identification*. USA, 80pp.

Carter, J. G. (1990) Skeletal biomineralization: pattern, processes and evolutionary trends. Van Nostrand Reinhold, New York, **1**, 832pp.

Carter, D. L., Heilman, M. D. and Gonzalez (1965) Ethylene glycol monoethyle ether for determining surface area of silicate minerals. *Soil Science*, **100**, no.5, 356-360.

Casey, J. P. (1961) *Pulp and paper. Chemistry and chemical technology, (second edition), paper testing and converting*. **3**, Interscience Publishers Ltd., London, 2113pp.

Casey, J. P. (1952) *Pulp and paper. Chemistry and chemical technology, properties of paper and converting.* **2**, Interscience Publishers Ltd., London, 1405pp.

Chang, L. L. P., Howie, R. A., and Zussman, J. (1996) *Rock-Forming Minerals. Non – silicate: sulphates, carbonates, phosphates, halides.* **5B**, (second edition), 383pp.

Chave, K. E., Deffeyes, K. S., Weyl, P. K., Garrels, R. M. and Thompson, M. E. (1964) Observations on the solubility of skeletal carbonates in aqueous solutions. *Science*, **137**, 33-34.

Choqette, P. W. and Pray, L. C. (1970) Geologic nomenclature and classification of porosity in sedimentary carbonates. *Bull. Am. Assoc. Petrol. Geol.*, **54**, 207-50.

Christidis, G. and Scott, P. W. (1993) Laboratory evaluation of bentonites. *Ind. Minerals*, **311**, 51-57.

Clarke, G. (1985) Special clays. *Ind. Minerals*, 216, 25-51.

Cocco, G. (1952) D. T. A. of some sulphates. *Periodico Di Mineralogia*, **21**, 103-141.

Conant, L. C. and Goudarzi, G. H. (1967) Stratigraphy and tectonic framework of Libya. *Bull. Am. Assoc. Petrol. Geol.*, **51**, 719-730.

Cronan, D. S. (1992) *Marine minerals in exclusive economic zones.* Chapman and Hall, London, 209pp.

Cuciureanu, G., Verbuta, A., Oita, N. and Craita, V. (1972) Delivery and stability of some antibiotics in bentonite. *Farmacia* (Bucharest), **20**, 119-127.

de Brodtkorb Milka, K. (1989) *Nonmetalliferous stratabound ore fields.* Van Reinhold, 332pp.

de Decker, M. (1997) Fillers and extenders. European market trends. *Ind. Minerals*, **363**, 29-35.

Dean, W. E. and Tung, A. L. (1974) Trace and minor elements in anhydrite and halite. Supai Formation (Permian), east-central Arizona. In: *4th symposium on salt* (ed A. H. Coogan), *North Ohio Geological Society*. 287 – 301.

Deer W. A., Howie R. A. and Zussman, J. (1992) *An introduction to the rock forming minerals*. (Second edition), Longman, 696pp.

Deer W. A., Howie R. A. and Zussman, J. (1962) Rock-forming minerals. Non-silicates, Vol. 5, Longmans, 371pp.

De Mille, J. B. (1947) *Strategic minerals: A summary of uses, world output, Stockpiles, Procurement*. McGraw-Hill Book Co. Inc., 626pp.

Desio, A. (1935) *Studi geologici sulla Cirenaica, sul Deserto Libico, sulla Tripolitania e sul Fezzan Orientale*. Missione Scientifica della R. Accad. D'Italia a Cufra (1931), **1**, 480pp.

Dickson, E. (1986) Refractory clays. In: raw materials for the refractories industry (ed E. M. Dickson). Second edition, 93-100.

Dickson, T. (1987) White carbonate fillers. An ocean of difference. *Ind. Minerals*, **239**, 65-73.

Dodd, J. R. (1967) Magnesium and strontium in calcareous skeletons: A review. *J. Paleontol.*, **41**, 1313 – 1331.

Dunham, R. J. (1962) Classification of carbonate rocks according to depositional texture. In: *Classification of carbonate rocks* (ed. W. E. Ham), *Am. Assoc. Petrol. Geol.*, Mem. 1, 108-121.

El Hawat, A. S. (1986a) Fine-grained current drift carbonates and associated facies in a slope to shelf shoaling-up sequence: the NE Libya. In: *7th European I.A.S.Mtg. (Abs)*. Krakow, Poland, 208-210.

El Hawat, A. S. (1986b) *Large-scale cross-bedded fine grained contributes and associated facies; A model from the Eocene of NE Libya. 12th. I.A.S.* Congress (Abs.). Canberra, Australia, 94pp.

El Hawat, A. S. and Salem, M. J. (1985) Stratigraphic reappraisal of Ar Rajmah Fm., Miocene, Al Jabal Al Akhdar, NE Libya: A case of field sedimentological approach. VIIIth Cong. Reg., Cong. Med. Neogene Stratig. (Abs.), *Hung. Geol. Survey*, Budapest, 206-208.

El Hawat, A. S. and Salem, M. J. (1987) A case study of the stratigraphic subdivision of Ar Rajmah Fm. and its implication on the Miocene of northern Libya. In: Proc. VIIIth Cong. Med. Neogene Stratig., *Budapest. Ann. Inst. Geol. Publ. Hung.*, Budapest, 173-184.

El Hawat, A. S. and Shelmani, M. A. (1993) *Short notes and guidbook on the geology of Al Jabal Al Akhdar, Cyrenaica NE Libya. Sedmentary basin of Libya*. Earth Science Society of Libya (ESSL), Benghazi, 70pp.

El Hawat, A. S., In Press Sedimentary basins of Egypt; an overview of dynamic stratigraphy. In: African sedimentary basins. (ed R. C. Selley). Elsevier, Amsterdam.

El-Arnauti, A. and Shelmani, M. (1985) Stratigraphic and structure setting. In: *Palynostratigraphy of northeast Libya* (eds. Thusu B. and Owens B.). *J. Micropalaeont.*, **4**, 1-10.

Eurybiades, B. and Niel Plummer (1985) Kinetic and thermodynamic factors controlling the distribution of SO_4^{2-} and Na^+ in calcites and selected aragonites. *Geochimica et Cosmochimica Acta*, **49**, 713-725.

Evans, A. M. (1993) *Ore geology and industrial minerals an introduction.* Blackwell Scientific Publications, 390pp.

Evan, G. and Shearman, D. J. (1964) Recent celestitíhe from the sediment of the Trucial coast of the Persian Gulf. *Nature*, 202, 385-386.

Flinter, B. H. (1959) The alteration of Malayan ilmenite grains and the question of ''arizonite''. *Econ. Geol.*, 54, 720-729.

Flugel, E. (1982) *Microfacies analysis of limestones. Springer.* Berlin, 633pp.

Friedman, G. M. (1965) Terminology of crystallization textures and fabrics in sedimentary rocks. *Jour. Sed. Petrology*, 35, 643-655.

Fuchthtbauer, H. and Peryt T. (1980) *The Zechstein Basin, with emphasis on carbonate sequences.* Contributions to sedimentology, no. 9, 328pp.

Gale, S. J. and Hoare, P. G. (1991) *Quaternary sediments. Petrographic methods for the study of unlithified rocks.* Belhaven Press, New York, 323pp.

Garea, B. B. and Braitwaite, C. J. R. (1996) Geochemistry, isotopic composition and origin of the Beda dolomites, Block NC 74 F, SW Sirte Basin, Libya. *Jour. Sed. Petrology*, 19 (3), 289-304.

Gillot, J. E. and Swenson, E. G. (1969) Mechanism of the alkali-carbonate rock reaction. *Quart. Jour. Eng. Geol.*, 2, 7-23.

Gordon, P. E. (1995) Strontium . U.S. Department of the Interior U.S. *Geological Survey.* Mineral industry surveys, 1 – 6.

Goudarzi, G. H. (1970) *Geology and mineral resources of Libya.* A Reconnaissance. U.S. Geol. Survey Prof. Paper, Washington, no. 660, 104pp.

Goudarzi, G. H. (1980) Structure of Libya. In: *The geology of Libya* (eds. M. J. Salem and M. T. Busrewil). *Academic Press, Tripoli*, **3**, 879-892.

Grahame, L. (1987) *Scanning electron microscopy and X-ray microanalysis*. Acol, London, 103pp.

Gregory, J. W. (1911) The geology of Cyrenaica. *Q. J. Geol. Soc. London*, **47**, 572-612.

Grey, I. E. and Reid, A. F. (1975) The structure of pseudorutile and its role in the alteration of ilmenite. *Amer. Mineral.*, **60**, 898-906.

Grim, R. E. (1968) *Clay mineralogy*. Second edition, McGraw-Hill, New York, 596pp.

Grim, R. E. and Guven, N. (1978) *Bentonites, geology, mineralogy, properties and uses*. Development in sedimentology, **24**, 256pp.

Gruver, R. M. (1951) Differential thermal-analysis studies of ceramic materials: III, characteristics heat effects of some sulphates. *Jour. Am. Ceramic Soc.*, **34**, 353-357.

Gruver, R. M. (1950) Differential thermal-analysis studies of ceramic materials: I, characteristics heat effects of some carbonates. *Jour. Am. Ceramic Soc.*, **33**, 96-101.

Gumati, S. M. and Anketell, J. M. (1982) *Structural analysis of western Sirte Basin, Libya*. Abstr. Bull. Am. Assoc. Petrol. Geol,. **66**, 591pp.

Gumati, Y. D. and Kanes, W. H. (1985) Early Tertiary subsidence and sedimentation facies, northern Sirte Basin, Libya. *Bull. Am. Assoc. Petrol. Geol.*, **69**, 39-52.

Haden, W. L. and Schwint, I. A. (1967) Attapulgite, its properties and applications. *Industrial and engineering chemistry*, **59**, no. 9, 59-69.

Hancock, J. M. and Kauffman, E. G. (1979) The great transgression of the Late Cretaceous. *J. Geol. Soc.*, **136**, 175-186.

Harben, P. (1988) CaCO₃ in paper. PCC versus the competition. *Ind. Minerals*, **366**, 39-49.

Harben P. (1988) Glass and ceramic spheres. Myriad names in growing market. *Ind. Minerals*, **248**, 53-54.

Harben, P. W. and Bates, R. L. (1990) *Industrial minerals, geology and world deposits.* Industrial mineral division, London, 312pp.

Harding, J. R. and Smith, R. A. (1986) Brickwork durability. *BDA design note 7*, 3-12.

Harding, T. P. (1983) Graben hydrocarbon plays and structural styles. *Geol. Mijnborw*, **63**, 3-23.

Harris, D. C. (1998) *Quantative chemical analysis.* 5th edition, W. H. Freeman and Company, New York, 227pp.

Harris, P. M. (1979) *Limestone and dolomite.* Mineral Resources Consultative Committee. Minerals Srategy and Econmics Reasearch Unit. Institute of Geological Sciences. Mineral Dossier no. **23**, 111pp.

Harrison, D. J. (1993) *Limestone.* Industrial mineral laboratory manual. *British Geological Survey.* Technical report, WG/92/29. Mineralogy and Petrology Series. 45pp.

Harrison, D. J. and Bloodworth, A. J. (1994) *Construction materials.* Industrial mineral laboratory manual. *British Geological Survey.* Technical report, WG/94/12. Mineralogy and Petrology Series. 100pp.

Hea, J. P. (1971) Petrography of the Paleozoic –Mesozoic sandstones of the southern Sirte Basin, Libya. In: *1st Symposium of Libya* (ed C. Gray), Univ. Libya Fac. Sci., Tripoli, 107-125.

Heinrich, K. F. J. (1981) *Electron beam X-ray microanalysis.* New York, 578pp.

Helmy, A. K., Ferreiro, E. A. and DeBussetti, S. G. (1994) Cation exchange capacity and condition of zero charge of hydroxy-Al montmorillonite. *Clays and clay minerals,* **42**, no. 4, 444-450.

Highley, D. E (1972) *Fuller's earth. Miner. Resour. Consult. Comm.,* Mineral Dossire **3**, HMSO, London.

Highley, D. E. (1990) Britain's industrial mineral resources and their exploitation. Erzmetall, **43**, 19-29.

Holloran (1974) In: bentonite in animal feed, a living mineral (ed A. Saeed). *Ind. Minerals,* **346**, 47-51.

Hull J. H. and Thomas I. A. (1974) Limestones and dolomite. In: the geology and mineral resources of Yorkshire. (eds D. H. Rayner and J. E. Hemingway). *The Yorkshire Geological Society,* 345-359.

''IM'' Pigments, Fillers and Extenders (1988). Calcium carbonate. *Ind. Minerals,* 39-48.

''IM'' Pigments, Fillers and Extenders (1988). European paper. Coated graphics provide market gloss. *Ind. Minerals,* 12-17.

''IM'' Pigments, Fillers and Extenders (1988). Plastic and rubber. Meeting the challenge of the future. *Ind. Minerals.*, 25-30.

Industrial Minerals (1999) Mineral spotlight: Celestite. *Ind. Mineral*, **380**, p.23.

Inglethorpe, S. D. J., Morgan, D. J., Highley, D. E. and Bloodworth, A. J. (1993) *Bentonite.* Technical report WG/93/20. Mineralogy and Petrology Series. Industrial mineral laboratory manual, British Geological Survey, 115pp.

JCPDS (1986) *Mineral powder diffraction file. Data Book.* USA, 1390pp.

Jean, P. S. and Jean, A. Cornee (1996) The Messinian reef complex of Milila, northeastern Rif, Morocco. In: *Models for carbonate stratigraphy from Miocene reef complexes of Mediterranean regions* (eds K. F. Evan, C. W. William and M. R. Jean), *S.E.P.M.*, 227-237.

Jepson, W. B. (1984) Kaolins: their properties and uses. *Phil. Trans. R. Soc. Lond.*, **A311**, 411-432.

Jones, T. R. (1983) The properties and uses of clays which swell in organic solvents. *Clay Minerals*, **18**, 399-410.

Jones, Tony (1997) Plastic fillers. A maturing market in Europe. *Ind. Minerals*, **356**, 61-63.

Jorgensen, D. B. (1994) Gypsum and anhydrite. In: *Industrial minerals and rocks.* 6th edition, (ed. Donald D. C.), Society for Minning, Metallurgy and Exploration, Inc. Littleton, Colorado, 571-581.

Jowfe Product Data Sheets . *National Oil Corporation. National Company For Oil Drilling Chemical and Equipments.* Jowfe Products Benghazi S. P. L. A. J.

Joyce, G. (1992) Celestite and strontium chemical trade. The Mexican wave. *Industrial mineral*, 21 – 33.

Kahle, C. (1965) Strontium in oolitic limestones. *Jour. Sed. Petrology*, **35**, No. 4, 846-856.

Kauffman, A. J. and Dilling, E. D. (1950) Differential thermal curves of certain hydrous and anhydrous minerals, with a description of the apparatus used. *Econ. Geol.*, **45**, 222-244.

Keegan, N. (1997) Minerals in paper. The weighting game. *Ind. Minerals*, **360**. 61-79.

Kellomaki, A., Nieminen, P. and Ritmaki, L. (1987) Sorption of ethylene glycol monoethyl ether on homoionic montmorillonites. *Clay Miner.*, **22**, 297-303.

Kendall, T. (1993) European Container glass industry. Recovery reflecting a greener image. *Ind. Minerals*, **306**, 35-48.

Kendall, T. (1996) Bentonite, major market review. *Ind. Minerals*, **344**, 25-37.

Kesler, S. E. (1994) *Mineral resources, economics and the environment.* Macmillan College Publishing Company, Inc., New York, 391pp.

Kinsman, D. J. (1969) Interpretation of Sr^{2+} concentrations in carbonate minerals and rocks. *Jour. Sed. Petrology*, **39**, 486-508.

Kleinsmeide, W. F. J. and Van Der Berg, N. J. (1968) Surface geology of the Jabal Al A khdar, northern Cyrenaica, Libya. In: *Geology and archaeology of northern Cyrenaica, Libya* (ed F. T. Barr), *Explor. Soc. Libya*, Tripoli, 115-123.

Klemme, H. D. (1971) Geothermal gradients, heat flow, hydrocarbon recovery. In: *Petroleum and global tectonics* (eds A. G. Fischer and S. Judson). Princetown Univ. Press, Princeton, 251-304.

Klen, L. (1974) *Geological map of Libya, 1:250,000 sheet Benghazi NI 34 – 14.* Explanatory Booklet, Indust. Resear. Cent., Tripoli, 56pp.

Klitzsch, E. (1968) Outline of geology of Libya. In: *Geology and archaeology of northern Cyrenaica, Libya* (ed F. T. Barr). *Petrol. Explor. Soc. Libya,* 10th Annual Field Conf., 71-78.

Klitzsch, E. (1971) The structural development of parts of North Africa since Cambrian time. In: *The Geology of Libya* (ed C. Grey). Univ. of Libya, Tripoli, 253-363.

Klitzsch, E. (1981) Lower palaeozoic rocks of Libya, Egypt and Sudan. In Lower Palaeozoic rocks of the Middle east, eastern and southern Africa and Antarctica. In: *Lower Palaeozoic rocks of the world* (ed C. H. Holland), **3**, 131-163.

Kogbe, C. A. (1980) The Trans-Saharan Seaway during the Cretaceous. In: *2nd Symposium of Libya* (eds M. J. Salem and M. T. Busrewil). *Univ. Libya Fac. Sci.,* Tripoli, **1**, 91-96.

Konrad, B. K. (1979) *Introduction to geochemistry.* second edition, McGraw-Hill, 617pp.

Kulp, J. L., Turkian, K. and Boyd, D. W. (1952) Strontium content of limestones and fossils. *Bull. Geol. Soc. of Am.,* 63, 701-716.

Langer, W. H. and Glanzman, V. M. (1993) National aggregates building America's future. *U. S. Geological Survey Circular.* USA, 1-15.

Larsen, G. and Chilingar, G. V. (1983) Developments in sedimentology (25 B). Diagenesis in sediments and sedimentary rocks, Elsevier, **2**, 572pp.

Lat, J. and Zamarsky, V. (1992) *The report on classification, evaluation and possible mining and processing methods of the potential bentonite deposit in Umm Ar Razam area in Libya.* PRC, National Oil Corporation, 200pp.

Lee, L. Fong (1995) *Report on a training program. Advanced material characterisation.* The University of Sheffield, England, under the sponsorship of Asian Development Bank, 54pp.

Lewis, D.W. and McConchie, D. (1994) *Analytical sedimentology.* Chapman and Hall, New York, 197pp.

Lloyd, C. P. and Murray, R. C. (1965) *Dolomitization and limestone diagenesis.* Society of Economic Paleontologists and Mineralogists, 180pp.

Long, J. V. P. (1977) Electron probe microanalysis. In: *physical methods in determinative mineralogy.* Second edition (ed J. Zussman J.). 273-341.

Loughbrough, R. (1993) Minerals for animal feed. In a stable market. *Ind. Minerals,* **306**, 19-34.

Lowenstam, H. A. (1964) *Sr/Ca ratio of skeletal aragonites from the recent marine biota at Palau and from fossil gastropod.* North-Holland Publishing Company, Amesterdam, 114-132.

Lumb M. D. (1978) *Luminescence spectroscopy.* Academic Press, London, 375pp.

Lumsden, D. N. (1979) Discrepancy between thin sections and X-ray estimates of dolomite in limestone. *Jour. Sed. Petrology,* **42**, 239-242.

Lynch, G. (1994) *Brickwork.* History, technology and practice. London, **1**, 260pp.

McMurry, J. (1998) *Fundmentals of organic chemistry.* 4th edition, Thomson Publishing Company, 566pp.

Machel, H. G. and Mountjoy, E. W. (1986) Chemistry and environments of dolomitization-a reappraisal. *Earth Sci. Rev.,* **23**, 175-222.

Mackenzie, R. C. (1975) *The differential thermal investigation of clays.* Mineralogical Society (Clay minerals group), London, 456pp.

MacKenzie, W. S. and Adams, A. E. (1994) *A colour Atlas of rocks and minerals in thin section.* 192pp.

Mann, S., Webb, J. and Williams, R. J. P. (1989) *Biomineralization.* 541pp.

Manning, D. A. C. (1995) *Introduction to industrial minerals.* Chapman and Hall. 276pp.

Marchetti, M. (1934) Note illustrative per un abbozzo di carta geologica della Cirenaica. *Boll. Soc. Geol. Ital.,* **53**, 309-325.

Martyn, P. (1996) Miocene reef distributions and their associations in the central Mediterranean region. In: *Models for carbonate stratigraphy from Miocene reef complexes of Mediterranean regions* (eds K. F. Evan, C. W. William and M. R. Jean). *S.E.P.M.,* 73-86.

Massa, D. and Delort, T. (1984) Evolution of the Sirte Basin (Libya) from Cambrian to Cretaceous. *Bull. Geol. Soc.,* France, **20**, 1087-1096.

Mattes, B. W. and Mountjoy, E. W. (1980) Burial dolomitization of the Upper Devonian Miette buildup, Jasper National Park, Alberta. In: *Concepts and models of dolomitizatio.* (eds D. H. Zenger, J. B. Dunhum and R. L. Ethington), *Spec. Publ. Soc. Palaeont. Mineral,* Tulsa **28**, 259-297.

McConnell, D. (1988) Minerals in paper. A quality paradox. *Ind. Minerals,* **247**, 155-157.

Mikbel, Sh. R. (1977) Basement configuration and structure of west Libya. *Libyan J. Sci.,* **7A**, Tripoli.

Mikbel, Sh. R. (1979) Structural and configuration map of the basement of east and central Libya. *N. Jb. Geol. Palaont. Abh.*, Stuttgart, **158**, 209-220.

Milliman, J. D. (1974) *Recent sedimentary carbonates.* Part 1, Springer-Verlag, 375pp.

Moore, C. H. (1989) *Carbonate diagensis and porosity.* Elsevier, Amsterdam, no. 46, 338pp.

Moore, D. M. and Reynolds, R. C. (1997) *X-ray diffraction and the identification and analysis of clay minerals.* Second edition, Oxford, 378pp.

Moore, J. W. (1976) *Environmental chemistry.* New York, USA, 500pp.

Moore, R. C. (1963) *Treatise on invertebrate palaeontology.* Geological Society of America, 498.

Moorlock, B. S. P. and Highley, D. E. (1991) *An appraisal of fuller's earth resources in England and Wales.* British Geological Survey. Technical report WA/91/75.

Morgan, D. J. (1994) *Minerals for development.* Mineralogy and Petrology Group, British Geological Survey, Technical report WG/94/13, 19pp.

Morse, J. W. and Mackenzie, (1990) *Geochemistry of sedimentary carbonates.* Developments in sedimentology, **48**, Elsevier, 707pp.

Mouzughi, A. G. and Taleb, M. T. (1980) Tectonic map of Libya. Petrol. Explor. Soc. Libya.

Muller, G. and Friedman, G. M. (1968) *Recent developments in carbonate sedimentology in central Europe.* Springer – Verlag, Berlin, 255pp.

Murray, H. H. (1984) Kaolin for pulp and paper. In: *raw materials for the pulp and paper industry* (eds P. Harben and E. Dickson), 39-42.

Murray, Fischer and Shade (1951) In: *The differential thermal investigation of clays* (ed. Mackenzie, R. C., 1957), Mineralogical Society, London, 456pp.

Nebergall, R. (1998) Bentonite in Mexico, a changing and rising market. *Ind. Minerals*, **365**, 47-55.

Nicholas, E. (1978) The behavior of Zn^{2+} and Mn^{2+} during carbonate diagenesis: theory and applications. *Jour. Sed. Petrology*, **48**, **3**, 799-814.

Nickless, E. F. P., Booth,S. J., and Mosley, P. N. (1976) *The celestite resources of the area north – east of Bristol*. 1st Geol. Sci., Miner. Assessment Rept. No. 25, 83pp.

Ober, J. A. (1994) Strontium minerals. In: *Industrial minerals and rocks*. 6th edition (ed. Donald D. C.), Society for Minning, Metallurgy and Exploration, Inc., Littleton, Colorado, 1003-1009.

O'Driscoll, M. (1990) Fine carbonate fillers. PCC breaks ground in paper. *Ind. Minerals*, **276**, 21-43.

O'Driscoll, M. (1988) Bentonite, overcapacity in need of market. *Ind. Minerals*, **250**, 43-64.

O'Driscoll, M. (1988) Burnt lime/dolime. Seeking markets green. *Ind. Minerals*, **248**, 23-51.

Odom, I. E. (1984) Smectite clay minerals: properties and uses. *Phil. Trans. R. Soc. Lond.*, **A311**, 391-409.

Odum, H. T. (1957) Biochemical deposition of strontium. *Publications of the Institute of Marine Science*, **4**, No. 2, 38-114.

Olaussen, S. (1981) Formation of celestite in the Wenlock, Oslo region Norway-evidence for evaporitic depositional environments. *Jour. Sed. Petrology*, **51**, 37-45.

Parkikh, C. (1998) Indian white mineral. *Ind. Minerals*, **365**, 69-75.

Peryt, T. M. and Wazny, H. (1980) Microfacies and geochemical development of the basin facies of the Zechstein limestone in Western Poland. In: *The Zechstein Basin with emphasis on carbonate sequences* (eds H. Fuchtbauer and T. Peryt), Stuttgart, 279-306.

Petroleum Research Centre (1987) *Evaluation of bentonite clay from Umm Ar Razam area.* National Oil Corporation, prepared by bentonite project group.

Pietersz, C. R (1968) Proposed nomenclature for rock units in northern Cyrenaica. In: *Geology and archaeology of northern Cyrenaica, Libya* (ed F. T. Barr). *Petrol. Explor. Soc. Libya*, 10th Annual Field Conf., 125-148.

Pokorny, V. (1963) *Principles of zoological micropalaeontology.* Berlin, **I**, 652pp.

Prentice, J. E. (1990) *Geology of construction materials.* Chapman and Hall, London, 202pp.

Prevot, J. L. and Lucas, J. (1986) Microstructure of apatite-replacing carbonate in synthesized and natural samples. *Jour. Sed. Petrology*, **56**, No. 1, 153-159.

Price, C. A. (1986) Testing porous building stone. Specification technical study **1**, *Arch. Jour.*, 62-64.

Przibram, K. and Caffyn, J. E. (1956) Irradiation colours and luminescence, a contribution to mineral physics. Pergamon Press Limited, London, 332pp.

Product data sheets. National Company for Oil Drilling Chemicals and Equipments (Jowfe). Benghazi-Libya.

Purser, B. H. (1998) Syn-rift diagenesis of Middle Miocene carbonate platforms on the north-western Red Sea coast, Egypt. In: *Sedimentation and tectonics of Rift Basins: Red Sea-Gulf of Aden* (eds. Purser B. H. and Bosence D. W. J.), Chapman and Hall, London, 369-389.

Purser, B. H., Jean, Claude, P. and Rosen, B. R. (1996) Miocene reefs of the northerwest Red Sea. In: *Models for carbonate stratigraphy from Miocene reef complexes of Mediterranean regions* (eds K. F. Evan, C. W. William and M. R. Jean), *S.E.P.M.*, 347-365.

Pusser, B., Tucker, M. and Zenger, D. (1994) *Dolomites.* International Association of Sedimentologists, no. **21**, Blackwell Scientific Publications, London, 451pp.

Reed, S. J. B. (1996) *Electron microprobe analysis and scanning electron microscopy in geology.* Cambridge University Press, 201pp.

Reyment, R. A. and Dingle, R. V. (1987) Palaeogeography of Africa during the Cretaceous period. *Palaeogeogr. Palaeoclim. Palaeoecol.*, **59**, 93-116.

Robinson, J. W. (1982) *Undergraduate instrumental analysis.* Third edition, Marcel Dekker, Inc., New York, 550 pp.

Robinson, P. (1980) Determination of calcium, Magnesium, manganese, strontium, sodium and iron in the carbonate fraction of limestones and dolomites. *Chemical Geology*, **28**, 135-146.

Rohlich, P. (1974) *Geological map of Libya; 1:250,000 sheet, Al Bayda sheet NI34-15, Explanatory Booklet.* Indust. Resear. Cent., Tripoli, 70pp.

Rohlich, P. (1980) Tectonic development of Al Jabal Al Akhdar. In: Geology of Libya. In: *Geology of Libya.* (eds M. J. Salem and M. T. Busrewil), *Academic Press*, London, **III**, 923-931.

Rollinson, H. (1993) *Using geochemical data: evaluation, presentation, interpretation.* Longman, 352pp.

Rosell, L., Orti, F., Kasprzyk, A., Playa, E. and Peryt, T. M. (1998) Strontium geochemistry of Miocene primary gypsum: Messinian of Southern-eastern Spain and Sicily and Badenian of Poland. Journal of Sedimentary Research, **68**, No.1, 63-79.

Russell, Alison (1988) Minerals in pharmaceuticals. The key is quality assurance. *Ind. Minerals*, **251**, 32-37.

Saeed, A. (1996) Bentonite in animal feed, a living mineral. *Ind. Minerals*, **346**, 47-51.

Sanford, R. M. (1970) Sarir Oil Field, Sirte Basin, Libya-Desert Surprise. In: geology of giant Petroleum Fields (ed. Halbouty M. T.), *Mem. Assoc. Petrol. Geol.*, **14**, 449-476.

Santaren, J. (1993) European market developments for absorbent clays. *Ind. Minerals*, **404**, 35-47.

Sassi, S. (1991) *Bentonite mining project, Libya.* Results of analyses and tests. University of Tunis II. 174pp.

Schmalz, R. F. (1965) Brucite in carbonate secreted by the red algae *Goniolithon sp.*, *Science*, **149**, 996-997

Scholle, P. A. (1978) *A colour illustrated guide to carbonate rock consistuents textures, cements and porosities.* Am. Assoc. Petrol. Geol. Mem. **27**, 241pp.

Searl, A. (1994) Discontinous solid solution in Ca-rich dolomites: the evidence and implications for the interpretation of dolomite petrographic and geochemical data. In: *Dolomite* (eds Bruce Puser, M. Tucker and Donald Zenger), 361-376.

Sedman, J. H. F. and Barlow, S. (1989) The durability of the bath building stone. *Proc. Ex. Ind. Conf.*, University of Birmingham, 82-91.

Selley, R. C. (1968) Facies profile and other new methods of graphic data presentation, application in quantitative study of Libyan Tertiary shoreline deposits. *Jour. Sed. Petrology*, **38**, 353-372.

Shah, N. R. (1997) Indian bentonite, focus on the Kutch region. *Ind. Minerals*, **359**, 43-47.

Shirmohammadi, N. H. and Shearman, D. J. (1966) On the distribution of strontium in some dolomitised and dedolomitised limestones from the French Jura: Abst. In Proc. Min. Soc., London, *Min. Mag.*, **35**, LXXII.

Shorre Olaussen (1981) Formation of celestite in the Wenlock, Oslo region Norway evidence for evaporitic depositional environments. *Jour. Sed. Petrology*, **51**, 37 – 45.

Sibley, D. F. (1980) Climatic control of dolomitization Seroe Domi Formation (Pliocene). In: *Concepts and models of dolomitization* (eds D. H. Zenger, J. B. Dunham and R. L. Ethington). *Soc. Econ. Palaeontologists Mineralogists Spec. Pub.* 28, 247-258.

Sibley, D. F. (1982) The origin of common dolomite fabrics: clues from the Pliocene. *Jour. Sed. Petrology*, **52**, 1087-1100.

Siegel, F. R. (1961) Variations of Sr/Ca ratios and Mg contents in recent carbonate sediments of the northern Florida Keys area. *Jour. Sed. Petrology*, **31**, No. 3, 336-342.

Sims, Catherine (1997) Spanish GCC. Amelee over Macael. *Ind. Minerals*, **361**, 27-37.

Sola, M. and Ozcicek B. (1990) On the hydrocarbon prospectivity of north Cyrenaica region, Libya. PRC, Tripoli, **2**, 25-41.

Sordon, J. (1980) Precise identification of illite/smectite interstratifications by X-ray powder diffraction. *Clays and Clay Minerals*, **28**, no.6, 401-411.

Stehli, F. G. and Hower, J. (1961) Mineralogy and early diagenesis of carbonate sediments. *Jour. Sed. Petrology*, **31**, 325-371.

Stockwell, L. E., Hillier J. A., Linley K. A., Mills A. J. and White R. (1998) World mineral statistics (1992-1996). British Geological Survey, 281pp.

Stowell, F. P. (1963) *Limestone. As a raw material in industry.* Imperial Chemical industries Ltd., London, UK, 55pp.

Taylor, G. D. (1994) *Material in construction.* Second edition, UK, 532pp.

Temple, A. K. (1966) Alteration of ilmenite. *Econ. Geol.*, **61**, 695-714.

Theng, B. K. G. (1974) *The chemistry of clay-organic reactions.* Adam Hilger Ltd., London, 362pp.

Theriault, F. and Hutcheon, I. (1987) Dolomitization and calcitization of the Devonian Grosmont Formation, northern Alberta. *Jour. Sed. Petrology*, **57**, 955-966.

Thomas, I. A. (1973) *Celestite* . Mineral Resources Consultative Committee, No. 6, 26pp.

Thompson, R. (1977) *The modern inorganic chemicals industry.* The Chemical Society, London, Special Publication no. 31, 466pp.

Tokuyama, A., Kitano Y. and Kaneshima, K. (1972) Geochemical behavior of chemical species in the processes of limestone foemation. Part I. Chemical

composition of corals and limestones in the Tyukyu Islands. *Geochem. J.*, **6**, 83-92.

Tony, G. (1991) *Laboratory assessment for Umm Ar Razam in drilling mud.* National Company for Drilling Chemicals and Equipments (Jowfe), National Oil Corporation, 17pp.

Tucker, M. (1988) *Techniques in sedimentology.* Blackwell Science, 394pp.

Tucker, M. E. (1979) *Sedimentology petrology.* Geoscience text, an introduction to the origin of sedimentary rocks. Second edition, Blackwell Science, 260pp.

Tucker, M. E., Wright, V. P. and Dickson, J. A. D. (1990) *Carbonate sedimentology.* Blackwell Scientific Publications, London, 482pp.

Tucker, M. E. (1991) *Sedimentary petrology, an introduction to the origin of sedimentary rocks.* Second edition, Blackwell Science, 260pp.

Turekian, K. (1955) Paleoecological significance of the strontium-calcium ratio in fossils and sediments. *Bull. Geol. Soc. of Am.*, **66**, 155-156.

Van Houten, F. B. (1983) Cretaceous rifting above a fixed mantle hotspot, Sirte Basin, north-central Libya. *Geology*, **11**, 115-118.

Velde, B. (1992) *Introduction to clay minerals, chemistry, origins, uses and environmental significance.* Chapman and Hall, London, 198pp.

Vidal, J. R. (1994) $CaCO_3$ fillers. Market trends and developments. *Ind. Minerals*, **326**, 63-65.

Walsh F. N. (1997) Inductively coupled plasma atomic emission sepectrometry (ICP-AES). In: *Modern analytical geochemistry, an introduction to quantitative chemical analysis for earth* (ed. Robin Gill), *Environmental and Materials Scientists*, Longman, 329pp.

Ward, W. C. and Halley, R. B. (1985) Dolomitization in a mixing zone of near-sea water composition, late Pleistocene, Northeastern Yucatan Peninsula. *Jour. Sed. Petrology*, **55**, 407-420.

Watson, D. M. and Rahuma (1992) Evaluation of bentonic clays of Umm Ar Razam area, Libya as potential drilling muds. *PRJ*, **4**, 46 – 51.

Weaver, C. E. (1975) Construction of limpid dolomite. *Geology*, **3**, 425-428.

Weber, J. N. and Kaufman, J. W. (1965) Brucite in the calcareous algae *Goniolithon*. *Science*, **149**, 996-997.

Wei Hong (1993) Celestite and strontianite. Review of ore processing and exploitation. *Ind. Mineral*, 55 – 59.

West, I. (1973) Vanished evaporites – significance of strontium minerals. *Jour. Sed. Petrology*, **43**, 278 – 279.

West, I. M. (1964) Evaporite diagenesis in the lower Perbeck beds of Dorset. *Proc. Yorkshire Geol. Soc.*, **34**,315-330.

Wilson, M. J. (1987) *A hand book of determinative methods in clay mineralogy.* Chapman and Hall, New York, 308pp.

Wood, M. W., and Shaw, H. F. (1976) The geochemistry of celesites from the Yate area near Bristol (U.K.). *Chemical Geology.* **17**, 179 – 193.

Wayne R. P. (1988) *Principles and applications of photochemistry.* Oxford Science Publications, 268pp.

Young, R. J. and Lovell, P. A. (1991) *Introduction to polymers.* Second edition, Chapman and Hall, 443pp.

Zenger, D. H. (1967) Coloration of the ''Pink *Chonete*'' (brachiopod) of the Onondaga limestone, New York. *Jour. Palaeontology*, **41**, 161-166.

Zert, B. (1974) *Geology map of Libya, 1:250,000 Dernah sheet NI 34-16. Explanatory Booklet.* Ind. Resear. Cent., Tripoli, 49pp.

APPENDICES

X.1 Limestone geochemistry

X.1.1 XRF analyses for major (wt. %) and trace (ppm) elements: (A5.1 – A5.9)

Sample no.	AH	AS	DE1	DE2	DE3	DE4	DE5	DE6	Qasar Libya (L)	Qasar Libya (U)
Oxides (wt. %)										
SiO$_2$	0.24	1.12	0.00	0.00	0.00	0.00	0.00	0.09	0.00	0.00
Al$_2$O$_3$	0.00	0.23	0.00	0.00	0.00	0.00	0.00	0.09	0.00	0.00
Fe$_2$O$_3$	0.00	0.11	0.00	0.00	0.00	0.00	0.00	0.02	0.00	0.00
MgCO$_3$	1.63	0.94	0.75	1.32	1.09	0.67	1.50	1.03	0.59	0.63
CaCO$_3$	98.67	98.09	100.40	99.72	99.83	100.20	99.14	99.31	100.60	100.48
S	0.00	0.00	0.00	0.00	0.00	0.00	0.00	0.00	0.00	0.00
K$_2$O	0.00	0.00	0.00	0.00	0.00	0.00	0.00	0.00	0.00	0.00
TiO$_2$	0.00	0.00	0.00	0.00	0.00	0.00	0.00	0.00	0.00	0.00
MnO	0.01	0.05	0.01	0.07	0.03	0.01	0.02	0.04	0.00	0.04
P$_2$O$_3$	0.01	0.00	0.00	0.00	0.00	0.01	0.00	0.01	0.00	0.00
Total	100.56	100.54	101.16	101.11	100.95	100.89	100.66	100.59	101.19	101.15
CaO	55.26	54.93	56.22	55.84	55.9.0	56.11	55.52	55.61	56.34	56.27
MgO	0.96	0.55	0.44	0.78	0.64	0.40	0.89	0.61	0.35	0.37
Limestone quality	VHP	HP				Very high purity (VHP)				VHP
Trace element (ppm)										
Nb	0	3	0	2	2	0	5	1	0	0
Zr	221	71	48	55	37	35	52	42	32	31
Y	38	45	41	42	39	42	37	43	40	41
Sr	2408	672	489	559	388	329	576	432	335	306
Rb	41	43	42	43	41	42	41	40	44	44
Zn	0	1	0	0	0	0	0	0	0	0
Cu	9	20	12	12	6	17	17	15	7	13
Ni	0	0	0	0	0	0	0	0	0	0
Cr	21	29	26	13	10	28	15	22	27	6
Ce	27	0	16	0	0	0	16	29	0	0
Nd	0	0	0	0	0	0	1	0	0	0
V	12	12	6	9	1	3	14	9	4	5
La	0	13	8	28	12	15	0	16	17	20
Ti	210	270	148	151	144	174	173	181	129	137
Ba	0	19	0	0	0	0	0	0	0	0
Sc	97	93	88	108	93	76	84	122	90	116

Table (A5.1) Chemical analysis for major and trace elements of Appollonia (L. to M. Eo.), Bachor quarry, and Darnah (Shahhat Susah road-cut) Formations, and Qasar Libya Quarry of Darnah Formation (M.-to U. Eo.).

Sample no.	SLP	SMP	SUP	SMUP	ST	Algal Lst L	Algal Lst U
Oxides (wt.%)							
SiO_2	6.74	16.03	4.40	14.24	6.22	0.00	5.06
Al_2O_3	2.16	5.12	1.32	4.35	1.86	0.00	1.44
Fe_2O_3	0.63	1.12	0.45	1.00	0.55	0.01	0.87
$MgCO_3$	2.82	3.93	2.71	3.18	1.30	1.14	1.98
$CaCO_3$	87.49	72.86	91.12	76.04	90.06	99.37	90.53
S	0.00	0	0.00	0.42	0.00	0.00	0.01
K_2O	0.10	0.23	0.07	0.24	0.06	0.00	0.15
TiO_2	0.08	0.21	0.05	0.16	0.08	0.00	0.10
MnO	0.01	0	0.03	0.01	0.02	0.06	0.02
P_2O_5	0.03	0.08	0.03	0.11	0.08	0.01	0.02
Total	100.06	99.58	100.18	99.75	100.23	100.59	100.18
CaO	48.99	40.80	51.03	42.58	50.43	55.65	50.70
MgO	1.66	2.32	1.6	1.88	0.77	0.67	1.17
Limestone quality	LP	I	LP	I	LP	VHP	LP
Trace element (ppm)							
Nb	8	9	0	6	4	3	5
Zr	79	106	144	150	147	58	105
Y	47	52	45	46	48	41	46
Sr	653	686	1484	1382	1475	605	711
Rb	49	54	46	53	47	43	49
Zn	21	31	7	31	15	0	11
Cu	8	13	25	14	14	5	16
Ni	0	0	11	0	0	0	0
Cr	63	89	54	97	70	24	57
Ce	32	54	24	33	45	73	53
Nd	31	15	0	0	0	0	2
V	32	51	22	42	43	18	32
La	0	9	27	16	32	0	15
Ti	790	677	540	1247	763	182	999
Ba	0	0	0	0	0	0	1
Sc	70	66	108	84	75	87	95

Table (A5.2) Chemical analysis for major and trace elements of Al Bayda Formation (L. Oligo.), Shahhat Susah Road – cut.

333

Sample no.	Bayda	A1	A2	A3	A4	A5	A6	A7
Oxides (wt. %)								
SiO_2	0.19	6.81	2.35	3.45	5.93	3.26	4.55	3.24
Al_2O_3	0.00	1.26	0.83	1.30	2.04	0.99	1.2	0.93
Fe_2O_3	0.00	0.88	0.33	0.54	0.82	0.44	0.87	0.92
$MgCO_3$	2.10	7.99	1.36	1.33	1.41	2.07	2.85	2.44
$CaCO_3$	98.13	82.27	95.39	93.54	89.71	93.38	90.43	92.50
S	0.00	0.01	0.00	0.00	0.00	0.00	0.00	0.00
K_2O	0.00	0.17	0.06	0.09	0.10	0.05	0.12	0.08
TiO_2	0.00	0.07	0.05	0.08	0.14	0.06	0.10	0.06
MnO	0.02	0.01	0.03	0.01	0.03	0.02	0.00	0.01
P_2O_5	0.01	0.12	0.00	0.00	0.01	0.00	0.01	0.01
Total	100.45	99.59	100.40	100.34	100.19	100.27	100.13	100.19
CaO	54.95	46.07	53.42	52.38	50.24	52.29	50.64	51.80
MgO	1.24	4.71	0.8	0.78	0.83	1.22	1.68	1.44
Limestone quality	HP	I	MP		Low purity (LP)			
Trace element (ppm)								
Nb	1	10	1	6	6	8	10	5
Zr	40	83	64	82	102	89	113	86
Y	37	43	46	47	44	44	45	46
Sr	381	599	541	619	612	619	532	580
Rb	39	50	46	44	48	43	49	45
Zn	0	14	7	6	9	8	12	14
Cu	13	17	24	23	20	21	10	17
Ni	0	0	0	0	1	0	0	0
Cr	9	82	65	58	52	46	64	60
Ce	0	0	45	32	39	1	20	5
Nd	0	7	13	23	9	0	0	0
V	29	25	16	37	39	31	73	42
La	0	10	0	11	26	0	15	2
Ti	236	1052	529	739	1206	685	945	664
Ba	0	9	0	0	0	0	0	0
Sc	80	72	80	88	92	98	74	83

Table (A5.3) Chemical analysis for major and trace elements of Al Bayda (L. Oligo.) and Al Abraq (M. to U. Oligo.) Formations, Deryanah Al Abyar Road-cut.

Sample no.	1	2	3	4	5	6	7	8	9	10	QM
Oxides (wt. %)											
SiO_2	30.27	18.60	23.46	38.90	25.82	33.04	35.03	36.71	17.65	32.94	0.00
Al_2O_3	4.11	4.50	7.07	4.92	5.33	8.56	6.29	8.42	4.61	8.76	0.00
Fe_2O_3	14.81	6.55	3.44	7.65	2.57	2.92	2.33	2.57	1.50	4.12	0.00
$MgCO_3$	3.54	2.68	2.64	3.47	2.66	3.37	3.02	3.85	2.50	3.02	1.44
$CaCO_3$	40.90	65.25	61.33	40.63	61.68	49.40	50.66	45.68	72.64	48.16	99.41
S	0.00	0.00	0.00	0.00	0.00	0.01	0.00	0.00	0.00	0.03	0.00
K_2O	4.30	1.31	0.86	2.41	0.82	0.97	1.11	1.01	0.44	0.95	0.00
TiO_2	0.22	0.26	0.38	0.43	0.43	0.61	0.51	0.55	0.26	0.76	0.00
MnO	0.02	0.01	0.02	0.01	0.00	0.00	0.00	0.00	0.01	0.02	0.05
P_2O_5	0.12	0.02	0.02	0.13	0.02	0.03	0.12	0.03	0.04	0.01	0.00
Total	98.29	99.18	99.22	98.55	99.33	98.91	99.07	98.82	99.65	98.77	100.90
CaO	22.9	36.54	34.34	22.75	34.54	27.66	28.37	25.58	40.68	26.97	55.67
MgO	2.10	1.58	1.56	2.05	1.57	1.99	1.78	2.27	1.48	1.78	0.85
Limestone quality						Impure (I)					VHP
Trace element (ppm)											
Nb	20	25	23	16	22	29	198	186	230	65	2
Zr	194	149	147	389	322	316	519	486	613	468	63
Y	45	47	45	48	49	44	68	60	76	48	37
Sr	161	214	348	254	260	354	1672	1447	1790	355	726
Rb	201	114	79	124	76	75	302	119	134	103	42
Zn	120	68	38	62	34	51	95	87	116	69	0
Cu	15	19	14	15	20	14	72	55	76	20	12
Ni	36	14	19	11	0	18	278	203	289	44	0
Cr	575	179	123	268	104	136	424	356	526	186	0
Ce	124	69	75	103	35	59	235	240	272	92	12
Nd	37	19	8	50	4	25	89	72	86	24	0
V	195	87	103	123	79	121	370	382	484	170	0
La	46	20	30	17	47	57	116	97	135	64	21
Ti	2005	1902	2676	3247	3161	4372	17518	17222	22549	6447	167
Ba	10	10	21	59	19	30	852	782	1051	135	17
Sc	28	66	67	28	61	45	33	23	25	34	101

Table (A5.4)   Chemical analysis for major and trace elements of Al Faidiyah Formation (U. Oligo.-L. Mio.), Wadi Al Qattarah Member of Ar Rajmah Formation (M. Mio.), Deryanah Al Abyar Road-cut.

Sample no.	LF1	UF0	UF1	UF2	UF3	UF4	UF5	UF6
Oxides (wt. %)								
SiO_2	23.80	0.29	0.00	0.00	0.00	0.00	0.00	0.00
Al_2O_3	10.17	0.00	0.00	0.00	0.00	0.00	0.00	0.00
Fe_2O_3	5.50	0.09	0.00	0.00	0.00	0.00	0.00	0.00
$MgCO_3$	2.56	1.14	0.45	0.89	0.74	0.47	0.65	0.71
$CaCO_3$	54.97	98.60	100.48	99.89	100.07	100.45	100.52	100.30
S	0.00	0.00	0.00	0.00	0.00	0.00	0.00	0.00
K_2O	0.59	0.00	0.00	0.00	0.00	0.00	0.00	0.00
TiO_2	1.14	0.00	0.00	0.00	0.00	0.00	0.00	0.00
MnO	0.05	0.00	0.02	0.00	0.02	0.03	0.02	0.00
P_2O_5	0.02	0.42	0.05	0.05	0.04	0.05	0.04	0.01
Total	98.80	100.54	101.00	100.83	100.87	101.00	101.23	101.02
CaO	30.78	55.22	56.27	55.94	56.04	56.25	56.29	56.17
MgO	1.51	0.70	0.27	0.53	0.44	0.28	0.38	0.42
Limestone quality	I	Very high purity (VHP)						
Trace element (ppm)								
Nb	110	0	1	0	0	0	47	0
Zr	566	22	32	21	16	24	580	27
Y	104	44	44	43	39	45	100	40
Sr	242	206	204	213	163	220	518	222
Rb	172	44	44	41	44	43	192	42
Zn	207	0	0	1	4	1	130	0
Cu	46	11	11	12	29	16	60	21
Ni	128	0	0	0	0	0	82	0
Cr	399	11	12	14	0	4	235	7
Ce	291	0	21	0	15	0	0	0
Nd	115	15	12	0	3	0	99	0
V	482	15	4	0	3	8	275	0
La	83	0	0	0	11	0	110	0
Ti	18934	185	150	149	169	149	856	151
Ba	155	35	0	0	0	0	739	0
Sc	39	93	121	92	107	83	62	92

Table (A5.5) Chemical analysis for major and trace elements of Al Faidiyah Formation (U. Oligo. to L. Mio.), Al Fatayah Quarry.

Sample no.	US	UL	UM	UU	ULst1	ULst2
Oxides (wt. %)						
SiO_2	23.57	23.45	23.22	23.86	6.20	11.33
Al_2O_3	10.30	10.09	9.87	10.55	2.04	1.75
Fe_2O_3	5.10	4.94	5.05	4.44	0.72	2.57
$MgCO_3$	2.10	1.98	1.97	1.61	3.02	4.94
$CaCO_3$	56.1	56.77	57.12	56.76	87.73	77.91
S	0.00	0.00	0.00	0.00	0.00	0.12
K_2O	0.62	0.64	0.63	0.63	0.14	0.59
TiO_2	1.03	1.04	1.02	1.08	0.12	0.10
MnO	0.05	0.03	0.04	0.05	0.06	0.01
P_2O_5	0.02	0.02	0.01	0.02	0.01	0.28
Total	98.89	98.96	98.93	99.00	100.04	99.60
CaO	31.42	31.79	31.99	31.79	49.13	43.63
MgO	1.24	1.17	1.16	0.95	1.78	2.91
Limestone quality	I				LP	I
Trace element (ppm)						
Nb	166	153	148	184	4	7
Zr	790	744	726	907	115	94
Y	144	137	133	116	60	53
Sr	314	317	310	352	585	611
Rb	177	167	161	158	70	47
Zn	254	209	212	187	11	1
Cu	40	37	36	37	19	6
Ni	110	96	89	110	14	7
Cr	449	410	416	499	108	36
Ce	410	385	346	299	53	0
Nd	174	164	171	144	0	0
V	435	401	384	431	73	58
La	173	159	146	176	28	1
Ti	18745	17765	17565	19761	946	710
Ba	21	6	0	83	66	9
Sc	53	51	32	37	71	69

Table (A5.6) Chemical analysis for major and trace elements of Al -
Faidiyah Formation (U. Oligo. to L. Mio.), Umm Ar -
Razam Quarry.

Sample no.	LB1	LB2	LB3	LB4	LB5	LB6	LB7	LB8
Oxides (wt. %)								
SiO_2	0.87	0.00	0.11	0.00	0.67	33.82	18.69	35.83
Al_2O_3	0.25	0.00	0.01	0.00	0.24	10.11	5.73	10.24
Fe_2O_3	0.09	0.00	0.00	0.00	0.06	3.55	1.50	3.24
$MgCO_3$	5.97	2.61	3.52	2.44	6.30	2.49	2.86	2.70
$CaCO_3$	92.78	97.7	96.65	98.11	92.66	46.35	69.53	44.09
S	0.00	0.02	0.00	0.00	0.00	0.00	0.01	0.00
K_2O	0.04	0.00	0.00	0.00	0.04	1.77	0.86	2.07
TiO_2	0.01	0.00	0.00	0.00	0.01	0.70	0.29	0.63
MnO	0.00	0.09	0.02	0.01	0.03	0.05	0.01	0.02
P_2O_5	0.03	0.00	0.03	0.01	0.03	0.07	0.09	0.08
Total	100.04	100.42	100.34	100.57	100.04	98.91	99.57	98.90
CaO	51.90	54.70	54.10	54.90	51.89	25.96	38.94	24.70
MgO	3.52	1.54	2.10	1.44	3.72	1.47	1.69	1.59
Limestone quality	LP	HP	MP	HP	LP	Weathering Clay		
Trace element (ppm)								
Nb	0	0	0	0	0	40	12	27
Zr	127	719	111	98	666	547	142	428
Y	40	34	41	42	31	78	48	61
Sr	1306	8042	1226	1082	7761	456	497	377
Rb	44	41	42	47	38	147	67	120
Zn	0	0	0	2	0	82	16	55
Cu	12	6	16	11	2	40	18	32
Ni	0	0	0	0	0	51	6	34
Cr	18	0	0	11	1	132	49	109
Ce	0	26	0	26	14	116	12	135
Nd	0	0	0	0	0	32	10	45
V	18	14	11	11	9	160	54	135
La	12	4	0	18	8	49	30	26
Ti	321	188	204	250	186	6634	2050	5089
Ba	1	0	0	0	25	394	135	348
Sc	87	79	77	100	87	38	73	54

Table (A5.7) Chemical analysis for major and trace elements of the lower part of Benghazi Member Member (M. Mio.), Benghazi Cement Quarry.

Sample no.	UBA1	UBA2	UBA3L	UBA3U	UBB1	UBB2L	UBB2U	UBB2MUP
Oxides (wt. %)								
SiO_2	0.07	0.57	0.63	0.00	0.00	0.00	0.00	0.01
Al_2O_3	0.03	0.24	0.33	0.01	0.00	0.00	0.00	0.05
Fe_2O_3	0.03	0.03	0.05	0.00	0.00	0.00	0.00	0.04
$MgCO_3$	30.38	25.21	22.88	28.85	24.81	28.01	19.89	29.70
$CaCO_3$	67.21	72.03	74.25	68.95	73.81	70.22	78.98	67.78
S	0.03	0.03	0.02	0.04	0.02	0.04	0.02	0.07
K_2O	0.00	0.01	0.01	0.00	0.00	0.00	0.00	0.00
TiO_2	0.00	0.01	0.01	0.00	0.00	0.00	0.00	0.00
MnO	0.00	0.00	0.00	0.00	0.00	0.00	0.03	0.00
P_2O_5	0.12	0.18	0.30	0.20	0.24	0.17	0.17	0.31
Total	97.87	98.31	98.48	98.05	98.88	98.44	99.09	97.96
CaO	37.60	40.34	41.60	38.61	41.34	39.32	44.23	37.96
MgO	17.92	14.87	13.50	17.02	14.64	16.53	11.74	17.52
Limestone quality				Impure (I)				
Trace element (ppm)								
Nb	0	3	0	2	0	3	0	0
Zr	27	34	34	30	21	29	28	39
Y	42	43	46	43	44	42	40	45
Sr	279	274	261	310	226	291	265	373
Rb	44	45	43	43	41	45	45	45
Zn	0	6	0	0	0	0	0	0
Cu	12	19	11	9	18	29	31	12
Ni	0	0	0	0	0	0	0	0
Cr	17	17	14	24	21	13	18	32
Ce	0	14	30	36	1	0	18	0
Nd	0	0	18	8	0	0	7	0
V	16	18	16	7	11	1	18	25
La	21	11	0	13	0	9	0	0
Ti	255	322	316	226	169	188	173	223
Ba	0	0	0	0	8	0	0	0
Sc	46	62	48	67	67	70	71	45

Table (A5.8) Chemical analysis for major and trace elements of the middle part of Benghazi Member (M. Mio.), Ar Rajmah Quarry.

Sample no.	RQ1L	RQ1U	RQ2	RQ3
Oxides (wt. %)				
SiO_2	0.00	0.00	0.00	0.00
Al_2O_3	0.00	0.00	0.00	0.00
Fe_2O_3	0.00	0.00	0.00	0.00
$MgCO_3$	22.40	1.78	1.74	1.14
$CaCO_3$	76.19	99.05	99.03	99.67
S	0.05	0.00	0.00	0.00
K_2O	0.00	0.00	0.00	0.00
TiO_2	0.00	0.00	0.00	0.00
MnO	0.00	0.07	0.00	0.03
P_2O_5	0.10	0.00	0.00	0.00
Total	98.74	100.90	100.77	100.84
CaO	55.47	55.47	55.46	55.81
MgO	13.22	1.10	1.03	0.70
Limestone quality	I	VHP		
Trace element (ppm)				
Nb	3	8	1	3
Zr	69	64	45	56
Y	39	44	41	45
Sr	728	680	500	610
Rb	44	45	44	42
Zn	0	0	0	0
Cu	7	20	14	19
Ni	0	0	0	0
Cr	13	6	6	7
Ce	21	0	0	25
Nd	7	0	0	0
V	12	3	3	5
La	0	2	0	0
Ti	196	152	156	134
Ba	0	0	0	0
Sc	61	99	96	80

Table (A5.9) Chemical analysis for major and trace elements of the upper part of Benghazi Member (M. Mio.), Wadi Al-Faj Quarry.

X.1.2 Calculation of the proportion in the blend: (A5.10 – A5.14)

Table(A5.10); Shows the blend proportions (wt. %) for limestone (LB1), and weathering clay (LB6, LB7, and LB8), of lower Benghazi Member of Ar Rajmah Formation in Benghazi cement quarry;

Component	LB1	LB6	LB1	LB7	LB1	LB8
SiO_2	0.87	33.82	0.87	18.69	0.87	35.83
Al_2O_3	0.25	10.11	0.25	5.73	0.25	10.24
Fe_2O_3	0.09	3.55	0.09	1.5	0.09	3.24
$MgCO_3$	5.97	2.49	5.97	2.86	5.97	2.7
$CaCO_3$	92.78	46.35	92.78	69.53	92.78	44.09
S	0	0	0	0.01	0	0
K_2O	0.04	1.77	0.04	0.86	0.04	2.07
TiO_2	0.01	0.7	0.01	0.29	0.01	0.63
MnO	0	0.05	0	0.01	0	0.02
P_2O_5	0.03	0.07	0.03	0.09	0.03	0.08
Total	100.04	98.91	100.04	99.57	100.04	98.9
CaO	97.89	37.14	97.89	61.46	97.89	34.89
Al_2O_3	0.47	14.47	0.47	9.04	0.47	14.47
SiO_2	1.64	48.39	1.64	29.50	1.64	50.64
Proportions In blend	60	40	26.47	73.53	62.1	37.9

Table(A5.11); Shows the blend proportions (wt. %) for limestone (LB2, & LB3), and weathering clay (LB6, LB7, and LB8),, of lower Benghazi Member of Ar Rajmah Formation in Benghazi cement quarry;

Component	LB2	LB6	LB2	LB7	LB2	LB8
SiO_2	0	33.82	0	18.69	0	35.83
Al_2O_3	0	10.11	0	5.73	0	10.24
Fe_2O_3	0	3.55	0	1.5	0	3.24
$MgCO_3$	2.61	2.49	2.61	2.86	2.61	2.7
$CaCO_3$	97.7	46.35	97.7	69.53	97.7	44.09
S	0.02	0	0.02	0.01	0.02	0
K_2O	0	1.77	0	0.86	0	2.07
TiO_2	0	0.7	0	0.29	0	0.63
MnO	0.09	0.05	0.09	0.01	0.09	0.02
P_2O_5	0	0.07	0	0.09	0	0.08
Total	100.42	98.91	100.42	99.57	100.42	98.9
CaO	100	37.14	100	61.46	100	34.89
Al_2O_3	0	14.47	0	9.04	0	14.47
SiO_2	0	48.39	0	29.50	0	50.64
Proportions In blend	59	41	25.4	74.6	61.5	38.5

341

Continued of table (A5.11)

Component	LB3	LB6	LB3	LB7	LB3	LB8
SiO_2	0.11	33.82	0.11	18.69	0.11	35.83
Al_2O_3	0.01	10.11	0.01	5.73	0.01	10.24
Fe_2O_3	0	3.55	0	1.5	0	3.24
$MgCO_3$	3.52	2.49	3.52	2.86	3.52	2.7
$CaCO_3$	96.65	46.35	96.65	69.53	96.65	44.09
S	0	0	0	0.01	0	0
K_2O	0	1.77	0	0.86	0	2.07
TiO_2	0	0.7	0	0.29	0	0.63
MnO	0.02	0.05	0.02	0.01	0.02	0.02
P_2O_5	0.03	0.07	0.03	0.09	0.03	0.08
Total	100.32	98.91	100.32	99.57	100.32	98.9
CaO	99.78	37.14	99.78	61.46	99.78	34.89
Al_2O_3	0.02	14.47	0.02	9.04	0.02	14.47
SiO_2	0.20	48.39	0.20	29.50	0.20	50.64
Proportions In blend	60	40	25.9	74.1	61.5	38.5

Table(A5.12); Show the blend proportions (wt. %) for limestone (LB4, and LB5), and weathering clay (LB6, LB7, and LB8), of lower Benghazi Member of Ar Rajmah Formation in Benghazi cement quarry;

Component	LB4	LB6	LB4	LB7	LB4	LB8
SiO_2	0	33.82	0	18.69	0	35.83
Al_2O_3	0	10.11	0	5.73	0	10.24
Fe_2O_3	0	3.55	0	1.5	0	3.24
$MgCO_3$	2.44	2.49	2.44	2.86	2.44	2.7
$CaCO_3$	98.11	46.35	98.11	69.53	98.11	44.09
S	0	0	0	0.01	0	0
K_2O	0	1.77	0	0.86	0	2.07
TiO_2	0	0.7	0	0.29	0	0.63
MnO	0.01	0.05	0.01	0.01	0.01	0.02
P_2O_5	0.01	0.07	0.01	0.09	0.01	0.08
Total	100.57	98.91	100.57	99.57	100.57	98.9
CaO	100	37.14	100	61.46	100	34.89
Al_2O_3	0	14.47	0	9.04	0	14.47
SiO_2	0	48.39	0	29.50	0	50.64
Proportions In blend	58.3	41.7	23.1	76.3	61.5	38.5

Continued of table (A5.12)

Component	LB5	LB6	LB5	LB7	LB5	LB8
SiO_2	0.67	33.82	0.67	18.69	0.67	35.83
Al_2O_3	0.24	10.11	0.24	5.73	0.24	10.24
Fe_2O_3	0.06	3.55	0.06	1.5	0.06	3.24
$MgCO_3$	6.3	2.49	6.3	2.86	6.3	2.7
$CaCO_3$	92.66	46.35	92.66	69.53	92.66	44.09
S	0	0	0	0.01	0	0
K_2O	0.04	1.77	0.04	0.86	0.04	2.07
TiO_2	0.01	0.7	0.01	0.29	0.01	0.63
MnO	0.03	0.05	0.03	0.01	0.03	0.02
P_2O_5	0.03	0.07	0.03	0.09	0.03	0.08
Total	100.04	98.91	100.04	99.57	100.04	98.9
CaO	98.28	37.14	98.28	61.46	98.28	34.89
Al_2O_3	0.45	14.47	0.45	9.04	0.45	14.47
SiO_2	1.27	48.39	1.27	29.50	1.27	50.64
Proportions In blend	60	40	28.6	71.4	61.5	38.5

Table(A5.13); Show the blend proportions (wt. %) for each limestone samples (LB1, LB2, LB3, LB4, LB5), and the average of weathering clay (A), of lower Benghazi Member of Ar Rajmah Formation in Benghazi cement quarry;

Component	LB1	A	LB2	A	LB3	A	LB4	A	LB5	A
SiO_2	0.87	29.4	0	29.4	0.11	29.4	0	29.4	0.67	29.4
Al_2O_3	0.25	8.7	0	8.7	0.01	8.7	0	8.7	0.24	8.7
Fe_2O_3	0.09	2.8	0	2.8	0	2.8	0	2.8	0.06	2.8
$MgCO_3$	5.97	2.7	2.61	2.7	3.52	2.7	2.44	2.7	6.3	2.7
$CaCO_3$	92.78	53.3	97.7	53.3	96.65	53.3	98.11	53.3	92.66	53.3
S	0	0.003	0.02	0.003	0	0.003	0	0.003	0	0.003
K_2O	0.04	1.6	0	1.6	0	1.6	0	1.6	0.04	1.6
TiO_2	0.01	0.54	0	0.54	0	0.54	0	0.54	0.01	0.54
MnO	0	0.03	0.09	0.03	0.02	0.03	0.01	0.03	0.03	0.03
P_2O_5	0.03	0.08	0	0.08	0.03	0.08	0.01	0.08	0.03	0.08
Total	100.04	99.2	100.42	99.2	100.32	99.2	100.57	99.2	100.04	99.2
CaO	97.89	43.9	100	43.9	99.78	43.9	100	43.9	98.28	43.9
Al_2O_3	0.47	12.8	0	12.8	0.02	12.8	0	12.8	0.45	12.8
SiO_2	1.64	43.3	0	43.3	0.20	43.3	0	43.3	1.27	43.3
Proportions In blend	53.9	46.1	52.6	47.4	52.9	47.1	52.6	47.4	45.5	54.5

Table(A5.14); Show the blend proportions (wt. %) for the average of limestone samples (LB$_{Average}$), and the average of weathering clay (A), of lower Benghazi Member of Ar Rajmah Formation in Benghazi cement quarry;

Component	LB$_{Average}$	A
SiO$_2$	0.33	29.4
Al$_2$O$_3$	0.1	8.7
Fe$_2$O$_3$	0.03	2.8
MgCO$_3$	4.17	2.7
CaCO$_3$	95.58	53.3
S	0.004	0.003
K$_2$O	0.016	1.6
TiO$_2$	0.004	0.54
MnO	0.03	0.03
P$_2$O$_5$	0.02	0.08
Total	100.30	99.2
CaO	99.20	43.9
Al$_2$O$_3$	0.19	12.8
SiO$_2$	0.61	43.3
Proportions In blend	53.1	46.9

X.1.3 EPMA (EDS & WDS) results: (A5.15)

Table (A5.15) EPMA (EDS &WDS) carbonate analyses of Benghazi Member of Ar Rajmah Formation. (The total in these tables below includes; SiO_2, K_2O, SO, Al_2O_3, SrO,and Na_2O)

	UBA1								
CaO	28.33	29.67	29.03	27.03	27.06	50.27	28.61	29.21	27.24
MgO	16.17	16.17	15.98	16.08	14.69	0.355	16.13	15.73	15.94
MnO	0.00	0.00	0.009	0.043	0.031	0	0	0	0.031
FeO	0.075	0.075	0.005	0.013	0.005	0	0.10	0	0
Total	53.01	45.01	46.07	43.39	42.52	51.11	44.94	46.94	43.71
Number of ions on the basis of two (O) excluding CO_2									
Ca	1.12	1.14	1.14	1.09	1.14	1.98	1.12	1.14	1.10
Mg	0.88	0.86	0.86	0.91	0.86	0.02	0.88	0.86	0.90
Mn	0.00	0.00	0.00	0.002	0.00	0.00	0.002	0.00	0.00
Fe	0.00	0.002	0.00	0.00	0.001	0.00	0.00	0.00	0.00
Total	2.00	2.002	2.00	2.002	2.001	2.00	2.002	2.00	2.00
	UBB1								
CaO	55.12	57.93	29.13	29.40	26.35	28.68	56.86	33.65	30.99
MgO	0.279	0.628	16.03	15.95	15.45	15.76	0.49	7.249	18.51
MnO	0.00	0.00	0.009	0.023	0.025	0.044	0.049	0.00	0.007
FeO	0.00	0.102	0.031	0.013	0.00	0.00	0.009	0.105	0.048
Total	55.39	58.81	45.66	45.96	42.19	44.90	57.51	47.18	49.58
Number of ions on the basis of two (O) excluding CO_2									
Ca	1.99	1.96	1.13	1.14	1.10	1.13	1.98	1.54	1.09
Mg	0.01	0.04	0.87	0.86	0.90	0.87	0.02	0.46	0.91
Mn	0.00	0.00	0.00	0.00	0.001	0.001	0.001	0.00	0.00
Fe	0.00	0.002	0.001	0.00	0.00	0.00	0.001	0.00	0.00
Total	2.00	2.002	2.001	2.00	2.001	2.001	2.001	2.00	2.00
	LB2						RQ1		
CaO	0.00	0.00	40.19	39.84	40.36	29.12	32.64	54.07	26.51
SrO	49.46	50.80	0.078	0.073	0.107	0.133	0.059	0.052	0.055
MgO	0.006	0.007	0.733	0.579	0.683	21.62	13.09	5.974	12.88
FeO	0.004	0.026	0.023	0.00	0.00	0.145	0.088	0.00	0.035
MnO	0.011	0.00	0.008	0.013	0.001	0.004	0.033	0.066	0.055
Total	49.49	50.96	41.09	40.55	41.25	51.89	46.57	60.21	40.00
Number of ions on the basis of two (O) excluding CO_2									
Ca	0	0.00	1.95	1.96	1.94	1.55	1.30	1.73	1.19
Sr	1.998	1.99	0.003	0.003	0.003	0.003	0.002	0.002	0.003
Mg	0.00	0.001	0.05	0.04	0.05	0.44	0.72	0.27	0.81
Fe	0.00	0.002	0.001	0.00	0.00	0.00	0.002	0.00	0.001
Mn	0.00	0.00	0.00	0.001	0.00	0.003	0.00	0.002	0.003
Total	1.998	1.998	2.004	2.004	1.99	1.99	2.02	2.004	2.007

		LB4	
CaO	26.308	54.148	30.015
SrO	0.033	0.034	0.080
MgO	19.623	0.776	18.687
FeO	0.019	0.036	0.031
MnO	0.024	0.017	0.001
Total	46.188	55.070	49.005
Number of ions on the basis of two (O) excluding CO_2			
Ca	0.98	1.96	1.08
Sr	0.001	0.001	0.002
Mg	1.02	0.04	0.92
Fe	0.001	0.001	0.001
Mn	0.001	0.00	0.00
Total	2.003	2.003	2.003

X.1.4 SEM-EDX results: (A5. 16)

Table (A5.16) SEM carbonate Analyses of Benghazi Member of Ar Rajmah Formation, Apollonia Formation, and Shahhat Marl of Al Bayda Formation:

	LB2											
CaO	54.20	40.12	53.69	36.17	52.31	34.87	52.95	33.96	35.45	50.67	54.40	33.36
MgO	0.307	11.43	0.45	16.14	0.393	16.87	0.302	17.46	15.60	0.445	0.502	16.26
MnO	0.00	0.00	0.00	0.00	0.00	0.00	0.00	0.00	0.00	0.00	0.00	0.00
FeO	0.00	0.00	0.00	0.00	0.00	0.00	0.00	0.00	0.00	0.00	0.00	0.00
Total	54.69	52.28	54.26	52.83	52.77	51.97	53.53	52.36	52.11	51.64	55.20	50.67
Number of ions on the basis of two (O) excluding CO$_2$												
Ca	1.98	1.43	1.98	1.24	1.98	1.20	1.98	1.17	1.24	1.98	1.97	1.19
Mg	0.016	0.57	0.023	0.76	0.02	0.80	0.016	0.83	0.76	1.024	0.03	0.81
Mn	0.00	0.00	0.00	0.00	0.00	0.00	0.00	0.00	0.00	0.00	0.00	0.00
Fe	0.00	0.00	0.00	0.00	0.00	0.00	0.00	0.00	0.00	0.00	0.00	0.00
Total	1.996	2.00	2.003	2.00	2.00	2.00	1.996	2.00	2.00	2.004	2.00	2.00

											LB5	
CaO	33.70	54.97	57.30	53.71	34.05	31.48	54.54	33.20	54.20	51.98	53.32	53.09
MgO	16.02	0.452	0.444	0.378	16.30	15.73	0.414	13.97	0.548	0.498	0.275	0.368
MnO	0.00	0.00	0.00	0.00	0.00	0.00	0.00	0.00	0.00	0.00	0.00	0.00
FeO	0.00	0.00	0.00	0.00	0.00	0.242	0.00	0.28	0.00	0.00	0.00	0.00
Total	50.37	55.72	58.03	54.19	51.58	52.56	55.20	49.31	55.08	52.73	53.74	53.69
Number of ions on the basis of two (O) excluding CO$_2$												
Ca	1.61	1.98	1.98	1.98	1.21	1.18	1.98	1.25	1.97	1.97	1.99	1.98
Mg	0.39	0.02	0.02	0.02	0.78	0.82	0.02	0.74	0.03	0.03	0.01	0.02
Mn	0.00	0.00	0.00	0.00	0.00	0.00	0.00	0.00	0.00	0.00	0.00	0.00
Fe	0.00	0.00	0.00	0.00	0.00	0.01	0.00	0.08	0.00	0.00	0.00	0.00
Total	2.00	2.00	2.00	2.00	2.00	2.01	2.00	1.998	2.00	2.00	2.00	2.00

CaO	33.34	34.07	33.48	33.09	34.11	32.73	51.53	50.28	51.84	32.92	33.90	30.97
MgO	15.83	14.44	15.61	15.25	15.78	13.77	0.308	1.507	0.337	15.79	15.25	13.23
MnO	0.00	0.00	0.00	0.00	0.00	0.00	0.00	0.00	0.00	0.00	0.00	0.00
FeO	0.00	0.00	0.00	0.26	0.00	0.00	0.00	0.00	0.463	0.00	0.00	0.00
Total	49.93	49.63	49.96	49.89	50.77	47.47	52.05	52.01	52.75	50.09	49.98	47.02
Number of ions on the basis of two (O) excluding CO$_2$												
Ca	1.20	1.26	1.20	1.21	1.22	1.28	1.98	1.92	1.97	1.20	1.22	1.25
Mg	0.80	0.74	0.79	0.78	0.78	0.72	0.02	0.8	0.02	0.80	0.78	0.75
Mn	0.00	0.00	0.00	0.00	0.00	0.00	0.00	0.00	0.00	0.00	0.00	0.00
Fe	0.00	0.00	0.00	0.01	0.00	0.00	0.00	0.00	0.01	0.00	0.00	0.00
Total	2.00	2.00	2.00	2.00	2.00	2.00	2.00	2.00	2.00	2.00	2.00	2.00

(The total in these tables above includes; SiO_2, K_2O, SO_3, Al_2O_3, and Na_2O)

												UBA1
CaO	33.00	33.48	33.49	41.41	33.21	42.61	32.28	34.56	34.12	50.29	51.18	54.91
MgO	15.80	15.20	14.93	7.114	14.74	8.044	14.93	13.62	3.20	0.67	0.377	0.88
MnO	0.00	0.00	0.00	0.00	0.00	0.00	0.00	0.00	0.00	0.00	0.00	0.00
FeO	0.00	0.00	0.00	0.00	0.00	0.00	0.00	0.00	0.00	0.00	0.00	0.00
Total	49.59	49.09	49.09	49.40	48.68	51.28	48.26	48.64	37.89	51.08	51.69	56.01
Number of ions on the basis of two (O) excluding CO_2												
Ca	1.20	1.22	1.32	1.61	1.23	1.58	1.22	1.29	1.72	1.96	1.98	1.96
Mg	0.80	0.78	0.77	0.39	0.77	0.42	0.78	0.71	0.28	0.04	0.02	0.04
Mn	0.00	0.00	0.00	0.00	0.00	0.00	0.00	0.00	0.00	0.00	0.00	0.00
Fe	0.00	0.00	0.00	0.00	0.00	0.00	0.00	0.00	0.00	0.00	0.00	0.00
Total	2.00	2.00	2.00	2.00	2.00	2.00	2.00	2.00	2.00	2.00	2.00	2.00

CaO	28.80	29.61	31.74	31.94	26.12	31.11	55.99	51.78	52.70	51.87	31.15	32.07
MgO	18.12	16.27	17.95	18.06	15.84	19.18	1.033	0.945	0.629	0.703	18.13	17.28
MnO	0.00	0.00	0.00	0.00	0.00	0.00	0.00	0.00	0.00	0.00	0.00	0.00
FeO	0.19	0.00	0.00	0.00	0.00	0.00	0.00	0.00	0.00	0.00	0.00	0.00
Total	48.33	47.45	51.00	51.28	42.28	51.10	57.16	52.94	53.44	52.67	50.33	50.39
Number of ions on the basis of two (O) excluding CO_2												
Ca	1.06	1.14	1.12	1.12	1.10	1.07	1.95	1.95	1.97	1.96	1.11	1.14
Mg	0.94	0.86	0.88	0.88	0.91	0.93	0.06	0.05	0.03	0.04	0.89	0.86
Mn	0	0.00	0.00	0.00	0.00	0.00	0.00	0.00	0.00	0.00	0.00	0.00
Fe	0.006	0.00	0.00	0.00	0.00	0.00	0.00	0.00	0.00	0.00	0.00	0.00
Total	2.006	2.00	2.00	2.00	2.01	2.00	2.01	2.00	2.00	2.00	2.00	2.00

CaO	30.19	31.01	29.21	30.33	29.48	30.63	31.79	32.25	29.32	31.59	29.78	30.10
MgO	21.12	16.63	18.15	17.26	18.06	18.11	18.02	16.94	16.40	17.91	19.07	18.31
MnO	0.00	0.00	0.00	0.00	0.00	0.00	0.00	0.00	0.00	0.00	0.00	0.00
FeO	0.00	0.00	0.00	0.00	0.00	0.00	0.00	0.00	0.00	0.00	0.00	0.192
Total	52.38	49.57	48.22	48.46	48.26	50.06	50.60	50.36	46.51	50.29	49.37	49.40
Number of ions on the basis of two (O) excluding CO_2												
Ca	1.02	1.15	1.07	1.11	1.08	1.10	1.12	1.16	1.12	1.12	1.06	1.09
Mg	0.98	0.85	0.93	0.89	0.89	0.90	0.88	0.84	0.88	0.88	0.94	0.91
Mn	0.00	0.00	0.00	0.00	0.00	0.00	0.00	0.00	0.00	0.00	0.00	0.00
Fe	0.00	0.00	0.00	0.00	0.00	0.00	0.00	0.00	0.00	0.00	0.00	0.006
Total	2.00	2.00	2.00	2.00	2.00	2.00	2.00	2.00	2.00	2.00	2.00	2.006

(The total in these tables above includes; SiO_2, K_2O, SO_3, Al_2O_3, and Na_2O)

					UBA3U							
CaO	31.05	32.50	31.09	31.04	52.46	47.82	44.76	52.47	51.61	51.91	41.82	41.20
MgO	18.15	16.38	17.13	18.66	0.418	0.575	0.432	0.385	0.735	0.371	0.80	0.65
MnO	0.00	0.00	0.00	0.00	0.00	0.00	0.00	0.00	0.00	0.00	0.00	0.00
FeO	0.00	0.00	0.00	0.00	0.00	0.00	0.00	0.00	0.00	0.00	0.584	0.661
Total	49.99	49.66	49.29	50.11	52.97	48.55	48.55	52.95	52.62	52.50	53.02	51.98
Number of ions on the basis of two (O) excluding CO_2												
Ca	1.10	1.16	1.13	1.09	1.98	1.97	1.97	1.96	1.96	1.98	1.93	1.92
Mg	0.90	0.84	0.87	0.91	0.02	0.03	0.03	0.04	0.04	0.02	0.05	0.05
Mn	0.00	0.00	0.00	0.00	0.00	0.00	0.00	0.00	0.00	0.00	0.00	0.00
Fe	0.00	0.00	0.00	0.00	0.00	0.00	0.00	0.00	0.00	0.00	0.02	0.02
Total	2.00	2.00	2.00	2.00	2.00	2.00	2.00	2.00	2.00	2.00	2.00	1.99

										UBB2 MUP		
CaO	32.71	31.17	30.96	31.11	30.93	31.32	31.77	29.40	29.75	41.81	47.58	38.36
MgO	15.71	16.64	15.99	15.69	16.13	16.01	16.13	18.16	17.42	11.03	11.05	2.39
MnO	0.00	0.00	0.00	0.00	0.00	0.00	0.00	0.00	0.00	0.00	0.00	0.00
FeO	0.00	0.00	0.00	0.00	0.00	0.00	0.00	0.00	0.00	0.00	0.00	0.00
Total	49.18	48.67	48.17	47.35	48.23	48.68	48.83	48.33	47.74	53.19	59.22	52.48
Number of ions on the basis of two (O) excluding CO_2												
Ca	1.20	1.15	1.16	1.17	1.16	1.17	1.18	1.07	1.10	1.47	1.52	1.37
Mg	0.80	0.85	0.84	0.83	0.84	0.83	0.82	0.93	0.90	0.53	0.48	0.63
Mn	0.00	0.00	0.00	0.00	0.00	0.00	0.00	0.00	0.00	0.00	0.00	0.00
Fe	0.00	0.00	0.00	0.00	0.00	0.00	0.00	0.00	0.00	0.00	0.00	0.00
Total	2.00	2.00	2.00	2.00	2.00	2.00	2.00	2.00	2.00	2.00	2.00	2.00

CaO	29.60	28.68	29.68	31.40	27.98	31.28	29.68	28.51	28.59	29.43	28.58	28.5
MgO	16.93	16.81	15.39	14.97	14.82	15.19	14.89	15.79	15.78	15.65	15.39	15.68
MnO	0.00	0.00	0.00	0.00	0.00	0.00	0.00	0.00	0.00	0.00	0.00	0.00
FeO	0.00	0.00	0.224	0.00	0.31	0.00	0.00	0.00	0.00	0.00	0.00	0.00
Total	47.58	46.69	46.21	47.50	45.12	47.32	45.50	44.95	45.36	46.29	45.20	45.04
Number of ions on the basis of two (O) excluding CO_2												
Ca	1.10	1.16	1.20	1.15	1.19	1.18	1.13	1.13	1.14	1.15	1.15	1.13
Mg	0.90	0.84	0.80	0.85	0.81	0.82	0.87	0.87	0.85	0.85	0.85	0.87
Mn	0.00	0.00	0.00	0.00	0.00	0.00	0.00	0.00	0.00	0.00	0.00	0.00
Fe	0.00	0.00	0.00	0.00	0.00	0.00	0.00	0.00	0.00	0.00	0.00	0.00
Total	2.00	2.00	2.00	2.00	2.00	2.00	2.00	2.00	1.99	2.00	2.00	2.00

(The total in these tables above includes; SiO_2, K_2O, SO_3, Al_2O_3, and Na_2O)

	UBB2											AH
CaO	28.92	28.10	28.17	28.49	28.84	46.58	46.38	46.47	48.06	46.41	46.66	52.32
MgO	15.74	15.46	15.47	16.20	15.59	0.34	0.79	0.604	0.261	0.248	0.552	0.69
MnO	0.00	0.00	0.00	0.00	0.00	0.00	0.00	0.00	0.00	0.00	0.00	0.00
FeO	0.00	0.00	0.00	0.00	0.00	0.00	0.00	0.00	0.00	0.00	0.00	0.00
Total	45.44	44.80	44.88	45.61	45.62	47.05	47.31	47.32	48.40	46.96	47.33	53.63
Number of ions on the basis of two (O) excluding CO_2													
Ca	1.14	1.14	1.14	1.12	1.13	1.98	1.95	1.96	1.98	1.98	1.97	1.922
Mg	0.86	0.86	0.86	0.88	0.87	0.02	0.05	0.04	0.02	0.02	0.03	0.035
Mn	0.00	0.00	0.00	0.00	0.00	0.00	0.00	0.00	0.00	0.00	0.00	0.00
Fe	0.00	0.00	0.00	0.00	0.00	0.00	0.00	0.00	0.00	0.00	0.00	0.00
Total	2.00	2.00	2.00	2.00	2.00	2.00	2.00	2.00	2.00	2.00	2.00	1.957

						SUP					ST	
CaO	52.60	52.21	50.60	51.65	49.35	51.92	51.37	44.64	48.61	49.54	49.29	49.50
MgO	0.323	0.09	1.12	0.18	0.544	0.771	0.674	0.42	0.464	0.15	0.33	0.66
MnO	0.00	0.00	0.00	0.00	0.00	0.00	0.00	0.00	0.00	0.00	0.00	0.00
FeO	0.00	0.201	0.00	0.00	0.00	0.00	0.00	0.43	0.00	0.00	0.00	0.00
Total	53.02	53.69	52.16	52.20	50.68	52.95	52.37	49.93	49.18	50.39	50.21	50.16
Number of ions on the basis of two (O) excluding CO_2													
Ca	1.97	1.92	1.904	1.95	1.91	1.93	1.93	1.65	1.96	1.96	1.94	1.95
Mg	0.012	0.05	0.06	0.01	0.04	0.04	0.04	0.022	0.03	0.01	0.02	0.04
Mn	0.00	0.00	0.00	0.00	0.00	0.00	0.00	0.00	0.00	0.00	0.00	0.00
Fe	0.00	0.01	0.00	0.00	0.00	0.00	0.00	0.012	0.00	0.00	0.00	0.00
Total	2.01	1.98	1.964	1.96	1.95	1.97	1.97	1.70	1.99	1.97	1.96	1.99

CaO	48.90	49.64	49.51	48.56	48.97							
MgO	0.291	0.17	0.40	0.58	0.543							
MnO	0.00	0.00	0.00	0.00	0.00							
FeO	0.00	0.00	0.00	0.00	0.212							
Total	49.41	50.05	50.20	49.14	49.86							
Number of ions on the basis of two (O) excluding CO_2													
Ca	1.95	1.97	1.94	1.95	1.94							
Mg	0.02	0.01	0.02	0.03	0.03							
Mn	0.00	0.00	0.00	0.00	0.00							
Fe	0.00	0.00	0.00	0.00	0.01							
Total	1.97	1.98	1.96	1.98	1.98							

(The total in these tables above includes; SiO_2, K_2O, SO_3, Al_2O_3, and Na_2O)

X.2 Clay mineralogy and geochemistry

X.2.1 Surface area method test: (A8.1)

Appendix 8.1: 2 – ethoxyethanol (ethylene glycol monoethyl ether [EGME]) surface area method test (British Geological Survey)

Equipment and reagents:

Rotary vacuum pump (e.g. Edwards model 5 single rotary pump)

Analytical balance, 200 g capacity, 0.1 mg readability

2 glass or Polycarbonate vacuum desiccators, small, approx. 15 cm in diameter including desiccant tray with a perforated cover

10 Aluminium weighing dishes, 6 cm diameter, labelled 1, 2, 3, 4, 5 & A, B, C, D, E

Dropper pipette

8 – 16 meshed, fused, granular anhydrous calcium chloride ($CaCl_2$), desiccant, GPR grade (ground to < 100 mesh and stored in an airtight container; can be recycled after use by placing in 105°C oven)

Anhydrous phosphorous pentoxide (P_2O_5), GPR grade

2 – ethoxyetnanol (ethylene glycol monoethyl ether, EGME), Analar quality

Control sample – Pure Ca-montmorillonite standard.

Method:

1 – Weigh aluminium dish to four figures. Record weight (M1). Add approximately 1.1 g of clay. Record weight (M2). Repeat this operation for a further four clay samples, including the control sample (in dish No. 3 or C).

2 - Place approx. 70 g of anhydrous phosphorous pentoxide in the tray of the first desiccator and replace desiccant tray cover. Arrange the five aluminium dishes in order (1, 2, 3, 4, 5 or A, B, C, D, E) around the circumference of the tray cover. Replace desiccator lid ensuring that no dishes are placed directly below air inlet valve.

3 – Evacuate for approx. 45 minutes and allow standing for 3-4 hours.

4 – Gradually release vacuum by SLOWLY opening air-inlet. Weigh dishes as quickly as possible (M3, 1st weighing). Replace immediately in desiccator and arrange the dishes in order 3, 4, 5, 1, 2, (or C, D, E, A, B) so that the control sample is in the first position. Evacuate for approx. 45 minutes and stand overnight under vacuum.

5 – Next morning, gradually release vacuum and rapidly weigh dishes again (M3, 2nd weighing). Immediately after weighing, add approx. 3 ml of EGME reagent to the dry clay in each dish and transfer samples to second desiccator containing dry calcium chloride desiccant. Arrange dishes in original order around circumference of the desiccant tray cover. Replace desiccator lid and allow standing for 1-1/2 hours. Evacuate for approx. 15 minutes with air-ballast setting of vacuum pump turned on, then evacuate for a further 45 minutes with the air ballast turned off. Allow to stand overnight under vacuum

6 – Next morning, gradually release vacuum and weigh dishes rapidly (M4).

Calculation:

Surface area = $[(M4 - M3_{lowest})/(M3_{lowest} - M1)]/K$

M1   Weight of dish (g)

M2   Weight of dish + sample (g)

M3   Weight of dish + dry sample (1st weighing) (g)*

M3   Weight of dish + dry sample (2nd weighing) (g)*

M4   Weight of dish + dry sample + 2-ethoxyethanol (g)

K   Weight of EGME required to form a monolayer over 1 m^2 of surface

      = 2.86×10^{-4} g/m^2

*   Select lowest value of M3

Moisture content (%) = $[(M2 - M3_{lowest})/(M2 - M1)]^{\times}100$

The weight results of Umm Ar Razam, Al Fatayah clays (Crude), and Control sample Pure Ca-montmorillonite (Standard).

Sample no.	M1 (g)	M2 (g)	M3 (1st) (g)	M3 (2nd) (g)	M4 (g)
Umm Ar Razam					
US	46.30	47.40	47.29	47.28	47.40
UL	46.50	47.60	47.49	47.49	47.60
UM	47.40	48.50	48.40	48.39	48.50
UU	46.61	47.71	47.61	47.60	47.72
Al Fatayah					
LF1	46.49	47.59	47.48	47.47	47.61
Control sample					
Pure Ca-montmorillonite	46.34	47.44	47.32	47.29	47.47

The weight results of Umm Ar Razam, Al Fatayah clays (grain size ranging from < 2 μm to > 0.5 μm), and Control sample pure Ca-montmorillonite.

Sample no.	M1 (g)	M2 (g)	M3 (1st) (g)	M3 (2nd) (g)	M4 (g)
Umm Ar Razam					
US	46.31	47.41	47.34	47.34	47.47
UL	46.50	47.60	47.53	47.53	47.66
UM	47.40	48.50	48.43	48.41	48.54
UU	46.61	47.71	47.63	47.62	47.75
Al Fatayah					
LF1	46.49	47.59	47.51	47.50	47.64
Control sample					
Pure Ca-montmorillonite	46.34	47.44	47.33	47.29	47.46

X.2.2 Swelling test: (A8.2)

Appendix 8.2: Laboratory procedure for bentonite swelling test (British Geological Survey)

Equipment & reagents:

Analytical balance, 0.01 g readability, 200 g capacity

6 watch glasses

6 10 ml measuring cylinders

Filter funnel

Drying oven (60 °C)

Spatula

Anhydrous sodium carbonate (Na_2CO_3), analytical grade

Distilled / deionised water

Method:

1. Take six 4g portions of <125 μm dry clay, and to five of these add 1, 2, 3, 4, 5, and 6% by weight of sodium carbonate. Gently grind the clays to mix in the sodium, add 15 ml distilled water and mix to a paste.

2. Dry at 60°C in oven overnight.

3. Crush the clay gently and screen through 500 and 250 μm. Weigh out 1 g of 500 – 250 μm material onto a watch glass.

4. Fill a 10 ml measuring cylinder to the mark with distilled water and place a filter funnel in the neck so that the tip is about 1 cm from the surface of the water.

5. Divide the clay sample roughly into 8 portions with a spatula and slowly add one portion every 5 minutes.

6. After each addition, lightly tap the bottom of the cylinder to settle the clay. The final surface of the clay should be level.

7. Leave the sample for 24 hours and read the volume of the clay to the nearest 0.1 ml. Multiply the result by 10. Samples of good bentonite should swell in excess of 10 ml. In such cases, addition of clay should be stopped when the swollen clay approaches the 9 ml mark. The amount of clay left is then weighed and the swelling volume for the total 1 g calculated.

Notes:

The relative quantities of clay and Na_2CO_3 required to obtain 1, 2, 3, 4, 5, & 6% concentrations in 4 g of material are as follows:

% Na_2CO_3	Wt. of Na_2CO_3 (g)	Wt. of clay (g)
0	0	4
1	0.04	3.96
2	0.08	3.92
3	0.12	3.88
4	0.16	3.84
5	0.20	3.80
6	0.24	3.76

The following tables below illustrate the measuring of the swollen clay of Umm Ar Razam and Al Fatayah quarries.

Sample no.US of Umm Ar Razam quarry of Al Faidiyah Fm.

Item	% Na_2CO_3	Wt.of Na_2CO_3 (g)	Wt.of clay(g)	Before 24 hrs (ml)	After 24 hrs (ml)	Swelling volume (ml)
1	0	0	4	4.00	4.00	-
2	1	0.04	3.96	6.3	6.3	-
3	2	0.08	3.92	6.00	6.00	-
4	3	0.12	3.88	6.00	6.00	-
5	4	0.16	3.84	6.00	6.00	-
6	5	0.20	3.80	7.00	7.1	1
7	6	0.24	3.76	6.9	7.00	1

Sample no.UL of Umm Ar Razam quarry of Al Faidiyah Fm.

Item	% Na_2CO_3	Wt.of Na_2CO_3 (g)	Wt.of clay(g)	Before 24 hrs (ml)	After 24 hrs (ml)	Swelling volume (ml)
1	0	0	4	5.5	5.5	-
2	1	0.04	3.96	6.5	6.5	-
3	2	0.08	3.92	8.1	8.1	-
4	3	0.12	3.88	7.2	7.2	-
5	4	0.16	3.84	8.00	8.00	-
6	5	0.20	3.80	7.00	7.05	0.5
7	6	0.24	3.76	6.6	6.7	1

Sample no.UM of Umm Ar Razam quarry of Al Faidiyah Fm.

Item	% Na_2CO_3	Wt.of Na_2CO_3 (g)	Wt.of clay(g)	Before 24 hrs (ml)	After 24 hrs (ml)	Swelling volume (ml)
1	0	0	4	4.5	4.5	-
2	1	0.04	3.96	7.2	7.2	-
3	2	0.08	3.92	7.00	7.00	-
4	3	0.12	3.88	7.1	7.1	-
5	4	0.16	3.84	6.7	6.7	-
6	5	0.20	3.80	6.1	6.1	-
7	6	0.24	3.76	6.00	6.00	-

Sample no.UU of Umm Ar Razam quarry of Al Faidiyah Fm.

Item	% Na_2CO_3	Wt.of Na_2CO_3 (g)	Wt.of clay(g)	Before 24 hrs (ml)	After 24 hrs (ml)	Swelling volume (ml)
1	0	0	4	4.5	4.5	-
2	1	0.04	3.96	5.00	5.00	-
3	2	0.08	3.92	6.00	6.00	-
4	3	0.12	3.88	6.00	6.00	-
5	4	0.16	3.84	5.5	5.5	-
6	5	0.20	3.80	6.8	6.8	-
7	6	0.24	3.76	6.8	6.8	-

Sample no. LF1 of Al Fatayah quarry of Al Faidiyah Fm.

Item	% Na_2CO_3	Wt.of Na_2CO_3 (g)	Wt.of clay(g)	Before 24 hrs (ml)	After 24 hrs (ml)	Swelling volume (ml)
1	0	0	4	2.5	2.5	-
2	1	0.04	3.96	7	7	-
3	2	0.08	3.92	7.7	7.8	1
4	3	0.12	3.88	8.2	8.2	-
5	4	0.16	3.84	8.00	8.00	-
6	5	0.20	3.80	9.6	9.6	-
7	6	0.24	3.76	8.9	8.9	-

X.2.3 Cation exchange capacity test: (A8.3)

Appendix 8.3: Cation exchange capacity ($BaCl_2/MgSO_4$ method; British Geological Survey)

Equipment and reagents:

250 ml wide-necked polythene bottle

250 ml measuring cylinder

5 ml pipette

100 ml pipette

Magnetic stirring plate + magnetic followers

pH meter (+pH calibration solutions)

Analytical balance, 200 g capacity, 0.1 mg readability

100 ml conical flask

50 ml burette

100 ml stoppered flask/bottle

PTFE/glass rod

Distilled or deionised water

Triethanolamine, general purpose reagent (GPR) quality

Barium chloride dihydrate ($BaCl_2.2H_2O$), analytical (Analar) quality

Magnesium sulphate heptahydrate ($MgSO_4.7 H_2O$), Analar quality

Ammonium chloride, Analar quality

Ammonia '880' solution (specific gravity 0.88)

Solochrome black 6B

Concentrated hydrochloric acid (HCl) solution, Analar quality

Di-sodium EDTA (ethylene-diamine-tetra-acetic-acid), Analar quality

Preparation of solutions:

1. Dilute (2M) HCl solution: slowly add 18 ml of concentrated HCl to 75 ml of distilled water (caution: DO NOT dilute by adding water to concentrated acid, always dilute by adding concentrated acid to water). Dilute to 100 ml with more deionised water.

2. Triethanolamine solution: dilute 90 ml of triethanolamine to 1 litre with distilled water. Add dilute (2M) HCl (approx. 180 ml) until a pH of 8.1 is obtained and dilute to 2 litres with distilled water.

3. 1 M barium chloride solution: dissolve 244 g of $BaCl_2.3H_2O$ in 1 litre of distilled water.

4. Buffered barium chloride solution: mix equal volumes of barium chloride and triethanolamine solutions.

5. 0.02 M EDTA solution: dissolve 3.723 g of disodium EDTA in 1 litre of distilled water, or use ampoules of concentrated EDTA solution available commercially (e.g. BDH Convol) and dilute according to the manufacturer's instructions.

6. Ammonia buffer: dissolve 7 g of ammonium chloride in 57 ml of ammonia '880' solution, and make up to 100 ml with distilled water (caution: carry out in a fume cupboard and DO NOT inhale fumes from ammonia '880' solution).

7. Indicator: dissolve 0.25 g of Solochrome Black 6B in 50 ml of ethanol.

8. Prepare 0.05 M $MgSO_4$ solution by dissolving 6.0195 g $MgSO_4$ in 1L deionised water.

Method:

1. Weigh 5 g of sample into a 250 ml polythene bottle and add a magnetic follower.

2. Note weight of bottle and contents (M1).

3. Add 100 ml of buffered barium chloride solution and agitate mixture for 1 hour on a magnetic stirring plate. Ensure that all the sample is dispersed – it may be necessary to dislodge some of the sample using a PTFE/glass rod. This stage can be omitted if samples are non-calcareous and non-saline.

4. Centrifuge at 1500 rpm for 15 minutes and discard the supernatant (if it is difficult to remove the majority of the solution by decantation then remove by a suction method instead).

5. Add a further 200 ml buffered barium chloride solution, agitate the mixture for 1 hour on magnetic stirring plate and then leave overnight.

6. Centrifuge at 1500 rpm for 15 minutes and discard the supernatant.

7. Add 200 ml of distilled water and agitate for a few minutes on a magnetic stirring plate. Centrifuge at 1500 rpm for 15 minutes and discard the supernatant.

8. Note weight of bottle and contents (M2).

9. Pipette 100 ml of $MgSO_4$ solution into the bottle, mix well and leave for approximately 2 hours, occasionally agitating on magnetic stirring plate.

10. Centrifuge at 1500 rpm for 15 minutes and decant the supernatant into a stoppered flask or bottle.

11. Pipette a 5 ml aliquot of this solution into a 100 ml conical beaker and add 5 ml of ammonia buffer, plus 6 drops of indicator.

12. Titrate with standard EDTA (titre A1 ml).

13. Titrate a 5 ml aliquot of 0.05 M $MgSO_4$ solution (titre B ml). The end-point is indicated by a blue to pink colour change.

Calculation:

The titration end-point (A1) must be corrected for the volume of residual water (retained by the sample after washing with distilled water). The corrected value (A2) can then be used to calculate the CEC value.

$$CEC = 8\ (B - A2) = \quad meq/100\ g$$

M1: weight of bottle plus dry contents (g)

M2: weight of bottle plus wet contents (g)

A2: corrected end-point = $[A1*(100+M2-M1)]/100$ ml

A1: titration end-point of sample (ml)

B: titration end-point of $MgSO_4$ solution (ml)

CEC values of Faidia Clay Member of Al Faidiyah Formation

Sample code	M1 (g)	M2 (g)	M2-M1	A1 (ml)	A2 (ml)	CEC (meq/100g)
Blank	46.273	49.433	3.16	24.15	24.91	2.32
UU	51.246	69.153	17.907	15.05	17.75	59.60
UM	52.114	70.648	18.534	15.80	18.73	51.76
UL	51.435	64.208	12.773	15.35	17.31	63.12
US	51.134	71.186	20.052	15.30	18.37	54.64
US/A	51.258	70.203	18.945	15.35	18.26	55.54
LF1	51.769	72.474	20.705	15.75	19.01	49.52

X.2.4 XRD results: (A8.4)

Table (A 8.4) Peak identification of clay minerals of Faidia clay Member, Al Faidiyah

        Formation (U. Oligocen-L. Miocene)

Sample No.	d (Å)				Clay Mineral	Remarks		
	Untreated	Glyco.	Heated			Size (μm)	Sequences	Location
			350°C	550°C				
UU	14.58	17.03	9.98	9.96	Smectite	<2.0 to >0.5	Upper	Umm Ar-Razam Quarry
	17.17	17.17	17.17	-	Kaolinite			
	3.53	-	3.53	3.52	Chlorite			
UU	15.1	17.39	9.97	9.8	Smectite	<0.5		
	17.17	17.17	17.17	-	Kaolinite			
	-	-	3.52	3.52	Chlorite			
UM	14.6	17.0	9.87	9.91	Smectite	<2.0 to >0.5		
	7.16	7.16	7.14	-	Kaolinite			
	-	3.52	3.52	3.52	Chlorite			
UM	14.0	17.55	9.93	10.06	Smectite	<0.5		
	7.16	7.16	7.16	-	Kaolinite			
	-	-	3.52	-	Chlorite			
UL	15.04	17.1	9.83	9.99	Smectite	<2.0 to >0.5		
	17.17	17.17	17.17	-	Kaolinite			
	-	-	-	3.51	Chlorite			
UL	15.35	17.41	9.97	9.90	Smectite	<0.5		
	7.16	7.16	7.16	-	Kaolinite			
	-	-	3.52	3.52	Chlorite			
US	14.89	17.33	9.95	9.79	Smectite	<2.0 to >0.5		
	7.16	7.16	7.17	-	Kaolinite			
	3.52	-	3.52	-	Chlorite			
US	14.85	17.52	9.89	9.85	Smectite	<0.5		
	17.17	17.17	17.17	-	Kaolinite			
	-	-	-	3.52	Chlorite			
LF1	15.31	17.44	9.9	10.04	Smectite	<2.0 to >0.5	Lower	Al-Fatayah Quarry
	17.17	17.17	17.17	-	Kaolinite			
	3.52	3.52	3.52	3.52	Chlorite			
LF1	15.31	17.44	9.9	9.77	Smectite	<0.5		
	17.17	17.17	17.17	-	Kaolinite			
	3.53	3.52	3.51	3.53	Chlorite			

X.3 Mineralogy and mineral chemistry of celestite-bearing formations

X.3.1 EPMA analyses of strontium contents of the main components of Formations present in the study area: (A.9.1-A.9. 3)

Table (A.9.1) 1- Ar Rajmah Formation (Middle Miocene).

Location	Formation	Age	Mg (wt. %)	Ca (wt. %)	Sr (wt. %)	MgCO$_3$ (mole %)	Atom ratio Sr/Ca x 1000
			Coralline algae				
			10.990	23.994	0.025	37.972	0.467
			0.386	35.802	0.041	1.334	0.519
			11.196	23.909	0.041	38.682	0.777
			10.864	23.724	0.014	37.535	0.277
			2.975	30.894	0.028	10.277	0.413
			0.427	37.893	0.019	1.474	0.225
			0.298	36.761	0.027	1.029	0.337
Benghazi Cement Quarry			0.349	37.894	0.015	1.205	0.184
			0.700	38.982	0.031	2.417	0.367
			0.491	37.389	0.042	1.697	0.517
			0.416	39.424	0.036	1.436	0.412
			8.064	22.093	0.028	27.863	0.578
			0.275	37.244	0.014	0.951	0.177
			0.532	34.937	0.020	1.838	0.266
			0.208	33.919	0.018	0.720	0.239
		Middle Miocene	1.826	35.484	0.031	6.308	0.403
			0.306	39.443	0.059	1.058	0.686
			11.955	24.686	0.017	41.307	0.313
			12.709	23.964	0.025	43.911	0.484
	Ar Rajmah		12.490	24.057	0.042	43.155	0.804
			10.568	24.563	0.033	36.513	0.614
			10.277	24.640	0.040	35.509	0.738
Ar Rajmah Quarry			10.540	25.089	0.053	36.418	0.971
			0.416	36.639	0.037	1.436	0.465
			Echinoderm fragments				
			0.394	39.932	0.077	1.363	0.881
			0.376	40.655	0.069	1.298	0.780
			0.311	39.512	0.078	1.073	0.901
			0.523	39.642	0.103	1.808	1.190
			0.470	39.227	0.065	1.623	0.759
			0.138	40.828	0.110	0.477	1.232
Benghazi Cement Quarry			0.170	40.608	0.096	0.586	1.086
			0.232	39.219	0.068	0.802	0.799
			0.200	39.442	0.073	0.691	0.843
			0.326	39.694	0.085	1.128	0.984
			0.259	39.008	0.068	0.895	0.803
			0.311	40.493	0.093	1.075	1.051
			0.363	40.288	0.082	1.254	0.931
			0.304	40.542	0.084	1.050	0.945
			0.318	40.351	0.081	1.100	0.920

Continued of Table (A.9.1)

Location	Formation	Age	Mg (wt. %)	Ca (wt. %)	Sr (wt. %)	MgCO$_3$ (mole %)	Atom ratio Sr/Ca x 1000
			Foraminifera				
			0.146	40.341	0.019	0.506	0.211
			0.265	40.118	0.075	0.916	0.858
			0.234	37.264	0.029	0.809	0.353
			0.386	39.967	0.044	1.334	0.503
			6.655	30.615	0.043	22.995	0.644
			0.272	38.931	0.096	0.939	1.123
			0.326	39.930	0.083	1.126	0.949
			0.264	39.869	0.087	0.911	0.999
			0.363	39.566	0.080	1.256	0.929
			0.215	39.860	0.065	0.741	0.747
			0.370	38.214	0.037	1.277	0.445
			0.315	38.849	0.054	1.088	0.637
			0.146	39.479	0.059	0.504	0.686
			0.254	38.589	0.046	0.878	0.541
			0.193	37.374	0.058	0.668	0.714
			0.305	39.668	0.040	1.052	0.458
			0.230	38.817	0.057	0.796	0.668
			0.219	39.045	0.074	0.756	0.872
Benghazi Cement Quarry	Ar Rajmah	Middle Miocene	Matrix				
			0.195	40.891	0.027	0.674	0.303
			0.336	39.403	0.053	1.159	0.618
			10.356	25.174	0.091	35.782	1.659
			0.450	39.651	0.098	1.554	1.132
			0.390	38.786	0.050	1.346	0.588
			0.468	38.801	0.014	1.617	0.169
			0.444	39.497	0.002	1.533	0.020
			0.543	38.864	0.043	1.877	0.508
			11.235	23.391	0.014	38.816	0.281
			4.947	30.147	0.031	17.092	0.475
			0.270	39.916	0.120	0.932	1.376
			11.440	25.158	0.060	39.526	1.092
			0.464	42.523	0.022	1.602	0.237
			0.224	42.121	0.068	0.775	0.744
			0.181	40.319	0.018	0.626	0.201
			8.882	30.684	0.048	30.689	0.719
			8.535	29.496	0.042	29.488	0.656
			6.710	30.384	0.033	23.182	0.496

Continued of Table (A.9.1)

Location	Formation	Age	Mg (wt. %)	Ca (wt. %)	Sr (wt. %)	MgCO$_3$ (mole %)	Atom ratio Sr/Ca x 1000
Benghazi Cement Quarry	Ar Rajmah	Middle Miocene	Cement				
			0.441	39.564	0.002	1.525	0.020
			0.552	39.226	0.000	1.907	0.000
			0.302	39.157	0.000	1.044	0.000
			0.211	39.533	0.000	0.729	0.000
			0.205	41.259	0.000	0.708	0.000
			0.387	40.274	0.000	1.338	0.000
			0.175	42.288	0.000	0.605	0.000
			0.323	40.077	0.000	1.117	0.000
and			0.269	42.083	0.000	0.928	0.000
			0.652	39.664	0.011	2.253	0.127
			0.261	40.351	0.000	0.903	0.000
			0.472	41.449	0.000	1.630	0.000
			0.419	40.096	0.000	1.447	0.000
			0.213	41.900	0.000	0.737	0.000
			0.233	41.359	0.000	0.804	0.000
			0.320	39.905	0.000	1.105	0.000
Ar Rajmah Quarry			0.162	40.260	0.000	0.561	0.000
			0.332	39.932	0.000	1.149	0.000
			0.267	40.643	0.000	0.924	0.000
			0.346	42.357	0.000	1.197	0.000

Table (A.9.2) 2- Apollonia Formation (Lower to Middle Eocene).

Location	Formation	Age	Mg (wt. %)	Ca (wt. %)	Sr (wt. %)	MgCO$_3$ (mole %)	Atom ratio Sr/Ca x 1000
Bachor Quarry	Apollonia	Lower to Middle Eocene	Matrix				
			0.177	40.231	0.007	0.611	0.077
			0.382	40.923	0.185	1.319	2.070
			0.137	39.759	0.265	0.473	3.045
			0.364	40.799	0.216	1.258	2.427
			0.252	39.288	0.118	0.869	1.368
			0.264	38.096	0.076	0.914	0.914
			0.302	40.019	0.353	1.044	4.040
			0.229	39.765	0.266	0.790	3.054
			0.297	37.575	0.091	1.025	1.112
			0.264	40.844	0.183	0.914	2.055
			0.299	40.679	0.022	1.033	0.247
			Cement				
			0.323	39.909	0.208	1.115	2.384
			0.363	39.774	0.282	1.256	3.248
			Forams				
			0.385	39.929	0.144	1.329	1.647
			0.518	41.395	0.240	1.789	2.654
			0.276	39.276	0.138	0.953	1.605
			0.336	39.658	0.518	1.159	5.969
			Coralline algae				
			0.275	39.605	0.008	0.951	0.088
			0.249	39.271	0.036	0.859	0.414
			0.249	39.350	0.041	0.861	0.482
			Echinoderm fragments				
			0.398	40.037	0.288	1.376	3.285
			0.352	39.570	0.249	1.216	2.874
			0.373	40.150	0.372	1.287	4.239
			0.411	40.066	0.234	1.420	2.674

Table (A.9.3) 3- Darnah Formation (Middle to Upper Eocene).

Location	Formation	Age	Mg (wt. %)	Ca (wt. %)	Sr (wt. %)	MgCO₃ (mole %)	Atom ratio Sr/Ca x 1000
Shahhat Susah road-cut	Darnah	Middle to Upper Eocene	Echinoid fragments					
			0.208	40.774	0.024	0.718	0.266
			0.130	40.629	0.035	0.449	0.390
			0.095	41.034	0.004	0.330	0.047
			0.212	41.338	0.037	0.731	0.412
			0.209	40.775	0.004	0.722	0.047
			0.232	39.973	0.019	0.800	0.223
			0.337	40.446	0.019	1.166	0.210
			0.227	40.964	0.027	0.785	0.302
			0.221	40.779	0.122	0.764	1.366
			0.157	40.484	0.041	0.544	0.468
			0.081	41.092	0.000	0.279	0.000
			0.246	40.750	0.048	0.848	0.541
			0.208	33.752	0.000	0.720	0.000
			0.652	36.275	0.074	2.253	0.928
			0.189	37.473	0.014	0.653	0.175
			1.043	37.491	0.130	3.604	1.589
			1.017	36.841	0.049	3.515	0.609
			0.647	38.060	0.147	2.234	1.768
			0.342	38.843	0.067	1.182	0.787
			0.401	37.809	0.052	1.384	0.624
			1.647	36.630	0.118	5.689	1.478
			0.528	37.255	0.004	1.823	0.052
			0.084	40.321	0.003.	0.292	0.029
			0.100	37.251	0.003	0.347	0.031
			1.774	38.987	0.178	6.130	2.093
			Forams					
			0.125	39.906	0.021	0.433	0.242
			0.172	39.261	0.028	0.594	0.325
			0.130	40.483	0.015	0.449	0.172
			0.065	40.446	0.011	0.225	0.124
			0.179	40.856	0.007	0.617	0.076
			0.117	39.259	0.000	0.405	0.000
			0.120	38.776	0.000	0.416	0.000
			0.089	37.709	0.000	0.307	0.000
			0.156	39.486	0.030	0.540	0.343
			0.197	40.089	0.002	0.680	0.019
			0.133	40.158	0.000	0.460	0.000
			0.101	40.106	0.019	0.349	0.212
			Coralline algae					
			0.212	40.389	0.004	0.733	0.048
			0.114	39.242	0.000	0.393	0.000
			0.300	40.685	0.029	1.035	0.323
			0.189	39.956	0.018	0.653	0.203
			Matrix					
			0.159	40.846	0.035	0.550	0.388
			0.125	40.984	0.019	0.433	0.217
			0.209	40.733	0.003	0.722	0.038
			0.167	39.272	0.034	0.575	0.394

Continued of Table (A.9.3)

Location	Formation	Age	Mg (wt. %)	Ca (wt. %)	Sr (wt. %)	MgCO$_3$ (mole %)	Atom ratio Sr/Ca x 1000
Shahhat Susah road-cut	Darnah	Middle to Upper Eocene	Cement				
			0.112	36.656	0.016	0.386	0.200
			0.112	37.515	0.000	0.386	0.000
			0.066	35.899	0.000	0.229	0.000
			0.077	36.891	0.002	0.265	0.021
			0.129	40.626	0.071	0.445	0.800
			0.088	40.031	0.000	0.302	0.000
			0.238	39.505	0.014	0.821	0.166
			0.110	39.597	0.000	0.380	0.000
			0.070	37.647	0.237	0.242	2.877
			0.035	35.724	0.107	0.122	1.364
			0.096	36.565	0.000	0.332	0.000

X.3.2 EPMA results: (A.9.4-A.9.17)

	Foraminifera				AH Coralline algae				Echinoderm fragments			

Oxides (wt. %)	Foraminifera				χ	σ	AH — Coralline algae			χ	σ	Echinoderm fragments				χ	σ
P₂O₅	0.024	0.036	0.01	0.054			0.010	0.010	0.008			0.044	0.012	0.012	0.046		
SO₃	0.012	0.048	0.015	0.000			0.117	0.088	0.078			0.032	0.123	0.077	0.057		
TiO₂	0.000	0.000	0.000	0.014			0.000	0.010	0.000			0.009	0.000	0.010	0.000		
MgO	0.633	0.852	0.454	0.552			0.453	0.409	0.410			0.655	0.579	0.613	0.676		
CaO	55.901	57.953	54.987	55.521			55.447	54.980	55.090			56.052	55.398	56.21	56.092		
MnO	0.000	0.000	0.002	0.000			0.000	0.000	0.001			0.000	0.000	0.000	0.000		
FeO	0.000	0.000	0.014	0.019			0.037	0.101	0.013			0.000	0.009	0.000	0.001		
NiO	0.033	0.041	0.000	0.026			0.000	0.000	0.000			0.007	0.024	0.029	0.020		
CuO	0.000	0.011	0.000	0.037			0.012	0.000	0.020			0.000	0.000	0.041	0.047		
SrO	0.170	0.284	0.163	0.612	0.310	0.210	0.009	0.042	0.049	0.033	0.021	0.340	0.294	0.440	0.277	0.338	0.073
BaO	0.001	0.018	0.000	0.000			0.000	0.007	0.000			0.000	0.000	0.000	0.000		
Na₂O	0.054	0.039	0.030	0.013			0.043	0.075	0.048			0.058	0.122	0.065	0.107		
K₂O	0.007	0.006	0.013	0.003			0.040	0.037	0.015			0.011	0.012	0.016	0.014		
Total	56.835	59.288	55.688	56.851			56.168	55.759	55.732			57.208	56.573	57.513	57.337		

Numbers of ions on the basis of 6 O excluding CO₂

Ions	Foraminifera				AH — Coralline algae			Echinoderm fragments			
P	0.002	0.003	0.001	0.004	0.001	0.001	0.001	0.004	0.001	0.001	0.004
S	0.001	0.004	0.001	0.000	0.011	0.008	0.007	0.003	0.011	0.007	0.005
Ti	0.000	0.000	0.000	0.001	0.000	0.001	0.000	0.001	0.000	0.001	0.000
Mg	0.093	0.120	0.068	0.081	0.067	0.061	0.061	0.095	0.085	0.089	0.098
Ca	5.882	5.841	5.913	5.863	5.898	5.898	5.911	5.863	5.858	5.856	5.850
Mn	0.000	0.000	0.000	0.000	0.000	0.000	0.000	0.000	0.000	0.000	0.000
Fe	0.000	0.000	0.001	0.002	0.003	0.008	0.001	0.000	0.001	0.000	0.000
Ni	0.003	0.003	0.000	0.002	0.000	0.000	0.001	0.001	0.002	0.002	0.002
Cu	0.000	0.001	0.000	0.003	0.001	0.000	0.001	0.000	0.000	0.003	0.003
Sr	0.010	0.016	0.010	0.035	0.001	0.002	0.003	0.019	0.017	0.025	0.016
Ba	0.000	0.001	0.000	0.000	0.000	0.000	0.000	0.000	0.000	0.000	0.000
Na	0.010	0.007	0.006	0.002	0.008	0.015	0.009	0.011	0.023	0.012	0.020
K	0.001	0.001	0.002	0.000	0.005	0.005	0.002	0.001	0.002	0.002	0.002
Total	6.002	5.997	6.002	5.993	5.995	5.999	5.996	5.998	6.000	5.998	6.000

Table (A.9.4) High resolution EPMA analyses and structure formulae of foraminifera, coralline algae and echinoderm fragments of the Apollonia Formation (Lower to Middle Eocene).

Table (A.9.5) High resolution EPMA analyses and structure formulae of matrix and cement of the Apollonia Formation (Lower to Middle Eocene).

Oxides (wt. %)	Matrix											χ	σ	Cement		χ	σ
P₂O₅	0.014	0.036	0.040	0.053	0.075	0.077	0.036	0.061	0.063	0.046	0.022			0.065	0.034		
SO₃	0.000	0.070	0.015	0.033	0.082	0.127	0.036	0.108	0.135	0.000	0.033			0.102	0.017		
TiO₂	0.006	0.000	0.001	0.013	0.000	0.032	0.013	0.004	0.016	0.005	0.000			0.008	0.000		
MgO	0.291	0.628	0.225	0.599	0.414	0.435	0.497	0.376	0.488	0.435	0.492			0.531	0.598		
CaO	56.323	57.292	55.663	57.118	55.003	53.335	56.026	55.671	52.605	57.182	56.950			55.872	55.683		
MnO	0.000	0.000	0.010	0.009	0.000	0.000	0.019	0.000	0.000	0.000	0.000			0.000	0.000		
FeO	0.000	0.000	0.000	0.009	0.046	0.066	0.000	0.000	0.080	0.000	0.006			0.011	0.012		
NiO	0.015	0.002	0.000	0.013	0.000	0.000	0.009	0.019	0.000	0.020	0.017			0.000	0.002		
CuO	0.000	0.000	0.001	0.000	0.000	0.009	0.015	0.005	0.037	0.000	0.000			0.013	0.022		
SrO	0.008	0.219	0.313	0.256	0.139	0.090	0.418	0.314	0.108	0.217	0.026	0.192	0.129	0.246	0.334	0.29	0.062
BaO	0.000	0.000	0.000	0.000	0.000	0.000	0.000	0.005	0.000	0.021	0.000			0.000	0.000		
Na₂O	0.000	0.070	0.000	0.013	0.028	0.060	0.060	0.000	0.115	0.025	0.000			0.019	0.044		
K₂O	0.000	0.003	0.003	0.008	0.035	0.036	0.018	0.009	0.058	0.006	0.006			0.005	0.000		
Total	56.657	58.320	56.271	58.124	55.822	54.267	57.147	56.572	53.705	57.957	57.552			56.872	56.746		

Numbers of ions on the basis of 6 O excluding CO₂

	Matrix													Cement			
P	0.001	0.003	0.003	0.004	0.006	0.007	0.003	0.005	0.006	0.004	0.002			0.005	0.003		
S	0.000	0.006	0.001	0.003	0.008	0.012	0.003	0.010	0.013	0.000	0.003			0.009	0.002		
Ti	0.000	0.000	0.000	0.001	0.000	0.002	0.001	0.000	0.001	0.000	0.000			0.001	0.000		
Mg	0.043	0.090	0.033	0.086	0.062	0.067	0.072	0.055	0.076	0.063	0.071			0.078	0.088		
Ca	5.952	5.872	5.936	5.877	5.890	5.867	5.878	5.891	5.850	5.910	5.915			5.871	5.876		
Mn	0.000	0.000	0.001	0.001	0.000	0.000	0.002	0.000	0.000	0.000	0.000			0.000	0.000		
Fe	0.000	0.000	0.000	0.001	0.004	0.006	0.000	0.000	0.007	0.000	0.001			0.001	0.001		
Ni	0.001	0.000	0.000	0.001	0.000	0.000	0.001	0.002	0.000	0.002	0.001			0.000	0.000		
Cu	0.000	0.000	0.000	0.000	0.000	0.001	0.001	0.000	0.003	0.000	0.001			0.000	0.000		
Sr	0.000	0.012	0.018	0.014	0.008	0.005	0.024	0.018	0.006	0.012	0.000			0.014	0.019		
Ba	0.000	0.000	0.000	0.000	0.000	0.000	0.000	0.000	0.000	0.001	0.000			0.000	0.000		
Na	0.000	0.013	0.000	0.002	0.005	0.012	0.011	0.000	0.023	0.005	0.000			0.004	0.008		
K	0.000	0.000	0.000	0.001	0.004	0.005	0.002	0.001	0.008	0.001	0.001			0.001	0.000		
Total	5.997	5.996	5.992	5.991	5.987	5.984	5.998	5.982	5.993	5.998	5.995			5.985	5.999		

Oxides (wt. %)	Coralline algae				χ	σ	Matrix				χ	σ
P₂O₅	0.057	0.026	0.022	0.024			0.000	0.024	0.016	0.004		
SO₃	0.045	0.007	0.022	0.000			0.000	0.000	0.034	0.039		
TiO₂	0.013	0.000	0.013	0.007			0.001	0.001	0.004	0.003		
MgO	0.349	0.187	0.493	0.311			0.262	0.206	0.344	0.274		
CaO	56.545	54.939	56.959	55.939			57.185	57.378	57.026	54.981		
MnO	0.018	0.002	0.000	0.000			0.000	0.000	0.000	0.000		
FeO	0.000	0.014	0.000	0.000			0.003	0.014	0.000	0.005		
NiO	0.026	0.032	0.000	0.000			0.005	0.005	0.010	0.000		
CuO	0.000	0.000	0.000	0.006			0.000	0.029	0.022	0.001		
SrO	0.005	0.000	0.034	0.021	0.015	0.016	0.041	0.023	0.004	0.04	0.027	0.017
BaO	0.000	0.008	0.000	0.001			0.000	0.000	0.015	0.000		
Na₂O	0.000	0.034	0.000	0.000			0.033	0.000	0.065	0.011		
K₂O	0.004	0.010	0.000	0.000			0.000	0.005	0.015	0.005		
Total	57.062	55.259	57.543	56.309			57.530	57.680	57.555	55.363		

Numbers of ions on the basis of 6 O excluding CO_2

	Coralline algae						Matrix					
P	0.005	0.002	0.002	0.002			0.000	0.002	0.001	0.000		
S	0.004	0.001	0.002	0.000			0.000	0.000	0.003	0.004		
Ti	0.001	0.000	0.001	0.000			0.000	0.000	0.000	0.000		
Mg	0.051	0.028	0.071	0.046			0.038	0.030	0.050	0.041		
Ca	5.923	5.957	5.916	5.946			5.956	5.960	5.930	5.946		
Mn	0.001	0.000	0.000	0.000			0.000	0.000	0.000	0.000		
Fe	0.000	0.001	0.001	0.000			0.000	0.001	0.000	0.000		
Ni	0.002	0.003	0.000	0.000			0.000	0.000	0.001	0.000		
Cu	0.000	0.000	0.000	0.000			0.000	0.002	0.002	0.000		
Sr	0.000	0.000	0.002	0.001			0.002	0.001	0.000	0.002		
Ba	0.000	0.000	0.000	0.000			0.000	0.000	0.001	0.000		
Na	0.000	0.007	0.000	0.000			0.006	0.000	0.012	0.002		
K	0.001	0.001	0.000	0.000			0.000	0.000	0.002	0.001		
Total	5.988	6.000	5.994	5.995			6.002	5.996	6.002	5.996		

Figure (A.9.6) High resolution EPMA analyses and structure formulae of coralline algae and matrix of the Darnah Formation (Middle and Upper Eocene).

Oxides (wt. %)	DE1 Foraminifera								x̄	σ
P_2O_5	0.030	0.000	0.047	0.091	0.000	0.059	0.000	0.004		
SO_3	0.028	0.031	0.015	0.007	0.000	0.055	0.040	0.012		
TiO_2	0.014	0.000	0.018	0.008	0.001	0.010	0.000	0.001		
MgO	0.206	0.283	0.214	0.107	0.294	0.193	0.198	0.146		
CaO	55.868	54.966	56.676	56.625	57.198	54.962	54.287	52.793		
MnO	0.000	0.009	0.028	0.000	0.000	0.000	0.000	0.000		
FeO	0.012	0.000	0.000	0.000	0.000	0.000	0.009	0.000		
NiO	0.013	0.008	0.005	0.022	0.007	0.003	0.009	0.000		
CuO	0.002	0.013	0.016	0.000	0.000	0.000	0.002	0.000		
SrO	0.025	0.033	0.018	0.013	0.008	0.000	0.000	0.000	0.012	0.125
BaO	0.000	0.012	0.002	0.007	0.000	0.000	0.000	0.000		
Na_2O	0.053	0.005	0.049	0.008	0.000	0.015	0.039	0.043		
K_2O	0.003	0.003	0.007	0.002	0.003	0.005	0.006	0.001		
Total	56.254	55.363	57.095	56.890	57.511	55.302	54.590	53.000		
Numbers of ions on the basis of 6 O excluding CO_2										
P	0.002	0.000	0.004	0.008	0.000	0.005	0.000	0.000		
S	0.003	0.003	0.001	0.001	0.000	0.005	0.004	0.001		
Ti	0.001	0.000	0.001	0.001	0.000	0.001	0.000	0.000		
Mg	0.030	0.043	0.031	0.016	0.043	0.029	0.030	0.023		
Ca	5.947	5.946	5.943	5.959	5.956	5.944	5.956	5.969		
Mn	0.000	0.001	0.002	0.000	0.000	0.000	0.000	0.000		
Fe	0.001	0.000	0.000	0.000	0.000	0.000	0.001	0.000		
Ni	0.001	0.001	0.000	0.002	0.001	0.000	0.001	0.000		
Cu	0.000	0.001	0.001	0.000	0.000	0.000	0.000	0.000		
Sr	0.001	0.002	0.001	0.001	0.000	0.000	0.000	0.000		
Ba	0.000	0.000	0.000	0.000	0.000	0.000	0.000	0.000		
Na	0.010	0.001	0.009	0.001	0.000	0.003	0.008	0.009		
K	0.000	0.000	0.001	0.000	0.000	0.001	0.001	0.000		
Total	5.996	5.998	5.994	5.989	6.000	5.988	6.001	6.002		

Table (A.9.7) High resolution EPMA analyses and structure formulae of Foraminifera of the Darnah Formation (Middle and Upper Eocene).

Oxides (wt. %) — DE1 — Echinoderm fragments

Oxides (wt. %)														χ	σ
P₂O₅	0.031	0.000	0.010	0.061	0.047	0.043	0.004	0.000	0.000	0.071	0.000	0.030	0.022		
SO₃	0.000	0.022	0.007	0.000	0.001	0.028	0.000	0.010	0.012	0.022	0.000	0.021	0.030		
TiO₂	0.000	0.025	0.000	0.000	0.007	0.000	0.004	0.011	0.019	0.013	0.000	0.001	0.000		
MgO	0.342	0.214	0.157	0.348	0.344	0.381	0.555	0.374	0.364	0.259	0.133	0.404	0.343		
CaO	57.083	56.881	57.447	57.873	57.085	55.962	56.625	57.350	57.091	56.677	57.529	57.050	47.253		
MnO	0.000	0.008	0.014	0.000	0.000	0.000	0.000	0.000	0.018	0.000	0.003	0.004	0.000		
FeO	0.001	0.000	0.015	0.002	0.003	0.000	0.025	0.017	0.000	0.006	0.000	0.000	0.000		
NiO	0.011	0.013	0.000	0.015	0.019	0.000	0.001	0.001	0.002	0.001	0.000	0.013	0.012		
CuO	0.032	0.000	0.001	0.023	0.005	0.000	0.000	0.000	0.000	0.014	0.000	0.000	0.000		
SrO	0.028	0.041	0.005	0.044	0.000	0.023	0.022	0.032	0.144	0.049	0.000	0.057	0.000	0.035	0.038
BaO	0.042	0.003	0.000	0.02	0.005	0.000	0.003	0.000	0.000	0.000	0.000	0.022	0.000		
Na₂O	0.000	0.028	0.005	0.000	0.005	0.056	0.000	0.030	0.000	0.000	0.039	0.021	0.048		
K₂O	0.000	0.001	0.000	0.008	0.000	0.010	0.012	0.003	0.000	0.000	0.012	0.003	0.010		
Total	57.570	57.236	57.661	58.394	57.516	56.503	57.250	57.828	57.650	57.112	57.716	57.626	47.718		

Numbers of ions on the basis of 6 O excluding CO_2

P	0.031	0.000	0.010	0.061	0.047	0.043	0.004	0.000	0.000	0.071	0.000	0.030	0.022		
S	0.000	0.022	0.007	0.000	0.001	0.028	0.000	0.010	0.012	0.022	0.000	0.021	0.030		
Ti	0.000	0.025	0.000	0.000	0.007	0.000	0.004	0.011	0.019	0.013	0.000	0.001	0.000		
Mg	0.342	0.214	0.157	0.348	0.344	0.381	0.555	0.374	0.364	0.259	0.133	0.404	0.343		
Ca	57.083	56.881	57.447	57.873	57.085	55.962	56.625	57.350	57.091	56.677	57.529	57.050	47.253		
Mn	0.000	0.008	0.014	0.000	0.000	0.000	0.000	0.000	0.018	0.000	0.003	0.004	0.000		
Fe	0.001	0.000	0.015	0.002	0.000	0.000	0.025	0.017	0.000	0.006	0.000	0.000	0.000		
Ni	0.011	0.013	0.000	0.015	0.003	0.000	0.000	0.001	0.002	0.001	0.000	0.013	0.012		
Cu	0.032	0.000	0.001	0.023	0.019	0.000	0.000	0.000	0.000	0.014	0.000	0.000	0.000		
Sr	0.028	0.041	0.005	0.044	0.005	0.023	0.022	0.032	0.144	0.049	0.000	0.057	0.000		
Ba	0.042	0.003	0.000	0.02	0.000	0.003	0.000	0.000	0.000	0.000	0.000	0.022	0.000		
Na	0.000	0.028	0.005	0.000	0.005	0.056	0.000	0.030	0.000	0.000	0.039	0.021	0.048		
K	0.000	0.001	0.000	0.008	0.000	0.010	0.012	0.003	0.000	0.000	0.012	0.003	0.010		
Total	57.570	57.236	57.661	58.394	57.516	56.503	57.250	57.828	57.650	57.112	57.716	57.626	47.718		

Table (A.9.8) High resolution EPMA analyses and structure formulae of echinoderm fragments of the Darnah Formation (Middle and Upper Eocene).

Oxides (wt. %)	DE5 Cement											χ	σ
P₂O₅	0.022	0.000	0.025	0.063	0.000	0.000	0.000	0.029	0.000	0.012	0.006		
SO₃	0.019	0.000	0.000	0.000	0.000	0.013	0.012	0.000	0.000	0.000	0.000		
TiO₂	0.000	0.000	0.000	0.000	0.000	0.000	0.000	0.01	0.000	0.001	0.000		
MgO	0.184	0.184	0.109	0.126	0.212	0.144	0.391	0.181	0.115	0.058	0.158		
CaO	51.319	52.521	50.258	51.647	56.877	56.043	55.307	55.436	52.706	50.014	51.191		
MnO	0.000	0.001	0.000	0.000	0.000	0.001	0.000	0.000	0.000	0.000	0.005		
FeO	0.000	0.000	0.011	0.006	0.005	0.027	0.025	0.012	0.027	0.000	0.000		
NiO	0.000	0.000	0.000	0.01	0.01	0.021	0.021	0.004	0.011	0.010	0.011		
CuO	0.000	0.000	0.000	0.021	0.025	0.003	0.003	0.006	0.000	0.000	0.000		
SrO	0.019	0.000	0.000	0.002	0.084	0.017	0.000	0.000	0.28	0.126	0.000	0.048	0.088
BaO	0.001	0.000	0.003	0.000	0.001	0.000	0.000	0.000	0.000	0.000	0.000		
Na₂O	0.011	0.000	0.000	0.000	0.046	0.057	0.000	0.000	0.000	0.000	0.000		
K₂O	0.002	0.000	0.003	0.010	0.025	0.003	0.006	0.006	0.007	0.004	0.000		
Total	51.577	52.706	50.409	51.885	57.285	56.288	55.782	55.684	53.146	50.225	51.371		
Numbers of ions on the basis of 6 O excluding CO_2													
P	0.002	0.000	0.002	0.006	0.000	0.000	0.000	0.002	0.000	0.001	0.001		
S	0.002	0.000	0.000	0.000	0.000	0.001	0.001	0.000	0.000	0.000	0.000		
Ti	0.000	0.000	0.000	0.000	0.000	0.000	0.000	0.001	0.000	0.000	0.000		
Mg	0.030	0.029	0.018	0.020	0.031	0.021	0.058	0.027	0.018	0.010	0.026		
Ca	5.959	5.971	5.975	5.962	5.955	5.968	5.934	5.963	5.961	5.978	5.972		
Mn	0.000	0.000	0.000	0.000	0.000	0.000	0.000	0.000	0.000	0.000	0.000		
Fe	0.000	0.000	0.001	0.001	0.000	0.002	0.002	0.001	0.002	0.000	0.000		
Ni	0.000	0.000	0.000	0.001	0.001	0.000	0.002	0.000	0.001	0.001	0.001		
Cu	0.000	0.000	0.000	0.002	0.002	0.002	0.000	0.000	0.000	0.000	0.000		
Sr	0.001	0.000	0.000	0.000	0.005	0.000	0.001	0.000	0.017	0.008	0.000		
Ba	0.000	0.000	0.000	0.000	0.000	0.000	0.000	0.000	0.000	0.000	0.000		
Na	0.002	0.000	0.000	0.000	0.009	0.011	0.000	0.000	0.000	0.000	0.000		
K	0.000	0.000	0.000	0.001	0.003	0.000	0.001	0.001	0.001	0.001	0.000		
Total	5.996	6.000	5.996	5.993	6.006	6.003	5.999	5.995	6.000	5.999	6.000		

Table (A.9.9) High resolution EPMA analyses and structure formulae of the cement of the Darnah Formation (Middle and Upper Eocene).

	DE5																			
Oxides (wt. %)	Echinoderm fragments												χ	σ	Foraminifera				χ	σ
P₂O₅	0.035	0.033	0.047	0.045	0.010	0.045	0.000	0.026	0.041	0.016	0.010	0.046			0.000	0.055	0.047	0.000		
SO₃	0.028	0.080	0.069	0.004	0.021	0.092	0.046	0.066	0.055	0.015	0.000	0.011			0.028	0.037	0.000	0.000		
TiO₂	0.000	0.001	0.02	0.000	0.005	0.000	0.000	0.005	0.000	0.004	0.000	0.02			0.014	0.003	0.012	0.000		
MgO	1.073	0.311	1.716	1.674	1.064	0.563	0.659	2.709	0.868	0.139	0.165	2.919			0.257	0.324	0.219	0.166		
CaO	50.785	52.462	52.488	51.577	53.284	54.380	52.932	51.282	52.157	56.450	52.152	54.582			55.281	56.124	56.221	56.149		
MnO	0.000	0.000	0.000	0.005	0.000	0.011	0.000	0.023	0.000	0.000	0.000	0.000			0.010	0.000	0.000	0.000		
FeO	0.016	0.095	0.033	0.019	0.028	0.050	0.000	0.020	0.020	0.000	0.022	0.011			0.010	0.000	0.017	0.006		
NiO	0.008	0.011	0.000	0.000	0.000	0.000	0.000	0.002	0.000	0.000	0.009	0.000			0.000	0.012	0.000	0.004		
CuO	0.000	0.039	0.000	0.035	0.011	0.000	0.000	0.000	0.000	0.000	0.000	0.000			0.000	0.000	0.000	0.000		
SrO	0.087	0.017	0.154	0.058	0.174	0.079	0.061	0.140	0.005	0.003	0.003	0.211			0.035	0.002	0.000	0.022	0.015	0.017
BaO	0.033	0.000	0.000	0.000	0.000	0.001	0.000	0.000	0.000	0.000	0.000	0.000	0.083	0.072	0.000	0.000	0.000	0.004		
Na₂O	0.089	0.022	0.093	0.024	0.383	0.057	0.157	0.359	0.122	0.000	0.011	0.132			0.026	0.011	0.000	0.008		
K₂O	0.009	0.004	0.014	0.009	0.027	0.019	0.007	0.012	0.012	0.008	0.010	0.011			0.017	0.010	0.000	0.001		
Total	52.163	53.075	54.634	53.450	55.007	55.297	53.862	54.393	53.517	56.635	52.382	57.943			55.678	56.578	56.516	56.360		
Numbers of ions on the basis of 6 O excluding CO₂																				
P	0.003	0.003	0.004	0.004	0.001	0.004	0.000	0.002	0.004	0.001	0.001	0.004			0.000	0.005	0.004	0.000		
S	0.003	0.008	0.007	0.000	0.002	0.009	0.004	0.006	0.005	0.001	0.000	0.001			0.003	0.003	0.000	0.000		
Ti	0.000	0.000	0.002	0.000	0.000	0.000	0.000	0.000	0.000	0.000	0.000	0.001			0.001	0.000	0.001	0.000		
Mg	0.170	0.049	0.259	0.258	0.161	0.085	0.102	0.408	0.134	0.021	0.026	0.413			0.038	0.048	0.032	0.025		
Ca	5.797	5.912	5.693	5.720	5.780	5.872	5.870	5.550	5.807	5.972	5.967	5.548			5.947	5.931	5.955	5.972		
Mn	0.000	0.000	0.000	0.000	0.000	0.001	0.000	0.000	0.000	0.000	0.000	0.000			0.001	0.000	0.000	0.000		
Fe	0.001	0.008	0.003	0.002	0.002	0.004	0.000	0.002	0.002	0.000	0.002	0.001			0.001	0.000	0.001	0.000		
Ni	0.001	0.001	0.000	0.000	0.000	0.000	0.000	0.000	0.000	0.000	0.001	0.000			0.000	0.000	0.000	0.000		
Cu	0.000	0.003	0.000	0.003	0.001	0.000	0.000	0.000	0.000	0.000	0.000	0.000			0.000	0.001	0.000	0.000		
Sr	0.005	0.001	0.009	0.004	0.010	0.005	0.004	0.008	0.000	0.000	0.000	0.012			0.002	0.000	0.000	0.001		
Ba	0.001	0.000	0.000	0.000	0.000	0.000	0.000	0.000	0.000	0.000	0.000	0.000			0.000	0.000	0.000	0.000		
Na	0.018	0.005	0.018	0.005	0.075	0.011	0.031	0.072	0.024	0.000	0.002	0.024			0.005	0.002	0.000	0.001		
K	0.001	0.001	0.002	0.001	0.004	0.002	0.001	0.002	0.002	0.001	0.001	0.002			0.002	0.001	0.000	0.000		
Total	6.000	5.991	5.997	5.997	6.036	5.993	6.012	6.002	6.026	5.996	6.000	6.005			6.000	5.991	5.993	5.999		

Table (A.9.10) High resolution EPMA analyses and structure formulae of the echinoderm fragments and foraminifera of the Darnah Formation (Middle and Upper Eocene).

Coralline algae

Oxides (wt. %)	LB1				χ	σ	LB3			χ	σ
P$_2$O$_5$	-	-	-	-			0.012	0.022	0.041		
SO$_3$	0.233	0.113	0.121				0.142	0.064	0.045		
TiO$_2$	0.000	0.000	0.018	0.010			0.004	0.000	0.000		
MgO	18.082	0.635	18.420	17.874			4.894	0.702	0.490		
CaO	33.592	50.123	33.473	33.213			43.251	53.050	51.465		
MnO	0.000	0.000	0.000	0.000			0.013	0.000	0.000		
FeO	0.027	0.001	0.016	0.014			0.000	0.000	0.055		
NiO	-	-	-	-			0.000	0.030	0.000		
CuO	-	-	-	-			0.001	0.000	0.020		
SrO	0.029	0.048	0.048	0.017	0.036	0.015	0.033	0.022	0.032	0.029	0.006
BaO	-	-	-	-			0.000	0.000	0.000		
Na$_2$O	0.125	0.038	0.099	0.079			0.027	0.000	0.093		
K$_2$O	00.053	0.030	0.002	0.000			0.010	0.000	0.034		
Total	52.142	50.987	52.199	51.456			48.387	53.890	52.275		

Numbers of ions on the basis of 6 O excluding CO$_2$

	LB1						LB3				
P	-	-	-	-			0.001	0.002	0.004		
S	-	-	-	-			0.015	0.006	0.004		
Ti	0.000	0.000	0.001	0.001			0.000	0.000	0.000		
Mg	2.561	0.104	2.595	2.564			0.811	0.108	0.078		
Ca	3.420	5.887	3.389	3.425			5.149	5.871	5.883		
Mn	0.000	0.000	0.000	0.000			0.001	0.000	0.000		
Fe	0.002	0.000	0.001	0.001			0.000	0.000	0.005		
Ni	-	-	-	-			0.000	0.003	0.000		
Cu	-	-	-	-			0.000	0.000	0.002		
Sr	0.002	0.003	0.003	0.001			0.002	0.001	0.002		
Ba	-	-	-	-			0.000	0.000	0.000		
Na	0.023	0.008	0.018	0.015			0.006	0.000	0.019		
K	0.006	0.004	0.000	0.000			0.001	0.000	0.005		
Total	6.015	6.006	6.008	6.007			5.986	5.991	6.002		

Table (A.9.11) High resolution EPMA analyses and structure formulae of coralline algae of the Ar-Rajmah Formation (Middle Miocene).

Continued of Table(A.9.11)

Oxides (wt. %)	LB4				χ	σ	LB5 Coralline algae						χ	σ	UBA3 U			χ	σ
P_2O_5	0.039	0.073	0.018	0.055			0.049	0.000	0.006	0.042	0.004	0.021			0.080	0.120	0.060		
SO_3	0.052	0.090	0.070	0.058			0.139	0.049	0.050	0.102	0.054	0.044			0.240	0.250	0.260		
TiO_2	0.011	0.007	0.002	0.000			0.006	0.000	0.000	0.002	0.002	0.000			0.000	0.020	0.000		
MgO	0.574	1.151	0.808	0.684			13.268	0.453	0.875	0.343	3.004	0.504			19.670	20.910	20.550		
CaO	53.051	54.575	52.344	55.194			30.930	52.141	48.912	47.486	49.678	55.220			34.560	33.550	33.680		
MnO	0.001	0.000	0.024	0.026			0.005	0.013	0.069	0.002	0.021	0.000			0.000	0.010	0.000		
FeO	0.002	0.035	0.023	0.000			0.041	0.000	0.000	0.000	0.066	0.000			0.030	0.020	0.000		
NiO	0.000	0.002	0.000	0.017			0.000	0.000	0.002	0.000	0.000	0.000			0.000	0.010	0.020		
CuO	0.023	0.000	0.000	0.000			0.000	0.000	0.003	0.005	0.000	0.000			0.000	0.000	0.000		
SrO	0.018	0.037	0.050	0.042	0.037	0.014	0.014	0.017	0.024	0.021	0.037	0.070	0.034	0.019	0.020	0.030	0.050	0.033	0.015
BaO	0.000	0.007	0.000	0.000			0.000	0.000	0.000	0.000	0.000	0.000			0.000	0.000	0.000		
Na_2O	0.000	0.009	0.065	0.013			0.096	0.014	0.020	0.148	0.008	0.025			0.110	0.100	0.090		
K_2O	0.002	0.006	0.005	0.000			0.014	0.000	0.013	0.034	0.021	0.001			0.000	0.010	0.000		
Total	53.773	55.992	53.409	56.089			44.595	52.687	49.974	48.185	52.895	55.885			54.700	55.020	54.690		
Numbers of ions on the basis of 6 O excluding CO_2																			
P	0.003	0.006	0.002	0.005			0.005	0.000	0.001	0.004	0.000	0.002			0.006	0.009	0.004		
S	0.005	0.008	0.007	0.005			0.015	0.005	0.005	0.011	0.005	0.004			0.020	0.021	0.021		
Ti	0.001	0.001	0.000	0.000			0.001	0.000	0.000	0.000	0.000	0.000			0.000	0.001	0.000		
Mg	0.089	0.170	0.125	0.101			2.220	0.071	0.145	0.059	0.464	0.075			2.622	2.750	2.725		
Ca	5.888	5.790	5.843	5.869			3.719	5.915	5.831	5.887	5.512	5.906			3.311	3.171	3.210		
Mn	0.000	0.000	0.002	0.002			0.000	0.001	0.007	0.000	0.002	0.000			0.000	0.001	0.000		
Fe	0.000	0.003	0.002	0.000			0.004	0.000	0.000	0.000	0.006	0.000			0.002	0.001	0.000		
Ni	0.000	0.000	0.000	0.001			0.000	0.000	0.000	0.000	0.000	0.000			0.000	0.001	0.001		
Cu	0.002	0.000	0.000	0.000			0.001	0.001	0.002	0.001	0.000	0.004			0.000	0.000	0.000		
Sr	0.001	0.002	0.003	0.002			0.002	0.003	0.004	0.001	0.002	0.005			0.001	0.001	0.002		
Ba	0.000	0.000	0.000	0.000			0.000	0.000	0.000	0.000	0.000	0.000			0.000	0.001	0.001		
Na	0.000	0.002	0.013	0.002			0.021	0.003	0.004	0.033	0.002	0.005			0.019	0.018	0.016		
K	0.000	0.001	0.001	0.000			0.002	0.000	0.002	0.005	0.003	0.000			0.000	0.001	0.000		
Total	5.989	5.983	5.998	5.987			5.990	5.996	5.997	6.000	5.996	5.996			5.981	5.975	5.979		

Echinoderm fragments

Oxides (wt. %)	LB1			χ	σ	LB3		χ	σ	LB5						χ	σ
P2O5	-	-	-			0.020	0.043			0.084	0.025	0.033	0.025	0.087	0.000		
SO3	0.049	0.000	0.036			0.033	0.106			0.031	0.000	0.044	0.000	0.047	0.026		
TiO2	0.000	0.000	0.000			0.000	0.000			0.005	0.001	0.006	0.000	0.000	0.003		
MgO	0.649	0.618	0.511			0.861	0.773			0.227	0.279	0.382	0.329	0.537	0.426		
CaO	55.905	56.917	55.317			55.499	54.918			57.159	56.851	54.906	55.219	55.572	54.611		
MnO	0.000	0.000	0.000			0.011	0.009			0.000	0.000	0.000	0.000	0.005	0.000		
FeO	0.000	0.000	0.006			0.011	0.000			0.000	0.029	0.036	0.000	0.000	0.000		
NiO	-	-	-			0.016	0.006			0.004	0.011	0.003	0.008	0.016	0.000		
CuO	-	-	-			0.004	0.000			0.009	0.023	0.000	0.023	0.000	0.015		
SrO	0.091	0.082	0.092	0.088	0.005	0.122	0.077	0.100	0.032	0.130	0.114	0.081	0.086	0.101	0.081	0.099	0.020
BaO	-	-	-			0.024	0.000			0.005	0.000	0.022	0.027	0.000	0.000		
Na2O	0.083	0.010	0.037			0.014	0.059			0.007	0.019	0.017	0.031	0.043	0.033		
K2O	0.074	0.000	0.039			0.001	0.005			0.000	0.002	0.019	0.007	0.000	0.007		
Total	56.849	57.640	56.037			56.616	55.996			57.661	57.354	55.549	55.755	56.408	55.202		
Numbers of ions on the basis of 6 O excluding CO_2																	
P	-	-	-			0.002	0.004			0.007	0.002	0.003	0.002	0.007	0.000		
S	-	-	0.000			0.003	0.010			0.003	0.000	0.004	0.000	0.004	0.003		
Ti	0.000	0.000	0.000			0.000	0.000			0.000	0.000	0.000	0.000	0.000	0.000		
Mg	0.095	0.089	0.076			0.126	0.114			0.033	0.041	0.057	0.049	0.079	0.064		
Ca	5.887	5.905	5.912			5.851	5.845			5.934	5.941	5.915	5.933	5.882	5.921		
Mn	0.000	0.000	0.000			0.001	0.001			0.000	0.000	0.000	0.000	0.000	0.000		
Fe	0.000	0.000	0.001			0.001	0.000			0.000	0.002	0.003	0.000	0.000	0.000		
Ni	-	-	-			0.001	0.000			0.000	0.001	0.000	0.001	0.001	0.000		
Cu	-	-	-			0.000	0.000			0.001	0.002	0.000	0.002	0.000	0.001		
Sr	0.005	0.005	0.005			0.007	0.004			0.007	0.006	0.005	0.005	0.006	0.005		
Ba	-	-	-			0.001	0.000			0.000	0.000	0.001	0.001	0.000	0.000		
Na	0.016	0.002	0.007			0.003	0.011			0.001	0.004	0.003	0.006	0.008	0.007		
K	0.009	0.000	0.005			0.000	0.001			0.000	0.000	0.002	0.001	0.000	0.001		
Total	6.013	6.001	6.006			5.996	5.990			5.986	5.999	5.993	6.000	5.987	6.002		

Table (A.9.12) High resolution EPMA analyses and structure formulae of echinoderm fragments of the Ar Rajmah Formation (Middle Miocene).

Oxides (wt. %)	LB1				LB3					LB4			LB5						χ	σ
	(Foraminifera)																			
P₂O₅	-	-	-	-	0.019	0.028	0.057	0.051	0.035	0.041	0.043	0.095	0.013	0.000	0.029	0.006	0.017	0.000		
SO₃	0.030	0.021	0.113	0.127	0.086	0.159	0.058	0.034	0.054	0.000	0.069	0.084	0.047	0.060	0.020	0.032	0.030	0.017		
TiO₂	0.000	0.015	0.014	0.000	0.000	0.014	0.000	0.000	0.002	0.000	0.000	0.006	0.017	0.000	0.001	0.000	0.005	0.011		
MgO	0.241	0.436	0.385	0.635	10.950	0.447	0.536	0.434	0.598	0.353	0.608	0.518	0.240	0.418	0.318	0.501	0.379	0.360		
CaO	56.477	56.165	52.169	55.954	42.861	54.504	55.902	55.816	55.393	55.804	53.499	54.388	55.271	54.024	52.324	55.535	54.344	54.663		
MnO	0.000	0.000	0.000	0.000	0.000	0.000	0.000	0.000	0.006	0.007	0.010	0.000	0.000	0.000	0.000	0.000	0.000	0.000		
FeO	0.000	0.000	0.025	0.000	0.010	0.000	0.000	0.000	0.005	0.006	0.000	0.000	0.000	0.010	0.000	0.000	0.023	0.021		
NiO	-	-	-	-	0.010	0.000	0.037	0.021	0.011	0.009	0.042	0.023	0.006	0.000	0.000	0.001	0.000	0.015		
CuO	-	-	-	-	0.000	0.004	0.000	0.019	0.020	0.003	0.007	0.000	0.000	0.009	0.000	0.011	0.012	0.000		
SrO	0.022	0.089	0.034	0.052	0.051	0.113	0.098	0.103	0.095	0.077	0.044	0.064	0.070	0.054	0.069	0.047	0.067	0.088	0.065	0.019
BaO	-	-	-	-	0.003	0.000	0.000	0.000	0.000	0.000	0.000	0.000	0.000	0.000	0.012	0.000	0.000	0.013		
Na₂O	0.103	0.127	0.030	0.052	0.055	0.116	0.045	0.064	0.000	0.021	0.034	0.010	0.009	0.102	0.111	0.029	0.079	0.095		
K₂O	0.010	0.017	0.042	0.013	0.015	0.000	0.000	0.001	0.000	0.001	0.011	0.014	0.000	0.011	0.005	0.009	0.003	0.004		
Total	56.884	56.871	52.812	56.838	54.060	55.385	56.733	56.543	56.219	56.322	54.367	55.202	55.673	54.688	52.889	56.171	54.959	55.287		
Numbers of ions on the basis of 6 O excluding CO_2																				
P	-	-	-	-	0.002	0.002	0.005	0.004	0.003	0.003	0.004	0.008	0.001	0.000	0.003	0.000	0.001	0.000		
S	-	-	0.001	-	0.008	0.015	0.005	0.003	0.005	0.000	0.007	0.008	0.004	0.006	0.002	0.003	0.003	0.002		
Ti	0.000	0.001	0.001	0.000	0.000	0.001	0.000	0.000	0.000	0.000	0.000	0.000	0.001	0.000	0.000	0.000	0.000	0.001		
Mg	0.035	0.064	0.061	0.093	1.566	0.067	0.079	0.064	0.088	0.052	0.093	0.078	0.036	0.064	0.050	0.074	0.057	0.054		
Ca	5.953	5.916	5.927	5.898	4.405	5.877	5.886	5.904	5.885	5.930	5.873	5.878	5.945	5.909	5.923	5.912	5.918	5.922		
Mn	0.000	0.000	0.000	0.000	0.000	0.000	0.000	0.000	0.000	0.001	0.001	0.000	0.000	0.000	0.000	0.000	0.000	0.000		
Fe	0.000	0.000	0.002	0.000	0.001	0.000	0.000	0.000	0.000	0.001	0.000	0.000	0.000	0.001	0.000	0.000	0.002	0.002		
Ni	-	-	-	-	0.001	0.000	0.003	0.002	0.001	0.001	0.003	0.002	0.000	0.000	0.000	0.000	0.000	0.001		
Cu	-	-	-	-	0.000	0.000	0.000	0.001	0.002	0.000	0.001	0.000	0.000	0.001	0.000	0.001	0.001	0.000		
Sr	0.001	0.005	0.002	0.003	0.003	0.007	0.006	0.006	0.005	0.004	0.003	0.004	0.004	0.003	0.004	0.003	0.004	0.005		
Ba	-	-	-	-	0.000	0.000	0.000	0.000	0.000	0.000	0.000	0.000	0.000	0.000	0.000	0.000	0.000	0.000		
Na	0.020	0.024	0.006	0.010	0.010	0.023	0.009	0.012	0.000	0.004	0.007	0.002	0.002	0.020	0.023	0.006	0.015	0.019		
K	0.001	0.002	0.006	0.002	0.002	0.000	0.000	0.000	0.000	0.000	0.001	0.002	0.000	0.001	0.001	0.001	0.000	0.000		
Total	6.010	6.012	6.005	6.006	5.998	5.992	5.993	5.996	5.989	5.996	5.993	5.982	5.993	6.005	6.006	6.000	6.001	6.007		

Table (A.9.13) High resolution EPMA analyses and structure formulae of foraminifera of the Ar Rajmah Formation (Middle Miocene).

Oxides (wt. %)	LB1	LB1	LB3	LB3	LB4	LB4	Matrix	Matrix	Matrix	Matrix	Matrix	Matrix	LB5	LB5	LB5	LB5	LB5	LB5	x̄	σ
P_2O_5	-	-	0.041	0.032	0.055	0.034	0.063	0.023	0.042	0.026	0.020	0.087	0.072	0.056	0.082	0.062	0.019	0.017		
SO_3	0.036	0.073	0.122	0.045	0.058	0.095	0.115	0.029	0.084	0.028	0.081	0.124	0.024	0.021	0.038	0.051	0.114	0.035		
TiO_2	0.022	0.008	0.014	0.011	0.016	0.012	0.019	0.014	0.014	0.000	0.000	0.000	0.013	0.013	0.007	0.009	0.012	0.015		
MgO	0.321	0.552	17.039	0.740	0.641	0.770	0.730	0.894	18.484	8.139	0.444	18.822	0.763	0.369	0.298	14.614	14.042	11.039		
CaO	57.247	55.164	35.244	55.512	54.301	54.322	55.296	54.409	32.747	42.205	55.883	35.221	59.532	58.970	56.446	42.958	41.294	42.538		
MnO	0.006	0.000	0.000	0.000	0.000	0.000	0.000	0.000	0.016	0.026	0.000	0.023	0.005	0.007	0.000	0.023	0.000	0.020		
FeO	0.000	0.088	0.051	0.000	0.002	0.010	0.000	0.052	0.149	0.090	0.000	0.142	0.031	0.000	0.030	0.000	0.083	0.153		
NiO	0.000		0.000	0.003	0.017	0.008	0.000	0.000	0.000	0.000	0.000	0.000	0.010	0.000	0.000	0.019	0.000	0.000		
CuO			0.010	0.010	0.002	0.016	0.000	0.014	0.000	0.016	0.000	0.015	0.000	0.000	0.011	0.002	0.024	0.000		
SrO	0.032	0.063	0.108	0.116	0.059	0.017	0.002	0.051	0.017	0.037	0.142	0.071	0.026	0.081	0.021	0.057	0.050	0.039	0.056	0.021
BaO			0.000	0.001	0.007	0.000	0.017	0.000	0.000	0.000	0.000	0.020	0.033	0.015	0.000	0.004	0.011	0.000		
Na_2O	0.033	0.015	0.135	0.020	0.012	0.051	0.026	0.066	0.085	0.029	0.100	0.092	0.027	0.000	0.022	0.025	0.044	0.031		
K_2O	0.018	0.024	0.040	0.012	0.012	0.002	0.009	0.030	0.048	0.032	0.013	0.068	0.052	0.010	0.017	0.000	0.070	0.059		
Total	57.714	55.988	52.804	56.502	55.182	55.337	56.277	55.582	51.686	50.629	54.689	56.683	60.588	59.542	56.972	57.824	55.763	53.946		

Numbers of ions on the basis of 6 O excluding CO_2

	LB1	LB1	LB3	LB3	LB4	LB4	Matrix	Matrix	Matrix	Matrix	Matrix	Matrix	LB5	LB5	LB5	LB5	LB5	LB5	x̄	σ
P	-	-	0.003	0.003	0.005	0.003	0.005	0.002	0.003	0.002	0.002	0.007	0.003	0.002	0.007	0.005	0.002	0.002		
S	-	-	0.011	0.004	0.006	0.009	0.011	0.003	0.008	0.003	0.008	0.011	0.024	0.021	0.003	0.005	0.011	0.003		
Ti	0.002	0.001	0.001	0.001	0.001	0.001	0.001	0.001	0.000	0.000	0.000	0.000	0.013	0.013	0.007	0.000	0.001	0.001		
Mg	0.046	0.082	2.390	0.109	0.096	0.115	0.107	0.133	2.617	1.263	0.444	2.617	0.763	0.369	0.298	2.055	1.975	1.553		
Ca	5.944	5.903	3.553	5.864	5.871	5.849	5.851	5.837	3.333	4.707	5.883	3.333	5.532	5.857	5.708	4.324	4.163	4.292		
Mn	0.000	0.000	0.000	0.000	0.000	0.000	0.000	0.000	0.001	0.002	0.000	0.002	0.005	0.007	0.000	0.023	0.000	0.020		
Fe	0.000	0.007	0.004	0.000	0.000	0.001	0.000	0.004	0.012	0.008	0.000	0.012	0.031	0.000	0.030	0.000	0.083	0.153		
Ni	-	-	0.000	0.000	0.001	0.001	0.000	0.000	0.000	0.000	0.000	0.000	0.010	0.000	0.000	0.019	0.000	0.000		
Cu	-	-	0.001	0.001	0.000	0.001	0.000	0.001	0.000	0.001	0.000	0.000	0.000	0.000	0.011	0.002	0.024	0.000		
Sr	0.002	0.004	0.006	0.007	0.003	0.001	0.000	0.003	0.001	0.002	0.142	0.071	0.026	0.081	0.021	0.057	0.050	0.039		
Ba	-	-	0.000	0.000	0.000	0.000	0.000	0.000	0.000	0.000	0.000	0.001	0.033	0.015	0.000	0.004	0.011	0.000		
Na	0.006	0.003	0.025	0.004	0.002	0.010	0.001	0.005	0.016	0.006	0.100	0.020	0.027	0.000	0.022	0.025	0.044	0.031		
K	0.002	0.003	0.005	0.002	0.002	0.000	0.001	0.004	0.006	0.004	0.013	0.092	0.052	0.010	0.017	0.000	0.070	0.059		
Total	6.003	6.002	5.999	5.995	5.987	5.991	5.982	6.001	5.998	5.998	5.998	54.689	59.542	59.542	56.972	57.824	55.763	53.946		

Table (A.9.14) High resolution EPMA analyses and structure formulae of matrix of the Ar Rajmah Formation (Middle Miocene).

Oxides (wt. %)	Coralline algae				χ	σ	Oyster				χ	σ	Echinoderm fragments				χ	σ
P$_2$O$_5$	0.058	0.113	0.079	0.059			0.057	0.006	0.010	0.025			0.041	0.006	0.077	0.059		
SO$_2$	0.180	0.175	0.196	0.056			0.107	0.095	0.096	0.110			0.058	0.024	0.025	0.031		
TiO$_2$	0.000	0.005	0.008	0.001			0.000	0.001	0.003	0.000			0.000	0.000	0.000	0.008		
MgO	17.387	16.909	17.342	0.684			0.193	0.203	0.214	0.250			0.512	0.597	0.5000	0.524		
CaO	34.388	34.496	35.124	51.295			54.211	54.451	55.325	54.920			56.69	56.403	56.759	56.492		
MnO	0.000	0.000	0.012	0.000			0.010	0.006	0.000	0.000			0.000	0.000	0.000	0.000		
FeO	0.056	0.000	0.003	0.098			0.000	0.004	0.009	0.011			0.014	0.000	0.019	0.000		
NiO	0.000	0.001	0.009	0.000			0.009	0.000	0.018	0.020			0.000	0.009	0.014	0.027		
CuO	0.000	0.000	0.000	0.000			0.000	0.000	0.013	0.000			0.000	0.000	0.003	0.000		
SrO	0.039	0.047	0.063	0.044	0.05	0.01	0.106	0.099	0.092	0.122	0.104	0.012	0.11	0.097	0.099	0.096	0.101	0.006
BaO	0.000	0.000	0.000	0.001			0.000	0.000	0.000	0.000			0.005	0.000	0.008	0.000		
Na$_2$O	0.080	0.096	0.124	0.096			0.167	0.212	0.165	0.156			0.075	0.070	0.068	0.000		
K$_2$O	0.019	0.022	0.005	0.063			0.000	0.000	0.001	0.006			0.067	0.012	0.019	0.018		
Total	52.207	51.864	52.965	52.397			54.860	55.077	55.946	55.620			57.572	57.218	57.591	57.255		
Numbers of ions on the basis of 6 O excluding CO$_2$																		
P	0.005	0.009	0.006	0.005			0.005	0.001	0.001	0.002			0.003	0.000	0.006	0.005		
S	0.016	0.016	0.017	0.006			0.010	0.009	0.009	0.010			0.005	0.002	0.002	0.003		
Ti	0.000	0.000	0.001	0.000			0.000	0.000	0.000	0.000			0.000	0.000	0.000	0.001		
Mg	2.454	2.405	2.416	0.108			0.029	0.031	0.032	0.037			0.074	0.087	0.072	0.076		
Ca	3.488	3.527	3.516	5.841			5.914	5.922	5.923	5.911			5.888	5.894	5.891	5.896		
Mn	0.000	0.000	0.001	0.000			0.001	0.001	0.000	0.000			0.000	0.000	0.000	0.000		
Fe	0.004	0.000	0.000	0.009			0.000	0.000	0.001	0.000			0.001	0.000	0.002	0.000		
Ni	0.000	0.000	0.001	0.000			0.001	0.000	0.001	0.001			0.000	0.001	0.001	0.002		
Cu	0.000	0.000	0.000	0.000			0.000	0.000	0.001	0.002			0.000	0.000	0.000	0.000		
Sr	0.002	0.003	0.003	0.003			0.006	0.006	0.005	0.007			0.006	0.006	0.006	0.005		
Ba	0.000	0.000	0.000	0.000			0.000	0.000	0.000	0.000			0.000	0.000	0.000	0.000		
Na	0.015	0.018	0.022	0.020			0.033	0.042	0.032	0.030			0.014	0.013	0.013	0.000		
K	0.002	0.003	0.001	0.009			0.000	0.000	0.000	0.001			0.008	0.002	0.002	0.002		
Total	5.986	5.981	5.984	6.001			5.999	6.012	6.005	6.001			5.999	6.005	5.995	5.990		

Table (A.9.15) High resolution EPMA analyses and structure formulae of the coralline algae shell fragments (Oyster) and echinoderm fragments of the Ar Rajmah Formation (Middle Miocene).

Oxides (wt. %)	Forams					χ	σ	Bivalve			χ	σ
P₂O₅	0.051	0.025	0.032	0.009	0.027			36.495	39.047	36.456		
SO₂	0.152	0.013	0.225	0.000	0.016			1.061	0.327	1.041		
TiO₂	0.000	0.000	0.000	0.000	0.011			0.002	0.016	0.016		
MgO	0.120	0.121	0.292	0.258	0.079			0.149	0.140	0.154		
CaO	16.418	27.521	47.444	50.004	14.451			50.470	50.305	50.105		
MnO	0.000	0.000	0.000	0.000	0.006			0.000	0.000	0.004		
FeO	0.014	0.009	0.048	0.025	0.029			0.185	0.321	0.195		
NiO	0.000	0.000	0.007	0.022	0.007			0.000	0.007	0.000		
CuO	0.000	0.001	0.000	0.001	0.000			0.000	0.000	0.002		
SrO	0.000	0.018	0.058	0.057	0.006	0.028	0.028	0.226	0.161	0.299	0.229	0.069
BaO	0.000	0.000	0.000	0.000	0.000			0.000	0.000	0.034		
Na₂O	0.130	0.060	0.195	0.072	0.101			1.120	1.024	1.100		
K₂O	0.037	0.002	0.022	0.002	0.012			0.021	0.017	0.015		
Total	16.922*	27.770*	48.323	50.450	14.745*			89.729	91.365	89.421		
Numbers of ions on the basis of 6 O								**Numbers of ions on the basis of 12.5 O**				
P	0.014	0.004	0.003	0.001	0.009			2.869	2.977	2.869		
S	0.047	0.002	0.024	0.000	0.006			0.092	0.027	0.092		
Ti	0.000	0.000	0.000	0.000	0.003			0.000	0.000	0.000		
Mg	0.059	0.036	0.050	0.043	0.045			0.021	0.019	0.021		
Ca	5.760	5.932	5.861	5.939	5.862			5.010	4.856	4.990		
Mn	0.000	0.000	0.000	0.000	0.002			0.000	0.000	0.000		
Fe	0.004	0.001	0.005	0.002	0.009			0.015	0.025	0.015		
Ni	0.000	0.000	0.001	0.002	0.002			0.000	0.000	0.000		
Cu	0.000	0.000	0.000	0.000	0.000			0.000	0.000	0.000		
Sr	0.000	0.002	0.004	0.004	0.001			0.013	0.010	0.017		
Ba	0.000	0.000	0.000	0.000	0.000			0.000	0.000	0.002		
Na	0.083	0.024	0.044	0.016	0.074			0.202	0.179	0.198		
K	0.016	0.001	0.003	0.000	0.006			0.002	0.002	0.002		
Total	5.983	6.002	5.995	6.007	6.019			8.223	8.094	8.201		

(Table header span: LB5)

* The total is very low (not correct), due to very high void space in the forams

Table (A.9.16) High resolution EPMA analyses and structure formulae of the shell fragments (forams & bivalve) of the Ar Rajmah Formation (Middle Miocene).

Table: **UBA3 U — Cement**

Oxides (wt. %)

Oxides (wt. %)																					χ	σ
P_2O_5	0.091	0.066	0.000	0.038	0.016	0.536	0.006	0.028	0.038	0.030	0.062	0.022	0.048	0.022	0.000	0.022	0.034	0.028	0.070	0.020		
SO_3	0.022	0.003	0.000	0.020	0.000	0.003	0.000	0.008	0.000	0.029	0.000	0.000	0.030	0.000	0.036	0.029	0.000	0.015	0.020	0.000		
TiO_2	0.000	0.005	0.003	0.000	0.005	0.000	0.000	0.005	0.001	0.008	0.000	0.000	0.002	0.000	0.008	0.010	0.001	0.009	0.000	0.010		
MgO	0.726	0.908	0.497	0.347	0.337	0.637	0.288	0.532	0.442	1.073	0.430	0.776	0.689	0.351	0.383	0.526	0.267	0.547	0.440	0.570		
CaO	55.389	54.916	54.820	55.346	57.763	56.383	59.203	56.108	58.916	55.530	56.492	58.029	56.134	58.660	57.902	55.867	56.364	55.905	56.900	59.300		
MnO	0.000	0.000	0.000	0.000	0.000	0.151	0.000	0.003	0.017	0.000	0.000	0.014	0.000	0.000	0.000	0.000	0.000	0.000	0.000	0.000		
FeO	0.000	0.000	0.000	0.000	0.010	0.000	0.000	0.010	0.000	0.016	0.000	0.009	0.000	0.009	0.014	0.035	0.000	0.001	0.020	0.000		
NiO	0.042	0.000	0.000	0.000	0.000	0.000	0.000	0.002	0.018	0.021	0.000	0.016	0.006	0.000	0.000	0.000	0.000	0.000	0.020	0.000		
CuO	0.026	0.038	0.013	0.054	0.016	0.000	0.000	0.033	0.011	0.015	0.022	0.000	0.007	0.000	0.000	0.000	0.011	0.033	0.000	0.010		
SrO	0.002	0.000	0.000	0.000	0.000	0.000	0.009	0.000	0.000	0.013	0.000	0.000	0.000	0.000	0.000	0.000	0.000	0.000	0.000	0.000	0.001	0.003
BaO	0.000	0.000	0.000	0.000	0.000	0.000	0.009	0.000	0.000	0.000	0.000	0.000	0.020	0.000	0.000	0.003	0.000	0.000	0.000	0.010		
Na_2O	0.016	0.043	0.030	0.010	0.000	0.021	0.014	0.003	0.020	0.010	0.028	0.058	0.000	0.000	0.016	0.000	0.000	0.022	0.010	0.050		
K_2O	0.006	0.000	0.007	0.003	0.001	0.017	0.000	0.007	0.004	0.000	0.004	0.000	0.001	0.000	0.002	0.000	0.000	0.001	0.000	0.010		
Total	56.320	55.979	55.370	55.818	58.148	57.748	59.520	56.739	59.467	56.745	57.038	58.924	56.937	59.042	58.361	56.492	56.677	56.561	57.480	59.950		

Numbers of ions on the basis of 6 O excluding CO_2

P	0.008	0.006	0.000	0.003	0.001	0.043	0.000	0.002	0.003	0.002	0.005	0.002	0.004	0.002	0.000	0.002	0.003	0.002	0.006	0.001
S	0.002	0.000	0.000	0.002	0.000	0.000	0.000	0.001	0.000	0.003	0.000	0.000	0.003	0.000	0.003	0.003	0.000	0.001	0.002	0.000
Ti	0.000	0.000	0.000	0.000	0.000	0.000	0.000	0.000	0.000	0.001	0.000	0.000	0.000	0.000	0.001	0.001	0.000	0.001	0.000	0.000
Mg	0.107	0.134	0.075	0.052	0.048	0.091	0.040	0.078	0.062	0.157	0.063	0.109	0.100	0.050	0.055	0.077	0.039	0.080	0.064	0.078
Ca	5.863	5.843	5.920	5.931	5.946	5.785	5.957	5.910	5.925	5.825	5.920	5.878	5.882	5.945	5.935	5.908	5.953	5.905	5.914	5.913
Mn	0.000	0.000	0.000	0.000	0.000	0.000	0.000	0.000	0.001	0.000	0.000	0.001	0.000	0.000	0.000	0.000	0.000	0.000	0.000	0.000
Fe	0.000	0.000	0.000	0.000	0.001	0.012	0.000	0.001	0.000	0.001	0.000	0.001	0.000	0.001	0.001	0.003	0.000	0.000	0.001	0.000
Ni	0.003	0.000	0.000	0.000	0.000	0.000	0.000	0.000	0.001	0.002	0.000	0.001	0.000	0.000	0.000	0.000	0.000	0.000	0.001	0.000
Cu	0.002	0.003	0.004	0.000	0.001	0.000	0.000	0.002	0.001	0.001	0.002	0.000	0.001	0.000	0.000	0.000	0.001	0.002	0.000	0.001
Sr	0.000	0.000	0.000	0.000	0.000	0.000	0.000	0.000	0.000	0.001	0.000	0.000	0.000	0.000	0.000	0.000	0.000	0.000	0.000	0.000
Ba	0.000	0.000	0.000	0.000	0.000	0.000	0.000	0.000	0.000	0.000	0.000	0.000	0.001	0.000	0.000	0.000	0.000	0.000	0.000	0.000
Na	0.003	0.008	0.006	0.002	0.000	0.004	0.003	0.000	0.004	0.002	0.005	0.011	0.000	0.000	0.003	0.000	0.000	0.004	0.002	0.005
K	0.001	0.000	0.001	0.000	0.000	0.002	0.000	0.001	0.000	0.000	0.000	0.000	0.000	0.000	0.000	0.000	0.000	0.000	0.000	0.001
Total	5.989	5.994	6.003	5.994	5.997	5.937	6.000	5.995	5.997	5.995	5.995	6.003	5.991	5.998	5.998	5.994	5.996	5.995	5.990	5.999

Table (A.9.17) High resolution EPMA analyses and structure formulae of the cement in the Ar Rajmah Formation (Middle Miocene).

X.3.3 EPMA for echinoid spines: (A.9.18-A.9.19)

Table (A.9.18) High resolution EPMA for echinoid spine (1), traverse 1 and 2 in Benghazi Member of the Ar Rajmah Formation (Middle Miocene).

Oxides (wt. %)	1 (Rim)	2	3	4	5	6	7	8
MgO	0.786	0.781	0.338	0.377	0.342	0.373	0.312	0.368
CaO	65.576	65.002	56.090	56.817	56.611	56.465	56.662	57.099
FeO	0.059	0.000	0.000	0.006	0.002	0.001	0.000	0.000
SrO	0.095	0.076	0.082	0.106	0.146	0.118	0.122	0.080
Total	66.516	65.859	56.510	57.306	57.101	56.957	57.096	57.547

Oxides (wt. %)	9	10	11	12 (Centre)	13 (Centre)	14	15	16
MgO	0.432	0.304	0.413	0.444	0.257	0.337	0.550	0.333
CaO	56.713	54.020	56.532	54.423	57.388	57.307	56.609	52.499
FeO	0.000	0.061	0.002	0.047	0.002	0.000	0.006	0.073
SrO	0.121	0.116	0.110	0.121	0.135	0.155	0.088	0.077
Total	57.266	54.501	57.057	55.035	57.782	57.799	57.253	52.982

Oxides (wt. %)	17	18	19	20	21	22	23	24
MgO	0.296	0.448	0.270	0.386	0.332	0.344	0.367	0.408
CaO	55.892	56.647	54.756	57.307	57.147	56.503	52.714	54.219
FeO	0.000	0.000	0.000	0.000	0.000	0.000	0.114	0.035
SrO	0.129	0.106	0.085	0.067	0.069	0.072	0.110	0.096
Total	56.317	57.201	55.111	57.760	57.548	56.919	53.305	54.758

Oxides (wt. %)	25 (Rim)							
MgO	0.343							
CaO	54.468							
FeO	0.075							
SrO	0.136							
Total	55.022							

Continued of Table (A.6.18), second traverse:

Oxides (wt. %)	1 (Rim)	2	3	4	5	6	7	8
MgO	0.387	0.453	0.333	0.310	0.337	0.340	0.403	0.368
CaO	56.563	56.720	55.193	55.490	56.900	56.324	56.285	56.228
FeO	0.015	0.016	0.000	0.000	0.000	0.021	0.000	0.000
SrO	0.122	0.092	0.116	0.081	0.123	0.113	0.125	0.111
Total	57.087	57.281	55.642	55.881	57.360	56.798	56.813	56.707

Oxides (wt. %)	9	10	11	12 (Centre)	13 (Centre)	14	15	16
MgO	0.308	0.490	1.159	0.309	0.307	0.307	0.280	0.261
CaO	56.184	50.635	46.646	56.508	58.148	52.593	57.311	54.505
FeO	0.004	0.091	0.354	0.000	0.000	0.011	0.000	0.077
SrO	0.114	0.098	0.079	0.120	0.121	0.096	0.092	0.121
Total	56.610	51.314	48.238	56.937	58.576	53.007	57.683	54.964

Oxides (wt. %)	17	18	19	20	21	22	23	24
MgO	0.409	0.338	0.778	0.366	1.158	0.304	0.486	0.423
CaO	56.940	54.027	55.678	56.930	55.498	52.865	53.669	56.714
FeO	0.000	0.019	0.000	0.000	0.005	0.119	0.071	0.011
SrO	0.124	0.123	0.080	0.102	0.100	0.093	0.084	0.133
Total	57.473	54.507	56.536	57.398	56.815	53.381	54.310	57.281

Oxides (wt. %)	25 (Rim)							
MgO	0.386							
CaO	54.816							
FeO	0.074							
SrO	0.082							
Total	55.358							

Table (A.9.19) High resolution EPMA for echinoid spine (2), traverse 1 and 2 in Benghazi Member of the Ar Rajmah Formation (Middle Miocene).

Oxides (wt. %)	1 (Rim)	2	3	4	5	6	7	8
MgO	15.501	0.372	0.412	0.552	0.436	0.327	0.631	0.352
CaO	40.948	58.791	52.759	47.181	58.679	57.985	57.789	57.824
FeO	0.000	0.050	0.085	0.262	0.000	0.008	0.013	0.000
SrO	0.362	0.106	0.113	0.090	0.103	0.06	0.110	0.127
Total	56.811	59.319	53.369	48.085	59.218	58.380	58.543	58.303

Oxides (wt. %)	9	10	11	12	13	14	15 (Centre)	16
MgO	0.448	0.255	0.522	0.382	0.402	0.270	0.359	0.473
CaO	59.048	49.833	58.499	59.442	54.601	59.587	59.021	56.458
FeO	0.005	0.102	0.002	0.000	0.058	0.017	0.000	0.019
SrO	0.097	0.067	0.099	0.110	0.124	0.141	0.151	0.101
Total	59.598	50.257	59.122	59.934	55.185	60.015	59.531	57.051

Oxides (wt. %)	17	18	19	20	21	22	23	24
MgO	0.529	0.360	0.301	0.770	0.320	0.570	0.389	0.328
CaO	58.762	53.129	54.434	58.481	49.745	58.553	59.378	59.631
FeO	0.007	0.156	0.141	0.011	0.330	0.000	0.071	0.000
SrO	0.120	0.074	0.076	0.123	0.056	0.101	0.112	0.142
Total	59.418	53.719	54.952	59.385	50.451	59.224	59.950	60.101

Oxides (wt. %)	25	26	27	28	29	30 (Rim)		
MgO	0.323	0.512	0.438	0.325	0.440	0.462		
CaO	58.991	56.619	58.445	59.946	57.382	58.411		
FeO	0.022	0.037	0.000	0.000	0.006	0.043		
SrO	0.132	0.025	0.121	0.094	0.114	0.113		
Total	59.468	57.193	59.004	60.365	57.942	59.029		

Continued of table (A.6.19), second traverse:

Oxides (wt. %)	1 (Rim)	2	3	4	5	6	7	8
MgO	0.961	0.200	0.289	0.391	0.329	0.266	0.386	0.660
CaO	58.453	57.051	55.337	59.559	57.533	48.360	58.155	58.803
FeO	0.009	0.000	0.069	0.000	0.000	0.371	0.000	0.000
SrO	0.132	0.064	0.049	0.103	0.094	0.051	0.144	0.127
Total	59.555	57.315	55.744	60.053	57.956	49.048	58.685	59.590

Oxides (wt. %)	9	10 (Centre)	11 (Centre)	12	13	14	15	16
MgO	0.227	0.256	0.382	0.425	0.252	0.396	0.488	0.427
CaO	58.771	58.929	59.253	58.661	57.226	58.952	58.690	57.096
FeO	0.000	0.009	0.011	0.037	0.000	0.011	0.000	0.000
SrO	0.148	0.134	0.148	0.147	0.064	0.078	0.099	0.075
Total	59.146	59.328	59.794	59.270	57.542	59.437	59.277	57.598

Oxides (wt. %)	17	18	19	20	21 (Rim)			
MgO	0.645	0.473	1.779	0.338	0.426			
CaO	40.679	51.971	57.054	57.707	57.702			
FeO	14.273	0.725	0.044	0.005	0.063			
SrO	0.053	0.077	0.066	0.114	0.109			
Total	55.650	53.246	58.943	58.164	58.300			